Regulatory Mechanisms of a Bacterial Multi-Kinase Network

by

Kimberly Ann Kowallis

B.S., Carlow University, 2011

Submitted to the Graduate Faculty of the

Dietrich School of Arts and Sciences in partial fulfillment

of the requirements for the degree of

Doctor of Philosophy

University of Pittsburgh

2020

UNIVERSITY OF PITTSBURGH

DIETRICH SCHOOL OF ARTS AND SCIENCES

This dissertation was presented

by

Kimberly Ann Kowallis

It was defended on

July 9, 2020

and approved by

Stephen G. Weber, Professor, Department of Chemistry

Kabirul Islam, Assistant Professor, Department of Chemistry

Vaughn S. Cooper, Professor, Department of Microbiology and Molecular Genetics

Dissertation Director: W. Seth Childers, Assistant Professor, Department of Chemistry

Regulatory Mechanisms of a Bacterial Multi-Kinase Network

Kimberly Ann Kowallis, PhD

University of Pittsburgh, 2020

Cells sense and respond to their environment through signaling pathways which often require processing several signals prior to implementing a biological response. Bacterial signaling pathways are responsible for processes such as virulence, biofilm formation, survival, and symbiosis that are of research interest for medical, environmental, and industrial advancements. Emerging discoveries suggest that the systems that control these responses are more complex and intertwined than the previously understood two-component systems. Proteins such as scaffolds and pseudokinases regulate the localization, activity, and timing of the phosphotransfer reactions that dictate cellular decisions. This dissertation describes regulatory mechanisms of a multi-kinase network that controls asymmetric division in the model bacterium *C. crescentus.*

It has been proposed that the novel pseudokinase DivL reverses signal flow by exploiting conserved kinase conformational changes and protein-protein interactions. Chapter 2 describes the development and characterization of a series of DivL-based modulators to synthetically stimulate reverse signaling of the network *in vivo*. I propose that synthetic stimulation and sensor disruption provide strategies to define signaling circuit organization principles for the rational design and validation of synthetic pathways.

In Chapter 3, I further dissect the roles of each DivL domain on subcellular localization and downstream activity. While not catalytically active, pseudokinases have been repurposed to serve functions including complex signal recognition, integration, competition, and intermolecular

allostery. I provide a refined model detailing how DivL plays each of these parts within its broader network.

The work in Chapter 3 also revealed multiple scaffolding interactions that orchestrate the multi-kinase network in time and space. In Chapter 4 I identify factors that lead to the accumulation of two biochemically distinct signaling hubs at opposite cell poles to provide the foundation for asymmetry. I also provide evidence that a scaffold not only recruits a key signaling protein to the correct location but mediates its switch between kinase and phosphatase activities that drives the cell cycle.

In each chapter, I discuss questions that remain and suggest future directions for study. Overall, this dissertation contributes strategies that can be used to interrogate other relevant multi-kinase networks in bacteria.

Table of Contents

List of Tables

List of Figures

Abbreviations

AMP, adenosine monophosphate; ATP, adenosine triphosphate; BODIPY, boron dipyrromethene; CC, coiled-coil; *C. crescentus*, *Caulobacter crescentus*; CtrA~P, phosphorylated CtrA; DivK~P, phosphorylated DivK; DivK$_{cs}$, cold-sensitive DivK strain; DHp, dimerization and histidine phosphorylation; DUF, domain of unknown function; *E. coli*, *Escherichia coli*; FRET, fluorescence resonance energy transfer; GFP, green fluorescent protein; HK, histidine kinase domain; kDa, kilodalton; LZ, leucine zipper; MKN, multi-kinase network; PAS, Per-Arnt-Sim domain; PEG 8000, polyethylene glycol molecular weight=8000 grams/mole; PodJ$_L$, long form of PodJ; PodJ$_S$, short form of PodJ; RD, receiver domain; RR, response regulator; sfGFP: super folder green fluorescent protein; SH3, SRC homology 3 domain; TM, transmembrane domain

Preface

For telling me to keep going, and when to take a break. For telling me I could do it. For prematurely calling me doctor every once in a while, just to keep my eye on the prize.

For listening to me talk about DivL, *Caulobacter*, or pseudokinases, even if just once. For all the troubleshooting, model building, figure scrawling, model busting, explain-this-to-me-one-more-time, mad scientist science talks.

For pouring yourself into all my projects with me. For welcoming me to come to you for anything, anytime. For the registering, the purchasing, the scheduling, the printing, the cleaning, the repairing, the training, the supplying, the…

For the lunch dates, coffee breaks, hot tea, bubble tea, craft nights, late nights, post-it quotes, workouts, snack raids, meme trades, playlist curations, pizza birthday celebrations, and for so many concerts.

For allowing me to teach you. For teaching me so much more.

For inspiring me with your own determination.

And for continuing to do so.

Thank you.

1.0 Introduction

This chapter was written in collaboration with Samuel W. Duvall, Wei Zhao, and W. Seth Childers. Adapted by permission from Springer Nature: Springer eBook "Manipulation of Bacterial Signaling Using Engineered Histidine Kinases" by Kimberly A. Kowallis, Samuel W. Duvall, Wei Zhao, W. Seth Childers Copyright (2020).

1.1 Potential for Engineering Histidine Kinases

Two-component systems allow bacteria to respond to changes through signal recognition by the histidine kinase (HK) and transfer of the phosphate to its response regulator (RR) [1, 2]. The RR can then activate a response, which is often gene transcription [3]. HKs are typically homodimeric, embedded in the membrane, and have one or more sensory domains that regulate the kinase domain. The HK domain, while highly conserved, contains many customizable functions including optional phosphatase activity, alteration of phosphotransfer partner specificity, and regulation of kinase heterodimerization (Figure 1.1). The variation of these functions in the kinase domains generates an array of different phenotypic responses (Figure 1.2). HKs exhibit the most remarkable diversity in the sensory domains with varied domain architectures and sensing capabilities [1]. As an example, *C. crescentus* cell-cycle kinase CckA homologs vary in the number and identity of PAS sensory domains across the alpha-proteobacteria (Figure 1.3). This highlights the potential evolution of new connections that can occur between input signals and output responses through domain shuffling of sensory domains. In contrast to many eukaryotic sensory

proteins that contain flexible linkers between domains, the linker region that connects the sensor to the kinase domain often contains one or more helical folds that allosterically transmit signals between domains [4-8].
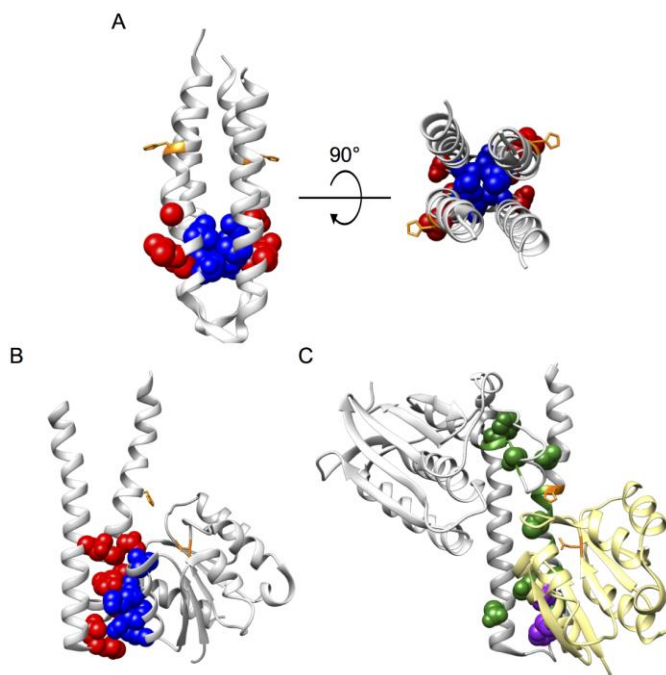
Figure 1.1: Customizable residues for the DHp bundle of a histidine kinase and the RD of a RR Phosphorylatable histidine and aspartic acid are colored orange. A) Residues involved in dimerization of the DHp are blue and buried in the bundle (PDB: 5B1N [9]. Residues in red are involved in RR specificity and are solvent exposed. B) The HK853-RR468 crystal structure (PDB: 3DGE [10]) highlights residues involved in the HK/RR specificity. Residues in red are located on the HK and blue are located on the RR. C) HK853-RR468 crystal structure (PDB: 3DGE [10]) with residues in cyan denoting the DXXN phosphatase motif, residues in green denoting the GXGXG motif, with second X (T in HK853) shown as spherical [10], blue showing the T267 and Y272 residues located on the HK capable of reducing phosphatase activity [10], and purple for the I17 and F20 residues located on the RR that can be mutated to prevent phosphate back-transfer [10].
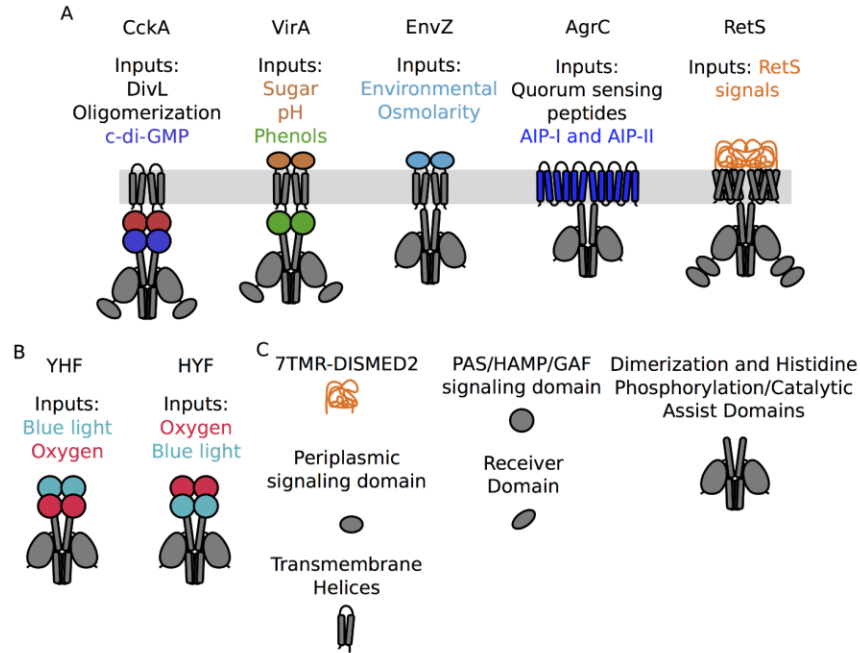
Figure 1.2: Sensing capacities and domain architectures of natural and synthetic HKs A) Domain architectures of 5 HKs with diverse sensing capabilities. Outputs include CckA activating transcription of cell-cycle regulated genes through the RR CtrA, VirA controlling virulence to plants and interkingdom gene transfer through the RR VirG, EnvZ controlling porin formation genes through the RR OmpR, AgrC activating virulence related genes, and RetS inhibiting GacS/GacA and PA1611 virulence pathways through heterodimer formation. B) Depiction of the synthetic chimeras of FixL and YtvA YHF and HYF HKs. C) Legend of domain representations.
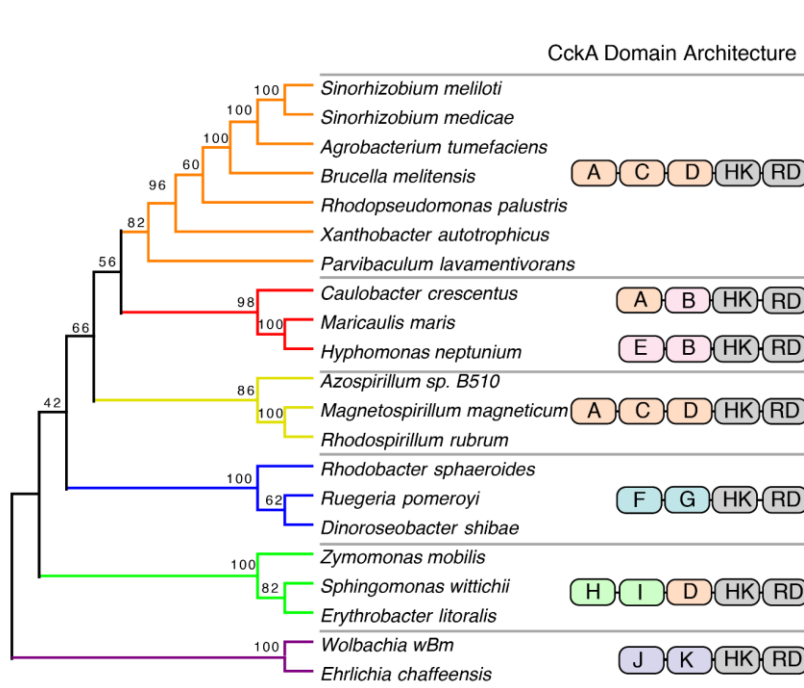
Figure 1.3: Analysis of CckA homologs in alphaproteobacteria species highlights the diversity in signaling domains

Methods such as cysteine cross-linking [5, 8, 11] and mutagenesis have greatly contributed to the understanding of HK signal transmission mechanisms, but not without the unpredictable effects that point mutations can have on protein folding and activity. Crystallography [7, 12-16] has also been a powerful technique to analyze the conformational states of HKs, but due to many HKs having one or more transmembrane domains, it is often difficult to isolate soluble full-length HKs. Furthermore, the transmembrane region is not dispensable for activity in some cases [17, 18]. Additionally, the central dimerization and histidine phosphotransfer (DHp) domain must interact with distinct domains to carryout kinase versus phosphotransfer functions, which leads to HK conformational diversity. To address these challenges, HK engineering strategies have provided a hypothesis-driven approach to test bacterial HK signal transmission mechanisms.

4

In this chapter we discuss various protein engineering strategies that have been taken to understand the mechanisms of HKs and two-component signaling networks. We review the design and characterization of chimeras that contain a sensory domain from one HK and the catalytic domain of another HK and examine how these strategies can help annotate unknown sensory functions [19, 20], discover phenotypes regulated by the signaling pathway [21, 22] and design sensors for small molecule detection [23, 24]. We also discuss a second strategy to test long-range HK allosteric signal transmission mechanisms that uses a leucine zipper to bias the conformational state to confer kinase activity, partial activity, or inactivity. Finally, we discuss strategies towards re-wiring two-component system network through heterodimerization [25], re-programming phosphotransfer RR specificity [26], and scaffold-dependent regulation [27].

1.2 Chimeric Histidine Kinases

First generation chimeric HKs reveal the importance of the connecting helical linker in signal transmission Early examples of engineered chimeric histidine kinases were generated by fusing the periplasmic and transmembrane domains of the *E. coli* aspartate sensing Tar chemoreceptor protein to the cytoplasmic HK domains of the osmolarity sensing protein EnvZ of *E. coli* [19, 28]. Construction and design of chimeric HKs has revealed that the linker region acts as a "structural joint" for transmitting signals between domains [29] and that linker compositional changes can place the kinase in the "on" or "off" state [30].

It was further shown that the C-terminal region of many classes of sensory domains (e.g. HAMP, PAS, and GAF domains) exploit a C-terminal helix that can allosterically transmit a signaling event from the sensor binding site to the histidine phosphorylation site [31, 32]. The function

of a chimeric HK is therefore dependent upon maintenance of the α-helix heptad periodicity. A second critical feature specific to PAS sensory domains is a structural motif that is positioned between the PAS domain and the C-terminal helix termed the DIT signal transmission motif [8, 20, 21, 33, 34]. The DIT motif is a set of residues at the N-terminus of the last helix in PAS domains, and can present itself as D-(A/I/V)-(T/S) [31]. This motif forms hydrogen bonding and salt bridge interactions that couple the PAS fold to the C-terminal α-helix such that signal can alter the conformation of downstream domains [31]. Mutations to the conserved aspartic acid and threonine to aliphatic amino acids have been shown to abolish signal transduction through the α-helix [7]. The DIT motif mutations therefore present an approach to test if signals are transmitted from a given PAS domain to downstream effector domains through the helical linker.

Aromatic Tuning to regulate HK interactions at the membrane-cytosolic interface

Transmission of a signal from the sensory domain in the periplasm to the cytoplasm is highly influenced by transmembrane helix interactions with the membrane. This can present a unique challenge when heterologously expressing a kinase from another organism, as changes in membrane composition can cause conformational changes and repositioning of the transmembrane helix and subsequently alter kinase activity [13, 35-37]. The configuration of aromatic residues near the membrane interface has been shown to modulate HK activity *in vivo* [36, 38]. The repositioning of aromatic residues at the membrane cytosolic interface to change the interactions between the transmembrane helix and the membrane has been termed aromatic tuning [39, 40]. As shown in Figure 1.4, the tryptophan is repositioned by one residue in both the N-terminal and C-terminal directions and this impacts the helix tilt angle within the membrane. This aromatic tuning strategy can optimize the responsiveness of chimeric HKs by expanding the sensor's dynamic range, and in some cases, restoring kinase activity to an unresponsive chimera [38].

6
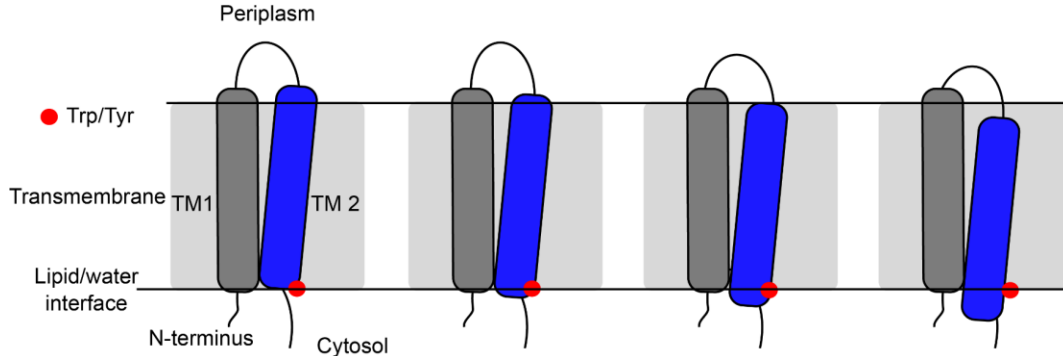
Figure 1.4: Aromatic tuning A) The impact of repositioning the aromatic tryptophan or tyrosine located at the lipid-water interface of the transmembrane and cytosol upon HK signaling. B) Aromatic tuning mutational strategy applied to the NavZ1 chimera [38].

Use of chimeric HKs to identify new signaling inputs Due to the lack of conservation among sensory domains, it has been difficult to determine physiological signal inputs of the vast majority of HKs. One approach is engineering HK chimeras in which a sensory domain of unknown function is attached to well-characterized kinase domain. Combined with the cognate RR, a transcriptional gene reporter can be used to identify factors that activate or repress the signaling domain (Figure 1.5A). This approach was used to characterize novel signals that regulate the sensory domain of the *Caulobacter crescentus* cell-cycle kinase CckA [21]. Prior to these studies, it was unclear what signals regulate CckA activity. In this study two design criteria were considered: first, selection of a well-understood kinase domain and downstream reporter and second, selection of the fusion site between the CckA sensor and the kinase. For this assay, the kinase should be orthogonal to the existing two-component systems encoded in the bacteria to insulate the chimeric HK from native two-component signaling networks. In this case Iniesta et al. selected a *C. crescentus* oxygen sensing FixL/FixJ β-galactosidase reporter used in strains with a knockout of the native FixL/FixJ signaling pathway [41]. To identify the best fusion sites a panel of

7

CckA-FixL chimeras was constructed and screened. The most responsive CckA-FixL chimera was coupled together with data from a transposon screen to identify protein signals that regulate CckA's activity and subcellular localization. This study revealed that a novel pseudokinase DivL promotes CckA activity through direct or indirect interaction with CckA's tandem sensory domain [21]. This example highlights the potential of coupling chimeric HKs together with fluorescent transcription reporter and high-throughput library approaches to identify signal inputs that modulate HKs that are critical for development or pathogenesis.
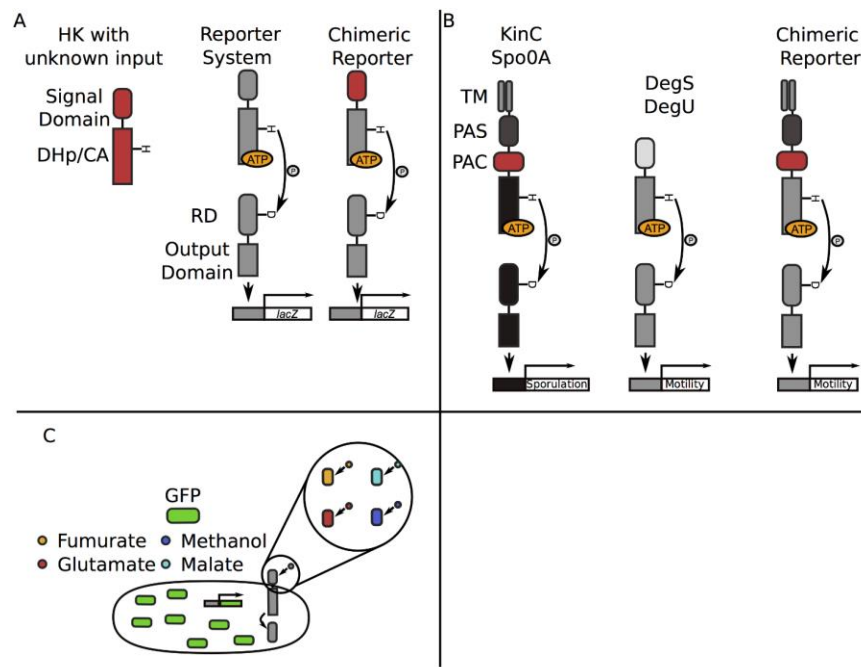
Figure 1.5: Design and application of chimeric histidine kinases to detect unknown and known signals A) General design of a HK chimera to report on the activity of an unknown signaling domain via β-galactosidase expression. B) A KinC/DegS reporter strain was generated such that membrane-damaging agent nyastatin could be sensed via KinC and trigger motility regulation through the DegS pathway. C) Small molecule reporters sensing fumarate, methanol, glutamate, and malate using the *E. coli* EnvZ/OmpR two-component system with GFP as a transcriptional readout.

8

Re-wired developmental response and identification of potassium leakage sensor domain *B. subtilis* is a model organism for bacterial differentiation into diverse cell types. The membrane potential sensing kinase KinC in *B. subtilis* has been implicated in formation of biofilms in response to membrane damage due to exposure to surfactins and other antimicrobial agents[22]. Therefore it was proposed that KinC was a potassium leakage sensing kinase. To identify the domains of KinC involved in sensing the effects of potassium leakage, the sensor of KinC was attached to the well characterized *B. subtilis* HK DegS, which controls genes that regulate swarming behavior, in a DegS knockout strain. Through a swarm size assay with the KinC-DegS chimera, it was demonstrated that the KinC sensory domain was a potassium leakage sensory directly or indirectly [22]. Wild-type cells typically respond to potassium leakage by upregulation of KinC biofilm genes, while the KinC-DegS chimera re-wires this response to potassium leakage to upregulate DegS-DegU motility genes (Figure 1.5B). This case illustrates the potential for synthetic developmental biology strategies to use HK chimeras to re-wire the behavioral logic of a bacterium.

Chimeric HKs as small molecule reporters HKs can also be repurposed as sensors for metabolic engineering [23, 24, 42, 43], optogenetic applications [44] or sensing disease related signals [45]. High-throughput screening methods using chimeric HKs have been designed to identify microorganisms that generate large quantities of chemicals for industrial processes [46, 47]. These chimeras use the EnvZ/OmpR two-component system that regulates GFP expression under *ompC* output. Unique chimeras were constructed using the sensor domains that detect malate (MalK), methanol (FlhS), glutamate (DegS), and fumarate (DcuS) (Figure 1.5C) [23, 24, 42, 43]. These small molecule fluorescent biosensors will now enable future screens of bacterial libraries for isolation of unique chassis for production of feedstock and small molecules.

Tuning the dynamic range of HK reporters by varying the degree of phosphatase function An inherent challenge to implementing HKs as cell based reporters is that each two component system has a defined signal detection range, and that range may not correspond to the application's required detection ranges [48]. Landry et al. utilized a computational model [49] that revealed decreasing phosphatase activity lowered the detection threshold without negatively affecting the dynamic range [50].

The catalytic phosphatase residues are found in a conserved DxxxQ/H motif in the HisKA_3 family or E/DxxT/N motif in the HisKA family just downstream of the phosphorylatable histidine. The proposed mechanism for the HisKA_3 family asserts that the glutamine or histidine align a water molecule for the hydrolysis of the phosphate group and that the aspartic acid forms a hydrogen bond with a conserved lysine of the response regulator [51]. Mutations to the glutamine/histidine or aspartic acid abolish or decrease phosphatase activity. The mechanism of the His_KA family appears to follow a similar mechanism as mutations to the threonine/asparagine result in loss of phosphatase activity [51, 52].

Other phosphatase activity mutants have been mapped to regions outside of the catalytic motif, and are thought to affect long-range conformational changes, interactions with the response regulator, the G2 box conformation, or nucleotide binding [10, 52, 53] (Figure 1.1C). Landry et al. successfully applied the conserved G2 box motif mutation as a sensor tuning strategy by engineering NarX kinase as a detector of nitrate from fertilizer [50]. The engineered system sensed a larger range of nitrate conditions in the native soil environment than the wild-type NarX kinase. The authors suggest that this sensor can be coupled with nitrogen-fixing systems for agricultural and environmental safety applications [54, 55]. Furthermore, this presents an attractive general

strategy that can be used to fine tune detection thresholds for histidine kinase biosensors in synthetic biology.

1.3 The Leucine Zipper Engineering Strategy

Studies of the long-range signal transmission from the sensory domain to the HK domain have led to a model of how these helical linkers propagate signal from the sensor to the HK domain. The model proposes that the helices form a coiled-coil interface that changes in response to signal binding. This conformational change is proposed to affect the position of the phosphorylatable histidine in relation to the ATP binding domain. This includes either taking on a kinase-active conformation or switching to a phosphotransfer or a phosphatase-active conformation (Figure 1.6) [7, 13, 15, 56, 57]. Other studies have suggested an electrostatic interaction between the signal transmission coiled-coil and the HK domain, which would similarly bias HK domain conformation [4, 5].
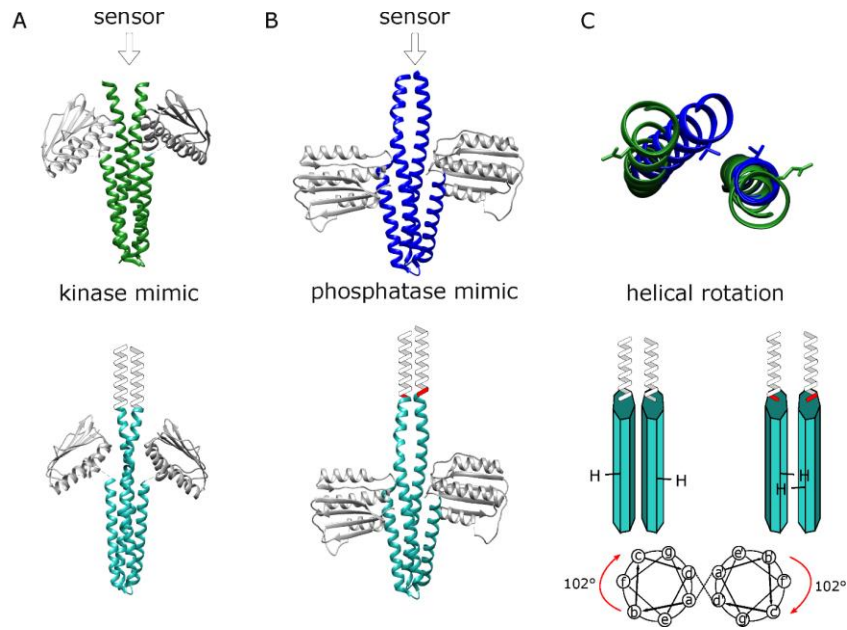
Figure 1.6: The leucine zipper engineering strategy Crystal structures of the (A top) kinase mimic (H188E, PDB: 3GIE [13]) and (B top) phosphatase mimic (H188V, PDB: 3EHJ[13]) of DesK show bending and helical rotation, apparent in (C top) an overlay of the DHp domains from above. A, B, C bottom) The leucine zipper fusion strategy is utilized to lock the kinase domain into distinct conformational states by addition or deletion of residues from the helical coil.

The ability to manipulate the conformation of the coiled-coil linkers has become a strategy for testing the HK signal transmission mechanism. The leucine zipper of the *S. cerevisiae* transcriptional activator GCN4 is a coiled-coil with a strong bias for one interface, with a K_d of dimerization in the 10 nM range [58]. Since the K_d of dimerization of the HK EnvZ is in the 0.4-10 µM range [25, 59], it is proposed that covalent attachment of the leucine zipper can stabilize the weaker HK coiled-coils in one conformation (Figure 1.6). This was first demonstrated to be an effective method to study signal transmission in a chemotaxis receptor [60] and later applied to the HKs VirA [4, 61, 62] and AgrC [11, 63]. The leucine zipper technique has been used to lock the catalytic domain of VirA in predicted kinase-on, kinase-off, and partial-kinase states and contributed to a three-state ratchet model for activation. The leucine zipper fusion strategy was applied to the AgrC kinase

domain and coupled with cysteine cross-linking to demonstrate the periodicity of the activation of AgrC [11, 63] in a mode similar to VirA kinase activation.

Leucine zipper fusions reveal a helical bundle ratchet model in VirA signal transmission VirA is a transmembrane hybrid HK that is expressed from a tumor-inducing plasmid in the plant-associated pathogen *A. tumefaciens*. VirA responds to at least four signals, including pH, temperature, and plant-derived phenolics and monosaccharides, and integrates these signals to phosphorylate the RR VirG, which activates virulence factors [64, 65]. The leucine zipper approach was applied to investigate the mechanism by which VirA can integrate multiple signals with a goal of understanding plant host-bacterial communication (Figure 1.7) [4, 61, 62].
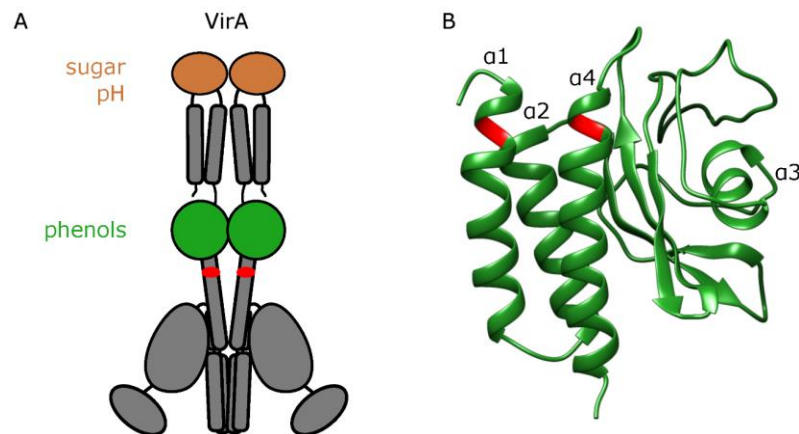
Figure 1.7: Application of the leucine zipper strategy to VirA A) The domain architecture of VirA and B) the homology model of the GAF domain of VirA compared to *Neisseria meningitdis* fRMsr [66]. Leucine zipper fusion sites are denoted in red.

The leucine zipper was fused directly to the N-terminus of either α1 or α4 within the GAF sensory domain.   At the fusion site an addition of 3 or 4 amino acids was incorporated to bias the coiled coil into a position corresponding to a 51° counterclockwise rotation or 51° clockwise rotation from the neutral position, respectively. It is important to note that the kinase domain in each leucine zipper fusion contained the mutation G665E, which exhibits higher basal kinase

activity but is still responsive to phenolic concentration [4, 61, 62, 67]. This allowed for detection of a negative impact of the leucine zipper fusion conformation upon kinase activity. The forced conformation of each fusion resulted in a distinct kinase activity measured by an *in vivo* β-galactosidase activity assay. These data contributed to a ratchet model of activation in which phenolic signal binding causes rotation within the helical bundle which positions the kinase domain in an active conformation [1, 4, 62].

It was further suggested that the rotation of the helical bundle places the phosphorylatable histidine into proximity with the ATP-binding domain, allowing phosphate transfer. To test this model, the leucine zipper fusion strategy was applied just 24 amino acids N-terminal to the phosphorylatable histidine, and the position of the histidine in each fusion was predicted. The panel of chimeras was extended to include a full heptad rotation of 7 fusion sites and the variable kinase activity in a β-galactosidase activity assay matched the prediction of the ratchet model. By comparing VirA to a protein with a solved x-ray crystal structure HK0853 [12], it was suggested that the active leucine zipper fusions correspond to a conformation in which the histidine would indeed be brought into proximity with the ATP-binding domain [4].

The leucine zipper fusion strategy was used to demonstrate the periodicity of AgrC AgrC is a homodimeric transmembrane quorum sensing HK that regulates virulence upon sensing homologous or heterologous autoinducing peptides in *S. aureus*. The linker between the sensor and kinase domain is predicted to have a helical fold [11]. A challenge in studying AgrC signal transmission *in vivo* is that the AgrC signaling cascade involves a positive feedback loop which can complicate transcriptional readouts [68]. Wang et al. used the leucine zipper fusion strategy to manipulate the conformation of this linker to study the AgrC signal transmission mechanism *in vitro* using nanometer-scale lipid bilayer discs [11, 63].

A panel of 15 leucine zipper fusions, corresponding to 2 heptad rotations, was constructed by fusing the GCN4 leucine zipper to the N-terminus of the AgrC linker, truncating one amino acid from the AgrC linker at a time. Each truncation results in a predicted 102° rotation of the helical linker per residue. An *in vitro* protein phosphorylation assay revealed that the kinase activity could be fit to a sine wave function as a function of linker length with a periodicity of 3.6 amino acids, corresponding to one turn of the helix. The activities of each leucine zipper fusion were compared to the basal, induced, and inhibited activities of full-length AgrC and equivalent activities were observed. These results indicated that AgrC transmits signals through conformational twisting of the sensor-kinase helical linker.

A cysteine cross-linking experiment of full-length AgrC resulted in characterization of the conformation of the linker in each signal-binding state. This data along with a study of AgrC homologs [63] allowed for defining the degree of rotation achieved by each state and led to a rheostat model in which each signal binding event results in a rotation in the linker and the attached kinase domain, dictating activity. This model is similar to the "ratchet model" of VirA, in that it revealed a periodic trend in which insertion of residues modulates activity between kinase active, partial kinase activity and inactivity.

This fine-tuning of the dynamic range of kinase response may be an evolutionary tactic to regulate the amplitude of HK response. More broadly we envision that the leucine zipper strategy could be used to test other modes of signal transmission such as reverse signaling [69, 70], phosphatase activity, and phosphotransfer activity. This strategy could also be applied to kinases with diverse sensory domain architectures in which helical regions are proposed to be involved with signal transmission [31]. Furthermore, designed leucine zipper fusions could be used to confer constitutive, intermediate, or null kinase activity to manipulate downstream responses.

The signal processing capabilities of tandem sensor kinases Several unannotated HKs contain two or more distinct sensory domains, raising the intriguing possibility that these HKs use Boolean-like logic to interrogate multiple environmental signals. As an example, Figure 1.8 indicates that several HKs encoded within the genome of *C. crescentus* contain two or more sensory domains in tandem. Indeed, the VirA HK processes phenolic signals and sugars in a AND gate manner that confirms the presence of two signals prior to triggering activation the VirA-VirG virulence regulon (Figure 1.2A) [4, 71]. However, a significant challenge remains in that we have poor knowledge of the identity of most HK sensory domains. The lack of knowledge about input signals prevents studying how most multi-sensor kinases processes signals.
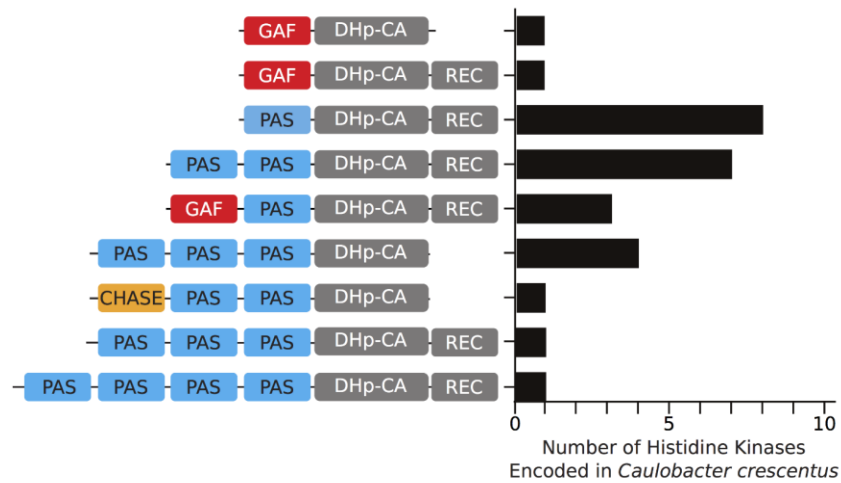
Figure 1.8: The domain architectures of all *Caulobacter crescentus* histidine kinases that contain a PAS or GAF sensory domain

To understand the large family of multi-sensor HKs, engineered synthetic tandem-sensor kinases composed of the oxygen sensing PAS domain of FixL and the blue-light sensing LOV domain of YtvA were developed (Figure 1.2B) [72]. Their designs indicated maintenance of α-helical

secondary structure in their fusions was critical for kinase functions. This synthetic tandem-sensor kinase demonstrated that independent sensory domains could regulate kinase in an additive manner. Furthermore, their studies revealed that sensory domains more proximal to the HK domain had a larger impact than the distal sensory domain. The examples of VirA and the synthetic tandem sensors reveal the capability to program advanced signal processing within the HK sensory domain. This could be commonly used in nature to ensure stringency of signaling response as highlighted in the VirA example [62], and also provides avenues to integrate and process signals for applications in synthetic biology.

1.4 Strategies to Engineer Kinase-Kinase and Kinase-Response Regulator Interactions

Regulation of multi-sensor kinases through oligomerization It has been proposed that a subset of multi-sensor domains control HK activity by toggling between dimer and tetramer states [73, 74]. The *B. subtilus* HK KinA regulates the sporulation pathways and utilizes a 4-PAS sensory domain. The input signal of KinA was not well understood but was predicted to be related to tetramerization [73, 75]. To tackle this problem, the diguanylate cyclase protein YdaM N-terminal PAS domains were fused to KinA kinase domain to promote tetramerization of to study how the sensory domain regulates KinA signaling activity [76]. The authors observed through crosslinking assays that the YdaM fusion placed KinA into a tetramer conformation that was constitutively active [74, 76]. This example illustrates that multiple sensor kinases may have the capacity to regulate oligomeric changes as a mechanism of HK activity control. Future work is needed to understand how broadly this oligomerization mechanism is used and if it is a common feature of multi-sensor HK as suggested by studies of KinA [76] and CckA [74] multi-sensor kinases.

Strategies to engineer HK heterodimerization Compared to eukaryotic signaling pathways, bacteria appear to exhibit minimal cross-talk between signaling pathways *in vivo* and *in vitro* even though the DHp/CA domains of HKs are conserved across bacteria [77]. Bacterial cell fitness is reliant on reducing unwanted cross-talk [77]. However, heterodimerization of HKs can generate more complex regulatory modes as highlighted by studies of the *P. aeruginosa* GacS and RetS HK heterodimer complex (Figure 1.9) [78, 79]. These results highlight the importance of understanding how to engineer desired HK dimerization modes in order to wire HK heterodimerization to productively integrate information from two pathways. Comparison of EnvZ and its closest HK homolog RstB revealed residues that are required for these HKs to remain homodimers or function as heterodimers. Using covariation analysis, the base of the DHp bundle was identified as the region most likely contributing to homodimerization. To test this, residues from RstB were swapped into EnvZ. After two residue mutations, the engineered EnvZ variant was no longer able to heterodimerize with wild-type EnvZ as determined by a fluorescence resonance energy transfer (FRET) competition assay, but maintained homodimerization ability [25]. A set of residues buried at the base of four-helix bundle was identified that is sufficient for regulating dimerization specificity, while leaving RR phosphotransfer specificity unperturbed (Figure 1.1A) [25].
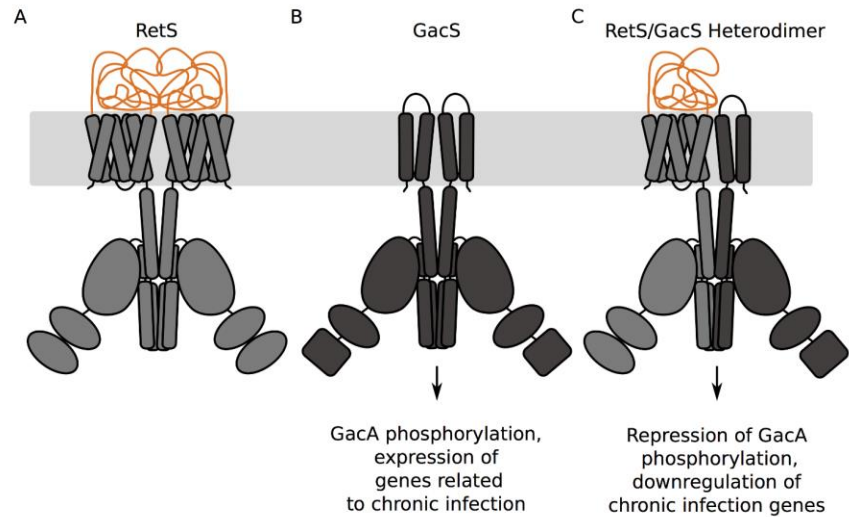
Figure 1.9: The RetS-GacS interactions dictate downstream regulation A) RetS homodimer, (B) GacS homodimer and a (C) RetS-GacS heterodimer. When GacS is a homodimer and receives input signals, GacA phosphorylation occurs and expression of genes related to chronic infection are transcribed. When RetS and GacS form a heterodimer, repression of GacA phosphorylation and downregulation of chronic infection genes occur.

The engineering of HK heterodimers may offer the potential to sense and integrate signals from each distinct sensory domain, however this remains to be explored. In addition, future work will determine the degree of HK heterodimerization specificity and the implication of this level of regulation in microbial development.

Strategies to re-wire HK and RR phosphotransfer HKs and RRs have co-evolved to exhibit specificity in phosphorylation activity in order to reduce HK-RR phosphotransfer cross-talk [80]. By rewiring HK-RR protein interaction interfaces, one can alter signaling flow from one HK to a different RR output, engineer a single HK to phosphorylate several RR outputs, or engineer the integration of many signals through many HKs that phosphotransfer to a single RR. The key interactions that modulate the phosphotransfer specificity are a suite of residues located on the solvent exposed surface of the DHp domain of the HK and the receiver domain of the

cognate RR. The key residues that determine the specificity for the DHp tend to be solvent exposed and located at the base of the four-helix bundle, as well as in the loop region (Figure 1.1A,B) [25, 26]. Skerker et al. identified residues within EnvZ that could be mutated to other HK residues (RstB, CpxA, PhoR, AtoS, and PhoQ) to confer phosphotransfer specificity to their RRs [26]. This was accomplished by identifying residues that co-vary between HKs and RRs [81, 82], and was consistent with the interaction interface observed with several HK-RR co-crystal structures [10, 83, 84]. The entire loop regions of each kinase were substituted into EnvZ, resulting in EnvZ variants that recognize and phosphorylate the corresponding RR targets [26].

RR specificity residues have been identified through covariation analysis and can be applied to specific HKs through secondary structure alignment of DHp domains [26]. By applying these HK-RR interface mutations or switching the entire DHp loop region, multiple phosphorylation partners could be under the control of a single HK. This re-wiring could also generate new connectivity between signaling input and outputs. This also provides an alternative approach to the sensor-HK chimeras that would allow one to retain much of the native HK function and just alter the residues to direct phosphotransfer to a desired RR.

Engineering assembly and activation of HK signaling Whitaker et al. took inspiration from eukaryotic signaling systems, which rely on scaffolds to colocalize and activate kinases, to design a modular prokaryotic system for synthetic biology [27, 85]. The downstream signaling of a chimeric HK [86] was re-wired to activate non-cognate RRs [87] in a scaffold-dependent manner (Figure 1.10). It has been demonstrated that HKs will transfer phosphate to non-cognate RRs with an increased effective concentration through direct tethering [88, 89]. Whitaker et al. sought to increase the local concentration of the HK and its downstream RRs by designing scaffolds with two protein-protein interaction domains, the SH3 peptide and leucine zipper, which recruited the

20

SH3-tagged HK and the leucine zipper-tagged RR, respectively. The advantage of scaffold-dependent co-localization is that the RR specificity of the HK was successfully adjusted by induction levels of the scaffold as determined by a fluorescent gene expression reporter assay. However, the system was sensitive to the expression level of each component.

The system was further engineered so that the scaffold is necessary not only for colocalization of the HK and RR, but also for HK activation. The kinase domain was engineered with an SH3 domain and an internal SH3 peptide such that the SH3 domain would block phosphotransfer to the RR until the scaffold SH3 peptide would compete for SH3 binding and activate the HK (Figure 1.10). Using the same fluorescent gene expression reporter, it was demonstrated that the scaffold was effective in colocalizing and activating two-component system signaling.
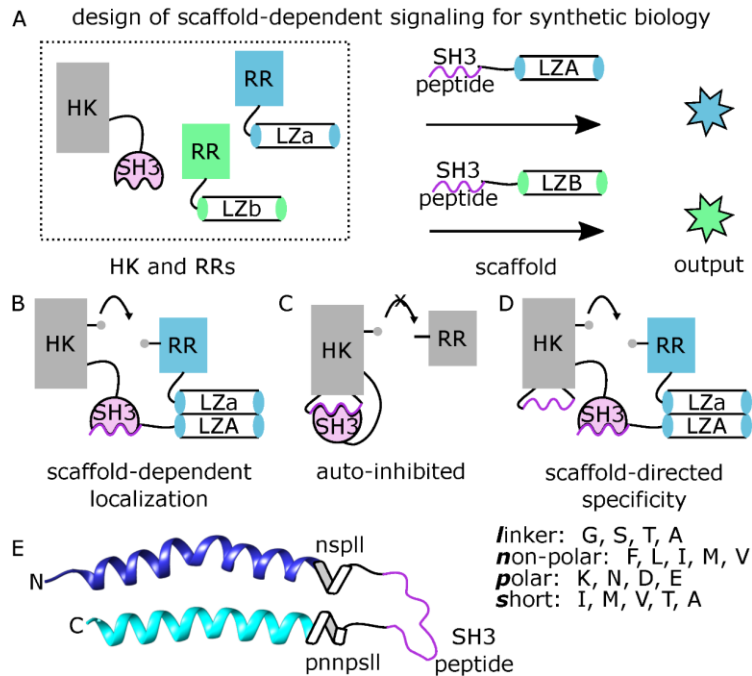
Figure 1.10: The design of scaffold-dependent signaling for HK synthetic biology (A) The SH3-bound HK and LZ-bound RRs are expressed in the cell. Induction of scaffold dictates the downstream activity of the HK. B) Scaffold-

dependent localization increases the effective concentration of the RR near the HK. C) The HK can be engineered with an autoinhibitory interaction. D) Induction of the scaffold co-localizes the components and relieves the autoinhibitory interaction to activate the signaling pathway. E) The design of the autoinhibitory interaction in the DHp of the chimeric HK TAZ1 (PDB: 5B1N [9]).

Insertion of the SH3 peptide into the kinase structure without affecting activity presented an interesting kinase engineering challenge. The turn between the helices in the DHp was chosen as the site for insertion because of its proximity to the RR binding site. However, direct insertion or the use of flexible linkers into this region did not yield an active kinase. A library of linkers, which mimicked the seven amino acids at the end of the DHp bundle, was created to extend the helical structure (Figure 1.10E). Additionally, two flexible amino acids were placed between the helical linker and the SH3 peptide at either end. Variants from the library were first screened for their ability to phosphorylate RR, and then for their conditional activation only in the presence of scaffold. The most promising library candidate was tested to confirm autoinhibition and scaffold-dependent activation. The modular signaling system designed here couples the roles of phosphotransfer and RR specificity and can therefore be extended to other two-component systems.

1.5 Conclusions and Outlook

The engineering strategies discussed here have contributed to an understanding of how bacteria use two-component systems to respond to their environment. However, several challenges remain in our capability to predictably engineer HK function. Most notable is poor access to diverse well-characterized sensory domains and the incapability to predict sensory

domain function based on primary sequence. Therefore further characterization of sensory domain structure and function is needed to understand the general design rules for how signals are perceived and distinguished. This includes investigation of how multi-sensor domains integrate multiple signals to regulate HK activity. A second major HK engineering opportunity is the engineering allosteric regulation through kinase-kinase interactions. Indeed, natural histidine kinase pairs suggest this as a mode of histidine kinase regulation, such as the *P. aeruginosa* RetS-GacS pair [79] and the *C. crescentus* DivL-CckA pair [21, 69, 90]. Further application of these HK engineering strategies and addressing these opportunities will enhance our understanding of bacterial impact upon human health and disease, agriculture, and environmental safety.

In this dissertation I demonstrate the use several of these histidine kinase engineering approaches, coupled with other standard molecular biology techniques, to probe a multi-kinase network in *C. crescentus*. In Chapter 2, I apply the leucine zipper approach to a novel pseudokinase modulator, DivL, to map out signal flow by measuring phenotypic changes *in vivo*. In Chapter 3, I utilize a FRET kinase sensor developed in our lab to identify the nature of the interaction between DivL and CckA. In Chapter 4, I describe scaffold-scaffold interactions that are required to orchestrate signaling and asymmetric division. We further use a chimeric reporter protein to report on a scaffold-kinase interaction that regulates the cell cycle.

2.0 Synthetic Control of Signal Flow Within a Bacterial Multi-Kinase Network

This chapter was written in collaboration with Elayna M. Silfani, Amanda Kasumu, Grace Rong, Victor So, and W. Seth Childers. Reprinted with permission from Kowallis, K. A., Silfani, E. M., Kasumu, A., Rong, G., So, V., and Childers, W. S. (2020) Synthetic Control of Signal Flow Within a Bacterial Multi-Kinase Network, ACS Synthetic Biology. Copyright (2020) American Chemical Society.

2.1 Introduction

Bacterial signaling systems are often arranged as parallel signaling arrays that include a set of sensor histidine kinases (HKs) that strictly regulate the phosphorylation of their own corresponding response regulator (RR) (Figure 2.1A)[91]. These signaling arrays offer orthogonal connectivity of single signals to single output responses. In contrast, productive cross-talk within multi-kinase networks (MKNs) appears to integrate many signals to regulate complex developmental processes such as sporulation[92], biofilm formation[93], quorum sensing[94], asymmetric cell division[69] and multi-cellular fruiting bodies[95]. Studies of these developmental networks point towards the importance of kinase-kinase interactions[21, 69, 79, 90, 96-98]. The current model of linear kinase signaling does not accommodate the possibility for kinases to interact in a reversed or lateral manner. Recent examples of interacting histidine kinases[93, 99] suggest allosteric mechanisms are in play, but the precise biophysical events remain unclear.
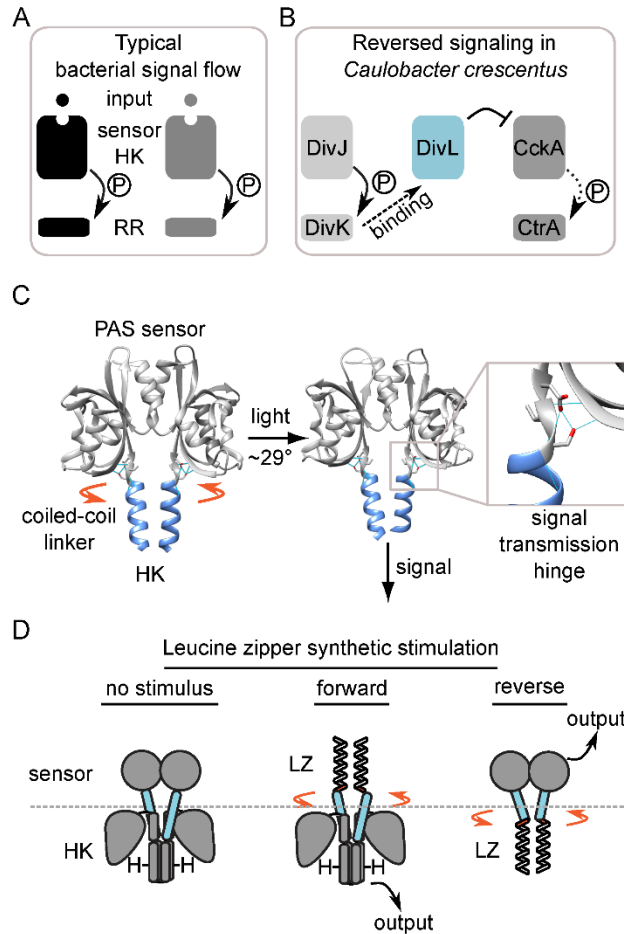
Figure 2.1: *Caulobacter crescentus* **uses the pseudokinase DivL to promote signaling cross-talk through reverse signaling** (A) In typical bacterial signal flow, orthogonal sensor histidine kinases receive a signal in the sensor domain, triggering auto-phosphorylation. The phosphate group is transferred to a corresponding response regulator, which elicits a distinct cellular response. (B) In the DivL pathway, the typical histidine kinase DivJ phosphorylates its response regulator DivK. DivL then recognizes phosphorylated DivK through a specific binding event and allosterically modulates the typical hybrid histidine kinase CckA, which prompts a cell-cycle regulating phosphorelay that regulates the master regulator CtrA[69, 100]. (C) Crystal structures of the light-responsive PpSB1-LOV protein in the dark and light-excited states[101] (PDB ID: 5J3Wand 5J4E) with the sensor in gray and the coiled-coil linker in blue reveals a ~29° rotation and translation in the coiled-coil linker. A magnified view shows the conserved signal transmission hinge motif residues (DVS) and the hydrogen bonds formed by this motif in light blue. (D) A cartoon of a typical histidine kinase and the strategy to synthetically stimulate forward signaling and reverse signaling (this study).

A well-studied bacterial MKN regulates asymmetric cell division in *Caulobacter crescentus* by regulating genes associated with division, replication, and motility (Figure 2.1B)[102-105]. Signaling cross-talk amongst four HKs that regulate phosphorylation of the cell-cycle master regulator CtrA[105] is achieved by an essential bacterial pseudokinase DivL. Past work has led to a reverse signaling model in which DivL's kinase domain has been repurposed as a sensor of the phosphorylation state of its RR DivK[69] and its sensory domain has been repurposed as an allosteric modulator of the downstream HK CckA[106, 107]. DivL thus couples the pathway that controls DivK phosphorylation with the CckA cell-cycle pathway (Figure 2.1B)[100, 108]. Neither DivK~P binding nor CckA regulation require DivL phosphorylation[106, 108, 109], nor does DivL exhibit kinase or phosphatase functions towards DivK[69], and thus the mechanism by which DivK~P recognition by DivL impacts the CckA pathway remains unclear.

Typical histidine kinases transmit signals through a conserved coiled-coil linker that directly connects the sensory domain to the four-helix bundle of the HK domain. Past structural analyses of the sensor-HK linker have indicated that the coiled-coil interface of these helices changes in response to signal recognition within the PAS sensory domains and this allosterically alters the downstream kinase helical bundle conformation (Figure 2.1C)[56, 110-114]. A set of conserved D-(A/I/V)-(T/S)-E residues at the C-terminal junction of the PAS domain and this coiled-coil linker forms a network of hydrogen bonds with the PAS domain fold (Figure 2.1C inset)[20, 115]. This hinge motif couples the conformational change that occurs in the PAS domain upon signal detection to the conformational re-arrangement that allows HK autophosphorylation[7, 116, 117]. We hypothesize that the long-range conformational changes that dictate canonical HK activity maintain a role in the reverse signaling mechanism utilized by the pseudokinase DivL[118]. In this case, DivK~P binds the catalytically dead DivL kinase domain which induces a bending or

twisting in the sensory helix. This conformational change is transferred to the repurposed sensor through the rigid signal transmission motif. However, we currently lack experimental strategies to directly test if reverse signaling occurs and if it is critical within a cellular context.

In bacterial signaling networks coiled-coils and helical bundles commonly serve as allosteric switches to propagate signals between domains[56, 110]. A protein engineering strategy to synthetically mimic forward signal response was implemented in the chemotaxis receptor Tar[60] and the HKs VirA[4, 61, 62] and AgrC[11, 63] by removing the sensory domain and covalently fusing a leucine zipper, which forms a coiled-coil with a strong bias for one interface, to the sensor helix coiled-coils (Figure 2.1D). These studies demonstrated that each engineered leucine zipper-sensor helix fusion induced the native helix into a distinct conformation, locking the catalytic domain in a distinct activity state[58]. This approach demonstrated that coiled-coils involved in allostery between two protein domains could be directly stimulated by fusion to a high affinity leucine zipper. To test our hypothesis that DivL utilizes its coiled-coil linker in a similar but reverse manner as the kinases in these studies, we removed the kinase domain and covalently attached the leucine zipper to the C-terminal end of the sensor helix coiled coils that extends from DivL's sensory domain (Figure 2.1D). Combining these protein engineering approaches to stimulate and disrupt reverse signal transmission allowed us to interrogate the DivL reverse signaling model *in vivo* and can be applied to map signaling flow within other complex bacterial signaling networks.

In order to apply the DivL synthetic stimulation strategy to learn about the cell-cycle MKN in *C. crescentus*, we needed to identify phenotypic *in vivo* readouts of stimulation. The *C. crescentus* cell-cycle MKN coordinates asymmetric division by regulating the activity of the master regulator CtrA which controls replication, division, and motility[119]. When a sessile stalked cell divides, the new cell pole is remodeled to form an incipient swarmer cell and the division

results in two distinct daughter cells (Figure 2.2A). DivL must modulate the active kinase CckA at the correct time and location for this process to occur correctly[106, 108, 120]. DivL localizes at the new cell pole through binding interactions with the scaffolds PodJ[121] and PopZ[122]. DivL localization to the new cell pole is correlated with CckA phosphorylation[21], however activation of the CtrA pathway eventually results in the loss of DivL's cell pole localization[90, 120]. To evaluate the effects of DivL synthetic simulation, we employed two distinct assays. First, a commonly used swarm assay was chosen for its sensitivity to CtrA-regulated motility, division and replication defects[123]. Secondly, given that DivL undergoes cell-cycle dependent changes in localization pattern[21, 90], we examined the possibility that signal flow through DivL controls its subcellular localization by visualizing fluorescently labelled DivL constructs.

2.2 Results and Discussion

DivL's sensor helix is required to impact swarm size Utilizing the leucine zipper fusion approach to study this MKN requires a minimal functional DivL construct and a coiled-coil fusion site within the sensor helix. In order to assess the importance of DivL's sensor helix and build a minimal functional construct, we referred to previous studies that demonstrated that a large portion of the DivL histidine kinase domain (HK), residues 566-769[124], is not essential for cell viability[109, 124]. The remaining minimal functional DivL maintains the multi-Per–Arnt–Sim (PAS) sensory domain, the sensor helix, and about one-half of the DivK~P binding site (Figure 2.2B-C). It is possible that the DivL(1-565) variant maintains a sufficient protein interaction interface to interact with DivK~P[69], so we designed two C-terminal truncations to remove the entire HK and the sensor helix. DivL 1-537 (DivL-537) lacks the entire HK and retains most of the sensor helix and DivL

28

1-518 (DivL-518), only retains the multi-PAS sensory domain (Figure 2.2B-C). We initially confirmed induced over-expression of each variant via Western blot analysis (Figure 2.3). Each variant was expressed in the wild-type background containing the endogenous full-length copy of DivL. Compared to a strain replicating an empty vector, over-expression of wild-type DivL reduced swarm size to $47 \pm 3\%$ (Figure 2.2D). In contrast, over-expression of DivL-518 resulted in a loss of the small swarm size phenotype characteristic of DivL over-expression (Figure 2.2D). While the endogenous copy of DivL may rescue more severe swarm phenotypes, when comparing to over-expression of wild-type DivL these results (Figure 2.2D) indicate that both the sensory domain and sensor helix are critical for DivL's over-expression impact on cell-cycle progression. Moreover, since the DivK~P binding site can be removed, it is non-essential for this function.
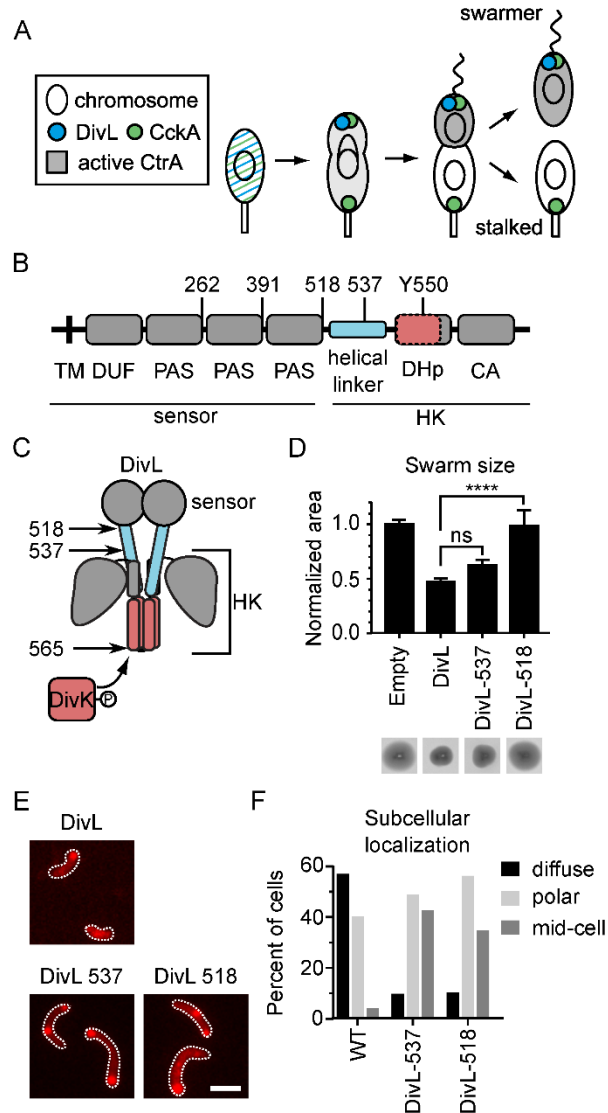
Figure 2.2: DivL's sensor helix is required for regulation of swarm size and accumulation at the cell poles (A) Cartoon depicting the *C. crescentus* life cycle. Localization of DivL, CckA, and active CtrA are dynamic and tightly regulated[21, 90, 104, 106, 108, 120, 125]. (B) Domain architecture model of a DivL monomer with the helical linker that connects the multi-PAS sensor and the HK shaded blue and the DivK binding site shaded red. (C) A structural representation of the domain architecture shown in B. (D) Quantification of the motility assay of *C. crescentus* strains over-expressing DivL-M2 catalytic domain truncations. Representative swarm images are show beneath the corresponding bar. *C. crescentus* were stabbed into 0.3% PYE agar supplemented with 0.3% xylose and incubated at 28 ℃ for 3 days. Error bars represent SD (N=3). Significance was determined with a Dunnett's multiple comparisons test by comparing the mean area of each strain to the mean area of DivL-WT (ns: P>0.05, *: $P \leq 0.05$, **: $P \leq 0.01$, ***: $P \leq 0.001$). (E)

30

Fluorescence microscopy to visualize the subcellular localization of DivL-mCherry DivK binding domain truncations expressed in *C. crescentus*. The variants were induced from the chromosomal xylose promoter in M2G supplemented with 0.03% xylose for 4 hours. Scale bar denotes 2 µm. (F) Quantification of the number of cells with diffuse, polar, or mid-cell localization of cells. N>101 cells.
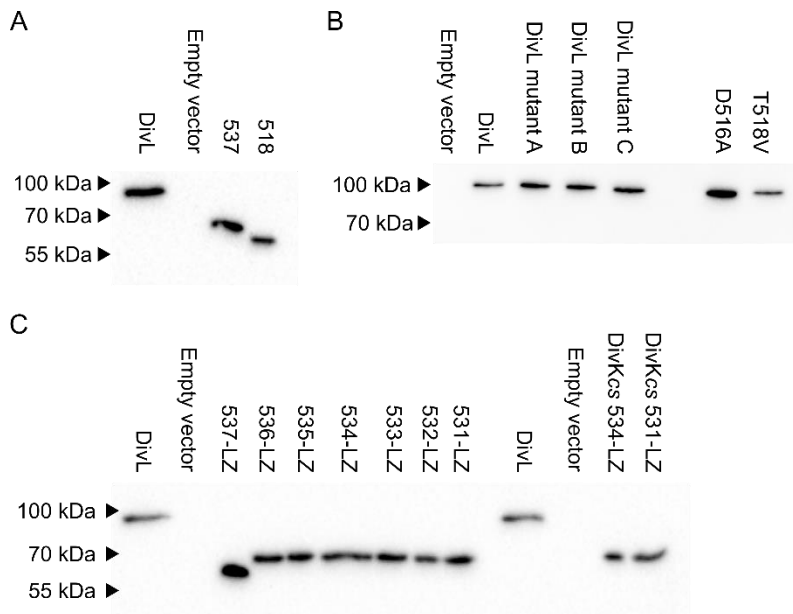
Figure 2.3: Western blot analysis of overexpression of DivL variants Western blots were performed to confirm overexpression of DivL variants in the strains used in the swarm assays. DivL mutants A-C in panel B were not used in the experiments for this manuscript.

DivL's sensory domain and C-terminus regulate foci accumulation at the poles

Studies have demonstrated the importance of subcellular localization to DivL's role in asymmetric cell division in *Caulobacter crescentus*[106, 108, 120]. DivL undergoes cell-cycle dependent changes in subcellular localization pattern from diffuse in swarmer cells to localized at one or both cell poles in pre-divisional cells. Consistent with past studies, we observed that for wild-type DivL about 40% of cells contained DivL accumulated at the cell poles, and about 55% of cells exhibited a diffuse DivL localization pattern when expressed in the wild-type background (Figure 2.2E-F). In

comparison, we observed that DivL-537 and DivL-518 exhibited similar levels of cell pole accumulation. However, for DivL-537 and DivL-518 there was a reduction in the cells displaying diffuse localization pattern and a corresponding increase in cells exhibiting mid-cell localized foci (Figure 2.2E-F). These results indicate that the sensor can form foci at the cell pole, and that the HK domain plays a role in regulating subcellular positioning or preventing mid-cell localized foci. This observation is consistent with earlier indications that the C-terminus of DivL is involved in DivL's new cell pole localization[21, 122, 126]. Moreover, we observed that the linker composition between the HK domain and the fluorescent protein fusion impacted cell pole binding (Figure 2.4). Monopolar DivL variants were frequently observed at the old cell pole but did not substantially impact fitness when presented as a sole copy (Figure 2.4). These studies of the C-terminal fusion linker indicate that DivL's C-terminal residues strongly influence new cell pole positioning. Collectively, these results in Figure 2.2 indicate that the sensory domain (DivL-518) is sufficient for cell pole accumulation in the wild-type background containing the endogenous copy of DivL.
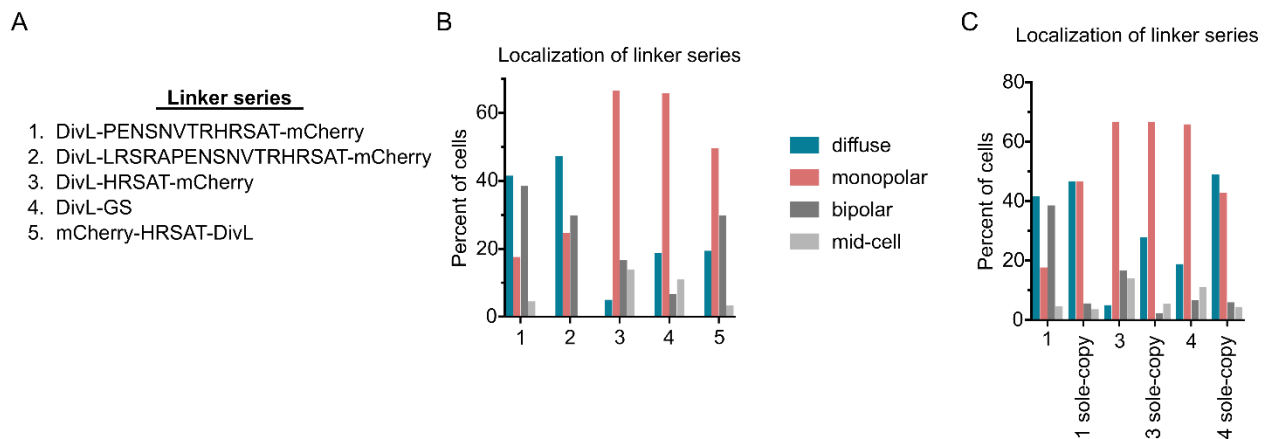
Figure 2.4: The DivL fluorescent protein affects subcellular localization (A) The designs and sequences of the mCherry and DivL linker series. (B) Fluorescence microscopy was used to visualize the subcellular localization of DivL-mCherry fusions expressed in *C. crescentus*. The variants were induced from the chromosomal xylose promoter in M2G supplemented with 0.03% xylose for 4 hours. The localization pattern differs depending on the design and

linker sequences. (C) The variants were expressed in a *divL* deletion strain and the localization patterns were analyzed. Upon deletion of wild-type DivL, more cells exhibited diffuse localization in each case, but the localization still varied based upon the design and linker sequences of the fusions. Monopolar foci were almost exclusively found at the stalked pole in all strains. N>115 cells for all samples.

DivL utilizes a conserved signal transmission motif Because truncating the sensor helix had an effect in the swarm assay, we analyzed this region for conservation amongst DivL alpha-proteobacterial homologs (Figure 2.5). By mapping the conserved residues onto the DivL HK crystal structure[69], we found high conservation at the coiled-coil interface. This conservation suggests that the helix may play a conserved role in signal transduction between the HK and sensory domains. The alignment also revealed a conserved PAS signal transmission motif at residues 516-519 that may be critical for transmission from the PAS sensory domain to the HK domain (Figure 2.6A-B)[20, 31]. Past studies of the blue light sensitive YF1 kinase have shown that a motif of conserved D-(A/I/V)-(T/S)-E residues at the junction couples the conformational change that occurs in the PAS domain upon signal detection to the conformational re-arrangement that allows HK autophosphorylation[7, 116, 117]. We incorporated mutations that disrupt functionality of the PAS signal transmission motif and examined their impact upon DivL over-expression mediated swarm size reduction in the wild-type background. Over-expression of wild-type DivL, confirmed by Western blot analysis (Figure 2.3), reduced swarm sizes to 49 ± 4% of the empty vector control (Figure 2.6C, 2.7). In contrast over-expression of the DivL D516A and T518V mutants partially recovered the wild-type swarm phenotype with milder reductions in swarm size of 76 ± 4% and 67 ± 6%, respectively. We also observed that signal transmission motif mutations had a mild impact upon DivL's subcellular localization (Figure 2.8). Overall these data indicate that a functional DivL signal transmission motif upstream of the sensor helix plays a role in the

33

reduction of swarm size upon DivL over-expression. This provides evidence that signal transmission between the kinase and sensory domains is needed to reduce swarm size upon DivL over-expression. Mutations to the remaining two signal transmission motifs within the DivL multi-PAS sensor (Figure 2.2B) may reveal how signals are propagated within the sensor in future studies.
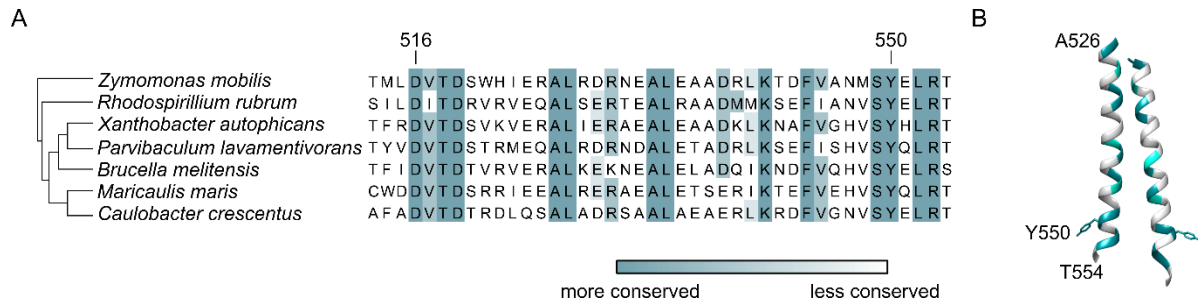
Figure 2.5: The DivL sensory linker is conserved at the coiled-coil interface (A) Alignment of the sensory helix of DivL homologs in the alpha-proteobacteria. More highly conserved residues are depicted by darker shades. The alignment maintains the tyrosine in the phosphorylatable position (Y550 in C. crescentus) and shows that the signal transmission motif DVT or DIT and coiled-coil interfaces are conserved across the class (D516-T518 in *C. crescentus*). (B) The structure of the sensory helix-DHp of C. crescentus DivL (PDB: 4Q20) [69] from residues A526-T554. The structure of the tyrosine in the phosphorylatable position Y550 is shown. Conservation is depicted in colors according to the alignment in Figure 2.5A.
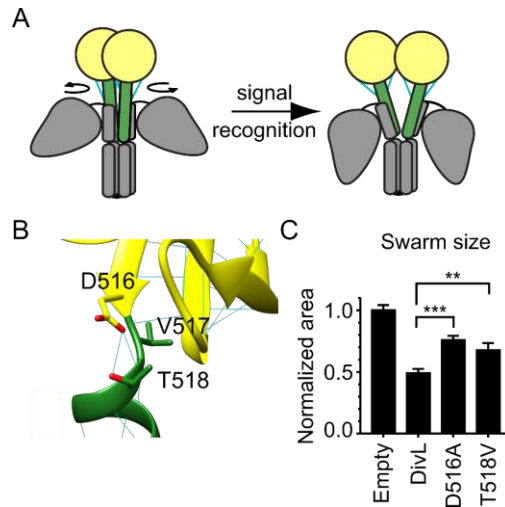
Figure 2.6: The conserved signal transmission motif is critical for DivL's regulation of swarm size (A) Cartoon of the conformational change that occurs at the signal transmission motif of sensor kinases. The signal transmission motif between the sensor (yellow) and the coiled-coil linker (green) contains residues that form several hydrogen bonds (blue) and serve as a conformational switch. (B) Homology model of DivL compared to YF1 (PDB ID: 4GCZ-A)[7] (C) Quantification of the motility assay of *C. crescentus* strains expressing DivL-M2 signal transmission motif mutations. *C. crescentus* were stabbed into 0.3% PYE agar supplemented with 0.3% xylose and incubated at 28 ℃ for 3 days. Error bars represent SD (N=3). Significance was determined with a Dunnett's multiple comparisons test by comparing the mean area of each strain to the mean area of DivL-WT (ns: P>0.05, *: P ≤ 0.05, **: P ≤ 0.01, ***: P ≤ 0.001).
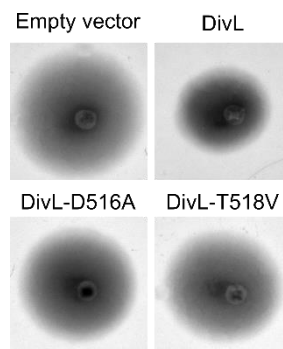
Figure 2.7: The conserved signal transmission motif is critical for DivL swarm activity Motility assay of C. crescentus strains expressing DivL-M2 point mutations to the signal transmission motif. Swarm areas are quantified in Figure 2.6C.
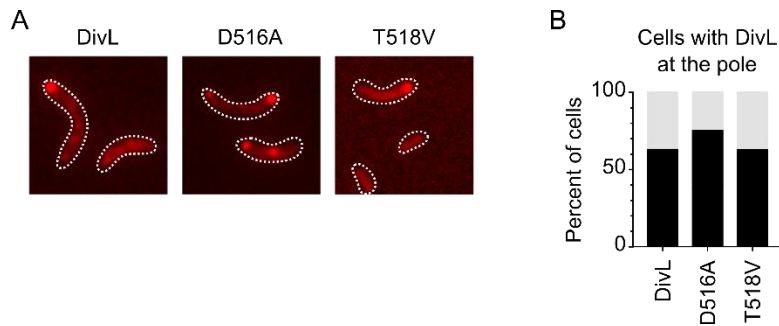
Figure 2.8: A DivL signal transmission motif mutations have a mild effect on subcellular localization (A) Fluorescence microscopy to visualize the subcellular localization of the DivL-mCherry signal transmission motif mutants expressed in *C. crescentus*. The variants were induced from the chromosomal xylose promoter in M2G supplemented with 0.03% xylose for 4 hours. (B) Quantification of the percent of cells with the DivL variants localized at the cell pole. N>110 for all samples.

Design of leucine zipper fusions strategy to synthetically trigger reverse signaling Past studies have demonstrated that the fusion of a high affinity leucine zipper to the coiled-coil sensor helix can stabilize the kinase domain into an active, neutral, or inactive conformation (Figure 2.9A)[4, 11, 61-63]. The fusion site of the rigid leucine zipper to the sensor helix of an HK dictates its coiled-coil interface, and the addition or removal of each residue results in a downstream helix rotation of 102°. We hypothesized that the leucine zipper fused to the C-terminus of the sensor helix could similarly lock DivL's multi-PAS sensor effector domain into distinct conformations that have varied impact upon the CtrA-mediated swarm size phenotypes and DivL's subcellular localization pattern (Figure 2.9A). We designed a series of DivL-LZ zipper fusions starting with DivL-537 as the core construct (Figure 2.9B) due to its moderate activity in the swarm assay (Figure 2.2C-D) and its ability to form foci (Figure 2.2E-F).
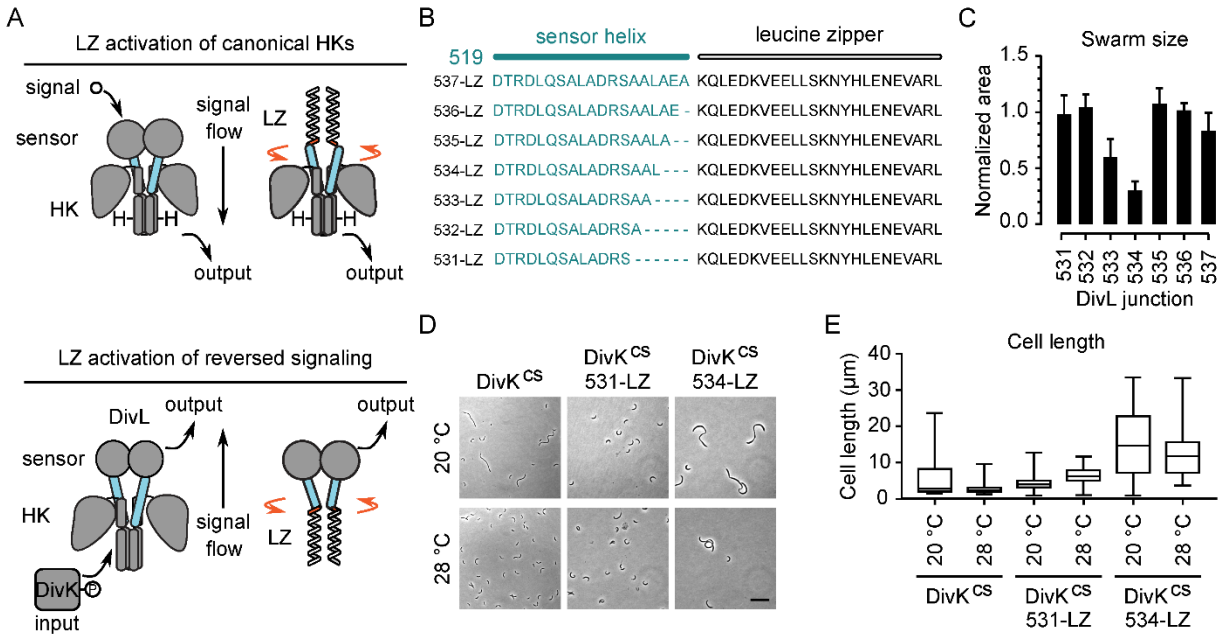
Figure 2.9: The leucine zipper fusion method was utilized to stimulate reverse signaling conformations and observe their effect on the cell cycle (A) A schematic of the leucine zipper fusion method as employed in previous studies of canonical histidine kinases[4, 11, 61-63] and how it is applied in this study to modulate DivL in reverse. (B) The sequences of the DivL-leucine zipper fusions used in this study, where each covalent fusion attached the GCN4 coiled-coil to the C-terminus of the PAS sensory helix. (C) Quantification of the motility assay of *C. crescentus* strains expressing DivL-M2 leucine zipper fusions. *C. crescentus* were stabbed into 0.3% PYE agar supplemented with 0.3% xylose and incubated at 28 ºC for 3 days. Error bars represent SD (n=3). (D) Phase microscopy to visualize the cell phenotypes of DivL leucine zipper fusions expressed in the DivK^CS strain. Strains were grown overnight in PYE medium and diluted in PYE supplemented with 0.03% xylose to induce over-expression. Cells were grown again overnight at 28 or 20 °C. Scale bar denotes 10 µm. (E) Quantification of cell lengths for each condition. The center line is the median and the box extends to the 25th and 75th percentiles. The whiskers lie at the minimum and maximum values. N>18 cells.

Leucine zipper-induced conformational changes periodically modulate cell cycle activity Upon over-expression of each of the DivL-LZ fusions in wild-type *C. crescentus,* confirmed by Western blot (Figure 2.3), we observed that the swarm area changed periodically

from 30-108% of wild-type as a function of the DivL linker length (Figure 2.9C, 2.10). This hallmark pattern indicates that DivL activity changes as the sensor helix is rotated, and that a specific coiled-coil interface induces a DivL sensor conformation which mediates swarm size reduction. In contrast, other coiled-coil interfaces have dampened or no impact on swarm size. Indeed, helical wheel analysis of the DivL-LZ chimeras indicate that DivL-534-LZ positions conserved leucine residues at the hydrophobic coil-coil interface (Figure 2.11). Meanwhile, other non-functional variants such as and DivL-536-LZ positions residues unfavorably for a coiled-coil conformation with conserved residues on the coiled-coil outer surface and negatively charged residues at the coil-coil interface (Figure 2.11). Remarkably, the synthetic leucine zipper activation strategy indicates that certain sensor helix conformations can signal in reverse to modulate DivL's *in vivo* regulatory functions.
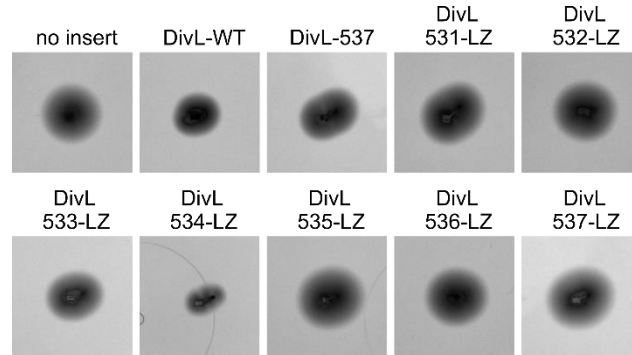
Figure 2.10: The leucine zipper fusion synthetically modulates the effect of DivL on the cell cycle Motility assay of C. crescentus strains expressing DivL-M2 leucine zipper fusions. Swarm areas are quantified in Figure 2.9C.

519- D T R D L Q S A L A D R S A A L A E A E -537

more conserved   less conserved

DivL-537-LZ

DivL-536-LZ   DivL-535-LZ

DivL-534-LZ   DivL-533-LZ

DivL-532-LZ   DivL-531-LZ
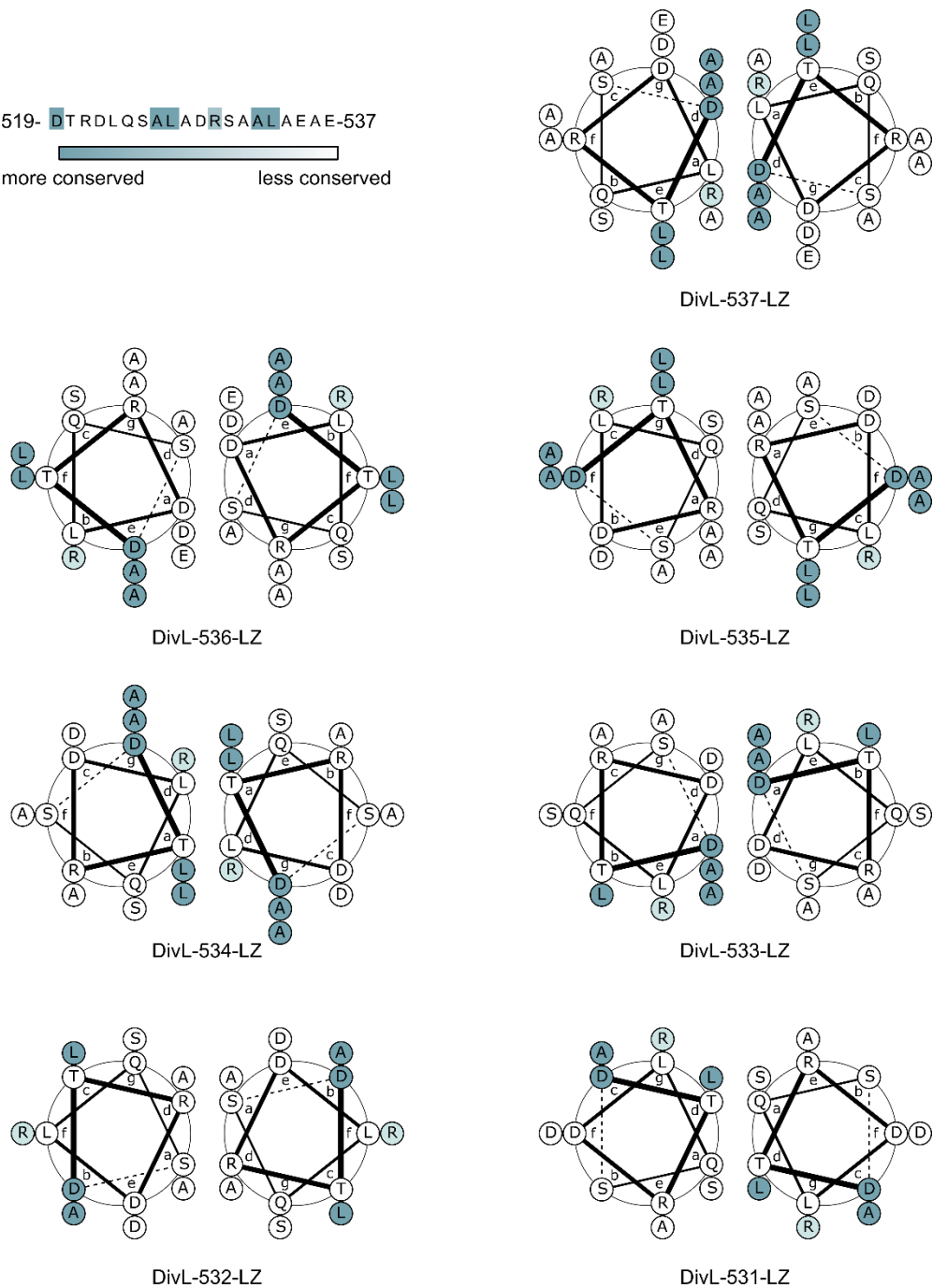
Figure 2.11: Helical wheel configuration of the sensor helix in each of the DivL-LZ fusions The amino acid sequence of the sensor helix starting at DivL-519 is arranged into a heptad configuration such that the leucine zipper fusion site is in the "b" position. Heptad wheel images were produced using DrawCoil 1.0 [127].

Due to the distinct activity of each of the DivL-LZ fusions in the swarm assay, we hypothesized that select fusions may mimic the DivL-DivK~P binding conformation. Such a variant would recover the phenotype that results when DivL is unable to bind DivK~P. We used a DivK cold-sensitive (DivK[cs]) genetic strain[123, 128, 129] in which DivK D90G exhibits decreased binding to DivL[90]. Growth of the DivK[cs] strain at 20 °C resulted in significantly longer cells, with 15% of cells longer than 10 µm, than at the permissive temperature 28 °C, with no cells longer than 10 µm (Figure 2.9D-E), as previously reported[128, 129]. Interestingly, we were unable to isolate DivK[cs] strains overexpressing DivL-WT and most of the DivL-LZ variant did not grow at 20 °C. Previous work from Tsokos and co-workers demonstrated that DivK[cs] is toxic to cells at cold temperatures due to loss of DivL-DivK~P binding[90]. Therefore, we suspect that over-expression of DivL in a strain in which DivK~P can no longer bind to DivL leads to increased CtrA pathway activation and complete loss of cell viability. Furthermore, our inability to culture select DivL-LZ variants suggest that the zipper-induced conformations are similarly toxic to cells. We did, however, isolate two DivL-LZ fusions: DivL-531-LZ and DivL-534-LZ. Supplementing the DivK[cs] strain with DivL-531-LZ resulted in fewer than 1% of cells with lengths longer than 10 µm at 20 °C (Figure 2.9D-E). In contrast, supplementing the DivK[cs] strain with DivL-534-LZ caused severe cell division phenotypes (63% of cells longer than 10 µm at 20 °C and 56% of cells longer than 10 µm at 28 °C) at both temperatures (Figure 2.9D-E). The DivL-531-LZ variant was able to rescue the DivK[cs] phenotype under cold temperature conditions, while the DivL-534-LZ variant induced a more severe phenotype. Interestingly, we observed that DivL-531-LZ was functional in the DivK[cs] background, while yielding no impact upon swarm size in the wild-type background (Figure 2.9C, 2.10). This suggests that dynamic feedback regulation mediated through DivK, in the wild-type strain, may be able to accommodate the functional impact of DivL-531-LZ in the

wild-type background. Overall, these results suggest that DivL-531-LZ adopts a sensory domain conformation that is similar to the DivL-DivK~P binding conformation to enable rescue of the cell filamentation defect. However, DivL-534-LZ may adopt an alternative sensory domain conformation that interacts with CckA in a manner similar to the free form of DivL that dominates and over-activates the CckA pathway in the DivKcs strain.

Leucine zipper-induced conformational changes periodically modulate DivL localization DivL undergoes cell-cycle dependent changes in subcellular localization pattern from diffuse in swarmer cells to localized at one or both cell poles in pre-divisional cells[106, 108]. DivL accumulates at the cell poles through direct binding interactions with two scaffolding proteins: PodJ[121] and PopZ[122]. However, the CtrA pathway activation indirectly negatively regulates DivL's localization at the cell poles[108, 120] through proteolytic regulation of the scaffolding protein PodJ[121]. Therefore, DivL's localization is controlled by both binding interactions with its cell pole localization factors and CtrA pathway activity. Given that we observed that removal of the HK domain impacts DivL's subcellular pattern (Figure 2.2E-F), we analyzed if synthetic stimulation of reverse signaling in the DivL-LZ chimeras could alter DivL's localization pattern in *C. crescentus* (Figure 2.12A-B). Strikingly, a periodic trend of cell pole accumulation emerged as a function of the DivL linker length (Figure 2.12A-B). Our analysis of DivL-518, which contains only the sensory domain and lacks the entire sensor helix and can accumulate at the cell poles (Figure 2.2E-F), indicates that the gradual truncation is not resulting in the loss of a protein binding site that is critical for localization. Rather, the periodic trend suggests that conformational changes mediated by the sensor-HK linker regulate DivL's subcellular localization pattern. These changes in DivL's localization could result from direct modulation of DivL's binding to cell-pole localized scaffold or this effect could occur indirectly through a protein that is regulated by the CckA

41

signaling pathway to control DivL accumulation at the cell pole. Notably, the DivL-LZ series does not exert the same impact upon swarm activity (Figure 2.9C, 2.10) and localization (Figure 2.12). The differences may arise due the two distinct mechanisms regulating DivL localization: direct binding interactions and negative feedback control via the CckA signaling pathway. For example, DivL-534-LZ exhibits small swarm size (Figure 2.9C) and loss of localization (Figure 2.12A-B). Therefore, we speculate DivL-534-LZ may have lost subcellular accumulation due to upregulation of the CtrA signaling pathway as indicated by its capacity to rescue the DivK^{cs} phenotype (Figure 2.9D-E). In contrast, DivL-532-LZ and DivL-535-LZ both exerted no reduction in swarm size (Figure 2.9C, 2.10) however have lost accumulation capabilities at the cell poles (Figure 2.12A-B). These variants may have lost affinity for cell pole scaffold directly, while having no direct impact upon CckA signaling.
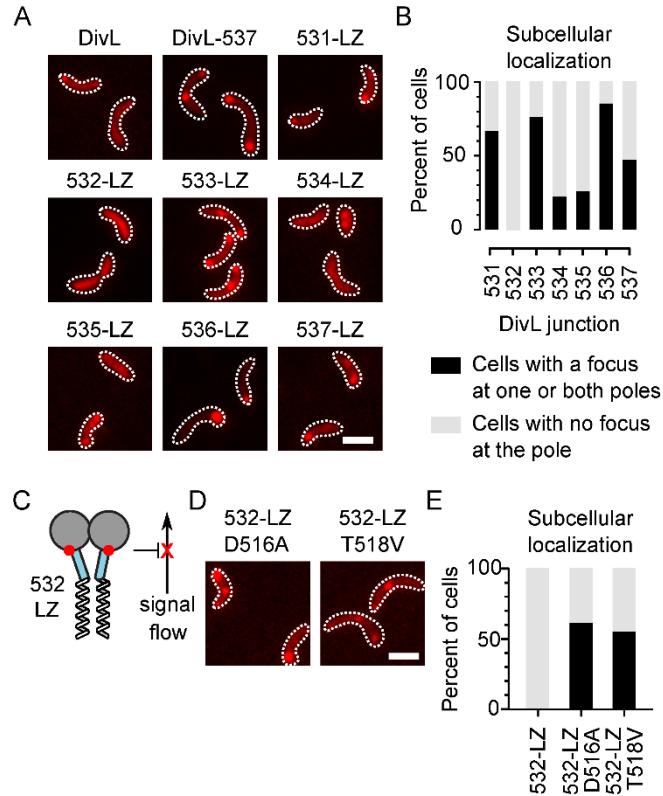
Figure 2.12: Synthetic stimulation and disruption of DivL localization mediated by leucine zipper fusion strategy and PAS sensor transmission motif mutations (A) Fluorescence microscopy to visualize the subcellular localization of DivL-mCherry leucine zipper fusions expressed in *C. crescentus*. The variants were induced from the chromosomal xylose promoter in M2G supplemented with 0.03% xylose for 4 hours. Scale bar denotes 2 μm. (B) Quantification of the percent of cells with the DivL-LZ variants localized at the cell pole. N>97 cells for all samples. (C) A cartoon of DivL's sensor domain fused to the leucine zipper with the signal transmission motif mutations indicated by a red X. (D) Fluorescence microscopy to visualize the subcellular localization of DivL-mCherry leucine zipper fusion mutants expressed in *C. crescentus*. The variants were induced from the chromosomal xylose promoter in M2G supplemented with 0.03% xylose for 4 hours. (E) Quantification of the percent of cells with the DivL-LZ variants localized at the cell pole. N>54 cells.

In designing the leucine zipper approach, we hypothesized that the effect of the leucine zipper upon DivL's sensory domain would require an intact PAS signal transmission motif. We introduced D516A and T518V mutations into the DivL-532-LZ chimera, which had a largely

43

diffuse population (Figure 2.12A-C). In comparison, the signal transmission mutants of DivL-532-LZ re-gained the ability to form foci (Figure 2.12D-E). This result indicates that the high affinity leucine zipper dimerization requires an intact PAS signal transmission motif to alter DivL's subcellular localization pattern. The leucine zipper DivL localization data support our hypothesis that DivL localization can be regulated by reverse signaling originating from the pseudo-HK domain. Regulation of this localization pattern could be direct by altering the binding affinity of DivL towards cell pole localized scaffolds or could be indirect through its impact upon CtrA regulated genes.

A possible explanation for the distinct activities and localization of the DivL-LZ fusions is that some may form inactive, misfolded aggregates. We chose to purify and analyze DivL-LZ-532 and DivL-LZ-536, lacking the transmembrane tether, by gel filtration due to their inactivity in the swarm assay and contrasting localization patterns (Figure 2.13). Both eluted as a single peak with an apparent molecular weight of approximately 86 kDa (compared to the predicted monomer molecular weight of 58 kDa). The results indicate that the DivL-LZ fusions have identical oligomerization profiles as well-folded proteins.
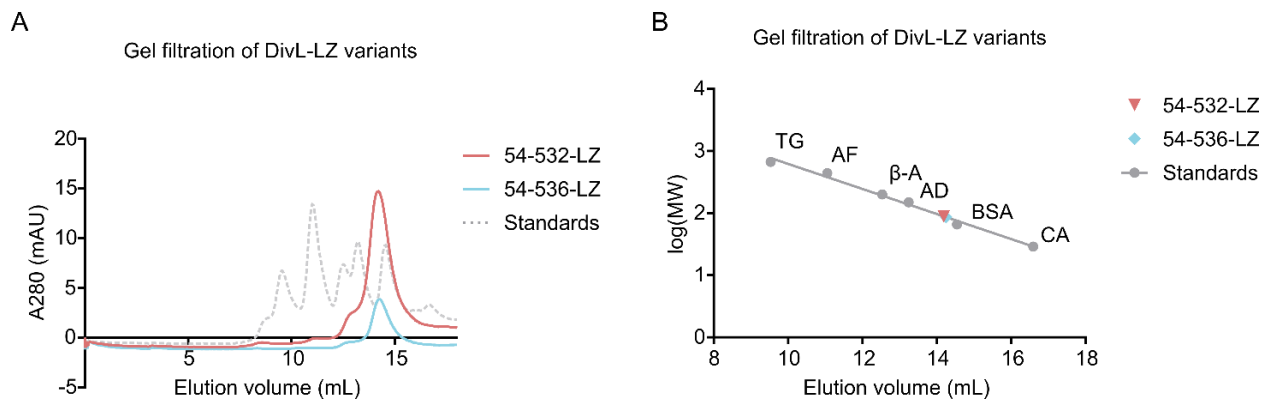
Figure 2.13: Gel filtration analysis of two DivL-LZ variants (A) Gel filtration elution curve of the protein standards (gray) and DivL-54-532-LZ (red) and DivL-54-536-LZ (blue) shows that both leucine zipper fusions were

eluted with the same volume of buffer. (B) A standard curve was created to calculate the apparent molecular mass of the leucine zipper fusions. The protein standard sizes were as follows: thyroglobulin (TG, 669 kDa), apoferritin (AF, 443 kDa), β-amylase (β-A, 200 kDa), alcohol dehydrogenase (AD, 150 kDa), bovine serum albumin (BSA, 66 kDa), and carbonic anhydrase (CA, 29 kDa).

Demonstration of techniques to probe reverse signaling Here we have demonstrated the potential of using synthetic stimulation and signal disruption strategies to probe signaling flux and directionality *in vivo* within complex bacterial multi-kinase networks. We applied this synthetic stimulation approach to directly test if a pseudokinase mediates pathway cross-talk by signaling in reverse. In this model, stimulation of the HK domain results in a conformational change in the sensor helix (Figure 2.2) through the signal transmission motif (Figure 2.6). Using the leucine zipper strategy (Figure 2.9, 2.12), we successfully demonstrated that DivL-531-LZ can mimic the allosteric effects of the DivL-DivK~P bound state and rescue CckA mediated phenotypes in the DivK^{cs} background (Figure 2.9D-E). We anticipate that biochemical studies of the DivL-LZ fusions in CckA kinase activity assays will help us to further characterize DivL's allosteric activator role. We now also propose that signaling flow within the cell cycle MKN helps to dictate the localization of one of its key players, DivL. We observed that the DivL-LZ chimera series had differential effects on CtrA regulated activity related to swarm size and DivL's localization pattern (Figure 2.9, 2.12). Swarm size activity is related to how DivL modulates CckA's kinase activity. In contrast, DivL's localization is regulated by both its affinity for cell pole recruitment factors (i.e. PodJ[121] and PopZ[122]) and a negative feedback within the CtrA signaling pathway that impacts these cell pole scaffolds[121, 130]. Therefore, we speculate that the DivL-LZ variants stimulate changes in both CckA pathway activity as well as DivL's direct affinity for cell pole recruitment factors.

Reverse signaling may be widespread Studies of pseudoenzymes have highlighted functions that extend beyond canonical enzymatic activity[131-133]. The current model of the DivL pseudokinase contributes to a new category of pseudoenzyme regulation that includes a ligand binding domain that regulates an enzymatic domain in a "forward signaling" manner. For example, a similar reverse signaling has also been observed with the *C. crescentus* signaling protein PopA[70]. PopA utilizes a catalytically dead diguanylate cyclase domain that has been repurposed as a c-di-GMP sensory domain to activate a previously upstream receiver domain to regulate the cell cycle. Thus, DivL and PopA provide two examples of pseudoenzymes that re-wire the input-output assignments and use reverse signaling flow.

Synthetic strategies to map-out signaling flow in signaling networks More broadly, we envision synthetic stimulation as a new systematic approach to interrogating signaling flow mechanisms within bacterial multi-kinase networks that orchestrate a range of bacterial developmental processes. As well, PAS domains are among one the most common bacterial signaling proteins[31, 134] and disruption of the PAS sensor transmission motif[7] provides an approach to understand their importance within multi-kinase networks. A strategy that combines synthetic stimulation and sensor disruption could be applied to systematically map out signaling flux within bacterial multi-kinase networks and reveal new network regulation mechanisms such as reverse signaling. Knowledge of how signals propagate through these natural multi-kinase networks can guide the development of advanced information processing systems in synthetic biology. Moreover, we propose that this combined synthetic stimulation and signal disruption approach will play a critical new role in the testing and validation of designed synthetic two-component signaling networks.

2.3 Methods

Construction of plasmids and strains All experiments were performed using *Caulobacter crescentus* NA1000 (also known as CB15N) and *Escherichia coli* DH5α (Invitrogen) and BL21 (Novagen). *C. crescentus* NA1000, WSC11311 *DivK341* (DivK^{cs}), and the ϕCR30 phage were kind gifts from Dr. Lucy Shapiro (Stanford University School of Medicine). DNA oligos, plasmids, and strains used in this study are listed in Tables 2.1-2.5.

Plasmid construction Restriction enzymes were purchased from Thermo Scientific or Invitrogen. PCR reactions were performed in 50 µL reaction mixtures containing 3% (v/v) DMSO, 1.3 M betaine, 0.3 µM each primer, and 0.2 mM each dNTP, and 1U Phusion High-Fidelity DNA Polymerase (Thermo Scientific). Gibson assembly (4) reactions were performed in 20 µL with 100 ng backbone and typically a 1:5 backbone:insert ratio, with 0.08U T5 Exonuclease (New England Biolabs), 1U Phusion High-Fidelity DNA Polymerase (Thermo Scientific), and 80U Taq DNA Ligase (New England Biolabs). An annealing temperature of 55 °C was used for most reactions. Plasmids and primers were designed using the J5 device editor software (5). Oligonucleotides were synthesized by IDT (Coralville, IA) and all DNA sequencing reactions were performed by The University of Pittsburgh Genomics Research Core or Genewiz (South Plainfield, NJ). DNA oligos, plasmid construction methods, plasmids, and strains used in this study are listed in Table S1-S5.

DivL-mCherry variants Plasmid WSC10153-pXCHYC6-divL was made by Gibson assembly of full-length divL into pXCHYC-6 (6) and served as the template for all further DivL plasmid designs. Full length divL was amplified from the template cosmid 2G1 (7) using primers KAK1 and KAK2. pXCHYC-6 was digested with SacI. This backbone and the insert were assembled using the Gibson assembly method (4) resulting in an integrating plasmid at the C. crescentus chromosomal xylose locus encoding C-terminal mCherry-tagged DivL. C. crescentus

47

cells were transformed by electroporation. Briefly, cells were grown in PYE medium overnight and rinsed three times with cold sterile water. Cells were resuspended in water and 80 µL of cells plus 10 µL of plasmid were electroporated with a time constant of 3.5-5.0 ms. Colonies were screened for integration at the xylose locus using RecUni-1, a primer that anneals to the plasmid, and RecXyl-2, a primer that anneals to the 5' region of the chromosomal promoter (6).

DivL-LZ fusion variants The leucine zipper sequence was embedded into the reverse primer with overhangs overlapping the DivL truncation and the backbone. PCR was used to amplify the DivL-LZ fusion, and Gibson assembly was used to insert the fusion into the PXCHYC-6-SacI or PCR-amplified pBXSPA-2 backbones described in these methods.

DivL-mCherry linker panel Cloning plasmid pWSC10153 resulted in the linker PENSNVTRHRSAT between DivL and mCherry. To vary this linker sequence, primers were used to amplify the original pXCHYC-6 backbone so that the DivL sequence would align with different regions of the multiple cloning site. The primers used to amplify the backbones and DivL inserts for this series are found in Table S1.

Table 2.1: Plasmid design of DivL-mCherry linker panel

Plasmid	Description	Forward primer backbone	Reverse primer backbone	Forward primer DivL	Reverse primer DivL
pKAK0141	pXCHYC-6 DivL LRSRAPENSNVTRHRSAT mCherry linker	KAK173	KAK174	KAK175	KAK176
pKAK0142	pXCHYC-6 DivL HRSAT mCherry linker	KAK177	KAK178	KAK179	KAK180
pKAK0143	pXCHYC-6 DivL GS mCherry linker	KAK181	KAK182	KAK183	KAK184
pKAK0145	pXCHYN-6 DivL mCherry HRSAT linker	KAK189	KAK190	KAK191	KAK192

Phage transduction Single-copy DivL-mCherry strains were made by using φCR30 phage transduction (8) to move the streptomycin divL gene replacement from WSC0427 (9) to the strains

48

containing the divL-mcherry copy under the xylose locus. To prepare ΔdivL phage, WSC0427 was grown in 2 mL of PYE medium supplemented with streptomycin and spectinomycin to stationary phase. Three dilutions of ϕCR30 phage in 5 μL was added to 0.5 mL of culture and incubated at room temperature for 15 minutes. The mixture was plated in top agar on a plain PYE plate and incubated at 28 °C overnight. The phage plaques were resuspended in 5 mL PYE and 100 μL chloroform, incubated for 10 minutes at room temperature, followed by centrifugation for 30 minutes at room temperature at 8,000 RPM.

As an example, to transduce the KAK43 strain, it was grown in 2 mL PYE supplemented with chloramphenicol overnight. Expression of DivL-mCherry was induced with 0.3% xylose for 2 hours. 100 μL of the phage prepared above was mixed with 0.5 mL cells and incubated at room temperature for 40 minutes. Cells were centrifuged at 15,000 g for 2 minutes and resuspended in 0.5 mL of PYE medium, then incubated with shaking at 28 °C for 2 hours. Cells were plated on PYE agar supplemented with 0.3% xylose, spectinomycin, and streptomycin. Colonies were screened for insertion of the streptomycin replacement at the divL locus using the primers KAKqc0046 that binds downstream of the divL locus and KAKqc0049 that binds in the streptomycin cassette. This resulted in strain KAK115: ΔdivL with pWSC10153 DivL-mCherry integrated at the xylose locus.

DivL point mutants DivL point mutants were designed as two-fragment Gibson assemblies with the point mutant embedded in the fragment amplification primers. pKAK0009-pXCHYC6-SacI-DivL-D516A was made by amplifying Insert 1 using primers KAK1 and KAKqc0019 and Insert 2 using primers KAKqc0018 and KAK2 from plasmid WSC10153 as a template. pXCHYC-6 was digested with SacI. This backbone and the inserts were assembled using

49

the Gibson assembly method resulting in an integrating plasmid at the C. crescentus chromosomal xylose locus encoding the C-terminal mCherry-tagged DivL mutant.

DivL-M2 variants pBXMCS-2 backbone was amplified by PCR using the primers KAK9 and KAK10. Fragments were amplified from WSC10153 or an already existing construct in pXCHYC-6. The backbone and insert were assembled using the Gibson assembly method resulting in a C. crescentus high-copy plasmid for the xylose-inducible expression of the C-terminal M2-tagged DivL variant.

Swarm plate assay Cells were grown to mid-log phase at 28 °C overnight in PYE (peptone yeast extract) medium and the appropriate antibiotic. Cells were normalized by dilution in PYE medium to the culture with the lowest OD600. Cells were stabbed into 0.3% PYE agar with the appropriate antibiotic and 0.3% xylose in 15 cm diameter culture plates using a Boekel replicator. Plates were incubated at 28 °C for 3 days. Plates were visualized using a ChemiDoc XRS+ system (Bio-Rad). Three replicate plates were analyzed. Swarm area was measured using ImageJ[135]. Swarm areas were normalized to the empty vector control on each plate. The error for the empty vector control was calculated by dividing the standard deviation of the areas by the average area. The error for the experimental areas was calculated as the standard deviation of the areas after normalization to the empty vector control. Significance was determined using Prism (GraphPad) with a Dunnett's multiple comparisons test by comparing the mean area of each strain to the mean area of DivL-WT (ns: $P>0.05$, *: $P \leq 0.05$, **: $P \leq 0.01$, ***: $P \leq 0.001$).

Fluorescence microscopy *C. crescentus* cells were grown in M2G medium with the appropriate antibiotics at 28 °C overnight to OD600=0.2-0.8. DivL-mCherry variants were induced with 0.03% xylose for 4 hours. Cells were diluted as needed an immobilized on a 1.5% agarose in M2G pad. DivK^{cs} strains were grown overnight in PYE medium and diluted in PYE

supplemented with 0.03% xylose to induce over-expression. Cells were grown again overnight at 28 or 20 °C. Phase microscopy was performed by using a Nikon Eclipse T*i*-E inverted microscope equipped with an Andor Ixon Ultra DU897 EMCCD camera and a Nikon CFI Plan-Apochromat 100X/1.45 Oil objective and intermediate 1.5x magnification. DIC (differential interference contrast) microscopy was performed with a Nikon CFI Plan-Apochromat 100X/1.45 Oil DIC objective with a Nikon DIC polarizer and slider in place. Carl Zeiss Immersol 518 oil was used. Excitation source was a Lumencor SpectraX light engine. mCherry was visualized with the DAPI/GFP/TRITC Chroma filter cube. Images were acquired with Nikon NIS-Elements AR software.

Fluorescence image analysis ImageJ[135] was used to adjust LUT, pseudocolor, and crop images. Image J Cell Counter and Nikon-NIS Elements AR were used to manually count cells and foci. ImageJ and MicrobeJ[136] were used for manual cell counting and cell length analysis. White outlines of the *C. crescentus* cell body were based on DIC or phase contrast imaging.

Multiple sequence alignments The DivL homolog sequences[137] were aligned using ClustalΩ in the MPI Bioinformatics Toolkit[138]. The phylogenetic tree was calculated in Jalview using BLOSUM62 Average Distance[139]. Protein visualization was performed with USCF Chimera[140].

Western blot Western blot analysis was used to determine protein levels of each DivL-M2 variant. Cells were grown in 2 mL PYE medium to early log phase at 28°C. Overnight induction with 0.3% xylose began at inoculation. 1 mL cells were harvested by centrifugation and resuspended in SDS 100 µL sample loading dye. Samples were treated by heating (75°C for 10 min). Samples volumes were normalized to the lowest OD600 upon collection and separated by 10% SDS–PAGE. Proteins were transferred onto a PVDF membrane (GE Healthcare). The

membrane was blocked in 5% milk (AmericanBio) overnight at 4°C. The anti-M2 (FLAG) antibody (Sigma-Aldrich) (1:5000 in TBST for 1 hour at 4°C) (Bulldog Bio) was used with a goat anti-rabbit IgG-peroxidase secondary antibody (Sigma-Aldrich) (1:10,000 in TBST for 1 hour at room temperature). PVDF membranes were treated with an ECL western blotting kit (Thermo Scientific) and visualized using a ChemiDoc XRS+ system (Bio-Rad). Colorimetric imaging was used to visualize the protein ladder, which was aligned with the blots to assign the size labels.

Protein purification Plasmids pKAK0137b and pKAK0137f were transformed into BL21 cells, and plated onto 100 µg/mL ampicillin LB plates and grown overnight at 37 °C. From a single colony, an overnight 10 mL 50 µg/mL ampicillin LB culture was inoculated and grown to saturation overnight. From this saturated culture two 1 L LB cultures were inoculated and grown to mid-log phase (0.6 OD). Expression of the DivL-LZ fusions was induced with 333 µM isopropyl-b-D-thiogalactopyranoside (IPTG) for 4 hours at 25 °C. The cells were harvested by centrifugation (4 °C for 20 minutes at 3,700 g). The resulting pellet was resuspended in 50 ml 50 mM HEPES pH=8, 0.5 M KCl and centrifuged (3,700 g at 4 °C for 20 minutes) to yield a cell pellet stored at -80 °C. Cells were thawed on ice and resuspended in 50 ml of lysis buffer (50 mM HEPES pH 8.0, 0.5 M KCl, 1 mM DTT, 25 mM imidazole, 10% glycerol, and 200 U of Benzonase Nuclease (Sigma) supplemented with SIGMAFAST protease inhibitor tablets (Sigma)). The cell suspension was lysed with three passes through the Emulsiflex at 20,000 psi. Insoluble cell debris was pelleted via centrifugation (30,000 g, 50 min at 4 °C). The resulting supernatant was incubated with 2 ml of a 50% slurry of HisPur Ni-NTA agarose resin (Thermo Fisher Scientific) at 4 °C for 2 hours. The Ni-NTA agarose was pelleted and washed with 30 ml of Ni-NTA wash buffer (50 mM HEPES pH=8], 0.5 M KCl, 1 mM DTT, 25 mM imidazole, and 10% glycerol). Then the DivL-LZ fusion was eluted from the agarose with Ni-NTA elution buffer (50 mM HEPES pH=8.0,

0.5 M KCl, 1 mM DTT, 250 mM imidazole, and 10% glycerol) and concentrated using Amicon Centrifugal Filter Units (30 kDa cutoff), aliquoted and frozen at 80 °C. The concentration was determined using the predicted molecular weight of 58 kDa and 78,630 M-1cm-1.

Gel filtration chromatography A gel filtration standard (Sigma) containing thyroglobulin (bovine), apoferritin (horse spleen), β-amylase (sweet potato), alcohol dehydrogenase (yeast), albumin (bovine serum) and carbonic anhydrase (bovine erythrocytes) was used to generate a molecular weight standard plot using a Superdex 200 10-300 GL column (GE Heathcare). A 1.9 mg/mL sample of DivL(1-536)-LZ and a 3.2 mg/mL sample of DivL(1-532)-LZ were loaded onto the column and eluted with 50 mM HEPES pH=8, 0.5 M KCl.

Table 2.2: DNA oligos

Name	Description
RecXyl-2	TCTTCCGGCAGGAATTCACTCACGCC
RecUni-1	ATGCCGTTTGTGATGGCTTCCATGTCG
WSC10295	TGGTACCTTAAGATCTCGAGCTATGACTTCGTACGACCTGATCCTCGC
WSC10296	TCGAATTCTCCGGGAAGCCGAGTTCGGGCTGCATGG
WSC10297	TGCATGGTACCTTAAGATCTCGAGCTATGACTTCGTACGACCTGATCCTCGCG
WSC10298	TGACGCGTAACGTTCGAATTCTCCGGCAGCTCCGAATAGCCGATGATCGTCG
WSC10299	TGACGCGTAACGTTCGAATTCTCCGGGGCTTCGGCCAGGGCCGC
WSC10301	CCAGCACGGCTCGACCCCGTGGGACCACAGGGC
WSC10302	GTGGTCCCACGGGGTCGAGCCGTGCTGGATCGC
WSC10303	TGACGCGTAACGTTCGAATTCTCCGGGGTGACGTCGGCGAAGGCG
KAKqc0018	GATCGCCTTCGCCGCCGTCACCGACACC
KAKqc0019	GGTGTCGGTGACGGCGGCGAAGGCGATC
KAKqc0020	CTTCGCCGACGTCGTCGACACCCGAGAC
KAKqc0021	GTCTCGGGTGTCGACGACGTCGGCGAAG
KAKqc0046	GGGCTGGTTCGAGGATGCCGCTTAG
KAKqc0049	GGAGAGAGCGAGATTCTCCGCGCTG
KAKqc0076	TGACGCGTAACGTTCGAATTCTCCGGCAGACGGGCGACCTCATTCTCGAGGTGGTAGTTCTTCGAGAGGAGTTCTTCGACCTTGTCTTCGAGTTGCTTGGCTTCGGCCAGGGCCGC
KAKqc0077	TGACGCGTAACGTTCGAATTCTCCGGCAGACGGGCGACCTCATTCTCGAGGTGGTAGTTCTTCGAGAGGAGTTCTTCGACCTTGTCTTCGAGTTGCTTTTCGGCCAGGGCCGCCGAGC
KAKqc0078	TGACGCGTAACGTTCGAATTCTCCGGCAGACGGGCGACCTCATTCTCGAGGTGGTAGTTCTTCGAGAGGAGTTCTTCGACCTTGTCTTCGAGTTGCTTGGCCAGGGCCGCCGAGCG
KAKqc0079	TGACGCGTAACGTTCGAATTCTCCGGCAGACGGGCGACCTCATTCTCGAGGTGGTAGTTCTTCGAGAGGAGTTCTTCGACCTTGTCTTCGAGTTGCTTCAGGGCCGCCGAGCGATC
KAKqc0080	TGACGCGTAACGTTCGAATTCTCCGGCAGACGGGCGACCTCATTCTCGAGGTGGTAGTTCTTCGAGAGGAGTTCTTCGACCTTGTCTTCGAGTTGCTTGGCCGCCGAGCGATCGGC
KAKqc0081	TGACGCGTAACGTTCGAATTCTCCGGCAGACGGGCGACCTCATTCTCGAGGTGGTAGTTCTTCGAGAGGAGTTCTTCGACCTTGTCTTCGAGTTGCTTCGCCGAGCGATCGGCCAGG
KAKqc0082	TGACGCGTAACGTTCGAATTCTCCGGCAGACGGGCGACCTCATTCTCGAGGTGGTAGTTCTTCGAGAGGAGTTCTTCGACCTTGTCTTCGAGTTGCTTCGAGCGATCGGCCAGGGC
KAKqc0108	TGACGCGTAACGTTCGAATTCTCCGGCAGACGGGCGACCTCATTCTCGAGGTGGTAGTTCTTCGAGAGGAGTTCTTCGACCTTGTCTTCGAGTTGCTTCACGCTGTCGACGAAGGC
KAK1	TGCATGGTACCTTAAGATCTCGAGCTATGACTTCGTACGACCTGATCCTCGC
KAK3	CGAGGTCGACGGTATCGATAAGCTTGATATGACTTCGTACGACCTGATCCTCGCG
KAK5	CGGCGCTTTTCCATCGAGAATTCGATGGCTTCGGCCAGGGCCGC
KAK7	CGGCGCTTTTCCATCGAGAATTCGATGAAGCCGAGTTCGGGCTGCATGG
KAK8	CGGCGCTTTTCCATCGAGAATTCGATGGTGACGTCGGCGAAGGCG

54

KAK9	ATCGAATTCTCGATGGAAAAGCGCCG
KAK10	ATCAAGCTTATCGATACCGTCGACCTCGAG
KAK132	CGGCGCTTTTCCATCGAGAATTCGATCAGACGGGCGACCTCATTCTCGAGG
KAK155	CCAACTAGTGAAAACCTGTATTTTCAGGGCGCTATGGCCTGGCTCGACGCCTTCGA
KAK158	GCTCGAGAATTCCATGGCCATATGGCTTCACAGACGGGCGACCTCATTCTCGA
KAK173	GCCCGAACTCGGCTTCTTAAGATCTCGAGCTCCGGAGAATTCG
KAK174	GGTCGTACGAAGTCATGGTACCATGCATATTAATTAAGGCGCCTGC
KAK175	CCTTAATTAATATGCATGGTACCATGACTTCGTACGACCTGATCCTCGC
KAK176	GCTCGAGATCTTAAGAAGCCGAGTTCGGGCTGCATGG
KAK177	CGAACTCGGCTTCCACCGGTCGGCCACCATGG
KAK178	GGTCGTACGAAGTCATACGCGTAACGTTCGAATTCTCCGG
KAK179	TCGAACGTTACGCGTATGACTTCGTACGACCTGATCCTCGC
KAK180	TGGCCGACCGGTGGAAGCCGAGTTCGGGCTGCATGG
KAK181	CGGCTTCGGATCCATGGTGAGCAAGGGCGAGGAGG
KAK182	CGTACGAAGTCATGGTGGCCGACCGGTGACG
KAK183	CCGGTCGGCCACCATGACTTCGTACGACCTGATCCTCGC
KAK184	CCTTGCTCACCATGGATCCGAAGCCGAGTTCGGGCTGCATGG
KAK189	ACTCGGCTTCTAACCTGCAGGCGCCTTAATTAATATGCATGG
KAK190	TGGCCGACCGGTGCTTGTACAGCTCGTCCATGCCGCC
KAK191	CGAGCTGTACAAGCACCGGTCGGCCACCATGACTTCGTACGACCTGATCCTCGC
KAK192	AGGCGCCTGCAGGTTAGAAGCCGAGTTCGGGCTGCATGG

Table 2.3: Gibson cloning strategy to generate plasmids

Plasmid	Plasmid Description	First Insert Forward Primer	First Insert Reverse Primer	Second Insert Forward Primer	Second Insert Reverse Primer
WSC10153	pXCHYC-6 DivL (1-769)	WSC10295	WSC10296		
pWSC10155	pXCHYC-6 DivL (1-537)	WSC10297	WSC10299		
pWSC10158	pXCHYC-6 DivL (1-518)	WSC10297	WSC10303		
pKAK0009	pXCHYC-6 DivL D516A	WSC10295	KAKqc0019	KAKqc0018	WSC10296
pKAK0010	pXCHYC-6 DivL T518V	WSC10295	KAKqc0021	KAKqc0020	WSC10296
pKAK0012	pBXMCS-2 DivL (1-537)	KAK3	KAK5		
pKAK0015	pBXMCS-2 DivL (1-518)	KAK3	KAK8		
pKAK0037	pBXMCS-2 DivL D516A	KAK3	KAK7		
pKAK0038	pBXMCS-2 DivL T518V	KAK3	KAK7		
pKAK0079	pXCHYC-6 DivL (1-537, LZ)	KAK1	KAKqc0076		
pKAK0080	pXCHYC-6 DivL (1-536, LZ)	KAK1	KAKqc0077		
pKAK0081	pXCHYC-6 DivL (1-535, LZ)	KAK1	KAKqc0078		
pKAK0082	pXCHYC-6 DivL (1-534, LZ)	KAK1	KAKqc0079		
pKAK0083	pXCHYC-6 DivL (1-533, LZ)	KAK1	KAKqc0080		
pKAK0084	pXCHYC-6 DivL (1-532, LZ)	KAK1	KAKqc0081		
pKAK0085	pXCHYC-6 DivL (1-531, LZ)	KAK1	KAKqc0082		
pKAK0096	pXCHYC-6 DivL (1-170, LZ)	KAK1	KAKqc0108		
pKAK0121a	pBXMCS-2 DivL (1-537, LZ)	KAK3	KAK132		
pKAK0121b	pBXMCS-2 DivL (1-536, LZ)	KAK3	KAK132		
pKAK0121c	pBXMCS-2 DivL (1-535, LZ)	KAK3	KAK132		
pKAK0121d	pBXMCS-2 DivL (1-534, LZ)	KAK3	KAK132		
pKAK0121e	pBXMCS-2 DivL (1-533, LZ)	KAK3	KAK132		
pKAK0121f	pBXMCS-2 DivL (1-532, LZ)	KAK3	KAK132		
pKAK0121g	pBXMCS-2 DivL (1-531, LZ)	KAK3	KAK132		

pKAK0137b	pTEV-5 DivL (1-532, LZ)	KAK155	KAK158		
pKAK0137f	pTEV-5 DivL (1-536, LZ)	KAK155	KAK158		
pKAK0141	pXCHYC-6 DivL LRSRAPENSNVT RHRSAT mCherry linker	KAK175	KAK176		
pKAK0142	pXCHYC-6 DivL HRSAT mCherry linker	KAK179	KAK180		
pKAK0143	pXCHYC-6 DivL GS mCherry linker	KAK183	KAK184		
pKAK0145	pXCHYN-6 DivL mCherry HRSAT linker	KAK191	KAK192		
pKAK0198	pXCHYC-6 DivL (1-532, LZ) D516A	KAK1	KAKqc0081		
pKAK0199	pXCHYC-6 DivL (1-532, LZ) T518V	KAK1	KAKqc0081		

Table 2.4: Plasmids

Plasmid	Description	Reference
pET-28b(+)	bacterial expression vector	Novagen
pTEV-5	bacterial expression vector	[141]
pXCHYC-6	C. crescentus integrating C-terminal mCherry fusion vector	[142]
pBXMCS-2	C. crescentus high-copy replicating C-terminal M2 fusion vector	[142]
WSC10153	pXCHYC-6 DivL (1-769)	This study
pWSC10155	pXCHYC-6 DivL (1-537)	This study
pWSC10158	pXCHYC-6 DivL (1-518)	This study
pKAK0009	pXCHYC-6 DivL D516A	This study
pKAK0010	pXCHYC-6 DivL T518V	This study
pKAK0012	pBXMCS-2 DivL (1-537)	This study
pKAK0015	pBXMCS-2 DivL (1-518)	This study
pKAK0037	pBXMCS-2 DivL D516A	This study
pKAK0038	pBXMCS-2 DivL T518V	This study
pKAK0079	pXCHYC-6 DivL (1-537, LZ)	This study
pKAK0080	pXCHYC-6 DivL (1-536, LZ)	This study
pKAK0081	pXCHYC-6 DivL (1-535, LZ)	This study
pKAK0082	pXCHYC-6 DivL (1-534, LZ)	This study
pKAK0083	pXCHYC-6 DivL (1-533, LZ)	This study
pKAK0084	pXCHYC-6 DivL (1-532, LZ)	This study
pKAK0085	pXCHYC-6 DivL (1-531, LZ)	This study
pKAK0096	pXCHYC-6 DivL (1-170, LZ)	This study
pKAK0121a	pBXMCS-2 DivL (1-537, LZ)	This study
pKAK0121b	pBXMCS-2 DivL (1-536, LZ)	This study
pKAK0121c	pBXMCS-2 DivL (1-535, LZ)	This study
pKAK0121d	pBXMCS-2 DivL (1-534, LZ)	This study
pKAK0121e	pBXMCS-2 DivL (1-533, LZ)	This study
pKAK0121f	pBXMCS-2 DivL (1-532, LZ)	This study
pKAK0121g	pBXMCS-2 DivL (1-531, LZ)	This study
pKAK0137b	pTEV-5 DivL (54-532, LZ)	This study
pKAK0137f	pTEV-5 DivL (54-536, LZ)	This study
pKAK0141	pXCHYC-6 DivL LRSRAPENSNVTRHRSAT mCherry linker	This study
pKAK0142	pXCHYC-6 DivL HRSAT mCherry linker	This study
pKAK0143	pXCHYC-6 DivL GS mCherry linker	This study
pKAK0145	pXCHYN-6 DivL mCherry HRSAT linker	This study
pKAK0198	pXCHYC-6 DivL (1-532, LZ) D516A	This study
pKAK0199	pXCHYC-6 DivL (1-532, LZ) T518V	This study

Table 2.5: *C. crescentus* **and** *E. coli* **strains**

Strain	Description	Plasmid(s)	Reference Source
E. coli DH5α	bacterial cloning strain		Invitrogen
E. coli BL21	bacterial expression strain		Novagen
C. crescentus NA1000	laboratory Caulobacter crescentus strain		Shapiro Lab
WSC0427	Δ*divL*(strep)	pMR20-divL	[143] Shapiro Lab
WSC1131	*DivK341* DivK^{cs}		[90] Shapiro Lab
WSC0300	C. crescentus pBXMCS-2		This study
WSC0302	*C. crescentus* pBXMCS-2 DivL (1-769)		This study
WSC0454	*C. crescentus* pXCHYC-6 DivL (1-537)	pWSC10155	This study
WSC0457	*C. crescentus* pXCHYC-6 DivL (1-518)	pWSC10158	This study
KAK12	DH5α pXCHYC-6 DivL (1-537)	pWSC10155	This study
KAK14	DH5α pXCHYC-6 DivL (1-518)	pWSC10158	This study
KAK20	DH5α pXCHYC-6 DivL (1-769)	pWSC10153	This study
KAK30	DH5α pBXMCS-2 DivL D516A	pKAK0037	This study
KAK33	DH5α pBXMCS-2 DivL T518V	pKAK0038	This study
KAK34	DH5α pXCHYC-6 DivL D516A	pKAK0009	This study
KAK36	DH5α pBXMCS-2 DivK	pBXSPA-DivK	This study
KAK43	NA1000 pXCHYC-6 DivL (1-769)	WSC10153	This study
KAK45	DH5α pBXMCS-2 DivL (1-537)	pKAK0012	This study
KAK47	DH5α pBXMCS-2 DivL (1-518)	pKAK0015	This study
KAK62	NA1000 pXCHYC-6 DivL HRSAT mCherry linker	pKAK0142	This study
KAK63	DH5α pXCHYC-6 DivL T518V	pKAK0010	This study
KAK64	NA1000 pBXMCS-2 DivL (1-537)	pKAK00012	This study
KAK65	NA1000 pBXMCS-2 DivL (1-518)	pKAK0015	This study
KAK92	NA1000 pXCHYC-6 DivL D516A	pKAK0009	This study
KAK102	NA1000 pXCHYC-6 DivL T518V	pKAK0010	This study
KAK115	NA1000 Δ*divL* pXCHYC-6 DivL (1-769)	pWSC10153	This study
KAK150	NA1000 pBXMCS-2 DivL D516A	pKAK0037	This study
KAK151	NA1000 pBXMCS-2 DivL T518V	pKAK0038	This study
KAK172	DH5α pXCHYC-6 DivL (1-537, LZ)	pKAK0079	This study
KAK176	DH5α pXCHYC-6 DivL (1-536, LZ)	pKAK0080	This study
KAK177	DH5α pXCHYC-6 DivL (1-535, LZ)	pKAK0081	This study
KAK178	DH5α pXCHYC-6 DivL (1-534, LZ)	pKAK0082	This study
KAK179	DH5α pXCHYC-6 DivL (1-533, LZ)	pKAK0083	This study
KAK180	DH5α pXCHYC-6 DivL (1-532, LZ)	pKAK0084	This study
KAK181	DH5α pXCHYC-6 DivL (1-531, LZ)	pKAK0085	This study
KAK197	NA1000 pXCHYC-6 DivL (1-536, LZ)	pKAK0080	This study
KAK198	NA1000 pXCHYC-6 DivL (1-535, LZ)	pKAK0081	This study
KAK199	NA1000 pXCHYC-6 DivL (1-533, LZ)	pKAK0083	This study

KAK200	NA1000 pXCHYC-6 DivL (1-532, LZ)	pKAK0084	This study
KAK201	NA1000 pXCHYC-6 DivL (1-531, LZ)	pKAK0085	This study
KAK202	NA1000 pXCHYC-6 DivL (1-537, LZ)	pKAK0079	This study
KAK205	NA1000 pXCHYC-6 DivL (1-534, LZ)	pKAK0082	This study
KAK209	DH5α pBXMCS-2 DivL (1-537, LZ)	pKAK0121a	This study
KAK214	DH5α pBXMCS-2 DivL (1-536, LZ)	pKAK0121b	This study
KAK229	DH5α pBXMCS-2 DivL (1-535, LZ)	pKAK0121c	This study
KAK230	DH5α pBXMCS-2 DivL (1-531, LZ)	pKAK0121g	This study
KAK232	DH5α pXCHYN-6 DivL mCherry HRSAT linker	pKAK0145	This study
KAK254	DH5α pTEV-5 DivL (54-536, LZ)	pKAK0137b	This study
KAK266	DH5α pXCHYC-6 DivL LRSRAPENSNVTRHRSAT mCherry linker	pKAK0141	This study
KAK267	DH5α pXCHYC-6 DivL GS mCherry linker	pKAK0143	This study
KAK270	DH5α pTEV-5 DivL (54-532, LZ)	pKAK0137f	This study
KAK276	DH5α pBXMCS-2 DivL (1-534, LZ)	pKAK0121d	This study
KAK277	DH5α pXCHYC-6 DivL HRSAT mCherry linker	pKAK0142	This study
KAK281	NA1000 pXCHYC-6 DivL LRSRAPENSNVTRHRSAT mCherry linker	pKAK0141	This study
KAK283	NA1000 pXCHYC-6 DivL GS mCherry linker	pKAK0143	This study
KAK293	DH5α pBXMCS-2 DivL (1-533, LZ)	pKAK0121e	This study
KAK294	DH5α pBXMCS-2 DivL (1-532, LZ)	pKAK0121f	This study
KAK299	NA1000 Δ*divL* pXCHYC-6 DivL HRSAT mCherry linker	pKAK0142	This study
KAK300	NA1000 Δ*divL* pXCHYC-6 DivL GS mCherry linker	pKAK0143	This study
KAK309	NA1000 pBXMCS-2 DivL (1-536, LZ)	pKAK0121b	This study
KAK310	NA1000 pBXMCS-2 DivL (1-535, LZ)	pKAK0121c	This study
KAK311	NA1000 pBXMCS-2 DivL (1-533, LZ)	pKAK0121e	This study
KAK312	NA1000 pBXMCS-2 DivL (1-532, LZ)	pKAK0121f	This study
KAK313	NA1000 pBXMCS-2 DivL (1-531, LZ)	pKAK0121g	This study
KAK324	NA1000 pBXMCS-2 DivL (1-537, LZ)	pKAK0121a	This study
KAK332	BL21 pTEV-5 DivL (54-536, LZ)	pKAK0137b	This study
KAK334	BL21 pTEV-5 DivL (54-532, LZ)	pKAK0137f	This study
KAK336	NA1000 pBXMCS-2 DivL (1-534, LZ)	pKAK0121d	This study
KAK340	NA1000 pXCHYN-6 DivL mCherry HRSAT linker	pKAK0145	This study
KAK351	DH5α pXCHYC-6 DivL (1-170, LZ)	pKAK0096	This study
KAK356	DH5α pXCHYC-6 DivL (1-532, LZ) D516A	pKAK0198	This study
KAK357	DH5α pXCHYC-6 DivL (1-532, LZ) T518V	pKAK0199	This study
KAK358	NA1000 pXCHYC-6 DivL (1-170, LZ)	pKAK0096	This study
KAK363	NA1000 pXCHYC-6 DivL (1-532, LZ) D516A	pKAK0198	This study
KAK364	NA1000 pXCHYC-6 DivL (1-532, LZ) T518V	pKAK0199	This study

3.0 A Bacterial Pseudokinase Utilizes Repurposed Modes of Action to Regulate an Active

Cell-Cycle Kinase

This chapter was written in collaboration with Samuel W. Duvall and W. Seth Childers and contains data from a manuscript in preparation.

3.1 Introduction

Pseudoenzymes are enzymes with mutations that are predicted to result in the loss of catalytic function[133]. Even though they appear to be "dead," pseudoenzymes are present across kingdoms in bacteria, archaea and eukaryotes. Characterization of individual pseudoenzymes have revealed a diverse set of functions outside of their prescribed enzymatic roles[133]. A well-studied group of pseudoenzymes is the pseudokinase. A surprising subset (about 10%) of human kinases are predicted to be pseudokinases[131]. Human pseudokinases have been of increasing research interest as many have been implicated in human diseases and are consequently attractive potential drug targets[132, 144]. Pseudokinases have been shown in eukaryotes to impact diverse biochemical systems by functioning as subcellular localization anchors, allosteric modulators of active enzymes, signal integrators, and competitors for substrate binding (Figure 3.1)[132].
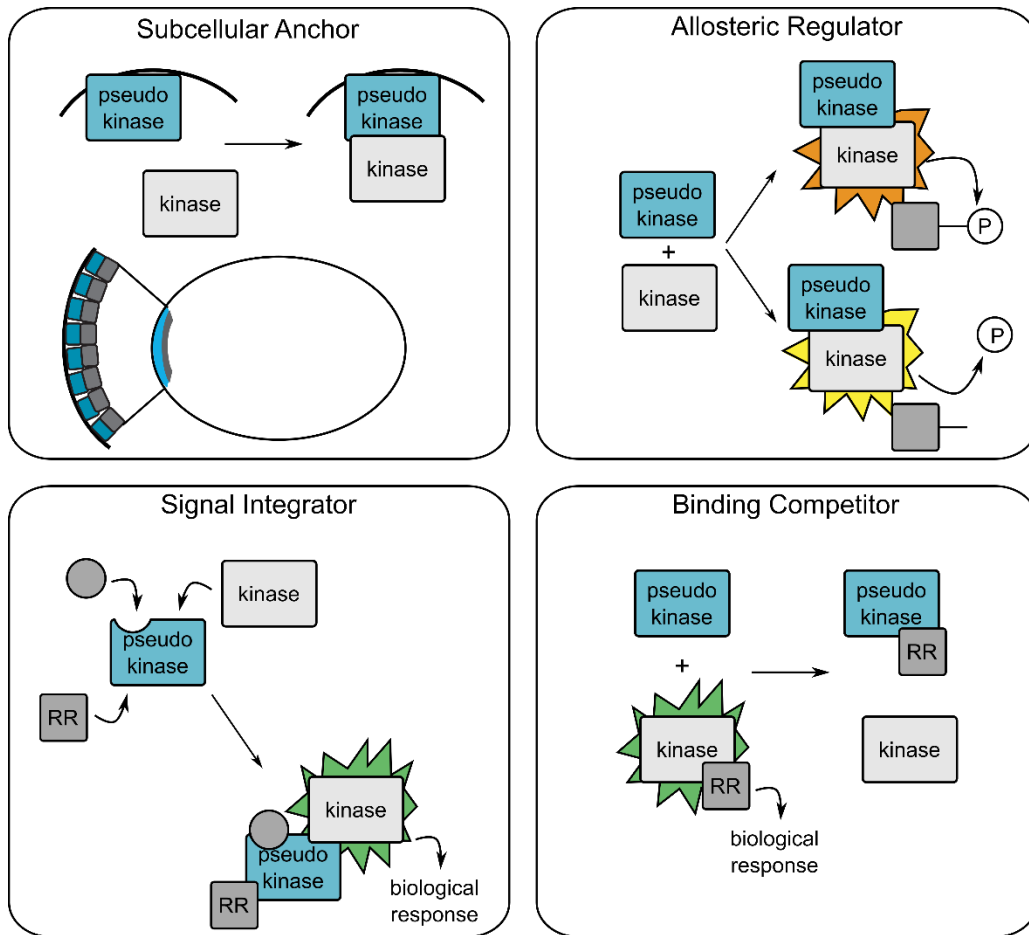
Figure 3.1: Eukaryotic pseudokinases are catalytically inactive but maintain essential roles These roles include anchoring an active kinase to a subcellular location, allosteric regulation of kinase or phosphatase activity, integrating multiple signals, and competitive binding[132].

Bacterial pseudokinases have received less attention, but emerging examples have been attributed to complex life cycles[118, 145] and pathogenesis[146-148]. Bacteria use two-component systems in order to adapt their behavior in response to the environment[1]. The two components are a histidine kinase (HK) and a response regulator (RR). The histidine kinase responds to a signal by auto-phosphorylating a conserved histidine. The phosphate group is then transferred to an aspartate residue on the RR, which goes on to elicit a cellular response, often by controlling transcription. The histidine kinase performs three distinct catalytic functions that can be disrupted

in pseudokinases: 1) autophosphorylation of the histidine within the kinase, 2) phosphotransfer to the response regulator, and 3) dephosphorylation of the response regulator[1]. A response regulator comprises an N-terminal receiver domain and a C-terminal effector domain. Phosphorylation by the histidine kinase occurs at the active site aspartic acid in the receiver domain. Additional residues in the active site coordinate a Mg^{2+} and align the aspartate to catalyze phosphotransfer or removal of the phosphate by water. A conformational change is transmitted to the effector domain to regulate output in response to phosphorylation state. Interestingly, pseudo-response regulators have also been discovered in bacterial[149] and plant[150] two-component systems.

One category of bacterial pseudokinases has mutations to the ATP binding pocket. One such pseudokinase in *C. crescentus*, ChpT, does not bind ATP or exhibit pseudokinase activity[145]. ChpT has, however, retained the ability to transfer a phosphate group from the hybrid histidine kinase CckA to the master regulator CtrA[145]. This phosphorelay is critical for *C. crescentus* to proceed through its asymmetric life cycle[125, 151, 152]. A phosphotransfer protein within the phosphorelay that controls sporulation in *B. subtilis* also resembles a histidine kinase but cannot bind ATP[153]. An interesting and recent addition to this category is SidJ from the intracellular pathogen *L. pneumophila*. This pseudokinase more closely resembles an atypical human kinase Haspin than a bacterial HK. Haspin is a constitutively active kinase that phosphorylates a threonine on histone H3 to regulate mitosis[154]. SidJ utilizes its kinase-like ATP binding domain to transfer AMP to its substrate, forming an acyl-adenylate intermediate for glutamylation[147]. SidJ is secreted into host cells and catalyzes inhibition of a ubiquitin ligase through polyglutamylation, ultimately allowing for *Legionella* replication within the host[147, 148].

A second category of bacterial pseudokinases is lacking a conserved phosphorylation site. The most well-characterized of this category is the *C. crescentus* pseudokinase DivL. Genetic

63

studies have demonstrated that the ATP binding domain can be removed without affecting cell viability and thus DivL does not require catalytic activity for function *in vivo*[143, 155]. Additionally, replacement of the phosphorylation site tyrosine with a non-phosphorylatable phenylalanine does not affect cell viability[21, 143]. DivL does not act as a kinase or phosphatase toward its cognate response regulator DivK *in vitro*[69]. Instead, the pseudo-HK domain has conserved its function to selectively bind the phosphorylated form of DivK (DivK~P)[69, 90].

Past efforts to understand how this bacterial pseudokinase is essential for cell viability with no apparent catalytic activity have revealed that DivL shares many features with its eukaryotic counterparts (Figure 3.1). DivL modulates the activity of an active histidine kinase CckA, and it does so in a switch-like manner in response to binding to the phosphorylated response regulator DivK[21, 90]. Moreover, DivL plays a role in anchoring CckA at the cell pole[21], which is critical for asymmetric regulation at each cell pole[156]. Thus, a critical cell-cycle pathway in *C. crescentus* utilizes not one but two pseudokinases, ChpT and DivL.

Another protein that has been coined as a bacterial pseudokinase due to its lack of catalytic kinase residues is RocA in Group A *Streptococcus* (GAS)[146]. GAS is a human pathogen causing infections ranging in severity from "strep throat" to necrotizing fasciitis[157]. Like DivL, its entire catalytic domain is dispensable for its enhancement of the activity of the CovRS (or CsrRS) virulence pathway[146]. RocA interacts with CovS through its transmembrane domain[96], which suggests a similar reverse signaling model as proposed for DivL in Chapter 2. Therefore, we propose that the DivL pseudokinase mechanisms that we uncover will allow for the further characterization of and discovery of similar pseudokinases in equally relevant bacterial models.

We still do not know what interactions are responsible for DivL's pseudokinase behaviors toward CckA. Previous studies, and the work described in Chapter 2[158], have indicated that DivL

regulates CckA activity through sensory domain interactions. A minimal functional DivL was identified that lacks most of the catalytic HK domain[155]. Construction of a chimeric CckA kinase activity reporter demonstrated that CckA's sensory domains were sufficient for DivL-dependent stimulation of CckA in *C. crescentus*[106]. In addition, *in vitro* studies of the DivL-CckA complex assembled on liposomes has shown that DivL's sensory domains are sufficient to regulate CckA function, and that CckA's sensory domains are required for this regulation[107]. In Chapter 2, we demonstrated that a truncated version of DivL that only contains the sensor can affect *C. crescentus* swarm motility, an output of the CckA pathway. In this study we applied a synthetic stimulation strategy to stimulate conformational changes within DivL's sensory domain and observed stimulation of the CckA-CtrA signaling pathway *in vivo*[158].

The role of the sensor domain in localization is less clear. Previous studies implicated the C-terminal residues of DivL in localizing to the new cell pole and recruiting CckA[21, 126, 143]. The 28 C-terminal residues of DivL were shown to be required for both DivL and CckA localization at new cell pole[21]. DivK binding to DivL is not required for DivL localization at the new cell pole[143], but a DivL variant that does not bind DivK was unable to recruit CckA to the new cell pole[90]. Furthermore, we demonstrated in Chapter 2 that a truncated DivL construct can localize to the new cell pole, and that this localization is dictated by a conformational change within the sensor-HK helix[159]. This indicates that there may be a redundant cell-pole targeting motif in the DivL sensory domain.

DivL's localization and CckA's localization and activity are intertwined. It makes sense that for asymmetric division to occur, localization of key cell-cycle regulators is critical (Figure 3.2)[21, 90, 125, 152, 160]. Asymmetric localization of the phosphatase PleC at the new cell pole and the kinase DivJ at the old cell pole generate differences in the levels of DivK phosphorylation at each

cell pole[161]. Current models suggest that when DivL and CckA are localized together at the old cell pole, DivK~P inhibits CckA activity by binding to DivL[90]. In contrast, when DivL and CckA are localized to the new cell pole in pre-divisional cells, where DivK is not phosphorylated, DivL activates CckA kinase activity[21, 90]. This results in an ultimate accumulation of phosphorylated CtrA in the new swarmer cell, which dictates its motility and inability to replicate and divide[105] (Figure 3.2).
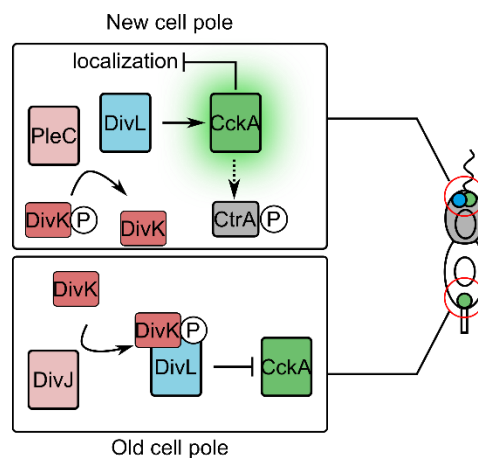
Figure 3.2: Cartoon of the relationship between DivL localization and CckA localization and activity At the new cell pole, DivK is dephosphorylated by PleC. DivL activates CckA activity and phosphorylated CtrA builds up in the developing swarmer cell. This pathway activation ultimately results in the loss of DivL and CckA at the pole. At the old cell pole, DivK is phosphorylated by DivJ. Phosphorylated DivK binds to DivL and this complex inhibits CtrA activity.

Studies using a CckA activity reporter determined that DivL localization to the new cell pole is correlated with CckA phosphorylation[21]. Apparent feedback mechanisms exist, however, as over-activation of CckA by the DivL-A601L mutant results in the loss of DivL's and CckA's cell pole localization[90, 120]. One such explanation for feedback is that DivL localizes at the new cell pole through binding interactions with the scaffolds PodJ[121] and PopZ[162], and PodJ localization

is dictated by CtrA-regulated proteolysis[163]. The complex relationships between localization and activity require us to examine both phenomena in our efforts to characterize the roles of DivL's sensory domain.

The N-terminal multi-sensor domain of DivL comprises a predicted transmembrane region (TM)[164] followed by four subdomains. First is a domain of unknown function, DUF3455, referred to hereafter as Domain A. Homology structure prediction did not result in any statistically significant hits for this domain, and the secondary structure prediction is distinct from the common Per-Arnt-Sim (PAS) sensory domain fold (Figure 3.3). The remaining three sensory domains have homology with the PAS domain, and these are referred to as PAS B, PAS C, and PAS D. The N-terminal sensory domain of CckA comprises a transmembrane region followed by two PAS sensory domains, referred to as PAS A and PAS B (Figure 3.4).
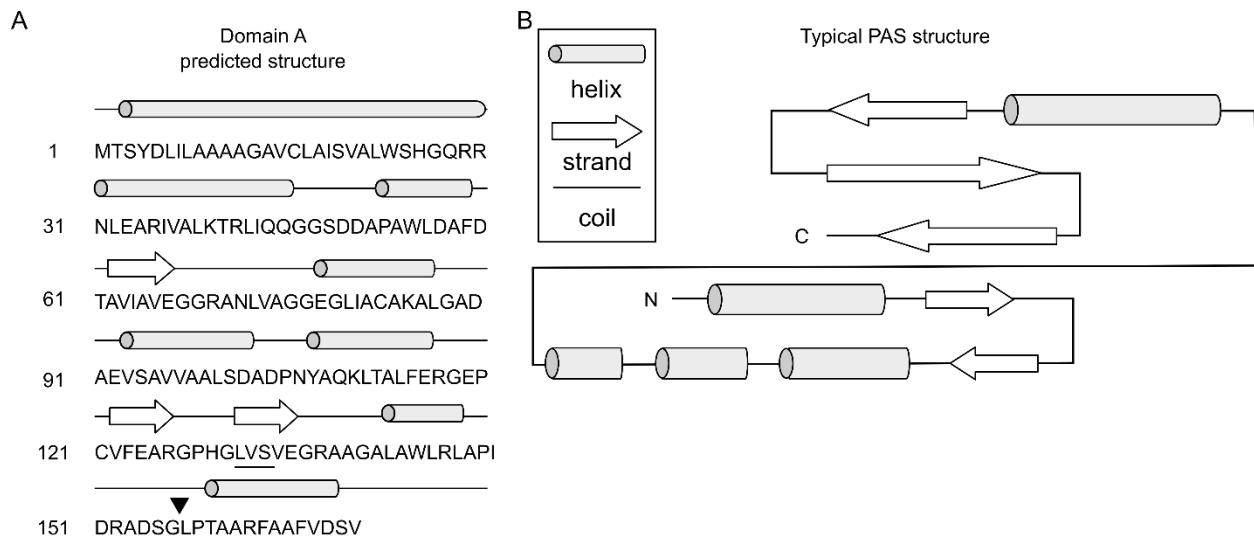
Figure 3.3: The DivL DUF Domain A does not have a predicted PAS-like structure (A) The secondary structure of Domain A was predicted based upon primary sequence by PSIPRED[165]. The arrow points to the designation of the end of DUF3455. The underlined residues indicate the signal transmission motif-like sequences that dictated the 133 and 170 cut-offs. (B) Representative topology of the PAS domain, adapted from Moglich, A., et al. *Structure* 17, 1282-1294 (2009).
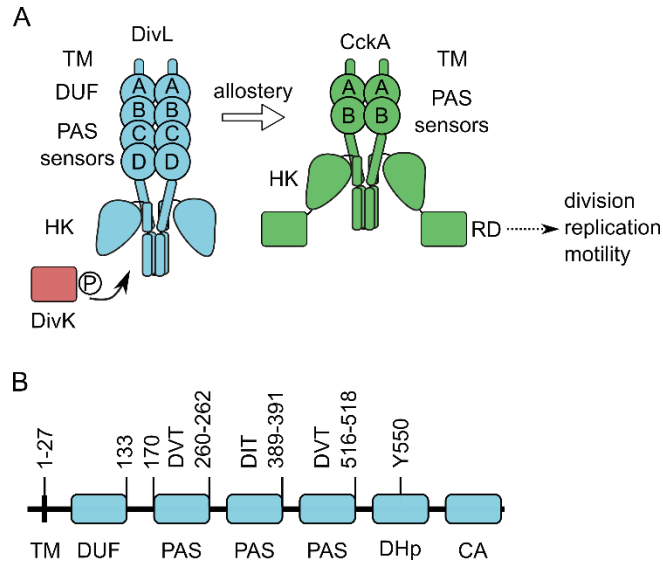
Figure 3.4: There are many potential domain interactions to allow for allostery between DivL and CckA DivL (blue) comprises a transmembrane (TM) region, a domain of unknown function (DUF), three PAS domains, and the HK. Phosphorylated DivK binds the HK region of DivL. CckA comprises a TM region, two PAS domains, and an HK domain. The allosteric interactions between DivL and CckA ultimately regulate division, replication, and motility. (B) Domain architecture of DivL with domain assignment cutoffs.

PAS domains are found in all kingdoms of life and regulate diverse processes by binding small molecules or facilitating protein-protein interactions and transmitting these signals to an output domain [31]. As discussed in Chapter 1, homologs of CckA (Figure 1.3) and DivL (Figure 3.5) have sensory domains with varying numbers and types of PAS domains. This indicates that PAS domains are modular and can be swapped to create new sensing and interaction capabilities.
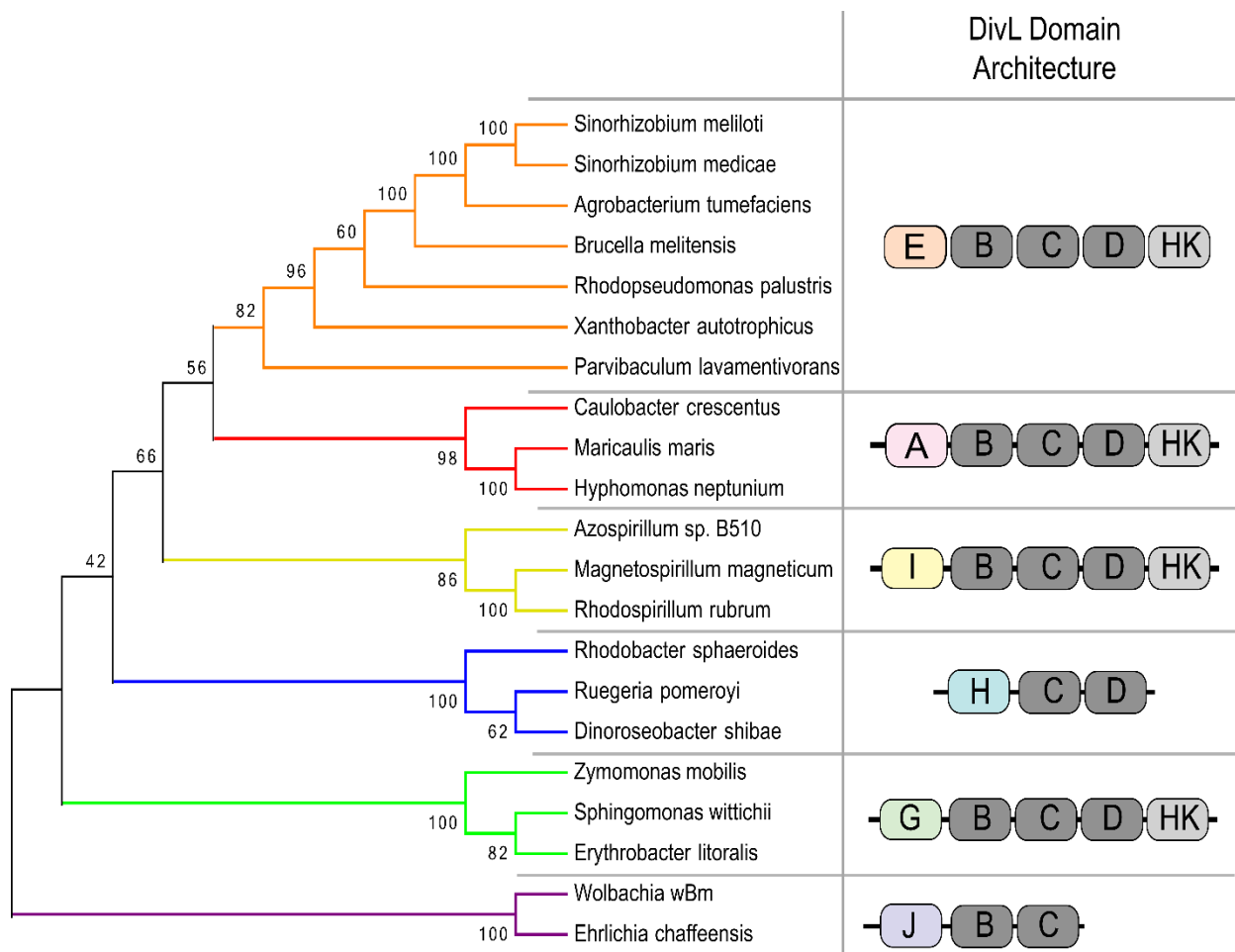
Figure 3.5: DivL homologs in alphaproteobacterial species show diversity and modularity in the composition of the sensory domain Analysis performed in collaboration with Wei Zhao.

Altogether, the combined five PAS domains and one DUF in DivL and CckA allow for the possibility of complex signal recognition, integration, competition, and intermolecular allostery (Figure 3.1). The distinct roles of the DivL sensory subdomains and a mechanism by which the DivL sensor communicates with the CckA sensor remain unknown. This information will contribute to the reversed signaling model in which DivK~P binding to DivL activates the sensory domain as an "effector" of CckA kinase activity[118]. The goal of the work described in this chapter is to interrogate the role of DivL's individual domains in performing each potential pseudokinase

function. From our experimental observations we propose a model for how DivL's subdomains work as an integrated system to orchestrate localization and enzymatic control of the DivL-CckA signaling complex.

3.2 Results

Domain A and the HK of DivL regulate cell-pole binding We designed and constructed a set of DivL variants with the sensory subdomains deleted individually to determine their roles in both DivL localization and CckA activity modulation. The ability for DivL to form foci at the cell poles is critical for both recruiting and regulating CckA[21, 90]. We, therefore, analyzed the role of each DivL sensory domain in DivL subcellular localization by creating variants with a C-terminal mCherry fluorescent protein fusion. DivL-mCherry expressed in the wild-type background exhibits diffuse localization in about 40% of cells and forms foci at one or both poles in about 50% of cells (Figure 2.2E-F). This is a similar subcellular distribution as observed when the fluorescently-labelled DivL is expressed as an additional copy[21, 126]. DivL was still able to localize to the cell poles when the HK domain was truncated (Figure 2.2E-F), so we deleted each sensory domain to identify their roles in dictating foci formation. Each domain deletion variant could form a focus except DivL-ΔA(Δ28-133) (Figure 3.6A, C). From these domain deletion localization experiments we conclude that the N-terminal Domain A is required for DivL to accumulate as a focus at the cell pole.
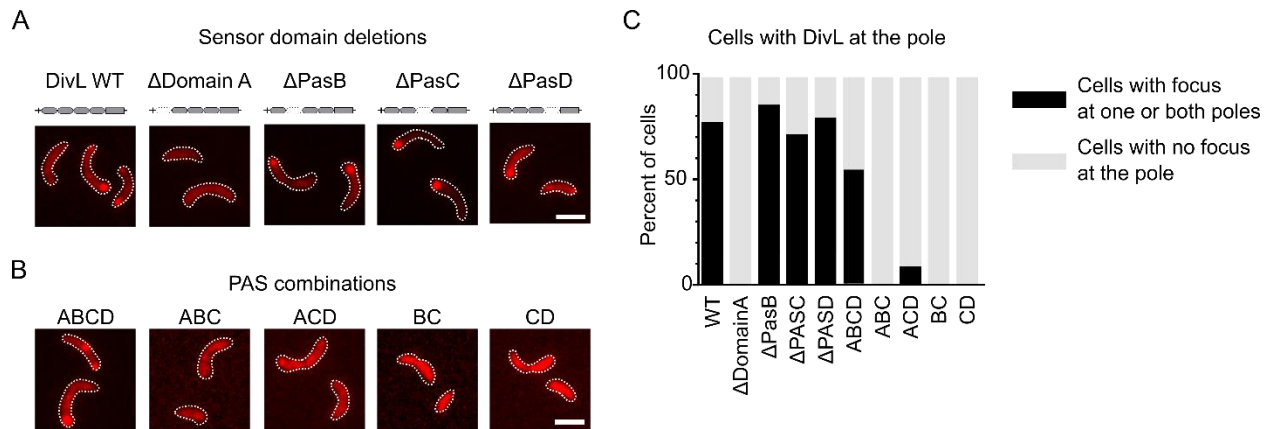
Figure 3.6: Domain A is required, but not sufficient, for DivL localization (A) Fluorescence microscopy to visualize the subcellular localization of DivL-mCherry domain deletion variants and (B) A panel of PAS domain combinations. The variants in A-B were induced from the chromosomal xylose promoter in M2G supplemented with 0.03% xylose for 4 hours. Scale bar denotes 2 µm. (C) Quantification of the percent of cells with DivL localization at the cell pole. N>36 cells.

We next asked if Domain A could serve independently as a minimal localization motif. We constructed several PAS domain combinations, based upon the conservation of these domains in select alphaproteobacteria (Figure 3.5). These constructs included DivL ABCD, ABC, ACD, BC and CD. We observed that the ABCD sensory domain construct, lacking the HK domain, accumulated as a focus in cells similar to wild-type. In contrast, removal of PAS B (i.e. ACD) or PAS D (i.e. ABC) from the ABCD construct abolished cell pole accumulation (Figure 3.6B-C). The ability to retain DivL's cell pole accumulation upon removal of PAS B or PAS D in the full-length construct, but not removal PAS B or PAS D in the context of ABCD construct suggest that these sensory domains and the HK domain may play redundant roles.

To further test the redundancy between the BCD domains and the HK domain, we constructed a DivL variant that lacked the BCD sensory domains termed TM-Domain A-HK. We observed that TM-Domain A-HK could accumulate at the cell poles in a similar manner as wild-

type DivL (Figure 3.7). This construct provided further support that DivL's BCD and HK domains play redundant roles in the recruitment of DivL to the cell poles. We next, asked if DivL's BCD and HK domains could be removed and retain DivL's cell pole accumulation. We observed that Domain A(28-133) with or without the transmembrane domain was unable to form foci and instead displayed diffuse localization (Figure 3.7A-C). We then defined a broader region of Domain A that is predicted to contain a helical coil leading into PAS B to determine if this C-terminal linker influenced Domain A's localization. This construct, DivL(28-170) also displayed diffuse localization with or without the transmembrane domain (Figure 3.7B-C). Removal of the transmembrane domain from either minimal TM-Domain A-HK construct resulted in loss of DivL's cell pole localization (Figure 3.7). From these experiments we conclude that Domain A in combination with the transmembrane or the C-terminal coiled-coil linker is insufficient for DivL's cell pole accumulation. Moreover, localization of DivL strictly requires Domain A and appears to work cooperatively with domains BCD or the HK domain to bind to factors at the cell poles.
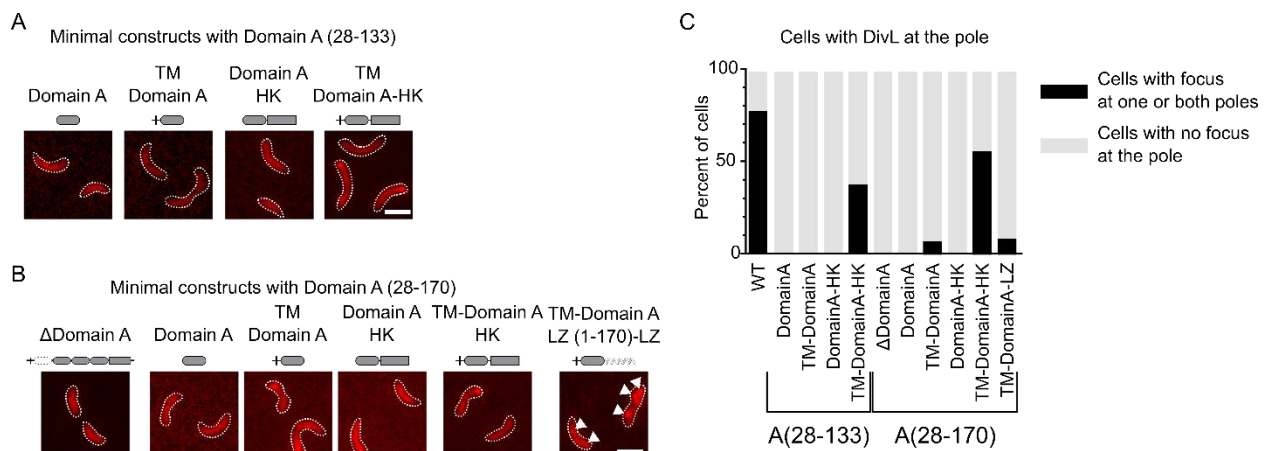
Figure 3.7: Domain A and the HK are minimally sufficient for DivL localization (A) a panel of potential minimal localization constructs in *C. crescentus* using Domain A (28-133). (B) A panel of potential minimal localization constructs using Domain A (28-170). Patchy localization is marked with a white arrow. The variants in A-B were

72

induced from the chromosomal xylose promoter in M2G supplemented with 0.03% xylose for 4 hours. Scale bar denotes 2 µm. (C) Quantification of the percent of cells with DivL localization at the cell pole. N>36 cells.

To probe whether domains BCD or the HK domain are merely serving to dimerize Domain A (1-170), we fused a leucine zipper to residue 170 to induce dimerization. This construct did not form distinct, round foci but appeared as irregular patches within the cell body, which may be due to misfolding or aggregation (Figure 3.7B-C, white arrows). These results suggest that dimerization of Domain A alone is insufficient to promote DivL accumulation at the cell poles. From this domain analysis, we conclude that direct or fuctional interactions between Domain A and the HK or BCD sensory domains may regulate DivL's localization pattern.

DivL's Domain A and the HK are sites of interaction for the scaffolds PopZ and PodJ
We next investigated whether Domain A mediates DivL's cell pole localization through protein-protein interactions with two key cell-pole scaffolds: PodJ or PopZ. Past studies from Curtis et al. have shown that PodJ plays a role in directly or indirectly recruiting DivL to one cell pole in *C. crescentus*[121]. Holmes et al. showed that PopZ and DivL interact in a heterologous *E. coli* reconstitution assay[162]. Similarly, we expressed DivL variants with either PodJ or PopZ in *E. coli* and measured their co-localization as an indication of interaction (Figure 3.8). A correlation score of 1 indicates complete co-localization and a score of -1 indicates no co-localization. Wild-type DivL co-localized with PopZ and to a lesser extent PodJ. We observed that DivL Domain A alone co-localized with both PopZ and PodJ. Expression of wild-type DivL and Domain A(33-133) disrupted the typical monopolar localization pattern of PopZ in *E. coli* indicative of an interaction[162]. We also observed that DivL-ΔTMΔA was able to co-localize with PopZ and PodJ. In fact, the populations of cells expressing PodJ with DivL-ΔTMΔA or DivL-Domain A(33-133) were not significantly different. These results are consistent with earlier studies that have

73

suggested a cell-pole binding site at the C-terminus of DivL[106, 122, 126]. Moreover, they suggest that DivL may have two distinct binding sites for PopZ and PodJ: Domain A and the HK domain. A potential localization factor that we have not thoroughly examined is the TM domain. Future localization studies in *C. crescentus* should include the DivL-ΔTMΔA construct that was found to co-localize with PopZ and PodJ in *E. coli* (Figure 3.8) to determine if the TM can inhibit localization in DivL-ΔA (Figure 3.6).
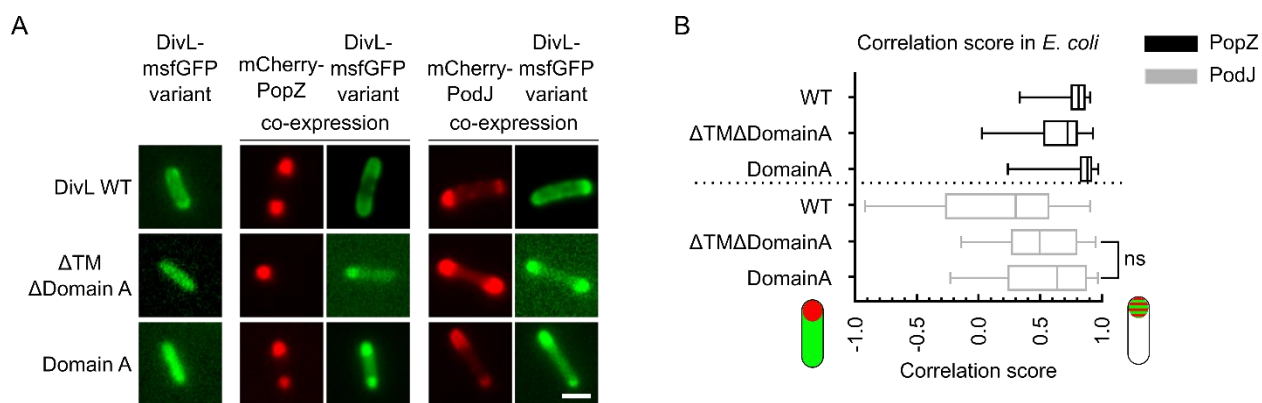
Figure 3.8: DivL has redundant binding sites for the scaffolds PopZ and PodJ (A) Heterologous expression of DivL-msfGFP variants with mCherry-PopZ or mCherry-PodJ in *E. coli*. DivL variants were induced from the pBAD plasmid with 10 mM arabinose for 2 hours. mCherry-PopZ and mCherry-PodJ were induced from the pACYC plasmid with 0.05 mM IPTG for 2 hours. Scale bar denotes 2 µm. (B) Quantification of co-localization between the DivL variants and PopZ or PodJ in Figure 7C. A correlation score of +1 indicates complete co-localization and a score of -1 indicates no co-localization. The center line is the median and the box extends to the 25th and 75th percentiles. The whiskers lie at the minimum and maximum values. Significance was determined using Tukey's multiple comparisons tests. Comparing the three DivL variants combined with the same scaffold have P-value<0.0037 except for the difference between DivL-ΔTM ΔDomain A compared to DivL-Domain A when co-expressed with PodJ. N>72 cells for all samples.

Signal stimulation of PAS C may regulate cell pole binding While deletion of the individual PAS domains did not result in a loss of cell pole localization, we asked whether disruption of potential PAS domain signal binding or protein-protein interactions could impact localization. One binding partner candidate that we know to interact with DivL is DivK~P[69, 90]. An *in vitro* binding assay demonstrated that PAS C and PAS D are both required for phospho-specific DivK binding[69]. Deletion of these domains did not impact DivL localization, so we used a homology model of the DivL PAS domains to predict conserved residues within the binding pocket or protein-protein interface and performed disruptive point mutations (Figure 3.9)[31]. The F292A mutation resulted in diffuse DivL localization while the V418A had a similar localization pattern as wild-type DivL-mCherry. Identification of F292 as a critical residue is consistent with the DivL-A288V genetic mutant characterized by Laub and co-workers[90]. This A288V mutation resulted in an elongated cell phenotype when expressed as the sole copy of DivL, which is characteristic of CckA mis-regulation. The residue A288 is adjacent to F292 within the same conserved small molecule binding pocket. The DivL-A288V mutation also caused the mis-localization of CckA, which could result from the possible mis-localization of DivL-A288V itself. Collectively we conclude that the PAS C small molecule binding site plays critical roles in regulating DivL localization and CckA kinase activity.
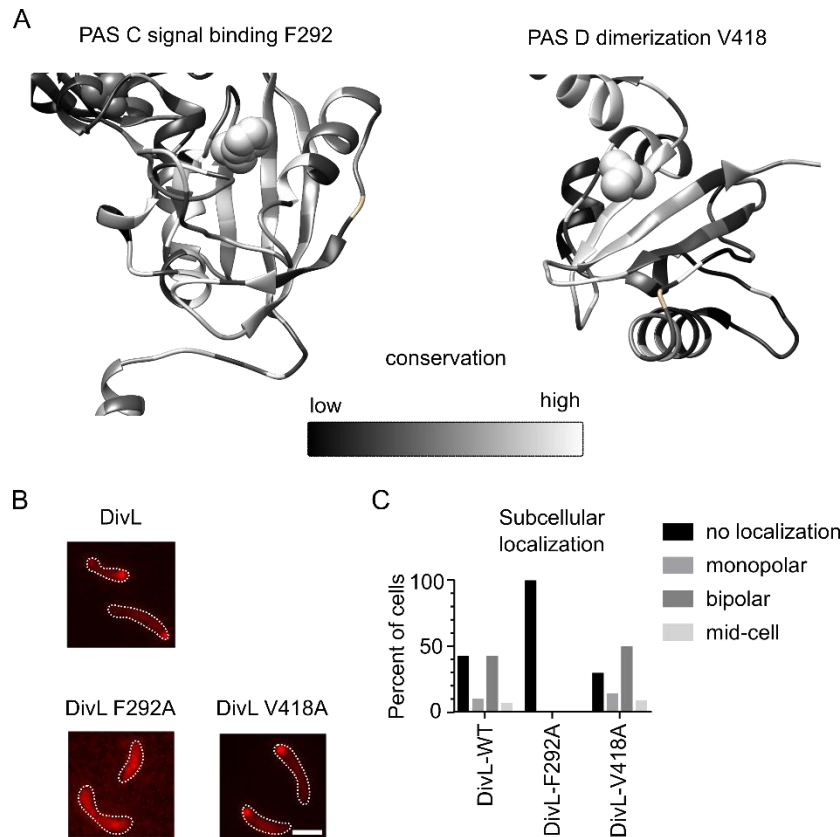
Figure 3.9: A predicted small molecule binding mutant in PAS C disrupts cell pole binding (A) Homology maps of DivL PAS C and PAS D. Regions that are more conserved among alphaproteobacterial DivL homologs are colored white and less conserved regions are colored black. The residues that were mutated are highlighted as spheres. (B) Fluorescence microscopy to visualize the subcellular localization of DivL-mCherry point mutants. The variants were induced from the chromosomal xylose promoter in M2G supplemented with 0.03% xylose for 4 hours. Scale bar denotes 2 µm. N>113

Several questions remain about the nature of the PAS C small molecular binding mutants. First, how do these DivL point mutants impact CckA kinase activity *in vivo* and *in vitro*? Secondly, do these point mutants impact DivL's ability to bind its cognate response regulator DivK in a phospho-specific manner? Finally, small molecule screens will be needed to identify small molecules that bind and regulate PAS C. In summary, interrogation of these questions will highlight the role of PAS C in the regulation of DivL-CckA signaling complex.

76

Integrating our results together with past studies[90] and our LZ stimulation studies (Chapter 2), we propose a model for how protein-protein interactions mediate DivL's cell pole localization (Figure 3.10A). PodJ and PopZ localize at the new cell pole where the transmembrane domain, Domain A, and the HK bind to these scaffolds to promote DivL's accumulation at the cell poles. DivK~P binding to the HK elicits a conformational change which is transmitted through the sensory helix to Domain A in order to regulate DivL's binding interactions with PopZ and PodJ. DivK~P, or a small molecule binding partner, similarly interacts with PAS C to regulate localization at the pole. Dynamic control of DivL scaffold binding must be required during the swarmer to stalked cell transition, where PopZ is still present at both poles, and PodJ accumulates at the new cell pole, but DivL remains diffuse (Figure 3.10B).
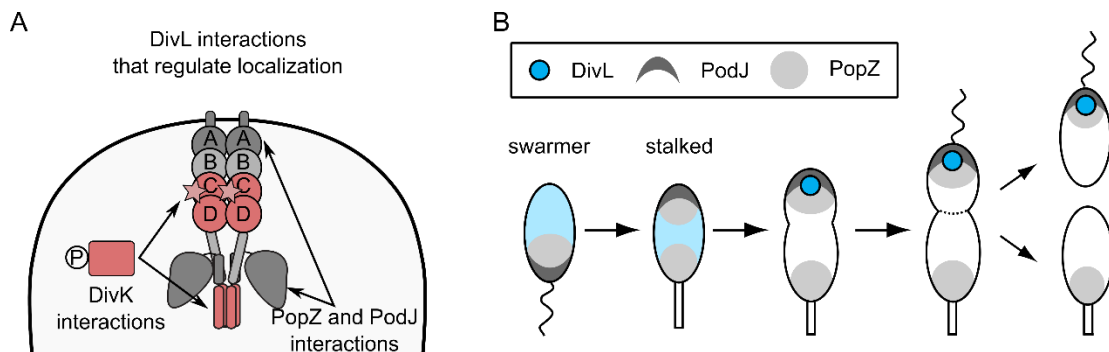
Figure 3.10: Annotation of the DivL domains that regulate localization (A) The transmembrane domain, Domain A and the HK (dark gray) regulate interactions with the scaffolds PopZ and PodJ (light gray background). PAS C and PAS D have been shown to regulate phospho-specific DivK binding (red)[69]. Point mutations within PAS C (red stars) that affect DivL and CckA[90] localization indicate that the interaction with another protein such as DivK~P regulates cell pole localization. (B) Cartoon of DivL, PodJ, and PopZ localization throughout the *C. crescentus* life cycle.

DivL's PAS B and PAS D are required for DivL-mediated regulation of the cell cycle

Previous models emphasize that DivL must localize at the correct pole at the correct time in the

cell cycle in order to modulate the active kinase CckA[106, 108, 120]. We have determined that Domain A and the HK mediate DivL localization at the pole through interactions with the scaffolds PodJ[121] and PopZ[162] (Figures 3.6-3.8, Figure 3.10). Additionally, point mutations to PAS C disrupted DivL localization (Figures 3.9-3.10) and CckA localization and activity[90]. The relationship between DivL localization and CckA activity are interconnected, as DivL localization to the new cell pole activates CckA kinase activity[21], but CckA activity causes DivL to become diffuse as a result of negative feedback[90, 120]. The leucine zipper experiments in Chapter 2 demonstrated that the sensor domain regulates the cell cycle through conformational changes in the sensor helix. We therefore, next investigated the roles of the individual sensory domains in CckA modulation.

We individually deleted each of the sensory subdomains, confirmed expression by Western blot analysis (Figure 3.11A), and evaluated the effect of their over-expression upon swarm size (Figure 3.11B-C). Swarm size may vary due to defects in swarmer cell motility, division, or chromosome replication[123]. Deletion of PAS B resulted in a small swarm size with an average area of 24% ± 3% of the empty vector control. In contrast, deletion of PAS D resulted in a larger swarm size with an average area of 90% ± 1% of the empty vector control. Over-expression of DivL-ΔA (Δ28-133) and DivL-ΔPAS C did not result in significantly different swarm areas compared to wild-type DivL. Intriguingly, the DivL-ΔA construct retains that capability to regulate swarm mobility (Figure 3.11). However, DivL-ΔA variant does not localize to the cell poles (Figure 3.6). This provides evidence that DivL can regulate the function of CckA away from the cell poles. Moreover, analysis of these DivL domain deletion variants indicate that PAS B and PAS D are involved in regulating swarm motility. Identification of PAS B's involvement in cell cycle regulation is consistent with a previous biochemical study that showed PAS B is required for inhibition of CckA autophosphorylation[107].
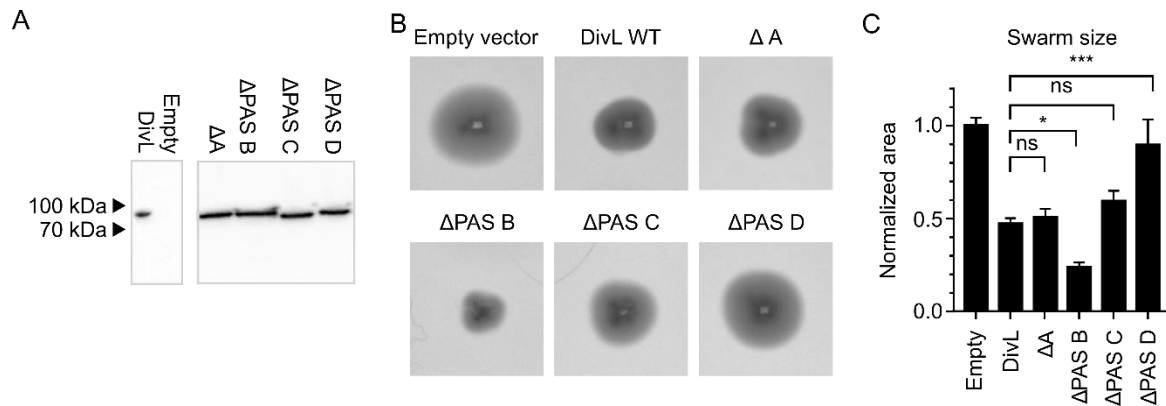
Figure 3.11: DivL's PAS-B and PAS-D are required for DivL mediated regulation of cell motility (A) Western blots were performed to confirm over-expression of DivL variants in the strains used in the PAS domain deletion swarm assays. (B) Motility assay of *C. crescentus* strains expressing DivL-M2 domain deletions. *C. crescentus* were stabbed into 0.3% PYE agar supplemented with 0.3% xylose and incubated at 28 ℃ for 3 days. (C) Quantification of the motility assay of *C. crescentus* strains expressing DivL-M2 domain deletions.

Functional PAS B and PAS D signal transmission motifs are required to mediate swarm-size reduction A conserved signal transmission motif is found at the C-terminus of PAS B, PAS C, and PAS D (Figure 3.12A). These 4 residues form a network of hydrogen bonds with themselves and the downstream signal transmission helix in order to transmit a conformational change in one domain to another. In Chapter 2 we made mutations to the signal transmission motif set of conserved D-(A/I/V)-(T/S)-E residues at the C-terminus of PAS D and found that the intact motif is required for DivL to reduce swarm size (Figure 2.6). We further made mutations to the signal transmission motif of PAS B (D260 and T262) and PAS C (D389 and T391) to map out the signal flow within the sensory domain (Figure 3.12). DivL variants with these mutations were over-expressed in *C. crescentus* cells. Western blot analysis showed that all of the variants were over-expressed but DivL-T391V (Figure 3.12B). Over-expression of DivL-WT reduced the swarm size to 49% ± 4% of the cells expressing the empty vector (Figure 3.12C-D). DivL-T262V over-expression resulted in a significantly larger swarm size compared to DivL-WT with an average

area of 73% ± 3%. Over-expression of DivL-ΔPAS B resulted in a smaller swarm size compared to wild-type DivL (Figure 3.11). This may mean that mutation of PAS B's signal transmission motif can not only inactivate but invert PAS B's signal response as demonstrated with similar mutations to the engineered light sensor YF1[7]. The mutations to the aspartates in the PAS B and PAS C signal transmission motif did not affect swarm size. Future studies will be required to investigate the impact of PAS C's D391A mutation, as in preliminary studies we did not observe expression of this variant by Western blot (Figure 3.12). In summary, we found that both PAS B and PAS D were required for DivL to exert its effect upon swarm motility (Figure 3.11), and it appears that the signal transmission motifs leading into these domains are critical for this function (Figure 3.12, 2.6).
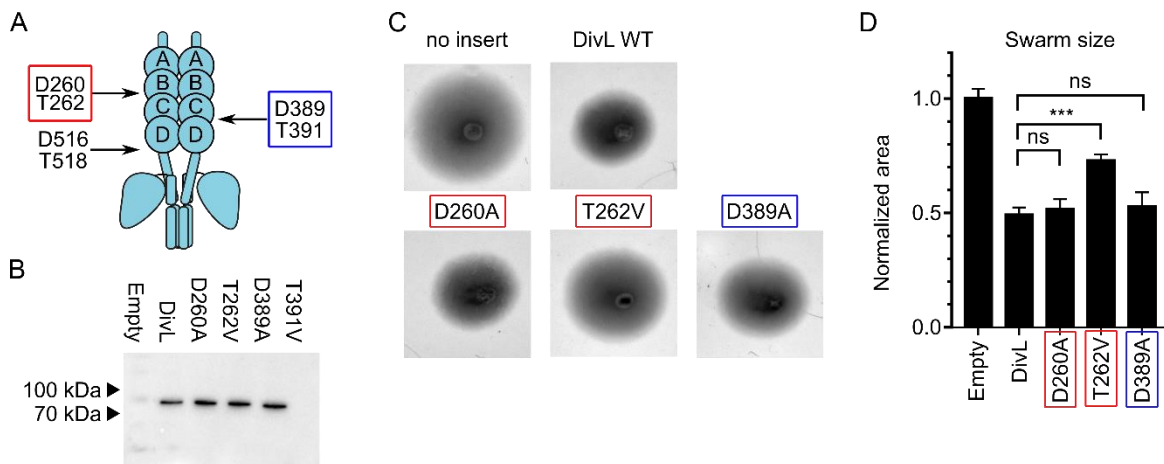
Figure 3.12: An intact PAS B signal transmission motif is required for swarm size reduction (A) Cartoon of DivL with the signal transmission motif residue numbers labelled. (B) Western blots were performed to confirm over-expression of DivL variants in the strains used in the DIT motif mutation swarm assays. (E) Motility assay of *C. crescentus* strains expressing DivL-M2 domain deletions. *C. crescentus* were stabbed into 0.3% PYE agar supplemented with 0.3% xylose and incubated at 28 ºC for 3 days. (F) Quantification of the motility assay of *C. crescentus* strains expressing DivL-M2 domain deletions. Error bars represent SD (n=3). Significance was determined

with a Dunnett's multiple comparisons test by comparing the mean area of each strain to the mean area of DivL-WT (ns: P>0.05, *: P ≤ 0.05, **: P ≤ 0.01, ***: P ≤ 0.001).

PAS B and the HK domain are not required to stimulate an increase in the CckA FRET sensor response The swarm assay detects defects in motility, replication, and division due to DivL variant over-expression in the bulk population[123]. In order to report directly on CckA activity at the subcellular level, Samuel Duvall in our lab recently developed and validated a CckA FRET (Fluorescence Resonance Energy Transfer) sensor[166]. This CckA FRET sensor is based upon conformational changes in CckA's structure and contains the FRET-active pair mClover3 and mRuby3 (R_0 of 6.43 nm) which undergo changes in FRET upon CckA conformational changes (Figure 3.13). FRET response is reported as the ratio of the FRET signal to the emission of the donor, mClover3. The FRET sensor was shown to detect changes in the CckA conformation throughout the cell cycle[152, 167], indicating that it is sensitive to changes in activity states. The FRET sensor also responded to over-expression of wild-type DivL, presumably because DivL can stimulate CckA conformational changes that promote phosphatase[168] or kinase[21, 90, 107] functions. Here we utilized the CckA-FRET sensor to determine which domains of DivL are required to modulate CckA's conformational state.
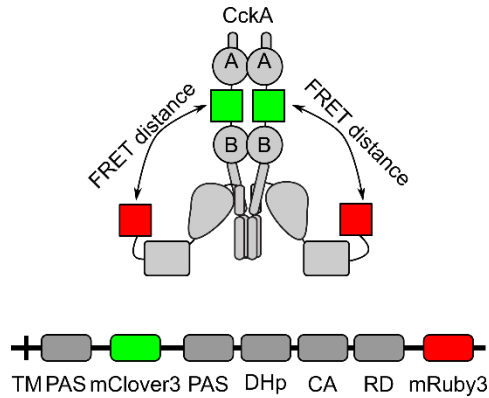
Figure 3.13: A cartoon of the CckA FRET sensor The mClover3/mRuby3 FRET pair is embedded into the *C. crescentus* CckA protein such that conformational changes produce measurable changes in the FRET interaction[166].

For this set of experiments, we over-expressed DivL domain deletion variants in a *C. crescentus* strain expressing a copy of the CckA FRET sensor under inducible control in addition to the native *cckA*. When over-expressing wild-type DivL, the FRET/mClover3 ratio at the new cell pole significantly increased. Over-expression of the sensor alone truncated at DivL-565 and DivL-ΔPAS B also led to increases in the observed FRET/mClover3 versus the wild-type strain (Figure 3.14A, C, F). Thus the HK domain and PAS B are not required to stimulate an increase in the FRET/mClover3 ratio. In a similar manner we also observed that the HK domain and PAS B were dispensable for DivL's over-expression impact upon swarm size reduction (Figure 2.2D, Figure 3.11)[143, 155]. Therefore, collectively we can conclude that DivL's PAS B and HK domains are not required to mediate changes in CckA conformational state and downstream signaling.
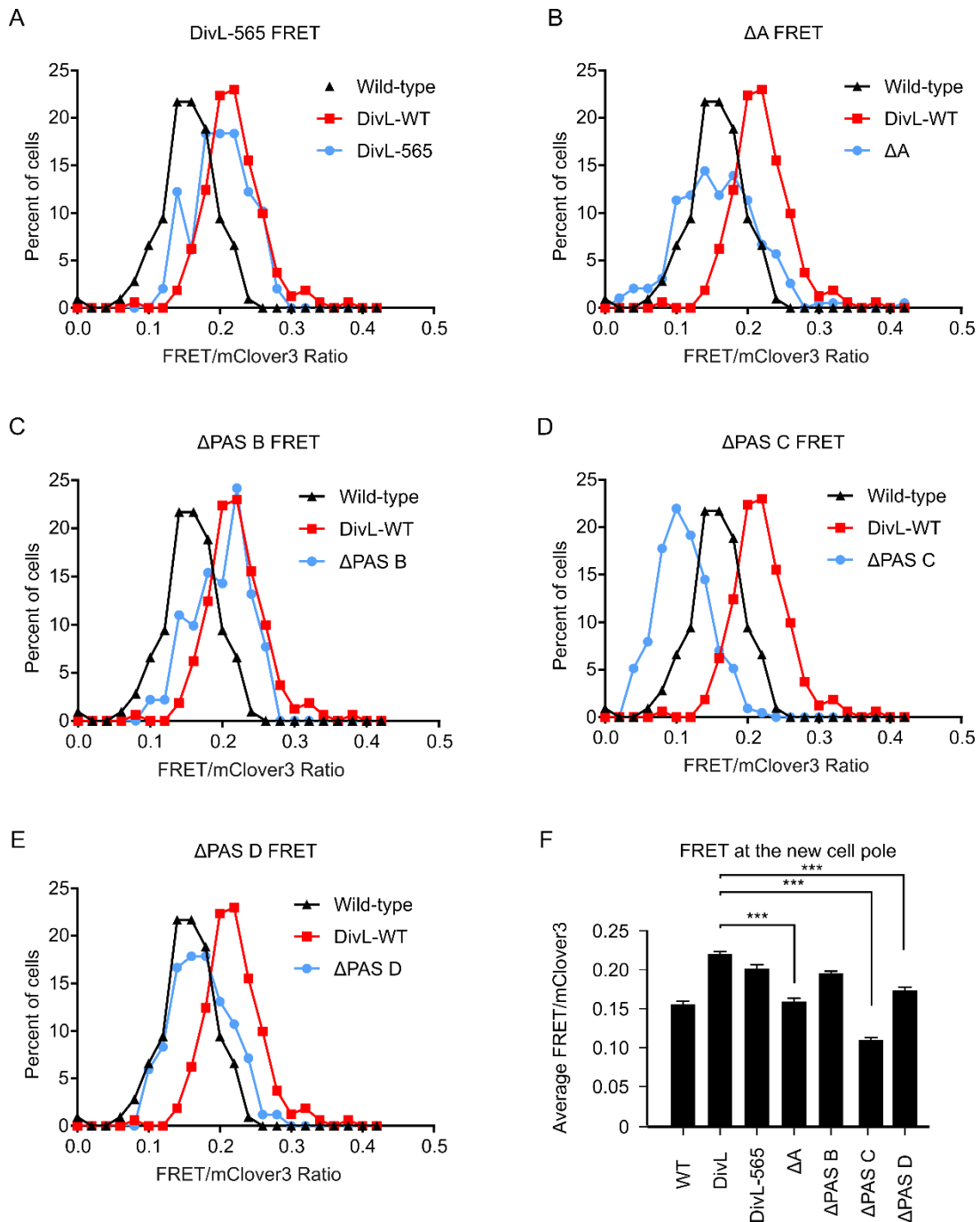
Figure 3.14: PAS C, PAS C, and PAS D regulate the CckA FRET sensor conformation (A)-(E) Histograms of the FRET/mClover3 ratio at the new cell pole in N>84 cells. Wild-type *C. crescentus* cells expressed the CckA FRET sensor induced with 0.03% xylose and over-expressing the DivL domain deletion variants induced with 0.5 mM vanillate for 3 hours. Fluorescence microscopy was used to visualize the subcellular localization of the CckA FRET sensor and to measure FRET intensities. (F) Average of the FRET ratio of the cells shown in the histograms in A-E.

PAS A and PAS D are required to stimulate an increase in the CckA's FRET sensor's FRET/mClover3 In contrast, the over-expression of DivL-ΔA resulted in a significant loss of DivL's effect on the CckA FRET sensor at the new cell pole (Figure 3.14B, F). This is consistent with the inability of DivL-ΔA to localize at the cell poles (Figure 3.6). Therefore, we conclude that the DivL-ΔA cannot exert an impact upon the CckA FRET sensor at the new cell pole due to its loss of new cell pole accumulation. Similarly, over-expression of DivL-ΔPAS D resulted in little change in the observed CckA FRET/mClover3 ratio (Figure 3.14E, F). Moreover, over-expression of DivL-ΔPAS D resulted in little change in swarm size compared to the empty vector (Figure 3.11C). These results suggest that PAS D may play a role in mediating the interaction between DivL and CckA.

DivL-ΔPAS C results in a decrease in the FRET/mClover3 ratio Expression of DivL-ΔPAS C had the remarkable effect of reducing the FRET/mClover3 ratio relative to wild-type Figure 3.14D, F). Notably, the deletion of PAS C did not affect subcellular localization (Figure 3.6) or swarm motility (Figure 3.11). However, disruptive point mutants with in PAS C disrupt DivL's cell pole localization (Figure 3.9) and impact CckA activity[90]. Therefore, PAS C may serve a unique role in localizing CckA at the cell pole and regulating CckA activity. The origins of the decrease in FRET/mClover3 ratio require more investigation but suggest that PAS C plays a role in modulating whether CckA exists in a conformational state that exhibits low or high FRET/mClover3 ratio states.

Each sensory domain has one or more roles in DivL function We have used DivL subcellular localization in *C. crescentus*, *E. coli* heterologous expression, swarm activity, and the CckA FRET sensor assays to annotate the roles of each of the DivL sensory domains. Our work has shown that Domain A, PAS C, and the HK domain play roles in DivL's localization at the cell

poles (Figure 3.15). Past work from Mann et al. have shown that PAS B is required for regulation of CckA phosphatase activity[107]. Here, we have shown that PAS B and PAS D play a role in regulating *C. crescentus* motility changes and CckA conformational changes upon DivL over-expression (Figures 3.10-3.12, Figures 3.14-3.15). We further found that functional signal transmission motifs of PAS B and PAS D are required to mediate these effects (Figure 3.12, Figure 2.6). This indicates that the PAS B and PAS D sensory motifs are necessary for transmitting signal from the HK into these sensory domains or from one sensory domain to another. We propose that PAS C makes a contact with DivK~P or another binding partner to modulate CckA activity[90] (Figure 3.15) and DivL localization (Figure 3.10). Our studies have identified that DivL interacts with three distinct signaling inputs via Domain A and the HK domain (PopZ, PodJ, DivK~P). These binding interactions control DivL's output (CckA activity) via PAS BCD (Figure 3.15).
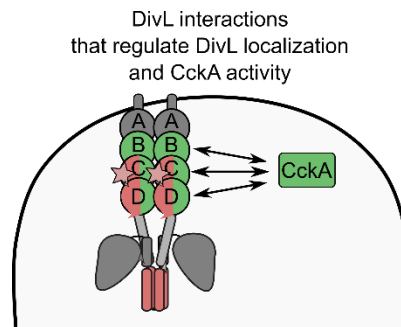
Figure 3.15: Annotation of the DivL domains that regulate DivL localization and CckA activity PAS B, PAS C, and PAS D regulate CckA activity (green). Domains that interact with the scaffolds PopZ and PodJ are colored dark gray and the domains that interact with DivK are colored red. PAS C and PAS D have been shown to regulate phospho-specific DivK binding (red)[69]. Point mutations within PAS C (red stars) that affect DivL and CckA[90] localization indicate that the interaction with another protein such as DivK~P regulates cell pole localization.

The CckA receiver domain competes with DivK for binding to DivL's HK domain

However, the mechanism of how DivL exerts its effect on CckA remains unclear. Does DivL

directly bind to CckA? How do conformational changes within DivL affect CckA activity? We followed up on our domain analysis with an initial *in vitro* binding assay to begin to answer these questions. When phosphorylated DivK binds to DivL, CckA activity changes[69, 90]. What remains unknown is how this binding event is propagated as a signal to CckA. One model is that DivL and CckA always interact, and DivK~P binding changes the conformation of the complex. Another model is DivL binds to either DivK~P or CckA in a competitive manner causing a conformational change in CckA depending on its interaction state. A fluorescence polarization experiment was performed to distinguish between these possibilities (Figure 3.16A). Purified DivK was labelled with a fluorescent BODIPY dye and phosphorylated by its kinase DivJ. It was then combined with DivL and fluorescence polarization was measured. As in a previous study[69], DivK~P was found to bind to DivL in solution. Purified CckA was added and the fluorescence polarization decreased, representing the release of free DivK-BODIPY into solution. This result indicates that the addition of CckA mediates the displacement of DivK~P from DivL through competitive binding. We thus propose that the phosphorylation state of DivK ultimately regulates CckA by interfering with the CckA-DivL interaction that induces kinase activity.
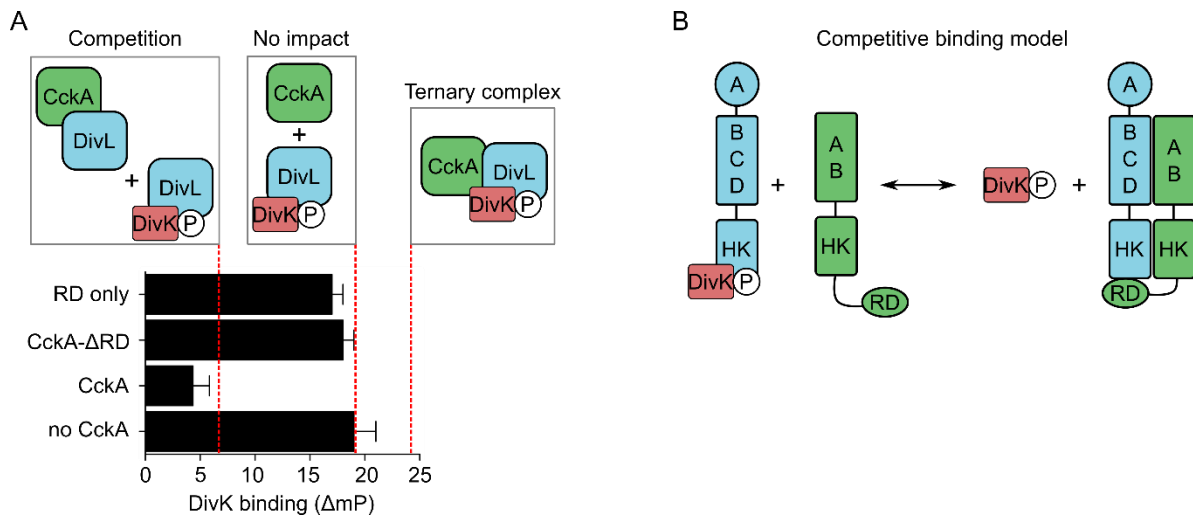
Figure 3.16: CckA disrupts the DivL-DivK~P complex *in vitro* (A) A fluorescence polarization binding assay determining if DivL binds DivK~P and CckA in a ternary complex or if DivK~P and CckA compete for DivL binding. BODIPY-labelled DivK was phosphorylated by its kinase DivJ and combined with DivL in solution. Each CckA construct was added to the existing mixture and fluorescence polarization was measured. Error bars represent SD (n=3). (B) A model showing that the receiver domain is important for the displacement of DivK~P from DivL.

The fluorescence polarization assay also included CckA-ΔRD and CckA-RD only to interrogate the role of the receiver domain (RD) in competing with DivK~P for DivL binding. When CckA-ΔRD was added, the DivL-DivK~P interaction was maintained. This indicates that the RD is needed to disrupt DivL-DivK~P binding. The RD is not the only domain required, however, as the RD alone was not able to disrupt DivL-DivK~P binding. We envision a model in which DivL and CckA form an interface at their sensory and HK domains. The position of CckA's RD domain is dictated by the presence or absence of DivK bound to DivL's HK domain (Figure 3.16B). In the absence of DivK~P, CckA's RD domain may bind to DivL's HK domain. However, DivK~P may compete with CckA's RD domain for interaction with interaction with the HK domain. We thus propose that this DivK~P mediated conformational change may regulate CckA's function as kinase or phosphatase.

87

PopZ and DivL both have roles in recruiting CckA to the new cell pole CckA exhibits

a complex localization pattern in which a fraction of pre-divisional cells are bipolar and some are

monopolar[152]. This raises the question of how CckA's localization pattern is dynamically

controlled in cells. The prevailing models suggest that DivL is required to anchor CckA at the cell

pole[21, 90]. In these studies, CckA did not accumulate at the new cell pole when DivL localization

is diffuse. We took advantage of our DivL-mCherry fusion that fails to localize to the new cell

pole (Figure 2.2E, Figure 3.17). This strain was viable and had a similar doubling time (152 ± 44

minutes) than wild-type cells (144 ± 20 minutes) when induced with 0.03% xylose. Surprisingly,

CckA-mClover was visualized at the new cell pole independent of DivL localization in 52% of

cells. This agrees with the findings in the initial CckA FRET sensor study[166] that suggest a model

in which CckA initially binds to PopZ at the new cell pole and DivL arrives later. We hypothesize

that complex binding interactions between DivL, DivK, CckA, and PopZ occur to orchestrate

CckA's dynamic cell cycle-dependent localization and activity changes.
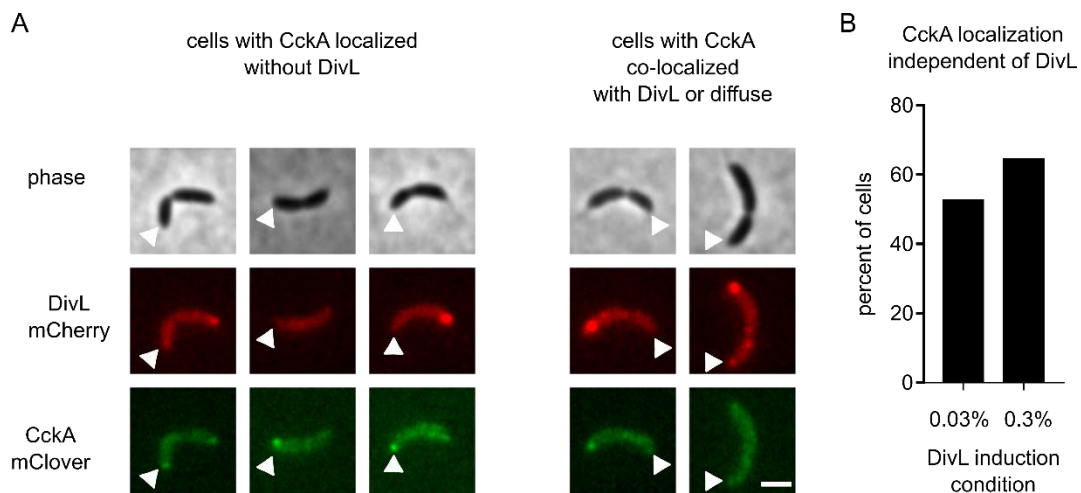
Figure 3.17: CckA can localize to the new cell pole without DivL localization at the new cell pole (A)
Fluorescence microscopy to visualize a sole-copy of xylose-inducible DivL-mCherry and CckA-mClover under the
cckA promoter. DivL-mCherry was expressed using 0.03% xylose for 3 hours. White arrows point to the new cell

pole. Scale bar denotes 2 µm. (B) Quantification of CckA localization in the strain in A at two different DivL-mCherry induction conditions. N>103 cells.

Initial studies show that DivL constructs have measurable effects on CckA activity *in vitro*. The CckA FRET activity reporter and swarm motility assay were useful for screening DivL variants for their effect upon CckA conformation and downstream cell cycle phenotypes. We developed an *in vitro* CckA kinase activity assay in order to directly measure DivL modulation of CckA activity in solution. Mann and co-workers have previously established a CckA radiometric phosphorylation assay in which CckA is recruited to liposomes that mimic the *C. crescentus* membrane[107, 168]. It was demonstrated that CckA activity depended on its density on the liposomes[168]. The addition of DivL to the CckA solution resulted in a decrease in CckA kinase phosphorylation, again in a liposome-dependent manner[107]. A DivL mutant that activates CckA activity *in vivo*[69, 90], DivL-A601L, however, stimulated CckA kinase activity[107]. This assay was used to evaluate several CckA domain deletions and DivL variants for their effects on CckA kinase activity (Figure 3.18A). We decided to combine this liposome assay with a coupled ATPase plate assay protocol that was established for CckA activity[145, 169] to gather data at more time points for kinetic analysis. We have performed preliminary work to establish this assay in the lab and begin to assess DivL variants for their effect on CckA activity *in vitro*.
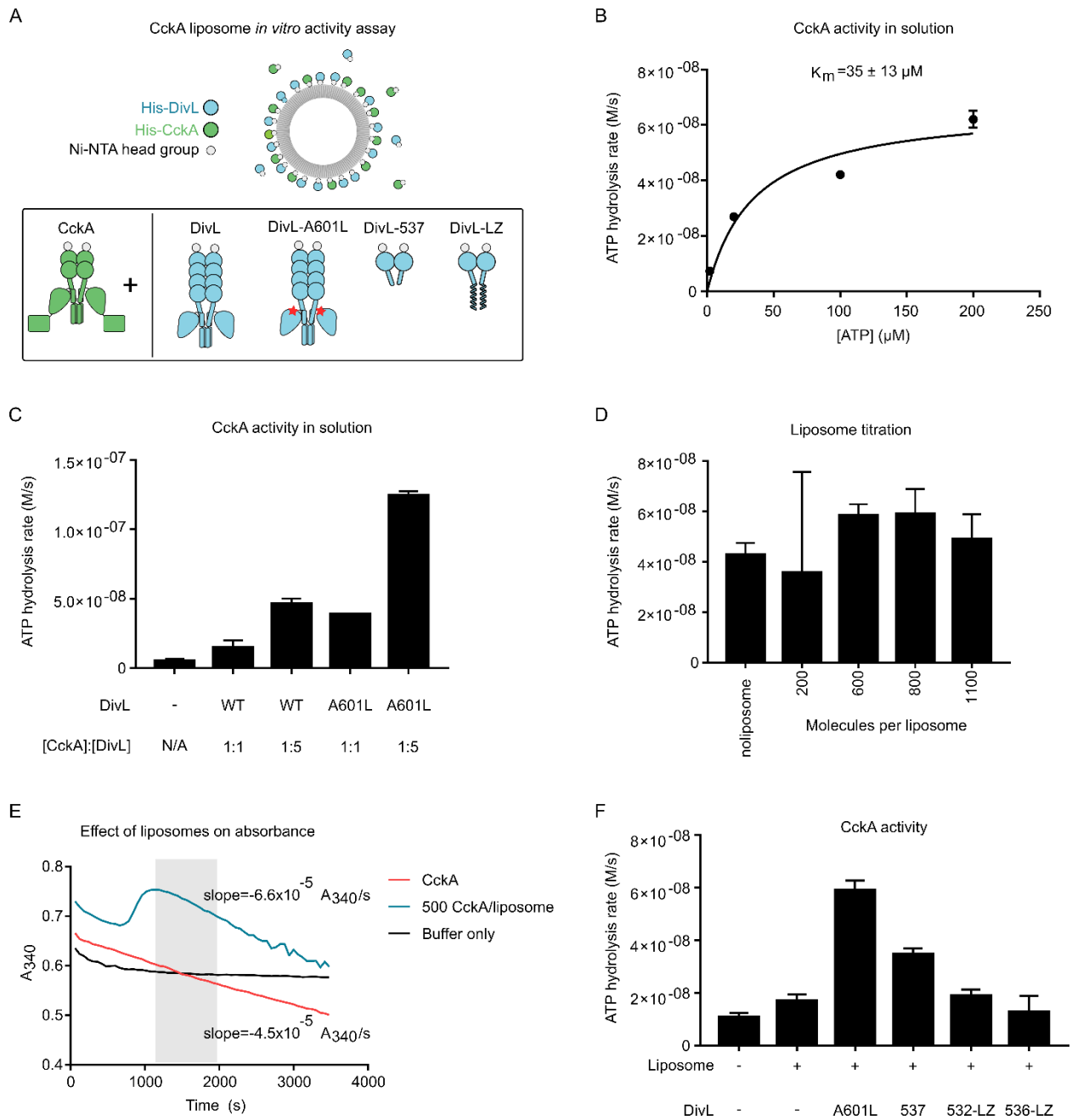
Figure 3.18: DivL modulates CckA kinase activity in solution and on liposomes (A) A cartoon of DivL and CckA

assembly on liposomes as described in previous studies[107, 168]. (B) Coupled enzyme assay with CckA at varying ATP

concentrations. 5 µM CckA was incubated in solution and autophosphorylation began with the addition of ATP. A_{340}

was measured every 60 seconds for an hour and the rate of ATP hydrolysis was calculated using the slope of A_{340} vs.

time. (C) DivL and DivL A601L stimulate CckA kinase activity in solution in a dose-dependent manner. The coupled

enzyme assay was performed with 2.5 µM CckA and either 2.5 µM or 5 µM DivL variant. (D) CckA coupled enzyme

with no liposome assembly or varying loading densities on liposomes. 5 µM CckA was incubated in solution with the calculated volume of liposomes needed to achieve each loading density. Autophosphorylation began with the addition of ATP. (E) Raw absorbance data over time for 5 µM CckA in solution alone or assembled at a half-maximum density of 500 molecules/liposome. Slopes used to determine ATP hydrolysis rates were calculated within the linear region shaded in gray. (F) Several DivL variants were screened for their effect upon CckA activity on liposomes. 5 µM CckA and 5 µM DivL variant were mixed in solution. Liposome solution was added for a loading density of 500 CckA molecules/liposome and 500 DivL molecules/liposome. All error bars represent SD of duplicate wells from one trial.

We first performed the coupled enzyme assay with CckA alone in solution (Figure 3.18B). After one trial, we observed that CckA activity was dependent upon ATP concentration with a K_m value of 35 ± 13 µM with 5 µM CckA. This is roughly similar to the K_m value found by Vo and co-workers of 17.9 ± 1.7 µM[169] for the same CckA concentration and confirms that our purified CckA was active. We next wanted to replicate the results of combining DivL or DivL-A601L with CckA. An initial trial demonstrated that both wild-type DivL and DivL-A601L increased CckA kinase activity in a concentration-dependent manner in solution (Figure 3.18C). Wild-type DivL being able to activate CckA in solution is in line with our predictions based on *in vivo* studies that show that DivL, unbound from DivK~P, activates CckA activity at the new cell pole[21, 90]. However, to address the discrepancy[107], we must rule out the possibility that the DivL variants were co-purified with another ATPase that could be contributing to the added kinase activity. A DivL-variant-only control, as well as the combination of each DivL variant with the catalytically dead CckA-H322A[169] will be performed during forthcoming assays. The discrepancy between these two assays may also arise from differences in protein purification batches or the type of assay (radiometric dot blot vs. coupled-enzyme).

We are eager to study the DivL variants that we used in the swarm and FRET assays *in vitro* to untangle the effects of localization, scaffold binding, and transcriptional feedback. We

started with preliminary studies of two DivL-LZ variants in the coupled enzyme kinase assay. This assay was performed with assembly of the proteins on the liposome. For CckA alone, the volume of liposome solution that was added to the mixture was calculated for a density of 500 molecules/liposome. The maximum loading density calculated previously[168] is 1100 molecules/liposome. When including DivL, CckA and DivL were mixed in solution and liposomes were added for a density of 500 CckA and 500 DivL molecules/liposome. Unlike previous studies[107, 168], we observed that CckA activity was not responsive to changes in loading density (Figure 3.18D). We noticed that adding the lipid solution into the assay interfered with the absorbance used to detect NADH oxidation (Figure 3.18E) so absolute rates may not be attainable with this set-up, and it appears that liposomes may not be necessary (Figure 3.18C). However, we found that we were able to compare rate changes for each of the DivL constructs.

Consistent with our initial trials in solution however, the addition of DivL-A601L on liposomes greatly increased CckA activity compared to CckA alone in solution or on liposomes. DivL-537, the base construct for the leucine zipper fusions, also activated CckA. Two of the leucine zipper constructs, DivL-532-LZ and DivL-536-LZ, did not have an activating effect on DivL-CckA complex. These constructs were initially chosen to be purified due to their differences in the DivL subcellular localization assay (Figure 2.12A-B) However, over-expression of these constructs resulted in similar, large swarm sizes, indicating that they both lost their ability to modulate the CckA pathway (Figure 2.9C, Figure 2.10). In addition, we observed that the impact of DivL-532-LZ and DivL-536-LZ upon CckA *in vitro* was similarly negligible. Future assays will expand upon these results and include DivL(54-769) as a control and the remaining DivL-LZ fusions. We hypothesize that the leucine zipper fusions will modulate CckA in a periodic manner, as described in the localization and swarm assays in Chapter 2.

3.3 Discussion

Here we have identified several of the ways that DivL acts as a pseudokinase to modulate a cell-cycle pathway. PAS B, PAS C, and PAS D all have modulating effects on the active kinase CckA (Figures 3.11-3.12, Figure 3.14). We identified a potential small molecule binding site within PAS C that regulates cell pole binding and the cell cycle[90] that could allow DivL to act as a bifunctional switch (Figure 3.9). Domain A and the HK are required for DivL to localize to the cell pole (Figures 3.6-3.7) where it may in turn anchor CckA[21, 90]. Moreover, our analysis suggests there may be complex and competitive binding interactions between DivL, DivK, CckA, and PopZ (Figures 3.8, Figure 3.16).

Together with the domain annotation, the competitive binding model led us to a refined model of how DivL regulates the CckA pathway (Figure 3.19). At the old cell pole, DivJ phosphorylates DivK~P[161], which binds to DivL[90]. This prevents CckA's RD domain from binding to DivL, which promotes CckA phosphatase activity at the old cell pole. At the new cell pole, DivK is de-phosphorylated by PleC and no longer binds to DivL[90]. CckA and DivL now interact within their sensory and HK domains, and CckA's RD binds to DivL's HK. According to previous studies, sequestration of the RD domain may promote CckA kinase activity[21, 90].
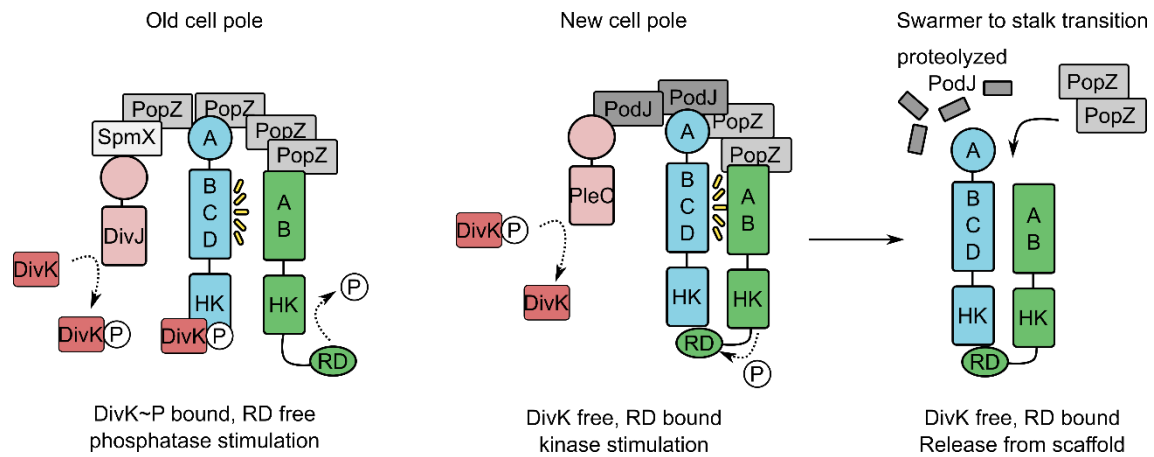
Figure 3.19: Model of DivL's pseudokinase functions regulating asymmetric localization and CckA pathway activity

In previous models, PodJ[121] and PopZ[162] scaffold DivL and CckA together and in proximity to DivJ or PleC to coordinate asymmetric activation of CckA[90]. Localization at the cell pole are mediated by Domain A in *C. crescentus* and may be regulated by the HK domain. Our leucine zipper fusion strategy allowed us to determine that changes in the DivL sensory domain conformation regulate binding to both poles. This indicates that the conformational change caused by DivK~P binding regulates DivL's interactions with PopZ, which is bipolar[170], or both PopZ and PodJ. DivK~P levels are lowest in the swarmer cell[171], and even though PopZ is present[170], DivL is diffuse. Thus our model proposes that during the swarmer to stalked transition, the loss of PodJ from the cell and the lack of DivK~P results in DivL unbinding from the cell pole (Figure 3.19).

DivL sensory domains have opposing roles in CckA regulation We discovered that deletion of PAS B and PAS D had an effect in the swarm motility assay (Figures 3.11-3.12) and that PAS D was required for CckA FRET sensor response (Figure 3.14). Critically, deletion of PAS B resulted in a significantly smaller swarm size. In contrast, PAS D is strictly required to mediate swarm size reduction and changes in the CckA-FRET sensor. These observations could

be rooted in CtrA pathway up- or down-regulation. Therefore, future *in vivo* studies are needed to determine how these DivL domain deletion constructs impact CckA phosphorylation levels and CtrA regulated genes. Notably, past *in vitro* studies identified PAS B as the domain that is required to repress kinase function and stimulate CckA phosphatase activity[107]. The PAS D deletion has not yet been analyzed in *in vitro* kinase studies, but we hypothesize that that DivL-ΔPas D would eliminate DivL's impact on CckA function. From these analyses we propose that PAS B and PAS D work cooperatively to regulate CckA functions. Given the essentiality of PAS D for CckA stimulation *in vivo* we propose that PAS D may serve as a binding site for CckA. We also anticipate that performing the *in vitro* CckA coupled enzyme assay with DivL-ΔPAS B, DivL-ΔPAS D, as well as those same constructs containing the activating mutation A601L, will allow us to assign the PAS domains' roles in CckA kinase and phosphatase activities.

DivL localization is regulated through multiple, and perhaps dynamic, scaffolding interactions We have characterized a novel protein structural fold with previously unknown function (DUF3455) (Figure 3.3) by finding that the N-terminal Domain A interacts with the scaffold proteins PopZ and PodJ (Figure 3.8). We also discovered that both Domain A and the HK bind to both cell pole localized scaffolds, PopZ and PodJ. Our leucine zipper results in Chapter 2 demonstrated that long-range signaling into Domain A regulate localization at the cell pole (Figure 2.12)[158], and we ask whether there are additional direct interactions between Domain A and the HK. The importance of Domain A binding to both PopZ and PodJ raises questions regarding the functional significance of DivL's binding to PopZ and PodJ. Do PodJ and PopZ serve as benign localization tethers? Or, given the proximity of domain A to the PAS BCD CckA stimulation domains, do PopZ and PodJ allosterically regulate CckA function? Do PopZ and PodJ bind

competitively, or do they form a complex? Do PopZ and PodJ interact to form a third unique binding site?

Interestingly, we observed that over-expression of the PopZ scaffold lowered the FRET signal[166]. Possible reasons for the change in the FRET ratio are that over-expression of PopZ 1) diluted the local concentration of CckA or 2) interfered with the interactions between DivL and CckA. Both of these events may change the conformational change of CckA and thus affect the FRET ratio. Here we observed that the deletion of PAS C also resulted in a decrease in the FRET ratio. The FRET ratio decrease that we observed here with the deletion of PAS C may indicate that PAS C regulates the binding interactions with the PopZ scaffold.

Signal integration via PAS C regulates CckA activity and DivL and CckA localization

As shown in Figure 3.7, deletion of the entire PAS C domain did not cause the loss of DivL localization. Therefore, discovery of a mutation within PAS C that disrupted DivL subcellular localization was an unexpected result. A potential model to accommodate these two results is that DivL-ΔPAS C may be in a conformation that is constitutively localized, or another region of DivL may also regulate localization control in the absence of PAS C. From these studies we propose that PAS C serves as a switch to regulate both the localization of DivL and its impact upon CckA signaling. A key question remains: what is the identity of this PAS C specific signal? In past work by Childers et al., DivL was shown to require both PAS C and PAS D for binding to DivK~P *in vitro*[69]. Moreover, this study showed that DivL variants that bind poorly to DivK~P show diminished cell pole accumulation[69]. Therefore, we propose a model in which DivK~P binds to PAS C, which serves as a conformational switch to enable DivL binding to cell-pole localized scaffolding proteins PopZ and PodJ.

3.4 Future Directions

Biochemical activity assays to analyze DivL's affect on CckA *in vitro* Together with previous data discussed earlier, our model (Figure 3.19) invokes that the DivL sensory subdomains have unique roles in allosteric modulation of CckA activity. We also proposed in Chapter 2 that this modulation can be periodically tuned, presumably in response to DivK~P. We have already made progress toward the use of a coupled ATPase activity assay to screen DivL variants modulating capabilities *in vitro* (Figure 3.18). Our initial studies began using two purified DivL-LZ fusion variants and we discussed that we plan to expand the assay using the full panel of LZ fusions. We hypothesize that the periodic trend that emerged in the swarm assay (Figures 2.9-2.10) will be observed here, with *in vitro* kinase activity relative to the DivL-LZ junction site.

We also intend to purify and analyze our panel of DivL domain deletions in this assay. These variants will allow us to define with more certainty the role that each DivL domain takes in regulating CckA kinase or phosphatase activity. For instance, because PAS B has previously been attributed to CckA phosphatase stimulation[107] and we observed a small swarm phenotype upon DivL-ΔPAS B over-expression, we predict that combining DivL-ΔPAS B with CckA in the activity assay will result in kinase stimulation. Similarly, since DivL-ΔPAS D resulted in a large swarm phenotype, we predict the opposite result for the combination of DivL-ΔPAS B with CckA: inhibition of kinase activity.

Ultimately, the intriguing possibility that PopZ, PodJ, or both regulate the CckA pathway can be addressed using this system. One model is that the scaffolds serve to regulate the accumulation of CckA to regulate its density-dependent activity[168]. In another model, DivL recognizes its subcellular localization by binding to the cell-pole scaffold, and this binding event

acts an input signal. The coupled enzyme activity assay will be performed CckA in solution with or without PopZ and PodJ. These results will be compared to the results when DivL is added.

Mapping out critical scaffold interactions within the DivL-CckA pathway We have identified that DivL interacts with PodJ, PopZ, CckA, and DivK~P in complex and dynamic ways. Several questions remain, including how DivL's Domain A and HK coordinate scaffold binding together, whether signals transmitted through the DivL sensor-HK helix dictate scaffold binding, and whether the observed CckA activity changes result from changing interactions with DivL. We propose that a series of *in vitro* binding assays are necessary to give us insight into these mechanisms.

We propose future work interrogating DivL's binding to PopZ and PodJ by using isothermal titration calorimetry (ITC) (Figure 20A)[172, 173]. Negative and positive controls for PopZ binding will be DivJ[170] and ZitP[172], respectively. Negative and positive controls for PodJ binding will be CckA[174] and PleC[175], respectively. ITC will be performed with full-length PopZ or PodJ with wild-type DivL, the DivL constructs used in the *E. coli* heterologous expression assay (Figure 3.8), and additional controls (Figure 3.20A). Maintenance of binding between either scaffold and DivL-ΔDomain A would indicate that Domain A is not the only basis for interaction, and perhaps the HK is sufficient for scaffold binding. Loss of binding between PopZ and DivL-ΔDomain A would reinforce the hypothesis that Domain A is responsible for DivL binding to PopZ or PodJ *in vivo* and *in vitro*.

ITC Assay: Binding to PopZ or PodJ

Titrant	DivL-WT	DivL-ΔTM 33-769	ΔDomain A 134-769	Domain A only 33-133	Domain A-HK 33-133, 519-769	DivL-BCD 134-518	DivL-LZ
Predicted outcome	binding	binding	reduced binding	reduced binding	binding	no binding	variable, based on fusion

B   FRET Assay: DivL binding competition

C   FP Assay: DivK~P binding to PAS C

D   FP Assay: DivK~P regulation of scaffolding

Predicted results

Low FRET

High FRET

High FRET

Fluorescence polarization

WT   A601L   F292A

DivL variant

Scaffold

Figure 3.20: Proposed experiments to refine the model presented in Figure 19 (A) ITC binding assays will be performed to determine the binding affinity of several DivL variants with PopZ or PodJ. (B) An in vitro FRET assay will be used to answer whether DivK~P can disrupt a DivL-CckA interaction. (C) Fluorescence polarization will be used to evaluate the PAS C F292A mutant for DivK~P binding capability. (D) Another fluorescence polarization assay will interrogate the role of DivK~P in DivL's interactions with the scaffolds PopZ and PodJ.

DivL-ΔHK (i.e. DivL-PAS ABCD) localized to the cell poles in *C. crescentus* in our assays (Figure 3.6) and also co-localized with PopZ and PodJ in *E. coli* (Figure 3.8). We hypothesize that the effect of periodic localization to the poles in the leucine zipper experiment arises from the sensor conformation dictating the ability of DivL-Domain A to bind PopZ or PodJ. We will

perform the ITC binding assay with PopZ or PodJ and two DivL-LZ variants which exhibited different localization patterns in *C. crescentus*, such as DivL-LZ-532 and DivL-LZ-536.

FRET-based studies to understand the interactions between CckA and DivL The model in Figure 3.19 could be refined if it was known how DivL and CckA interact throughout the cell cycle. CckA can disrupt the DivL-DivK~P complex, but does DivK~P similarly disrupt a DivL-CckA interaction? Are changes in DivL's regulation of CckA activity dictated by disruption or reconfiguration of a DivL-CckA complex? Here we propose a FRET-based *in vitro* binding assay in which purified DivL-mClover and CckA-mRuby are allowed to incubate in solution before the addition of DivK~P. A predicted loss of FRET upon DivK~P addition would indicate that DivL and CckA were bound together, but disrupted by DivK~P (Figure 3.20B). In contrast, DivK~P may only disrupt the interaction between CckA's RD domain and DivL's HK domain. In this model, the addition of DivK~P would not disrupt DivL-CckA sensory domain interactions. Therefore, DivL-mClover and CckA-mRuby would exhibit high FRET. The proposed FRET experiment will play a critical role in distinguishing these DivK-CckA-DivL competition models (Figure 3.20B).

Proposed experiments to determine the role of PAS C in DivL function We do note that DivL localization is unaffected in a strain expressing a DivK mutant that does not bind DivL (DivK[cs])[90, 143], leading us to consider the possibility of a second binding partner to PAS C. We hypothesize that the inactive DivL mutant in PAS C, that fails to activate the CckA signaling pathway in vivo, binds DivK~P more tightly[90]. To test this idea, we propose to measure the binding affinity of DivL-F292A to DivK~P in a fluorescence polarization assay (Figure 3.20C)[69].

Based on the localization differences between the DivL-LZ fusion constructs that mimic different DivK~P binding states, we also hypothesize that DivK~P alters DivL's ability to bind to

PodJ or PopZ (Figure 3.20D). To test this idea, we propose binding assays between DivL and PodJ or PopZ in the presence and absence of DivK~P (Figure 20D). A second potential model is that PAS C contains a small molecular binding site. Therefore, we also propose future biochemical screens for a small molecule that binds to PAS C. These proposed experiments will help dissect the role of DivL's PAS C in regulating interactions with DivK, PodJ and PopZ.

Determination if DivL-CckA signaling mechanisms are utilized by other bacterial pseudokinases We propose that the techniques we have developed in the synthetic stimulation study (Chapter 2) and the pseudokinase annotations in this chapter can be expanded to discover and characterize more bacterial pseudokinases. Another allosteric regulator of an active kinase termed a pseudokinase is RocA in Group A Streptococcus (GAS)[146], the pathogen responsible for "strep throat" and necrotizing fasciitis[157]. RocA regulates the activity of the active CovRS (or CsrRs) virulence pathway independent of its entire catalytic domain[146]. RocA interacts with CovS through its transmembrane domain[96], which we speculate may be a repurposed sensor domain. Apart from its apparent similarities to DivL, RocA is of interest because a hyper-virulent clinical isolate contains mutations and a truncation within the HK domain[176]. We hypothesize that the kinase domain of RocA may have evolved to respond to a response regulator ligand, and that may be why mutations of this protein in the M3 serotype causes a loss of RocA activity.

Response regulators bind to the dimerization and histidine phosphotransfer (DHp) domain of histidine kinases, and coevolution of certain residues within the DHp and RR dictate binding and phosphotransfer specificity (Figure 1.1A-B)[26]. DivJ and PleC, which act as a kinase and phosphatase toward DivK in cells[161, 177], respectively, share 5 out of these 12 residues in common. DivL also maintains the ability to bind to DivK~P at the conserved DHp-RR interface, and DivJ, PleC, and DivL share 2 of these residues in common. In order to predict potential RR binders with

RocA, we performed an initial survey of these critical residues in RocA compared to the other HKs in GAS (Figure 3.21). We identified three HK sequences that have at least 2 RR docking residues in common with RocA: FasB, FasC, and Spy1622. The hyper-virulent RocA mutant in the M3 serotype in fact contains a mutation to one of the residues RocA shares with FasB and Spy1622. Interestingly, RocA regulates CovS phosphatase activity under acid stress in stationary phase[178], and FasB, FasC, and Spy1622 are growth-phase and pH-dependent[179, 180]. With this evidence at hand, we propose a fluorescence polarization binding experiment[69] to determine if the response regulator of FasB and FasC, FasA, can bind to RocA, especially in a phospho-specific manner. At this time, a response regulator has not been identified for Spy1622.
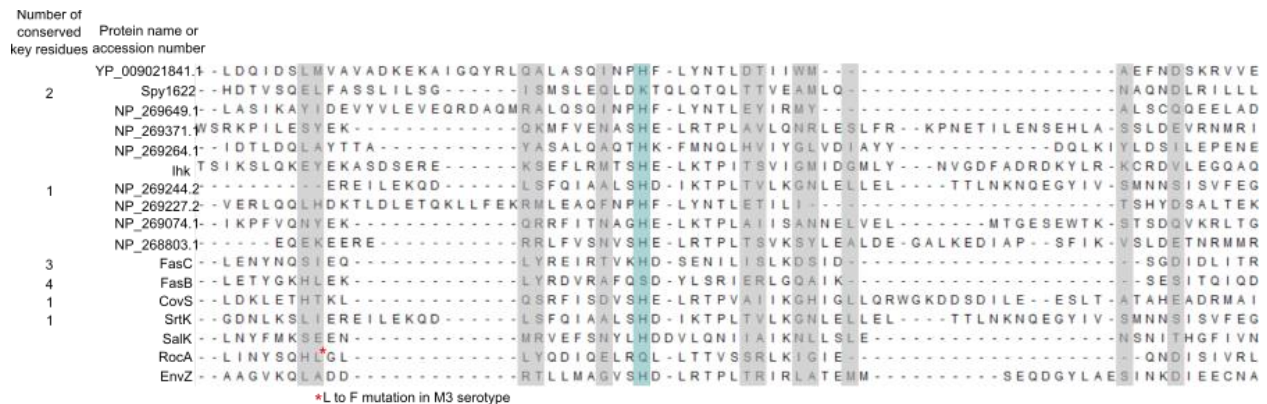
Figure 3.21: RocA has common RR docking residues with FasB, FasC, and Spy1622 Alignment of the RocA DHp domain with the other identified HKs from *S. pyogenes* and a well-studied HK EnvZ from *E. coli*. Conserved RR docking residues are shaded in gray[26]. The phosphorylation site is shaded in blue.

The leucine zipper fusion strategy described in Chapter 2 can be used regardless of the discovery of a RocA-binding response regulator. We demonstrated that this strategy can synthetically stimulate conformations of a reverse signaling pseudokinase to mimic a binding event in the HK domain. We hypothesize that leucine zipper stimulation of the RocA membrane

sensor will modulate CovS phosphatase activity towards CovR[178]. Since RocA and CovS comprise membrane spanning sensors, a phosphorylation assay can be done using nanodisc assemblies [11, 181]. This proposed experiment will build upon our experience in stimulating reversed signaling in a bacterial pseudokinase and expand the *in vitro* technology to using the leucine zipper on one protein to allosterically regulate a second protein.

3.5 Methods

Construction of plasmids and strains All experiments were performed using *Caulobacter crescentus* NA1000 (also known as CB15N) and *Escherichia coli* DH5α (Invitrogen) and BL21 (Novagen). *C. crescentus* NA1000, WSC11311 *DivK341* (DivK^{cs}), and the φCR30 phage were kind gifts from Dr. Lucy Shapiro (Stanford University School of Medicine). DNA oligos, plasmid construction methods, plasmids, and strains used in this study are further described in the Supplemental Text and listed in Table S1-S5.

Plasmid construction Restriction enzymes were purchased from Thermo Scientific or Invitrogen. PCR reactions were performed in 50 μL reaction mixtures containing 3% (v/v) DMSO, 1.3 M betaine, 0.3 μM each primer, and 0.2 mM each dNTP, and 1U Phusion High-Fidelity DNA Polymerase (Thermo Scientific). Gibson assembly (4) reactions were performed in 20 μL with 100 ng backbone and typically a 1:5 backbone:insert ratio, with 0.08U T5 Exonuclease (New England Biolabs), 1U Phusion High-Fidelity DNA Polymerase (Thermo Scientific), and 80U Taq DNA Ligase (New England Biolabs). An annealing temperature of 55 °C was used for most reactions. Plasmids and primers were designed using the J5 device editor software (5). Oligonucleotides were synthesized by IDT (Coralville, IA) and all DNA sequencing reactions were performed by The

University of Pittsburgh Genomics Research Core or Genewiz (South Plainfield, NJ). DNA oligos, plasmid construction methods, plasmids, and strains used in this study are listed in Tables 3.1-3.4.

DivL-mCherry variants Plasmid WSC10153-pXCHYC6-divL was made by Gibson assembly of full-length *divL* into pXCHYC-6 (6) and served as the template for all further DivL plasmid designs. Full length *divL* was amplified from the template cosmid 2G1 (7) using primers KAK1 and KAK2. pXCHYC-6 was digested with SacI. This backbone and the insert were assembled using the Gibson assembly method (4) resulting in an integrating plasmid at the C. crescentus chromosomal xylose locus encoding C-terminal mCherry-tagged DivL. C. crescentus cells were transformed by electroporation. Briefly, cells were grown in PYE medium overnight and rinsed three times with cold sterile water. Cells were resuspended in water and 80 µL of cells plus 10 µL of plasmid were electroporated with a time constant of 3.5-5.0 ms. Colonies were screened for integration at the xylose locus using RecUni-1, a primer that anneals to the plasmid, and RecXyl-2, a primer that anneals to the 5' region of the chromosomal promoter (6).

DivL point mutants DivL point mutants were designed as two-fragment Gibson assemblies with the point mutant embedded in the fragment amplification primers. pKAK0001-pXCHYC6-SacI-DivL-F292A was made by amplifying Insert 1 using primers KAK1 and WSCp89 and Insert 2 using primers WSCp88 and KAK2 from plasmid WSC10153 as a template. pXCHYC-6 was digested with SacI. This backbone and the inserts were assembled using the Gibson assembly method resulting in an integrating plasmid at the C. crescentus chromosomal xylose locus encoding the C-terminal mCherry-tagged DivL mutant.

DivL-M2 variants pBXMCS-2 backbone was amplified by PCR using the primers KAK9 and KAK10. Fragments were amplified from WSC10153 or an already existing construct in pXCHYC-6. The backbone and insert were assembled using the Gibson assembly method resulting

in a C. crescentus high-copy plasmid for the xylose-inducible expression of the C-terminal M2-tagged DivL variant.

pBAD-DivL-msfGFP variants The pBAD-DivL-msfGFP plasmid was isolated from a strain generously given by Dr. Grant Bowman (University of Wyoming Department of Molecular Biology)[162]. The pBAD backbone, excluding DivL, was amplified using the primers KAK321 and KAK322. A divL fragment encoding 134-769 was amplified from plasmid WSC10153. The backbone and insert were assembled using the Gibson assembly method resulting in an E. coli arabinose-inducible plasmid encoding C-terminal msfGFP-tagged DivL 134-769.

pTEV-His-DivL variants The pTEV-5 backbone was digested with NheI. Fragments were amplified from WSC10153 or an already existing construct in pXCHYC-6. The backbone and insert were assembled using the Gibson assembly method resulting in an IPTG-inducible His-tagged DivL variant.

Western blot Western blot analysis was used to determine protein levels of each DivL-M2 variant. Cells were grown in 2 mL PYE medium to early log phase at 28°C. Overnight induction with 0.3% xylose began at inoculation. 1 mL cells were harvested by centrifugation and resuspended in SDS 100 µL sample loading dye. Samples were treated by heating (75°C for 10 min). Samples volumes were normalized to the lowest OD600 upon collection and separated by 10% SDS–PAGE. Proteins were transferred onto a PVDF membrane (GE Healthcare). The membrane was blocked in 5% milk (AmericanBio) overnight at 4°C. The anti-M2 (FLAG) antibody (Sigma-Aldrich) (1:5000 in TBST for 1 hour at 4°C) was used with a goat anti-rabbit IgG-peroxidase secondary antibody (Sigma-Aldrich) (1:10,000 in TBST for 1 hour at room temperature). PVDF membranes were treated with an ECL western blotting kit (Thermo Scientific) and visualized using a ChemiDoc XRS+ system (Bio-Rad). Colorimetric imaging was used to

visualize the protein ladder (Thermo Scientific), which was aligned with the blots to assign the size labels.

Swarm plate assay Cells were grown to mid-log phase at 28 °C overnight in PYE (peptone yeast extract) medium and the appropriate antibiotic. Cells were normalized by dilution in PYE medium to the culture with the lowest OD600. Cells were stabbed into 0.3% PYE agar with the appropriate antibiotic and 0.3% xylose in 15 cm diameter culture plates using a Boekel replicator. Plates were incubated at 28 °C for 3 days. Plates were visualized using a ChemiDoc XRS+ system (Bio-Rad). Three replicate plates were analyzed. Swarm area was measured using ImageJ[135]. Swarm areas were normalized to the empty vector control on each plate. The error for the empty vector control was calculated by dividing the standard deviation of the areas by the average area. The error for the experimental areas was calculated as the standard deviation of the areas after normalization to the empty vector control. Significance was determined using Prism (GraphPad) with a Dunnett's multiple comparisons test by comparing the mean area of each strain to the mean area of DivL-WT (ns: P>0.05, *: $P \leq 0.05$, **: $P \leq 0.01$, ***: $P \leq 0.001$).

Fluorescence microscopy *C. crescentus* cells were grown in M2G medium with the appropriate antibiotics at 28 °C overnight to OD600=0.2-0.8. DivL-mCherry variants were induced with 0.03% xylose for 4 hours. Cells were diluted as needed and immobilized on a 1.5% agarose in M2G pad. DivK^{cs} strains were grown overnight in PYE medium and diluted in PYE supplemented with 0.03% xylose to induce over-expression. Cells were grown again overnight at 28 or 20 °C. Phase microscopy was performed with a Nikon Eclipse T*i*-E inverted microscope equipped with an Andor Ixon Ultra DU897 EMCCD camera and a Nikon CFI Plan-Apochromat 100X/1.45 Oil objective and intermediate 1.5x magnification. DIC (differential interference contrast) microscopy was performed with a Nikon CFI Plan-Apochromat 100X/1.45 Oil DIC

objective with a Nikon DIC polarizer and slider in place. Carl Zeiss Immersol 518 oil was used. Excitation source was a Lumencor SpectraX light engine. Chroma filter cube CFP/YFP/MCHRY MTD TI was used to image mCherry (630/60M). Chroma filter cube DAPI/GFP/TRITC was used to image EGFP, and mClover 3(515/30M). Images were acquired with Nikon NIS-Elements AR software.

Fluorescence image analysis ImageJ[135] was used to adjust LUT, pseudocolor, and crop images. ImageJ Cell Counter and Nikon-NIS Elements AR were used to manually count cells and foci. ImageJ and MicrobeJ[136] were used for manual cell counting, cell length analysis and correlation scores. White outlines of the *C. crescentus* cell body were based on DIC or phase contrast imaging.

FRET microscopy and image processing Simultaneous FRET imaging required a Hamamatsu W-View Gemini Image Splitter in the light path between the Nikon TiE and the camera. A GFP/mCherry dichroic mirror, GFP emission filter, and mCherry emission filter were used. Alignment of the channels was done using the supplied alignment slide. Alignment of the channels was done before each imaging event. Each strain was imaged under the same conditions (600 millisecond Autoexposure, 100 Gain, 2x2 binning for capture, and 15% power). Background from the fluorescent channels was subtracted in the Nikon software. In ImageJ a mask was generated by thresholding cell signal above background. The original image was then multiplied by the masked image to remove background signal and the mCherry emission channel image was divided by the GFP emission channel (32-bit image) to generate a ratiometric FRET image. Image AnalysisFor each experiment, 4 images were uploaded into MicrobeJ (Phase, GFP channel, mCherry channel, and ratiometric image). The phase image was used to generate a cell outline using the Medial Axis setting. Cell poles were outlined using the MicrobeJ automatic pole settings

which to draw a shape around the cell pole. MicrobeJ was preset to mark the stalk pole as the pole with higher intensity in the GFP channel. After software chose the poles, manual adjustment was done by choosing cells with a visible stalk and cells with incorrect pole alignment were corrected manually. MicrobeJ's data analysis tool was then used to average the intensity of the cell pole and body. Data was exported to Prism (GraphPad) in order to generate histograms and average data. Student's t-test was used to determine significant difference in populations. Error bars are reported as standard error of the mean.

Protein purification Expression plasmids were transformed into BL21 cells, and plated onto 100 µg/mL ampicillin LB plates and grown overnight at 37 °C. From a single colony, an overnight 10 mL 50 µg/mL ampicillin LB culture was inoculated and grown to saturation overnight. From this saturated culture two 1 L LB cultures were inoculated and grown to mid-log phase (0.6 OD). Expression of the DivL-LZ fusions was induced with 333 µM isopropyl-b-D-thiogalactopyranoside (IPTG) for 4 hours at 25 °C. The cells were harvested by centrifugation (4 °C for 20 minutes at 3,700 g). The resulting pellet was resuspended in 50 ml 50 mM HEPES pH=8, 0.5 M KCl and centrifuged (3,700 g at 4 °C for 20 minutes) to yield a cell pellet stored at -80 °C. Cells were thawed on ice and resuspended in 50 ml of lysis buffer (50 mM HEPES pH 8.0, 0.5 M KCl, 1 mM DTT, 25 mM imidazole, 10% glycerol, and 200 U of Benzonase Nuclease (Sigma) supplemented with SIGMAFAST protease inhibitor tablets (Sigma)). The cell suspension was lysed with three passes through the Emulsiflex at 20,000 psi. Insoluble cell debris was pelleted via centrifugation (30,000 g, 50 min at 4 °C). The resulting supernatant was incubated with 2 ml of a 50% slurry of HisPur Ni-NTA agarose resin (Thermo Fisher Scientific) at 4 °C for 2 hours. The Ni-NTA agarose was pelleted and washed with 30 ml of Ni-NTA wash buffer (50 mM HEPES pH=8], 0.5 M KCl, 1 mM DTT, 25 mM imidazole, and 10% glycerol). Then the DivL-LZ fusion

was eluted from the agarose with Ni-NTA elution buffer (50 mM HEPES pH=8.0, 0.5 M KCl, 1 mM DTT, 250 mM imidazole, and 10% glycerol) and concentrated using Amicon Centrifugal Filter Units (30 kDa cutoff), aliquoted and frozen at 80 °C. The concentration was determined using the predicted molecular weight of 58 kDa and 78,630 M-1cm-1.

Fluorescence polarization assay DivK was labeled at Cys-99 using thiol-reactive BODIPY FL Naminoethyl malemide (Invitrogen). DivK was mixed together with 10-fold excess BODIPY FL N-aminoethyl malemide and allowed to react for 2 hours at room temperature, and unreacted dye was quenched with mercaptoethanol. BODIPY-DivK was purified via dialysis to remove unreacted fluorescent dye. BODIPY-DivK~P was generated by mixing 250 nM DivJ with 1 mM ATP and 5 mM MgCl$_2$ and incubated for 40 min. For binding assays using unphosphorylated DivK, 1 mM nonhydrolyzable AMP-PNP and 5 mM MgCl2 were included in the buffer. BODIPY-DivK,P or BODIPY-DivK was then incubated with varying kinase concentrations for 45 minutes to reach binding equilibrium. Fluorescent DivK was excited at 470 nm and emission polarization was measured at 530 nm in a Molecular Devices SpectraMax M5 plate reader. Fluorescent polarization measurements were performed in triplicates, and three independent trials were averaged with error bars representing the standard deviation.

Coupled enzyme assay ATPase activity was measured using a coupled-enzyme assay. CckA was mixed in kinase buffer (50 mM HEPES pH=8, 50 mM KCl) supplemented with 0.1 mM ATP, 10 mM MgCl2, 3 mM phosphoenolpyruvate, 0.2 mM NADH, 2 units of pyruvate kinase, and 6.6 units of lactate dehydrogenase (P0294, Sigma). DivL constructs and/or liposomes were added to the reported concentrations. Reactions were performed in duplicate in a 200 ml volume and loaded into a clear polystyrene 96 well-plate. Each reaction was initiated by the addition of ATP, and 340 nm absorbance was recorded every 60 s for 60 min on a Tecan Infinite

200 Pro plate reader. The slope of a stable, linear absorbance decay was measured to calculate ATP hydrolysis rates using a NADH extinction coefficient of 6220 $M^{-1}s^{-1}$[169]. Background rates of ATP hydrolysis and NADH oxidation were measured and subtracted from observed CckA construct ATP hydrolysis rates. The mean observed rates and Michaelis-Menten plot were determined and analyzed using Prism (GraphPad).

Multiple sequence alignments The DivL homolog sequences[137] were aligned using ClustalΩ in the MPI Bioinformatics Toolkit[138]. The phylogenetic tree was calculated in Jalview using BLOSUM62 Average Distance[139]. Protein visualization was performed with USCF Chimera[140].

Table 3.1: DNA oligos

Name	Description
RecXyl-2	TCTTCCGGCAGGAATTCACTCACGCC
RecUni-1	ATGCCGTTTGTGATGGCTTCCATGTCG
WSCp88	CCGTGGCGATCGCCAGCCAGACGCG
WSCp89	CGCGTCTGGCTGGCGATCGCCACGG
WSC10295	TGGTACCTTAAGATCTCGAGCTATGACTTCGTACGACCTGATCCTCGC
WSC10296	TCGAATTCTCCGGGAAGCCGAGTTCGGGCTGCATGG
WSC10297	TGCATGGTACCTTAAGATCTCGAGCTATGACTTCGTACGACCTGATCCTCGCG
WSC10304	CGCGACCCTCGACCCCGTGGGACCACAGGGC
WSC10305	GTGGTCCCACGGGGTCGAGGGTCGCGCGGCG
WSC10306	GGACATCCTCGATCTCCACGCTGTCGACGAAGGCGG
WSC10307	CGTCGACAGCGTGGAGATCGAGGATGTCCGCGACGC
WSC10171	TGACGCGTAACGTTCGAATTCTCCGGGAAGCCGAGTTCGGGCTGC
WSC10306	GGACATCCTCGATCTCCACGCTGTCGACGAAGGCGG
WSC10307	CGTCGACAGCGTGGAGATCGAGGATGTCCGCGACGC
WSC10308	GGCGCAGCTCGCCGGTGACGTCGGCGCAGAACAC
WSC10309	CGCCGACGTCACCGGCGAGCTGCGCCTGAAAGC
WSC10310	GGTCTCGGGTGTCGGTGATGTCGGAATAGATCAGCAGC
WSC10311	TATTCCGACATCACCGACACCCGAGACCTGCAGAGCG
KAKqc0010	GTGTTCTGCGCCGCCGTCACCGAGATC
KAKqc0011	GATCTCGGTGACGGCGGCGCAGAACAC
KAKqc0012	CTGCGCCGACGTCGTCGAGATCGAGGATG
KAKqc0013	CATCCTCGATCTCGACGACGTCGGCGCAG
KAKqc0014	CTGATCTATTCCGCCATCACCGGCGAG
KAKqc0015	CTCGCCGGTGATGGCGGAATAGATCAG
KAKqc0016	CTATTCCGACATCGTCGGCGAGCTGCG
KAKqc0017	CGCAGCTCGCCGACGATGTCGGAATAG
KAKqc0108	TGACGCGTAACGTTCGAATTCTCCGGCAGACGGGCGACCTCATTCTCGAGGTGGTAGTTCTTCGAGAGGAGTTCTTCGACCTTGTCTTCGAGTTGCTTCACGCTGTCGACGAAGGC
KAK1	TGCATGGTACCTTAAGATCTCGAGCTATGACTTCGTACGACCTGATCCTCGC
KAK2	TGACGCGTAACGTTCGAATTCTCCGGGAAGCCGAGTTCGGGCTGCATGG
KAK3	CGAGGTCGACGGTATCGATAAGCTTGATATGACTTCGTACGACCTGATCCTCGCG
KAK7	CGGCGCTTTTCCATCGAGAATTCGATGAAGCCGAGTTCGGGCTGCATGG
KAK9	ATCGAATTCTCGATGGAAAAGCGCCG
KAK10	ATCAAGCTTATCGATACCGTCGACCTCGAG
KAK31	TGACGCGTAACGTTCGAATTCTCCGGCACGCTGTCGACGAAGGC
KAK32	TGACGCGTAACGTTCGAATTCTCCGGCGAAACAAGGCCATGGGG
KAK33	TGCATGGTACCTTAAGATCTCGAGCTATGCAGCGACGGAACCTGGAGGC
KAK35	CGTCGACAGCGTGGACACCCGAGACCTGCAGAGCG
KAK36	GGTCTCGGGTGTCCGAAACAAGGCCATGGGG
KAK37	TGGCCTTGTTTCGGACACCCGAGACCTGCAGAGCG

KAK63	TGACGCGTAACGTTCGAATTCTCCGCGGTGACGTCGGCGAAGGCG
KAK64	TGACGCGTAACGTTCGAATTCTCCGCGGTGATGTCGGAATAGATCAGCAGC
KAK91	TGCATGGTACCTTAAGATCTCGAGCTATGGTCGAGCCGTGCTGGATCGC
KAK92	TGACGCGTAACGTTCGAATTCTCCGGGGTGATGTCGGAATAGATCAGCAGC
KAK93	TGCATGGTACCTTAAGATCTCGAGCTATGGAGATCGAGGATGTCCGCGACGC
KAK94	TGACGCGTAACGTTCGAATTCTCCGGGGTGACGTCGGCGAAGGCG
KAK155	CCAACTAGTGAAAACCTGTATTTTCAGGGCGCTATGGCCTGGCTCGACGCCTTCGA
KAK158	GCTCGAGAATTCCATGGCCATATGGCTTCACAGACGGGCGACCTCATTCTCGA
KAK323	TTTTTGGGCTAACAGGAGGAATTAACCAATGGTCGAGGGTCGCGCGGCG
KAK324	TTACTGCCGCCGCCGCCGCTCTCGAGGAAGCCGAGTTCGGGCTGCATGG
KAK325	TTTTTGGGCTAACAGGAGGAATTAACCAATGGAGGCGCGTATCGTCGCGC
KAK326	TTACTGCCGCCGCCGCCGCTCTCGAGCGAAACAAGGCCATGGGGACCG
SWD211	GGTACCTTAAGATCTCGAGCTCCGGAGAACCCGCCACCCAGCTCGCTG
SWD212	CCTCGCCCTTGCTGGTGGCCGACCGGTGACGCGTAACGTTCGACGCCGCCTGCAGCTGCTG
SWD213	CCGGTCGGCCACCAGCAAGGGCGAGGAGCTGTTCACC
SWD214	CTAGTGGATCCCCCGGGCTGCAGCTATTAGCTCACCATCGGATCTTCGCCGC
SWD485	GCCCGAACTCGGCTTCTAGCTCTTAAGATCTACGTACCGGTGCTAGCTG
SWD486	CGTACGAAGTCATCTCACCACGTGGTACCTCGAGAATTCATATGC
SWD487	GGTACCACGTGGTGAGATGACTTCGTACGACCTGATCCTCGCG
SWD488	CGTAGATCTTAAGAGCTAGAAGCCGAGTTCGGGCTGC
SWD659	CGGCTATTCGGAGCTGTAGCTCTTAAGATCTACGTACCGGTGCTAGCTG
SWD660	GGTACGTAGATCTTAAGAGCTACAGCTCCGAATAGCCGATGATCGTCG

Table 3.2: Gibson cloning strategy to generate plasmids

Plasmid	Plasmid Description	First Insert Forward Primer	First Insert Reverse Primer	Second Insert Forward Primer	Second Insert Reverse Primer
pWSC10159	pXCHYC-6 DivL (1-27, 134-769)	WSC10297	WSC10304	WSC10305	WSC10171
pWSC10160	pXCHYC-6 DivL (1-170, 264-769)	WSC10297	WSC10306	WSC10307	WSC10171
pWSC10161	pXCHYC-6 DivL (1-262, 392-769)	WSC10297	WSC10308	WSC10309	WSC10171
pWSC10162	pXCHYC-6 DivL (1-391, 519-769)	WSC10297	WSC10310	WSC10311	WSC10171
pKAK0001	pXCHYC-6 DivL F292A	KAK1	WSCp89		
pKAK0003	pXCHYC-6 DivLV418A	WSCp88	KAK2		
pKAK0016	pBXMCS-2 DivL (1-27, 134-769)	KAK3	KAK7		
pKAK0017	pBXMCS-2 DivL (1-170, 264-769)	KAK3	KAK7		
pKAK0018	pBXMCS-2 DivL (1-262, 392-769)	KAK3	KAK7		
pKAK0019	pBXMCS-2 DivL (1-391, 519-769)	KAK3	KAK7		
pKAK0033	pBXMCS-2 DivL D260A	KAK10	KAKqc0011	KAKqc0010	KAK9
pKAK0034	pBXMCS-2 DivL T262V	KAK3	KAKqc0013	KAKqc0012	KAK7
pKAK0035	pBXMCS-2 DivL D389A	KAK3	KAKqc0015	KAKqc0014	KAK7
pKAK0036	pBXMCS-2 DivL T391V	KAK10	KAKqc0017	KAKqc0016	KAK7
pKAK0045	pXCHYC-6 DivL (1-170)	KAK1	KAK31		
pKAK0046	pXCHYC-6 DivL (1-133)	KAK1	KAK32		
pKAK0047	pXCHYC-6 DivL (28-170)	KAK33	KAK31		
pKAK0048	pXCHYC-6 DivL (28-133)	KAK33	KAK32		
pKAK0049	pXCHYC-6 DivL (1-170, 519-769)	KAK1	KAK34	KAK35	KAK2
pKAK0050	pXCHYC-6 DivL (1-133, 519-769)	KAK1	KAK36	KAK37	KAK2
pKAK0051	pXCHYC-6 DivL (28-170, 519-769)	KAK33	KAK34	KAK35	KAK2
pKAK0052	pXCHYC-6 DivL (28-133, 519-769)	KAK33	KAK35	KAK37	KAK2
pKAK0072	pXCHYC-6 DivL (1-170, 263-518)	KAK1	WSC10306	WSC10307	KAK63
pKAK0073	pXCHYC-6 DivL (1-391)	KAK1	KAK64		
pKAK0088	pXCHYC-6 DivL (171-391)	KAK91	KAK92		

pKAK0089	pXCHYC-6 DivL (263-518)	KAK93	KAK94		
pKAK0096	pXCHYC-6 DivL (1-170, LZ)	KAK1	KAKqc0108		
pKAK0137b	pTEV-5 DivL (1-532, LZ)	KAK155	KAK158		
pKAK0137f	pTEV-5 DivL (1-536, LZ)	KAK155	KAK158		
pKAK0207	pBAD DivL (134-769),msfGFP	KAK323	KAK234		
pKAK0208	pBAD DivL (33-133), msfGFP	KAK325	KAK326		
pSWD63	pGFPC-4 CckA (1500bp), mClover3	SWD211	SWD212	SWD213	SWD214
pSWD208	pVMCS-1 DivL (1-565)	SWD649	SWD486	SWD487	SWD660
pSWD209	pVMCS-1 DivL (1-27, 134-769)	SWD485	SWD486	SWD487	SWD488
pSWD210	pVMCS-1 DivL (1-170, 264-769)	SWD485	SWD486	SWD487	SWD488
pSWD211	pVMCS-1 DivL (1-391, 519-769)	SWD485	SWD486	SWD487	SWD488
pSWD228	pVMCS-1 DivL (1-262, 392-769)	SWD485	SWD486	SWD487	SWD488

Table 3.3: Plasmids

Plasmid	Description	Reference
pET-28b(+)	bacterial expression vector	Novagen
pTEV5	bacterial expression vector	[141]
pTEV6	bacterial expression vector with MBP solubilization tag	[141]
pXCHYC-6	C. crescentus integrating C-terminal mCherry fusion vector	[142]
pBXMCS-2	C. crescentus high-copy replicating C-terminal M2 fusion vector	[142]
N/A	pBAD DivL (1-769), msfGFP	[162]
pWZ013-30	pCDFDuet1-mcherry-PodJ	[174]
WSC10153	pXCHYC-6 DivL (1-769)	This Study
pWSC10159	pXCHYC-6 DivL (1-27, 134-769)	This Study
pWSC10160	pXCHYC-6 DivL (1-170, 264-769)	This Study
pWSC10161	pXCHYC-6 DivL (1-262, 392-769)	This Study
pWSC10162	pXCHYC-6 DivL (1-391, 519-769)	This Study
pKAK0001	pXCHYC-6 DivL F292A	This Study
pKAK0003	pXCHYC-6 DivLV418A	This Study
pKAK0016	pBXMCS-2 DivL (1-27, 134-769)	This Study
pKAK0017	pBXMCS-2 DivL (1-170, 264-769)	This Study
pKAK0018	pBXMCS-2 DivL (1-262, 392-769)	This Study
pKAK0019	pBXMCS-2 DivL (1-391, 519-769)	This Study
pKAK0033	pBXMCS-2 DivL D260A	This Study
pKAK0034	pBXMCS-2 DivL T262V	This Study
pKAK0035	pBXMCS-2 DivL D389A	This Study
pKAK0036	pBXMCS-2 DivL T391V	This Study
pKAK0045	pXCHYC-6 DivL (1-170)	This study
pKAK0046	pXCHYC-6 DivL (1-133)	This study
pKAK0047	pXCHYC-6 DivL (28-170)	This study
pKAK0048	pXCHYC-6 DivL (28-133)	This study
pKAK0049	pXCHYC-6 DivL (1-170, 519-769)	This study
pKAK0050	pXCHYC-6 DivL (1-133, 519-769)	This study
pKAK0051	pXCHYC-6 DivL (28-170, 519-769)	This study
pKAK0052	pXCHYC-6 DivL (28-133, 519-769)	This study
pKAK0072	pXCHYC-6 DivL (1-170, 263-518)	This study
pKAK0073	pXCHYC-6 DivL (1-391)	This study
pKAK0088	pXCHYC-6 DivL (171-391)	This study
pKAK0089	pXCHYC-6 DivL (263-518)	This study
pKAK0096	pXCHYC-6 DivL (1-170, LZ)	This Study
pKAK0137b	pTEV-5 DivL (54-536, LZ)	This Study
pKAK0137f	pTEV-5 DivL (54-532, LZ)	This Study

pKAK0207	pBAD DivL (134-769), msfGFP	This Study
pKAK0208	pBAD DivL (33-133), msfGFP	This Study
pWSC10036	pTEV5-DivL(152-769)	[69]
pWSC10038	pTEV5-DivL(152-769) A601L	[69]
pJAB27	pET-28b(+) CckA(70-691) expression vector	[69]
pWSC29	pET-28b(+) DivJ(195-596)	[69]
pWSC31	pET-28b(+) DivK	[69]
pSWD63	pGFPC-4 CckA (1500bp), mClover3	This Study
pSWD208	pVMCS-1 DivL (1-565)	This Study
pSWD209	pVMCS-1 DivL (1-27, 134-769)	This Study
pSWD210	pVMCS-1 DivL (1-170, 264-769)	This Study
pSWD211	pVMCS-1 DivL (1-391, 519-769)	This Study
pSWD228	pVMCS-1 DivL (1-262, 392-769)	This Study

Table 3.4: *C. crescentus* **and** *E. coli* **strains**

Strain	Description	Plasmid(s)	Reference Source
E. coli DH5α	bacterial cloning strain		Invitrogen
E. coli BL21	bacterial expression strain		Novagen
C. crescentus NA1000	laboratory Caulobacter crescentus strain		
JH42	BL21(DE3) pACYC-mCherry-PopZ		[162]
JH79	BL21 (DE3) pACYC-mCherry-PopZ + pBAD-DivL-msfGFP		[162]
WSC0300	C. crescentus pBXMCS-2		[142]
WSC0302	*C. crescentus* pBXMCS-2 DivL (1-769)		this study
WSC1233	DH5α pCDFDuet1-mcherry-PodJ	pWZ013-30	[174]
WSC1368	BL21(DE3) pCDFDuet1-mcherry-PodJ	pWZ013-30	[174]
WSC0458	*C. crescentus* pXCHYC-6 DivL (1-27, 134-769)	pWSC10159 NA1000	this study
WSC0459	*C. crescentus* pXCHYC-6 DivL (1-170, 264-769)	pWSC10160 NA1000	this study
WSC0460	*C. crescentus* pXCHYC-6 DivL (1-262, 392-769)	pWSC10161 NA1000	this study
WSC0461	*C. crescentus* pXCHYC-6 DivL (1-391, 519-769)	pWSC10162 NA1000	this study
KAK15	DH5α pXCHYC-6 DivL (1-27, 134-769)	pWSC159	this study
KAK16	DH5α pXCHYC-6 DivL (1-170, 264-769)	pWSC160	this study
KAK17	DH5α pXCHYC-6 DivL (1-262, 392-769)	pWSC161	this study
KAK18	DH5α pXCHYC-6 DivL (1-391, 519-769)	pWSC162	this study
KAK20	DH5α pXCHYC-6 DivL (1-769)	WSC10153	this study
KAK23	DH5α pBXMCS-2 DivL D260A	pKAK0033	this study
KAK26	DH5α pXCHYC-6 DivL F292A	pKAK0001	this study
KAK27	DH5α pBXMCS-2 DivL T262V	pKAK0034	this study
KAK28	DH5α pXCHYC-6 DivLV418A	pKAK0003	this study
KAK43	NA1000 pXCHYC-6 DivL (1-769)	WSC10153	this study
KAK48	DH5α pBXMCS-2 DivL (1-27, 134-769)	pKAK0016	this study
KAK49	DH5α pBXMCS-2 DivL (1-391, 519-769)	pKAK0019	this study
KAK51	DH5α pBXMCS-2 DivL (1-170, 264-769)	pKAK0017	this study
KAK52	DH5α pBXMCS-2 DivL (1-262, 392-769)	pKAK0018	this study
KAK66	NA1000 pBXMCS-2 DivL (1-262, 392-769)	pKAK0018	this study
KAK67	NA1000 pBXMCS-2 DivL (1-391, 519-769)	pKAK0019	this study
KAK68	NA1000 pBXMCS-2 DivL (1-27, 134-769)	pKAK0016	this study
KAK69	NA1000 pBXMCS-2 DivL (1-170, 264-769)	pKAK0017	this study
KAK88	NA1000 pXCHYC-6 DivL F292A	pKAK0001	this study
KAK89	NA1000 pXCHYC-6 DivLV418A	pKAK0003	this study
KAK117	DH5α pXCHYC-6 DivL (28-170)	pKAK0047	this study
KAK119	DH5α pXCHYC-6 DivL (28-133)	pKAK0048	this study
KAK122	DH5α pXCHYC-6 DivL (1-170)	pKAK0045	this study
KAK123	DH5α pXCHYC-6 DivL (1-133)	pKAK0046	this study

KAK124	DH5α pXCHYC-6 DivL (1-170, 519-769)	pKAK0049	this study
KAK125	DH5α pXCHYC-6 DivL (1-133, 519-769)	pKAK0050	this study
KAK126	DH5α pXCHYC-6 DivL (28-170, 519-769)	pKAK0051	this study
KAK127	DH5α pXCHYC-6 DivL (28-133, 519-769)	pKAK0052	this study
KAK130	DH5α pBXMCS-2 DivL D389A	pKAK0035	this study
KAK137	NA1000 pBXMCS-2 DivL D260A	pKAK0033	this study
KAK138	NA1000 pBXMCS-2 DivL T262V	pKAK0034	this study
KAK139	NA1000 pBXMCS-2 DivL D389A	pKAK0035	this study
KAK140	NA1000 pXCHYC-6 DivL (1-170)	pKAK0045	this study
KAK141	NA1000 pXCHYC-6 DivL (1-133)	pKAK0046	this study
KAK142	NA1000 pXCHYC-6 DivL (28-170)	pKAK0047	this study
KAK143	NA1000 pXCHYC-6 DivL (28-133)	pKAK0048	this study
KAK144	NA1000 pXCHYC-6 DivL (1-170, 519-769)	pKAK0049	this study
KAK145	NA1000 pXCHYC-6 DivL (1-133, 519-769)	pKAK0050	this study
KAK146	NA1000 pXCHYC-6 DivL (28-170, 519-769)	pKAK0051	this study
KAK147	NA1000 pXCHYC-6 DivL (28-133, 519-769)	pKAK0052	this study
KAK149	NA1000 pBXMCS-2 DivL T391V	pKAK0036	this study
KAK174	*divL::spec* pXCHYC-6 DivL (1-769) *cckA::cckA-mclover3*	WSC10153	this study
KAK186	DH5α pXCHYC-6 DivL (1-170, 263-518)	pKAK0072	this study
KAK188	DH5α pXCHYC-6 DivL (171-391)	pKAK0088	this study
KAK191	DH5α pXCHYC-6 DivL (171-391)	pKAK0089	this study
KAK215	NA1000 pXCHYC-6 DivL (1-170, 263-518)	pKAK0072	this study
KAK221	NA1000 pXCHYC-6 DivL (171-391)	pKAK0088	this study
KAK222	NA1000 pXCHYC-6 DivL (263-518)	pKAK0089	this study
KAK228	NA1000 pXCHYC-6 DivL (1-391)	pKAK0073	this study
KAK254	DH5α pTEV-5 DivL (54-536, LZ)	pKAK0137b	this study
KAK270	DH5α pTEV-5 DivL (54-532, LZ)	pKAK0137f	this study
KAK332	BL21 pTEV-5 DivL (54-536, LZ)	pKAK0137b	this study
KAK334	BL21 pTEV-5 DivL (54-532, LZ)	pKAK0137f	this study
KAK392	DH5α pBAD DivL (134-769), msfGFP	pKAK0207	this study
KAK393	DH5α pBAD DivL (33-133), msfGFP	pKAK0208	this study
KAK406	BL21 pBAD DivL (33-133), msfGFP+ pACYC-mCherry-PopZ	pKAK0208, pACYC-mCherry-PopZ	this study
KAK411	BL21 pBAD DivL (33-133), msfGFP	pKAK0208	this study
KAK423	BL21 pBAD DivL (134-769), msfGFP +pCDFDuet1-mcherry-PodJ	pKAK0207, pWZ013-30	this study
KAK424	BL21 pBAD DivL (33-133), msfGFP +pCDFDuet1-mcherry-PodJ	pKAK0208, pWZ013-30	this study
KAK427	BL21 pBAD DivL (134-769), msfGFP	pKAK0207	this study
KAK428	BL21 pBAD DivL (134-769), msfGFP +pACYC-mCherry-PopZ	pKAK0207, pACYC-mCherry-PopZ	this study
SWD193	DH5α pGFPC-4 CckA (1500bp), mClover3	pSWD63	[166]
SWD491	DH5α pVMCS-1 DivL (1-27, 134-769)	pSWD209	this study

SWD485	DH5α pVMCS-1 DivL (1-170, 264-769)	pSWD210	this study
SWD557	DH5α pVMCS-1 DivL (1-262, 392-769)	pSWD228	this study
SWD492	DH5α pVMCS-1 DivL (1-391, 519-769)	pSWD211	this study
SWD504	DH5α pVMCS-1 DivL (1-565)	pSWD208	this study
SWD212	NA1000 cckA::cckA-mClover3	pSWD63	[166]
SWD513	NA1000 FRET+pVMCS-1 DivL (1-27, 134-769)	pSWD95, pSWD209	this study
SWD510	NA1000 FRET+pVMCS-1 DivL (1-170, 264-769)	pSWD95, pSWD210	this study
SWD611	NA1000 FRET+pVMCS-1 DivL (1-262, 392-769)	pSWD95, pSWD228	this study
SWD509	NA1000 FRET+pVMCS-1(1-391, 519-769)	pSWD95, pSWD211	this study
SWD525	NA1000 FRET+pVMCS-1 DivL (1-565)	pSWD95, pSWD208	this study
SWD608	NA1000 FRET Sensor only	pSWD95	[166]

4.0 A Bacterial Scaffolding Protein Regulates Cell Polarity and Cell-cycle Progression in *C.*

crescentus

This chapter was written in collaboration with Wei Zhao, Chao Zhang, Samuel W. Duvall, Dylan T. Tomares, Haley N. Petitjean, and W. Seth Childers. It contains data from two manuscripts in preparation: "Scaffold-scaffold interactions regulate cell polarity in a bacterium" by Wei Zhao*, Samuel W. Duvall*, Kimberly A. Kowallis, Chao Zhang, Dylan T. Tomares, Haley N. Petitjean, W. Seth Childers and "A bacterial scaffolding protein allosterically regulates histidine kinase activity to coordinate cell-cycle progression in *Caulobacter Crescentus*" by Chao Zhang*, Wei Zhao*, Kimberly A. Kowallis, and W. Seth Childers. Some of this data appears in the pre-print entitled "A circuit of protein-protein regulatory interactions enables polarity establishment in a bacterium" by Wei Zhao, Samuel W. Duvall, Kimberly A. Kowallis, Dylan T. Tomares, Haley N. Petitjean, and W. Seth Childers, *bioRxiv* 503250.

4.1 Introduction

Cells must orchestrate a vast number of signaling events in time and space to allow for complex processes such as cytoskeletal dynamics, division, and morphogenesis[182, 183]. This is often accomplished by scaffolding proteins that can direct signal flow in time and space. Scaffolding proteins utilize a variety of mechanisms to recruit proteins to subcellular locations and increase local concentrations in order to promote discrete interactions[182]. Scaffolds can also control the activity of their client proteins[182]. These roles are crucial in establishing polarity, which requires

robust localization of signaling antagonists at opposite sides of the cell[184]. In bacteria, several recent studies have implicated asymmetric scaffolding in both pathogenesis[185, 186] and antibiotic resistance[187], but it is still unclear whether bacteria use similar mechanisms as eukaryotic cells to achieve asymmetry.

A puzzling question regarding bacterial scaffold proteins that recruit proteins to cytosolic microdomains is in how the scaffolds themselves localize to specific subcellular niches. Several localization mechanisms have emerged from studies of individual proteins in bacteria (Figure 4.1)[188]. First, one scaffold can recruit another scaffold to create a polar complex[183]. In the absence of an existing scaffold, however, a protein may recognize characteristics that are unique to the poles, such as lipid[189] or peptidoglycan[175] composition. Some proteins also recognize the concave curvature at the cell pole[190]. A final mechanism for cell pole localization is through nucleoid occlusion. A large portion of the bacterial cytoplasm is occupied by the chromosome, or nucleoid. The cell poles provide void spaces where proteins can self-assemble. Finally, proteins at the pole can be inherited during cell division to produce two newly asymmetric daughter cells[191, 192]. These and other studies have provided an outline of methods for determining how an uncharacterized scaffold may localize to one or both cell poles in bacteria.
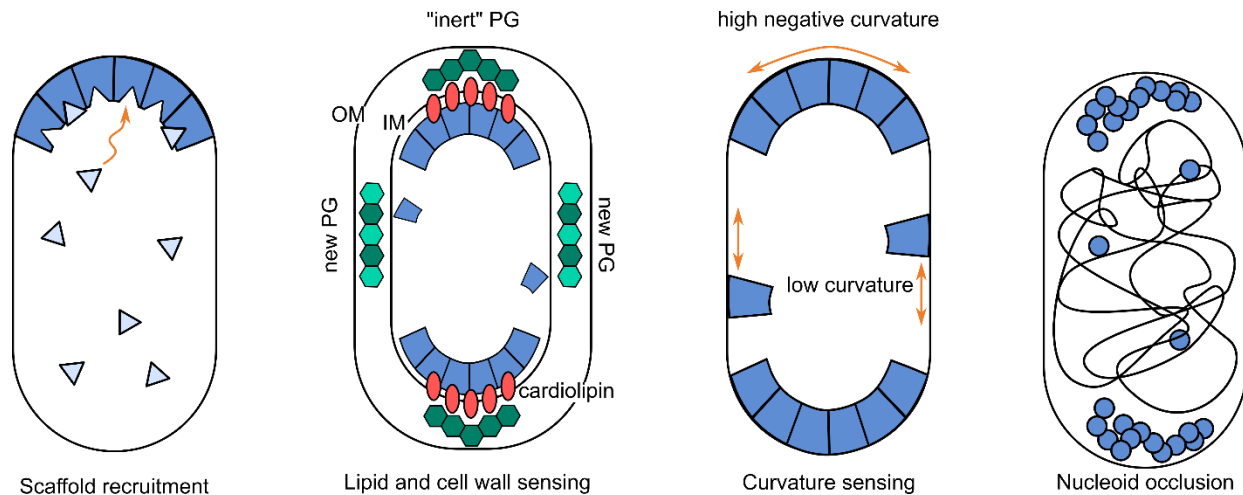
Figure 4.1: Mechanisms of protein localization at the bacterial cell poles First, one scaffold can recruit another to create a complex at the cell pole. Second, proteins may recognize cell wall or membrane components that are unique to a certain locale, such as "inert" peptidoglycan or cardiolipin at the poles. Third, large oligomers of proteins can detect areas of curvature and may favorably localize to the negative curvature at the poles. Fourth, the chromosome, or nucleoid, may leave little space for a self-assembled protein and thus drive scaffold assembly at the cell poles. Adapted from Laloux, G. & Jacobs-Wagner, C. *J Cell Sci*. 127(Pt 1):11-19 (2014).

In eukaryotes, a large subset of cellular microdomains are formed through biomolecular condensation. These include liquid-like, phase-separated regions within the cytoplasm that can concentrate specific proteins and nucleic acids and guide reaction specificity[193]. Sharing functions with organelles but not bound by a membrane, they are permeable to a wider range of biomolecules and more responsive to changes in environmental conditions. Many examples have been characterized in eukaryotes[193] and there have been recent examples from our lab[194, 195] and others[196] described in the microbiology literature. Proteins that form biomolecular condensates are often composed of folded domains that make specific interactions connected by flexible linkers or intrinsically disordered domains[197]. Intrinsically disordered domains have also been attributed to selective recruitment of client proteins[122, 193, 197]. Intrinsically disordered domains have low

sequence complexity but offer several features that lend them to condensate formation and protein recruitment such as charged-block patterns, aromatic residues that can participate in cation-pi or pi-pi interactions, and polar patches. These types of interactions are weak and transient, but in larger numbers, contribute to phase separation. Recognizing these motifs in uncharacterized scaffolds may lead to the discovery of more of these condensate forming proteins.

Scaffolds can regulate signaling pathways beyond subcellular localization[182, 198] (Figure 4.2). Recruitment of reaction components to the same locale can increase reaction rates[199]. Similarly, through competitive binding interactions, scaffolds can physically block interactions between proteins or between proteins and lipids in order to inhibit reactions[200]. Scaffolds can also allosterically regulate the activity of a signaling pathway component. An example of this is the scaffold Ste5 which puts its client into a conformation that is favorable for phosphorylation[201]. The well-characterized scaffolds which direct complex signaling networks allosterically come from eukaryotic systems. Emerging examples of complex regulation in bacteria[121, 183, 194, 196] indicate that the same scaffold functions may be at play in these systems.
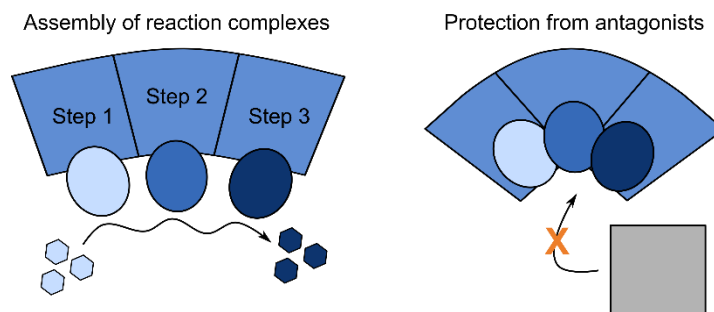
Figure 4.2: Scaffolds can promote or inhibit reactions by increasing the concentration of components or competing for binding Adapted from Shaw, A. & Filbert, *Nat. Rev. Immunol.* 9, 47–56 (2009).

The model bacterium for cell polarity *Caulobacter crescentus* undergoes an intricate life cycle that is largely achieved by scaffolds that organize the asymmetric localization of several developmental client proteins at opposite cell poles. As a result, each division cycle creates non-identical daughter cells, one motile swarmer cell and one sessile stalked cell (Figure 4.3A)[102, 103, 202]. The swarmer cell later differentiates into a stalked cell to initiate another round of replication[203]. One critical difference between the stalked cell and the swarmer cell that is established by asymmetric scaffolding is the activity of the master regulator CtrA[90, 103, 152, 161, 177, 204]. CtrA is responsible for the transcription of more than 90 genes that drive the cell cycle[105]. Additionally, CtrA~P prevents additional chromosome replication until the swarmer cell differentiates into a stalked cell[205]. Scaffolds selectively localize the kinase DivJ and phosphatase PleC at opposite poles where they regulate the response regulator DivK, and ultimately, CtrA (Figure 4.3A)[108, 177]. In swarmer cells, CtrA is phosphorylated, beginning flagellar and pili biogenesis and initiating chemotaxis[105]. In stalked cells, CtrA is not phosphorylated, the holdfast forms, and chromosome replication is allowed[105, 205].
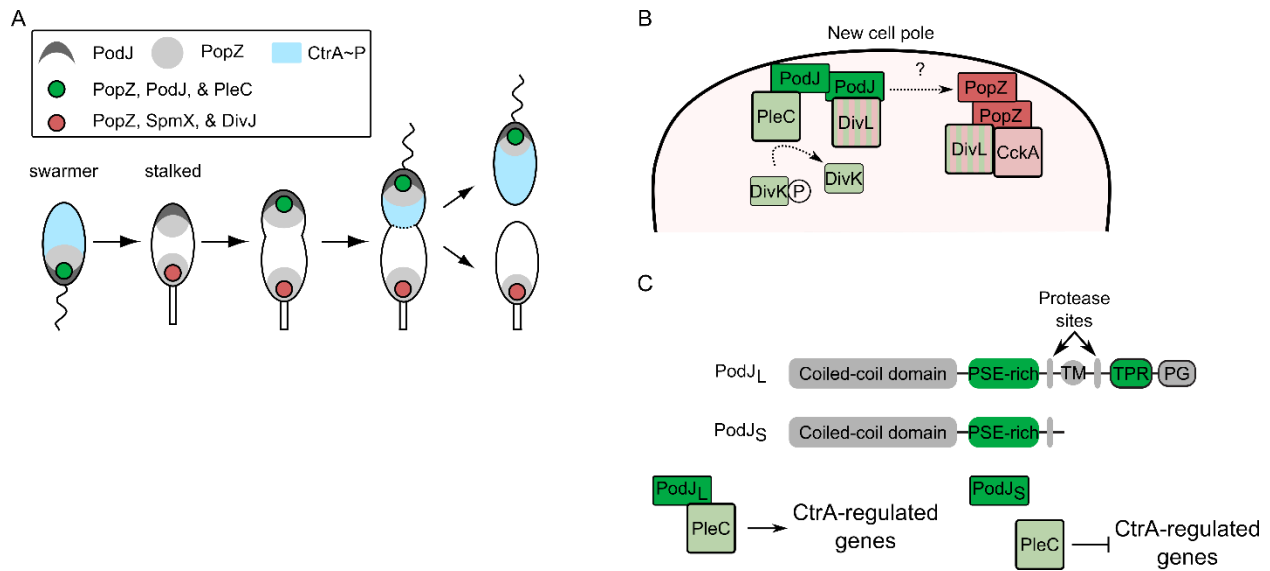
Figure 4.3: The scaffolds PopZ and PodJ regulate cell polarity and the cell cycle in *C. crescentus* (A) A cartoon showing the *C crescentus* life cycle. A motile swarmer cell differentiates into a sessile stalked cell, which elongates and eventually divides into one stalked and one swarmer daughter cells. The PodJ-rich polar region remodels into a SpmX-rich region upon differentiation into a stalked cell. Then the new cell pole becomes PodJ-rich. Upon division, each cell inherits a distinct polar composition. Ultimately, regulation of the master regulator CtrA controls replication and cell type. (B) Several key players in the *C. crescentus* cell cycle rely on PodJ (PleC, DivL) (green) and PopZ (CckA) (red) scaffolds within the PopZ microdomain at the new cell pole (light pink). (C) PodJ undergoes proteolysis throughout the cell cycle and proteolysis correlates with PleC localization (putative interaction domains shaded green) and downstream CtrA regulation.

Two scaffold proteins that are integral to asymmetry in *C. crescentus* are PopZ and PodJ. PopZ self-assembles into a micron-sized biomolecular condensate at both cell poles (Figure 4.3A)[122, 170, 191, 196, 202]. Like many of its eukaryotic scaffold counterparts, PopZ is largely disordered, a quality that allows it to specifically recruit multiple client proteins[122]. A favored model for how PopZ accumulates at the cell pole in *C. crescentus* and the divergent *E. coli* is nucleoid occlusion[191, 192, 206]. Interestingly, the hubs at the cell poles are asymmetrically inherited during division, conferring asymmetry to the daughter cells[191, 192]. Single-molecule tracking

125

experiments[196] and FLIP studies[122] have shown that PopZ dynamically recruits multiple protein clients at each cell pole in pre-divisional cells[122].

Some of the clients that are scaffolded by PopZ localize to both cell poles. The kinase CckA and its modulator DivL bind to both PopZ microdomains (Figure 4.3B)[122]. PopZ serves as an attachment site for the ParB-parS centromere as it moves from the old cell pole to the new cell pole during chromosome segregation[122, 191]. Only at the old cell pole, however, PopZ recruits a second scaffold SpmX, which recruits the kinase DivJ[183]. However, the mechanisms that enable one scaffold to promote the formation of two compositionally distinct biomolecular condensates at each pole remains unclear.

A unique feature within the PopZ subdomain at the new cell pole is the scaffolding protein PodJ. The cytoplasmic portion of PodJ comprises a series of coiled-coil folds followed by an intrinsically disordered PSE-rich region. As with PopZ[122, 196, 197] and other eukaryotic scaffolds, this may also form a biomolecular condensate. Within the periplasm, PodJ contains a tetrapeptide co-repeat (TPR) domain and a peptidoglycan binding sensing (PG) domain that is critical for robust polar localization[175] and is thus hypothesized to recognize the inert peptidoglycan at the cell poles[207]. The exact mechanism of how PodJ localizes to the cell pole remains unknown.

Studies have shown that PodJ localization is required for the phosphatase PleC to be recruited at the new cell pole (Figure 4.3B)[208, 209]. The peptidoglycan binding domain and portions of the PSE-rich domain have been implicated in recruiting PleC to the pole[175]. We also demonstrated that PodJ is a DivL binding partner in *E. coli* in Chapter 3 (Figure 3.8). Intriguingly, deletion of PodJ also resulted in a decrease in the PopZ client CckA at the cell pole[121]. The downstream effects of deleting or truncating the PodJ scaffold were down-regulation of the CtrA pathway[121, 175] and the CtrA-regulated gene *pilA*[121, 175, 208]. Since several key players in the CtrA

pathway rely on either PodJ (PleC, DivL) or PopZ (DivJ, CckA) to localize together at the new

cell pole, these studies suggest that there may be physical and functional interactions between PodJ

and PopZ (Figure 4.3B). Here we characterize the physical interactions between PopZ and PodJ

that allow them to coordinate the signaling interactions between their respective clients within the

new cell pole microdomain to ensure reliable asymmetric cell division.

Not only is PodJ required for PleC localization at the new cell pole[208, 209], it was further

noticed that PleC is no longer fully functional when it is delocalized in a p*odJ* deletion strain[208].

Delocalized PleC results in a 50% decrease in *pilA* levels[208]. However, inactive but localized PleC

mutants affect not only *pilA* promoter activity, but cause stalk biogenesis, motility[210], and

holdfast[211] defects. Thus, it seems that PodJ is involved in regulating some, but not all, PleC

functions. PleC's undergoes an activity switch from phosphatase to kinase that correlates with its

subcellular position. When PleC is localized at the new cell pole, it functions as a phosphatase[161].

In contrast, when it is localized at the old cell pole in the swarmer-to-stalk transition, it functions

as a kinase[212]. Therefore, PleC's kinase-to-phosphatase switch may be influenced by protein-

protein interactions at each cell pole. These studies have led to a collective model in which PleC

localization at the cell pole, facilitated by PodJ, is required for its full impact on select cell

processes[121, 175, 208]. We speculate that PodJ has a role beyond merely tethering PleC to the pole,

and that it allosterically regulates PleC activity.

Upon cell division, full-length PodJ$_L$ is proteolyzed into a shortened form PodJ$_S$[163, 213] via

a set of proteases (Figure 4.3C)[121, 163, 213]. This proteolytic processing of PodJ correlates with a

downregulation of CtrA-regulated genes[175]. Notably, the deletion of PodJ's cytoplasmic domain or

periplasmic domains results in a decrease in pilA promoter activity[209] and reduction of PleC cell

pole localization[175]. These past studies suggest that both PodJ's cytoplasmic and periplasmic

domains play roles upon CtrA pathway regulation. In fact, there are existing examples in which modifications of the scaffold, rather than the active enzyme, can regulate a signaling pathway[182, 200]. Here, we test the model that PodJ's proteolytic processing serves as a direct input signal to coordinate PleC signaling activity. We have taken a synthetic biology approach to reconstitute PodJ scaffolding and PleC signaling to map out the set of molecular interactions that transmit signals from PodJ to PleC.

Despite many studies dedicated toward understanding the cell polarity circuit in *C. crescentus*, many questions about these scaffolding interactions remain. Two separate scaffolds are responsible for the correct localization and activity of several clients within the same signaling pathway[122, 208, 209], and how these scaffolds cooperate in their common task is unknown. There is also speculation that allosteric regulation of the cell cycle pathway is at play[121, 175, 208]. In this chapter, we will interrogate these roles to uncover a novel scaffold-scaffold interaction and a scaffold that acts as an activity switch within the cell cycle pathway.

Overall within this chapter, we will interrogate how the PodJ scaffold accumulates at the cell poles, the roles of the PodJ-PopZ scaffold-scaffold interaction, and if and how the PodJ scaffolds impact the activity of associated signaling proteins.

4.2 Results

PodJ domain architecture predictions suggest self-assembly and peptidoglycan sensing as localization mechanisms Previous studies[121, 175] and primary sequence structure prediction allowed us to map out PodJ's domain architecture in order to perform an analysis of domains involved in localization and interaction with other proteins (Figure 4.4). The PodJ

128

scaffold domain architecture includes a N-terminal cytosolic domain composed of a coiled-coil rich region that is adjacent to an intrinsically disordered region[175]. Previously, Curtis *et al.* demonstrated that deletion of 589-639, enriched in positively charged residues, reduces activity from CtrA-dependent promoters[121]. Our structure prediction results showed a larger intrinsically disordered domain that includes the PSE-rich region from residues 471-588 (Figure 4.4). Oligomerization domains, that increase multivalency, followed by disordered linkers are common domain architectures that can promote phase separation[122, 193, 194]. Therefore, if PodJ exhibits self-assembly or phase separation capabilities it may suggest that PodJ accumulates at the cell poles via nucleoid occlusion mechanism (Figure 4.1). A second mechanism that has been suggested for PodJ localization is an interaction with the cell wall at the poles[175]. The C-terminal end of PodJ passes through the membrane into the periplasm and contains the TPR and PG domains (Figure 4.3C)[175]. Previous domain analysis has implicated a portion of the intrinsically disordered domain and the periplasmic domain in new cell pole targeting of PodJ [175]. However, it remains unclear how these domains contribute to PodJ's subcellular accumulation. We therefore asked whether PodJ is able to self-assemble in the absence of other scaffolds.
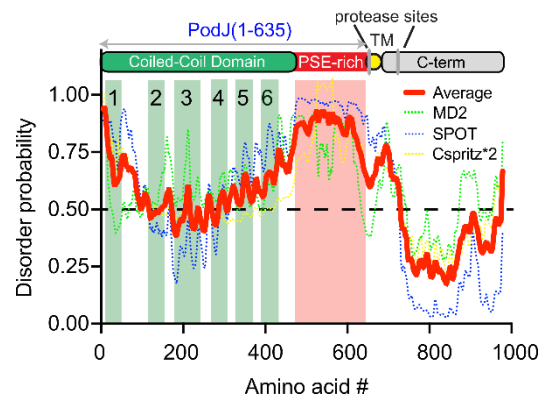

Figure 4.4: **PodJ comprises motifs predicted to self-assemble and recruit protein clients** PodJ domain organization predicted by HHpred and adapted from previous studies[121, 175]. The coiled-coil rich region was analyzed

by PCOILS and modeled with MODELLER. The probability of intrinsic disorder over the primary sequence of PodJ (red line), represented as the average scores from four disorder prediction algorithms: Meta disorder MD2, SPOT, Cspritz*2, and MFDp2. Analysis was perfomed in collaboration with Wei Zhao.

PodJ forms a focus at the poles independent of PopZ Self-assembly of PopZ drives the formation of a biomolecular condensate at both cell poles[162, 191, 196]. PopZ recruits the oligomeric SpmX to the old cell pole, which then recruits the kinase DivJ[183]. We first asked whether the new cell pole is assembled in a similar manner. To interrogate whether PodJ relies upon PopZ to localize to the cell pole, we visualized sfGFP-PodJ in wild-type *C. crescentus* and a Δ*popZ* strain. We observed that sfGFP-PodJ was able to accumulate at the poles in over 90% of cells in the Δ*popZ* strain (Figure 4.5A). The deletion of PopZ resulted in an increase in cells with bipolar PodJ localization, but the ability to accumulate at the cell poles was unaffected.
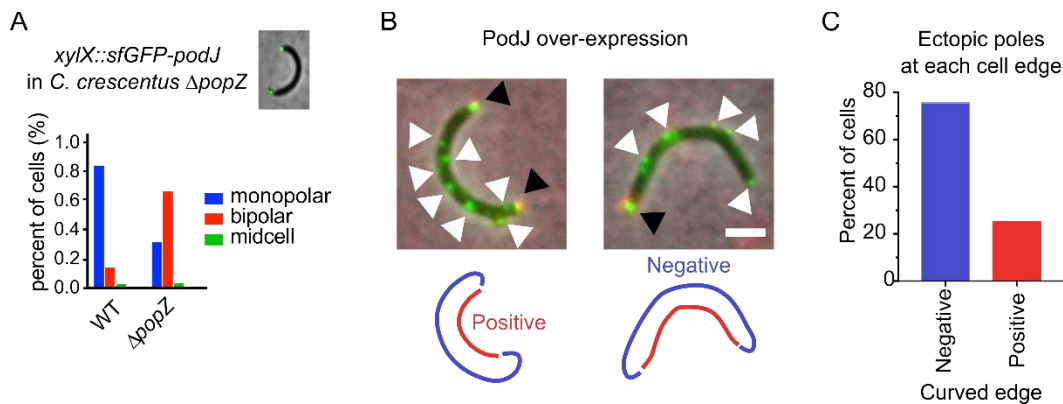
Figure 4.5: PodJ can accumulate as a focus independent of PopZ (A) sfGFP-PodJ was expressed from the xylose locus in wild-type *C. crescentus* and a *popZ* deletion strain. n>161 cells. (B) mNeonGreen-PodJ was over-expressed from a high copy xylose inducible plasmid in a *C. crescentus* strain expressing mCherry-PopZ from the *popZ* locus. Black arrows point to PodJ foci with PopZ colocalized. White arrows point to PodJ-only foci. 27% of the PodJ foci were co-localized with PopZ. Outlines below the cells distinguish between postive and negative curvature. n=164 cells. Scale bar denotes 2 µM. (C) Percent of ectopic sfGFP-PodJ foci which localized to the negative or positive

curvature along the edges of the cell. N=520 foci. Imaging sfGFP in the Δ*popZ* strain was performed in collaboration with Wei Zhao.

SpmX forms ectopic poles upon over-expression, and these new poles nucleate new PopZ microdomains[183]. We observed that over-expression of PodJ also results in the formation of ectopic poles, indicating that PodJ plays a role in maintaining cell polarity and shape (Figure 4.5B). However, this process is independent of PopZ. Only 27% of the PodJ foci, at the typical poles or ectopic poles, were co-localized with PopZ. This observation suggests that PodJ accumulation as a focus can occur independent of the PopZ scaffold. We also noticed that 75% of the ectopic poles along the side of the cells formed along the concave edge of the cells. This suggests that there may be a mechanism by which PodJ recognizes the negative curvature at the poles and along one side of the cell (Figure 4.1). We would not expect the formation of seemingly randomly placed ectopic poles based on the PG sensing model[175] or the nucleoid occlusion model.

PodJ accumulates at the cell poles in *E. coli* independent of specific *C. crescentus* proteins To test if PodJ subcellular accumulation was independent of any other *C. crescentus* specific factors, we heterologously expressed PodJ in *Escherichia coli* BL21 cells. Notably, the γ-proteobacterium *E. coli* is highly divergent from the α-proteobacterium *C. crescentus* and does not contain any clear homologs of the *C. crescentus* scaffolding proteins or new cell pole signaling proteins. YFP-PodJ accumulated at both cell poles in *E. coli* (Figure 4.6A-B), suggesting that PodJ cell pole accumulation was independent of known *C. crescentus* polarity proteins.
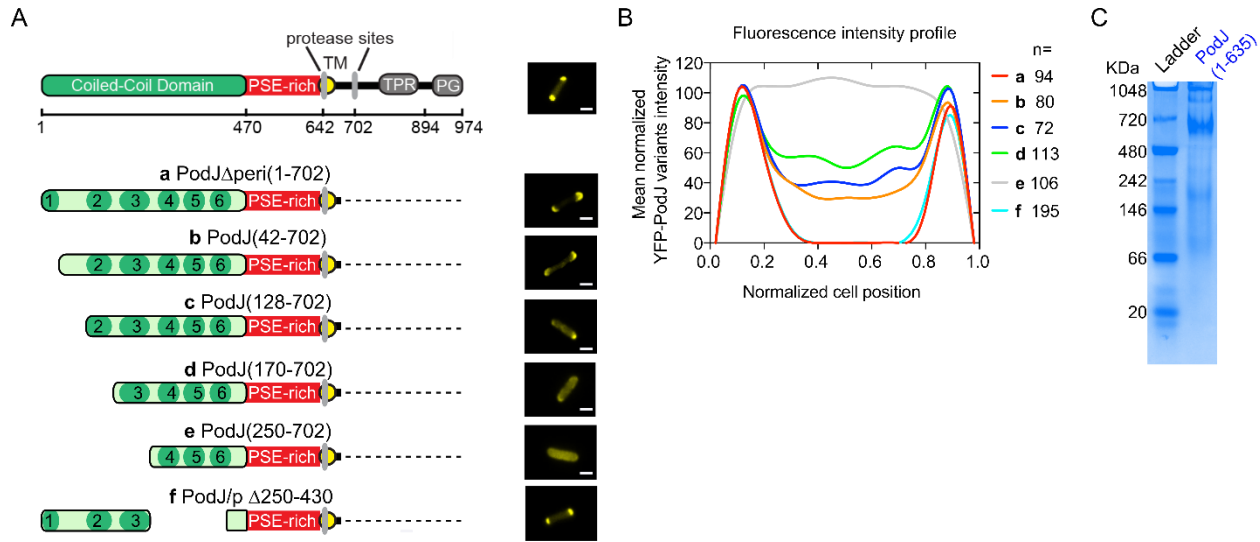
Figure 4.6: PodJ self assembles *in vitro* and in *E. coli* through coiled-coils 1-3 (A) Heterologous expression of YFP-labelled PodJ variants in *E. coli*. (B) Fluorescence intensity profiles normalized to cell length show the average distribution of each YFP-PodJ variant across the cell body. (C) Native gel analysis of purified PodJ 1-635 in which the protein is subjected to nondenaturing gel electrophoresis at 4°C and subsequently stained with Coomassie blue stain. Several distinct bands represent high-order oligomers of PodJ monomers (71 kDa). Experiments were performed in collaboration with Wei Zhao.

To identify a minimal focus assembly construct, we screened a set of PodJ domain deletion variants for their capabilities to maintain cell pole accumulation (Figure 4.6A-B). Amongst this set, the construct representing the proteolyzed form of PodJ that lacks the periplasmic domains, PodJΔperi, accumulated at the cell poles similar to the wild-type PodJ in *E. coli* (Figure 6A-B). In contrast, the PodJ localization pattern gradually changed from bipolar to diffuse when we truncated the coiled-coil (CC) domains 1 to 3 (Figure 4A-B), indicating that residues 1-249 were critical for cell pole accumulation of PodJ.

PodJ self-assembled into a high order oligomer *in vitro* Since PodJ accumulated at the cell poles independent of other known scaffolding proteins *in vivo*, we hypothesized that PodJ is a self-assembled protein. We therefore purified the cytoplasmic portion of PodJ, PodJ(1-635), and

analyzed the protein through native gel analysis (Figure 4.4C). The result showed PodJ oligomerization into an array of large complexes of PodJ monomers (71 kDa) ranging in size from approximate 8-mers (710 kDa) to 14-mers (994 kDa). These results indicate that PodJ is a self-assembled scaffolding protein, which suggest that coiled-coil multivalent interactions could contribute to PodJ's localization pattern.

PodJ forms liquid-liquid phase separated droplets in solution Given the high degree of oligomerization of PodJ in solution, we tested whether PodJ undergoes liquid-liquid phase separation to form a biomolecular condensate. PodJ's predicted secondary structure contains a characteristic coiled-coil and intrinsically disordered domains[175] that have been shown in other proteins to promote formation of biomolecular condensates[193, 197]. Cellular assemblies that are predicted to form biomolecular condensates often form spherical, liquid-like droplets in solution[214]. To test if PodJ forms biomolecular condensates, we combined purified sfGFP-PodJ(1-635) at a concentration of 20 µM in a Tris buffer with 300 mM sodium chloride and changed the concentration of PEG 8000. We observed that liquid-like, rounded droplets were visible using phase contrast and fluorescence microscopy (Figure 4.7). The size of these condensates was dependent upon PEG concentration, with the largest size at 2% PEG. At a lower salt concentration of 150 mM sodium chloride, the droplet size decreased. These results indicate that PodJ forms a PEG and salt-dependent biomolecular condensate.
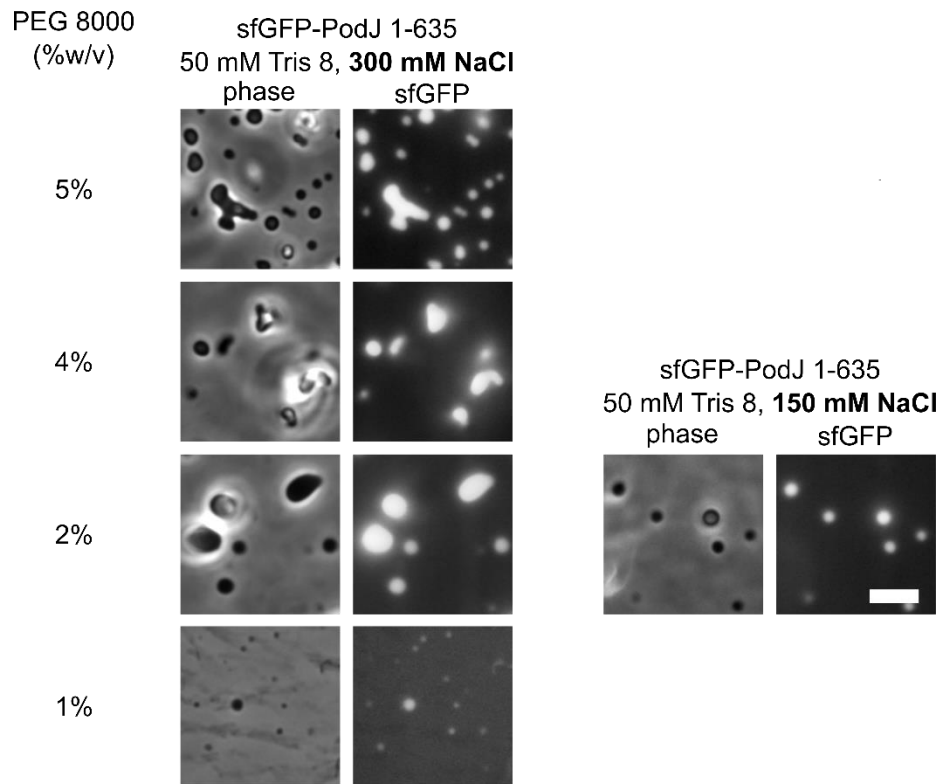
Figure 4.7: PodJ self assembles into a salt- and PEG-dependent condensate in solution Purified sfGFP-PodJ 1-635 were mixed with a Tris buffer and varying amounts of salt and PEG 8000. The solutions were then sealed onto a glass slide to be imaged. Scale bar denotes 5 µm.

During our initial screen of a wider range of PEG conditions and using potassium chloride, we assessed the ability of PodJ(250-635), which lacks CC1-3, to form a condensate (Figure 4.8). This region was required for accumulation in *E. coli* (Figure 4.6), so we predicted that this construct would not form droplets *in vitro*. However, this construct formed droplets of similar sizes and numbers as PodJ(1-635) for each condition. Therefore, CC1-3 is critical for cell pole accumulation in *E. coli*. However, it is not required for the formation of biomolecular condensates *in vitro*. The CC1-3 deletion construct retains the intrinsically disordered PSE-rich domain, which is predicted to promote biomolecular condensate formation. Therefore, future investigations will

be needed to interrogate the roles of the PSE-rich domain and the remaining CC4-6 in self-assembly in *C. crescentus* and in solution.
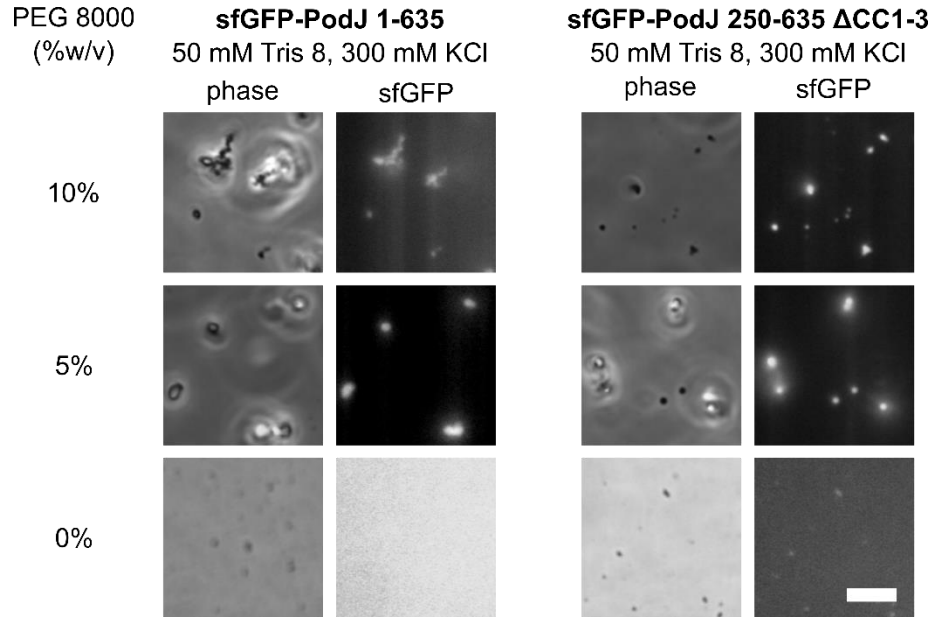
Figure 4.8: CC1-3 is not required for liquid-liquid phase separation in solution Purified sfGFP-PodJ 1-635 or sfGFP-PodJ 250-635 were mixed with a Tris buffer and varying amounts of salt and PEG 8000. The solutions were then sealed onto a glass slide to be imaged. Scale bar denotes 5 μM.

PopZ binds directly to coiled-coil region 4-6 of PodJ in *E. coli* To determine if PopZ and PodJ interact directly, we heterologously expressed fluorescent protein fusions of PodJ and PopZ in *E. coli*. As shown in Figure 4.9A, when PopZ is expressed in *E. coli*, about 80% of cells exhibit monopolar localization. However, PopZ co-localizes in a bipolar pattern in about 60% of cells when co-expressed with YFP-PodJ. To determine the PopZ binding site within PodJ, we screened the capability of PopZ to bind to the library of PodJ domain deletion variants through co-expression in *E. coli* (Figure 4.9B). We found that deletion of the C-terminal periplasmic domain in PodJ did not disrupt the PodJ-PopZ interaction (Figure 4.9B). In contrast, deletion of its CC4-6

domains disrupted PopZ co-localization with PodJ. We then expressed YFP-CC4-6 alone and observed that it was dispersed through the cytoplasm in *E. coli*. However, mCherry-PopZ was able to recruit this PodJ variant to the cell pole when co-expressed in *E. coli*. These data indicate that coiled-coil 4-6 in PodJ functions as a PopZ interaction site.
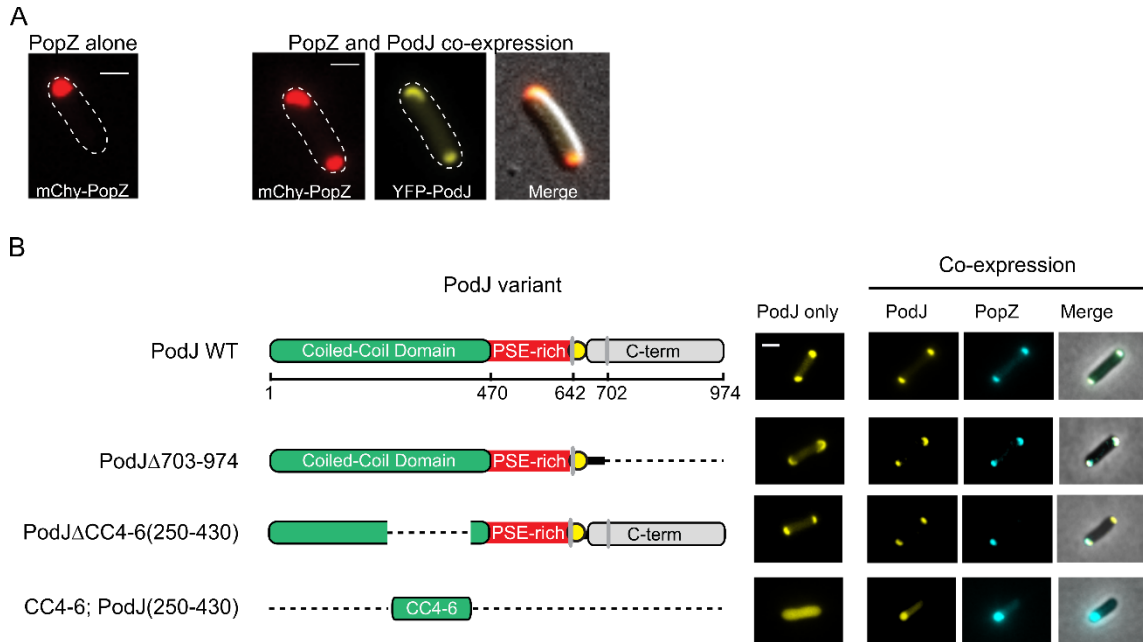
Figure 4.9: PodJ interacts with PopZ through coiled-coils 4-6 in *E. coli* (A) Expression of mCherry-PopZ alone and co-expressed with YFP-PodJ in *E.* coli. (B) Co-expression of YFP-PodJ variants and mCherry-PopZ in *E. coli*. Experiments were performed in collaboration with Wei Zhao.

PodJ's coiled-coil region 4-6 is required to recruit PopZ to the new cell pole in *C. crescentus* We next wondered whether this PodJ-PopZ interaction site is important in *C. crescentus* polarity. We observed sfGFP-PodJΔCC4-6 in the *C. crescentus podJ* deletion strain was able to localize at the new cell pole (Figure 4.10A). However, this PodJ variant recruited about 2-fold less PopZ to the new cell pole than full length sfGFP-PodJ. This resembles the PopZ localization pattern in a strain in which *podJ* is entirely deleted. (Figure 4.10B). A comparison of

PopZ cell pole intensity ratio (old:new) shows that the ratio increases in the Δ*podJ* strain and in cells expressing PodJΔCC4-6, indicating that PodJΔCC4-6 lacks a functional PopZ binding site (Figure 4.10C). PodJΔCC4-6 exhibits mild localization at the mid-cell in *C. crescentus* (Figure 4.10A). This could mean that once established, the PodJ-PopZ interaction stabilizes PodJ at the new cell pole. It could also indicate that PodJ contains binding site that interacts with a component of the division plane, such as the protein TipN, which localizes to the mid-cell at the time of division and becomes an inherited marker of the new cell poles[215].
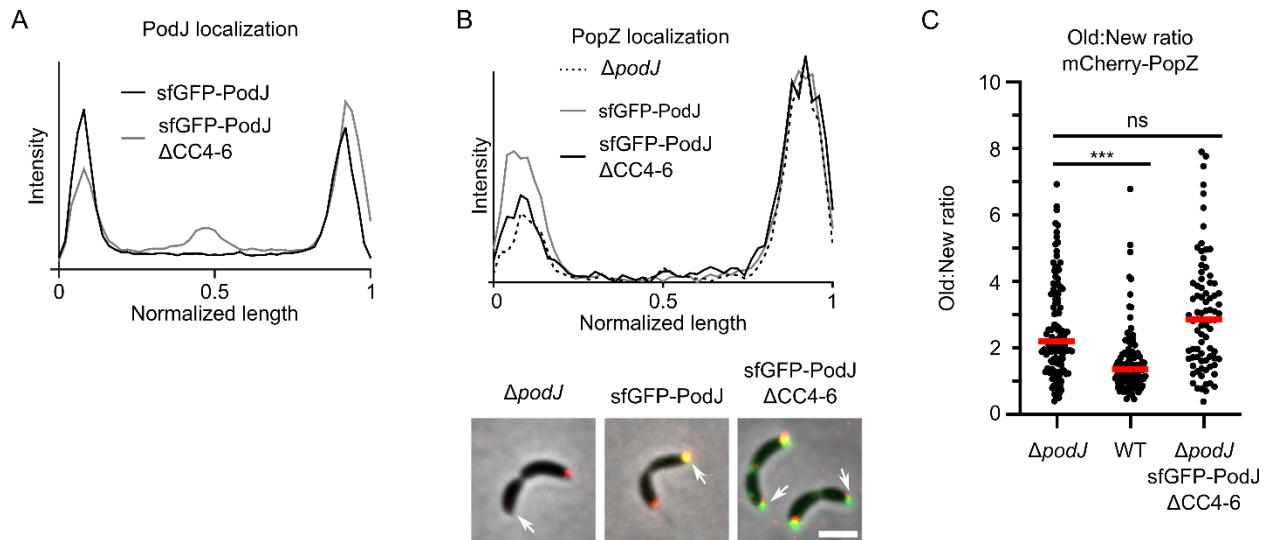
Figure 4.10: PodJ coiled-coils 4-6 are required to robustly recruit PopZ to the new cell pole in *C. crescentus* mCherry-PopZ was expressed from the chromosomal *popZ* locus in the *podJ* deletion strain, a *podJ* deletion strain supplemented with sfGFP-PodJ from the chromosomal xylose locus with 0.03% xylose for 3 hours, and a *podJ* deletion strain similarly supplemented with sfGFP-PodJ-ΔCC4-6. (A) Fluorescence intensity profiles show the average fluorescence intensity of sfGFP-PodJ variants across the cell body. (B) Fluorescence intensity profiles show the average fluorescence intensity of mCherry-PopZ in each of the strains. Representative cell images are shown. Arrows point to the new cell pole. Scale bar denotes 2 μm. (C) Analysis of the strains in B to determine ratios of the fluorescence intensity at the old and new cell poles. Experiments were performed in colloboration with Sam Duvall.

We present a model of our findings regarding PodJ's assembly at the new cell pole and its interactions with PopZ (Figure 4.11). We discovered that PodJ accumulates at the cell pole in *C. crescentus* and *E. coli* independent of other protein scaffolds, including PopZ (Figures 4.5-4.6). PodJ self-assembles in solution (Figure 4.6C), and preliminary results show that PodJ forms a biomolecular condensate *in vitro* (Figure 4.7-4.8). The *E. coli* experiments indicated that PodJ's coiled-coil 1-3 region is critical for self-assembly, but this was not required for condensate formation *in vitro*. We hypothesize that the PodJ oligomeric complex recognizes the cell pole by sensing negative curvature due to the bias of ectopic poles on the concave side of *C. crescentus* cells (Figure 4.5B). Once at the pole, PodJ can promote new cell pole accumulation of PopZ through its coiled-coil 4-6 domain.
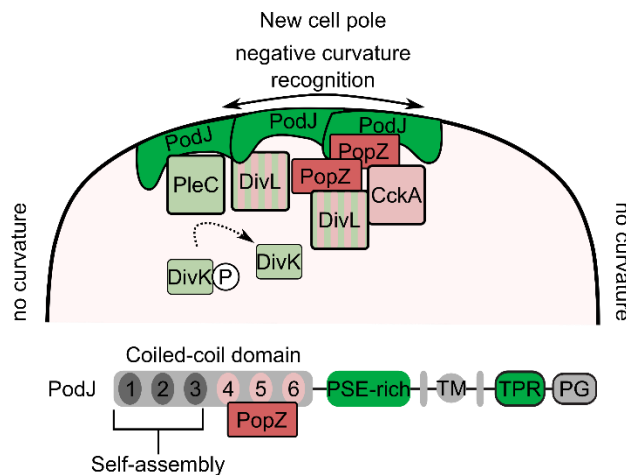
Figure 4.11: Model of PodJ's self-assembly and accumulation at the new cell pole and recruitment of PopZ.

PleC is recruited to the cell poles by PodJ's PSE-rich domain in *E. coli* We next addressed how PodJ recruits PleC to the new cell pole, and whether it plays a role in regulating PleC activity. Previous domain analysis has indicated that the peptidoglycan binding domain and

a portion of the disordered PSE-rich domain of PodJ contribute to PleC's new cell pole localization in *C. crecentus*[121, 175]. However, it is unclear whether these regions are direct PleC binding sites or if they indirectly mediate PleC localization. To interrogate the interactions between PodJ and PleC, we heterologously co-expressed full-length PleC together with a library of PodJ variants in *E. coli* (Figure 4.12). Co-expression of PodJ and PleC resulted in the recruitment of PleC to the cell poles, indicating that PodJ and PleC interact directly in *E. coli*. Deletion of the periplasmic domain of PodJ did not affect PleC recruitment or PodJ cell pole localization. Further removal of the transmembrane region does not affect PodJ binding to PleC.
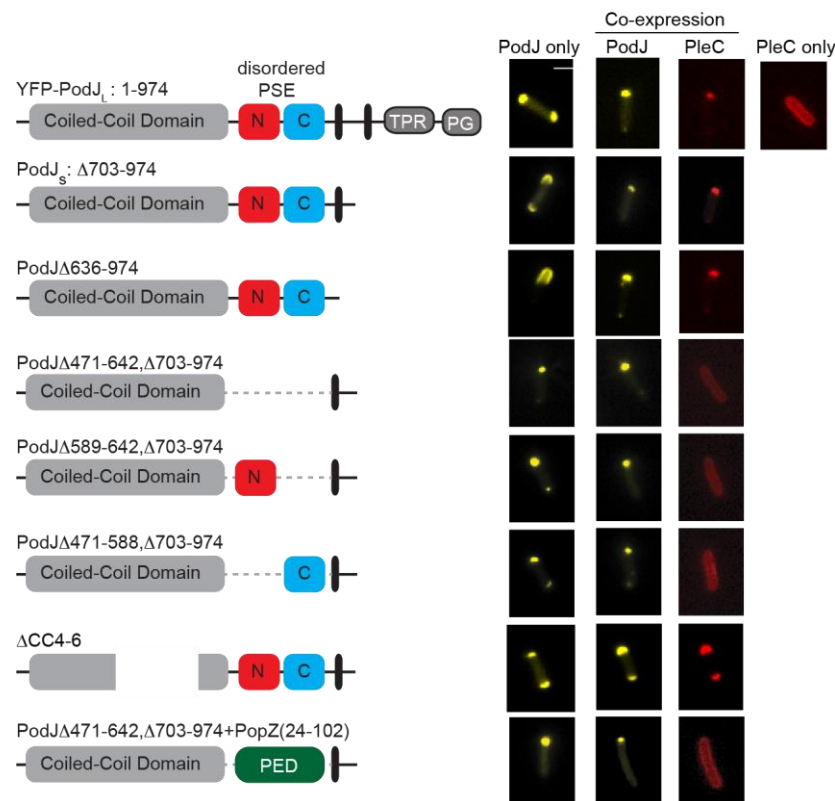
Figure 4.12: The PodJ scaffold interacts with the histidine kinase PleC through the disordered PSE domain

Co-expression of PleC-mCherry with a panel of YFP-PodJ variants in *E. coli*. YFP-PodJ was induced with 0.5 mM

IPTG and PleC-mCherry was induced with 1mM arabinose for 2 hours. Experiments were performed in collaboration with Wei Zhao.

Previously, Curtis *et al.* demonstrated that deletion of 589-639, enriched in positively charged residues, reduces activity from CtrA-dependent promoters[121]. Our earlier domain architecture prediction identified a larger intrinsically disordered region with two distinct compositions. Residues 471 to 588 are abundant in prolines (18.6%), glutamate/aspartate (20.3%) and serine (9.3%) and residues 589 to 642 are abundant in arginine/lysine (22.2%), glycine (14.8%), and serine (14.8%). Our results showed that this larger intrinsically disordered region was needed in its entirety to recruit PleC to the cell poles (Figure 4.12). The deletion of the N-terminal disordered region or C-terminal disordered region individually resulted in the loss of PleC recruitment to the cell poles by PodJ in *E. coli*. To determine if any disordered peptide sequence would recruit PleC, we replaced PodJ's PSE-rich domain with a similar negatively charged PED-rich domain from the scaffolding protein PopZ[122, 216]. One notable difference between the two disordered regions is that PopZ's disordered domain is more homogenously negatively charged and lacks a positively charged block. Additionally, PodJ's PSE-rich domain is 171 residues long while PopZ's PED-rich domain 78 residues long and may form a smaller interface surface with which to interact with PleC. The disordered domain from the PopZ scaffold was unable to promote PleC recruitment to the cell poles, suggesting that the PodJ PSE-rich domain specifically recruits PleC to the cell poles (Figure 4.12).

PleC interacts with PodJ through its tandem cytoplasmic sensory domain We next asked which domains within PleC serve as the site of PodJ interaction. PleC is composed of a N-terminal sensory domain and a C-terminal histidine kinase domain. The sensory domain contains a periplasmic region and two PAS domains in the cytoplasm. To test the interaction domain(s)

140

with PodJ, we heterologously expressed PleC domain deletion variants together with PodJ in *E. coli* (Figure 4.13). PleC variants that lack the periplasmic domain, PAS A, PAS B, or the HK maintained their ability to co-localize with PodJ. This ability to delete each domain within PleC individually suggested that PleC may have redundant sites of interaction with PodJ. We observed that the deletion of both PAS A and PAS B results in complete loss of PleC's cell pole localization. We tested whether each of these domains were sufficient for PodJ binding and found that PAS A, PAS B, and PAS AB colocalized with PodJ at the pole. These results suggest that PodJ interacts with PleC's PAS A and PAS B sensory domains.
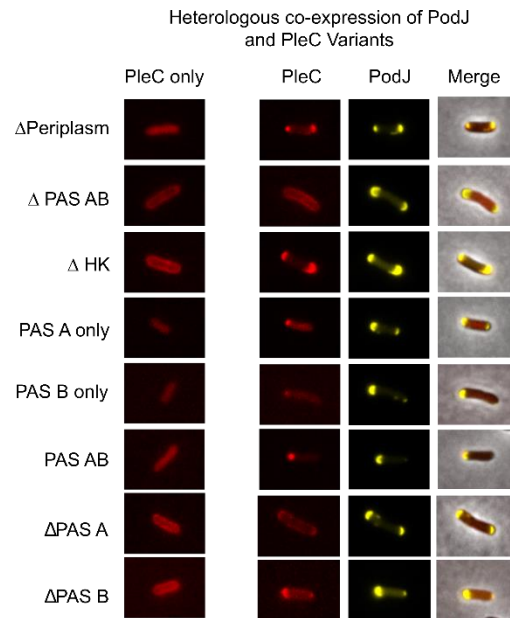
Figure 4.13: PodJ interacts with PleC PAS A and PAS B domains Co-expression of YFP-PodJ with a panel PleC-mCherry variants in *E. coli*. YFP-PodJ was induced with 0.5 mM IPTG and PleC-mCherry was induced with 1mM arabinose for 3 hours. Experiments were performed in collaboration with Wei Zhao.

PleC's PAS sensory domain interacts with PodJ's intrinsically disordered domain at the new cell pole in C. crescentus Past work has shown that PleC-GFP localizes at the new cell

pole in pre-divisional *C. crescentus* cells[217], and was dependent upon PodJ[175]. Therefore, as a control, we observed that expression of PleC-mCherry in a *podJ* deletion background resulted in the loss of localization (Figure 4.14A). Supplementation of the *podJ* deletion strain with xylose-induced sfGFP-PodJ restored PleC's localization to the new cell pole. Past studies have shown that the deletion of PodJ's the C-terminal portion of the intrinsically disordered region partially disrupted PleC's localization at the cell poles[121, 175]. Because deletion of PodJ-PSE disrupted binding by PleC in *E. coli*, we asked if deletion of the disordered domain would disrupt PleC's cell pole localization in *C. crescentus*. Expression of sfGFP-PodJ without the intrinsically disordered domain, PodJΔPSE, accumulated at the cell poles in *C. crescentus*. However, PodJΔPSE was unable to recruit PleC to the new pole in *C. crescentus*. Therefore, we conclude that PodJ serves as a scaffold that recruits PleC through its intrinsically disordered domain.
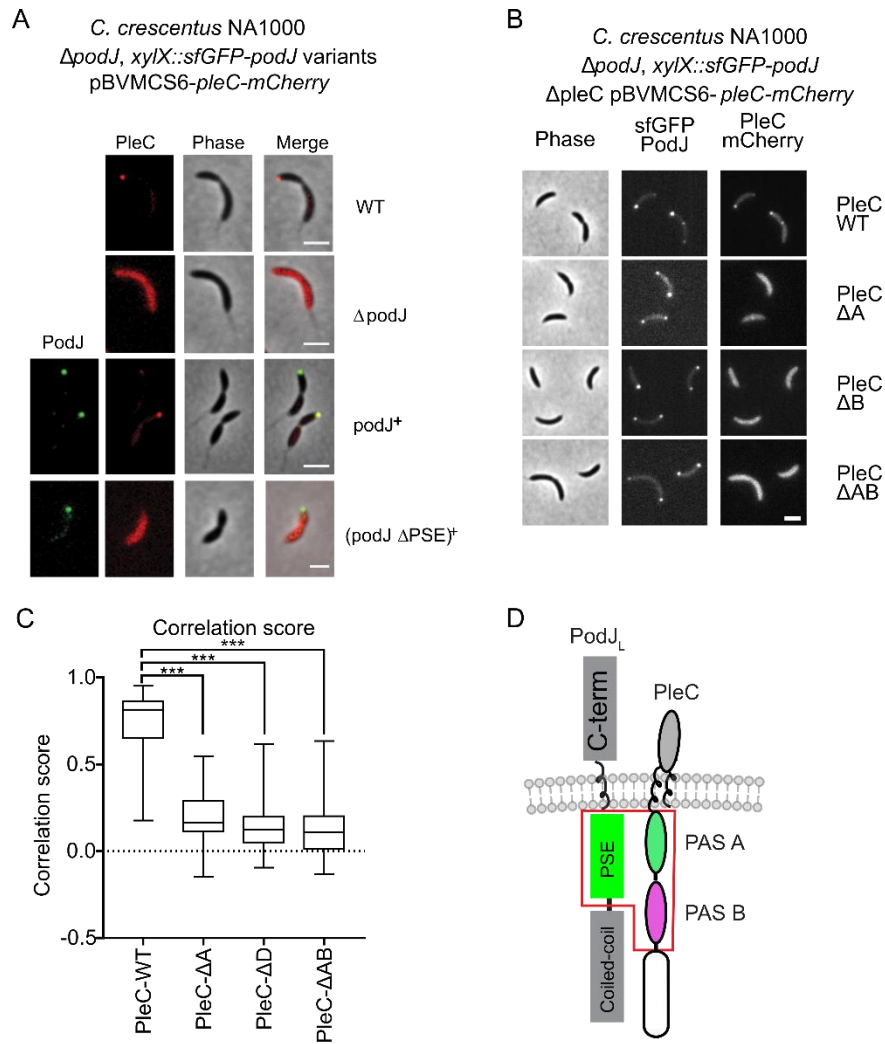
Figure 4.14: The PodJ-PleC interaction sites are conserved in *C. crescentus* (A) Localization of PleC-mCherry expressed in wild-type *C. crescentus*, the *podJ* deletion strain, and a *podJ* deletion strain supplemented with sfGFP-PodJ or sfGFP-PodJ-ΔPSE. Cells were induced with 0.03% xylose for sfGFP-PodJ and 0.05 mM vanillate for PleC-mCherry for 5 hours. Scale bar denotes 2 µm. (B) Localization of PleC-mCherry variants with sfGFP-PodJ in the *C. crescentus pleC* and *podJ* deletion strain. Cells were induced with 0.03% xylose for sfGFP-PodJ and 0.5 mM vanillate for PleC-mCherry for 5 hours. Scale bar denotes 2 µm. (C) Quantification of co-localization between the PleC variants with PodJ in Figure 4.14B. A correlation score of +1 indicates complete co-localization and a score of -1 indicates no co-localization. The center line is the median and the box extends to the 25th and 75th percentiles. The whiskers lie at the minimum and maximum values. Significance was determined using Dunnett's multiple comparisons test. ***:

p<0.001. (D) A cartoon showing the proposed PodJ-PleC interaction site. PodJ's PSE region binds to PleC's PAS A and PAS B. PodJ variant imaging was performed in collaboration with Wei Zhao.

Our heterologous expression experiments in *E. coli* also indicated that PleC's PAS A and PAS B are required to interact with PodJ's PSE-rich domain (Figure 4.13)**.** We therefore asked whether the PodJ interaction sites are sufficient for PleC's cell pole localization in *C. crescentus* (Figure 4.14B-C). In *C. crescentus* strains with *pleC* and *podJ* deleted, PleC-mCherry and sfGFP-PodJ co-localize to the new cell pole. However, the deletion of PleC's PAS A, PAS B, or both PAS AB results in a diffuse PleC localization pattern. In contrast, *E. coli* expression of PleC's PAS A or PAS B alone maintained a reduced ability to co-localize with PodJ (Figure 4.13), indicating that the requirement for both PAS-A and PAS-B may be more stringent in *C. crescentus.* However, we can now propose a model in which PodJ's intrinsically disordered PSE-rich domain interacts with PleC's PAS A and PAS B at the new cell pole in *C. crescentus* (Figure 4.14D).

Disruption of the PodJ-PleC interaction has downstream effects on the cell cycle We observed that despite the loss of PleC binding to PodJ at the new cell pole, the cells in Figure 4.14B did not have noticeable cell cycle defects. However, under inducible control from the xylose locus, PodJ appears to be over-expressed and localized to both poles. Perhaps this PodJ expression condition does not mimic the wild-type and compensates for the loss of the PodJ-PleC interaction. We expressed the same PleC-mCherry domain deletions in a Δ*pleC C. crescentus* strain and observed the same effects on localization but an impaired division phenotype (Figure 4.15A-B). Deletion of both PAS domains or each individual PAS domain resulted in a diffuse localization pattern. The PleC-ΔPAS A variant did exhibit mild localization at the stalked cell pole in 18% of cells, where it may retain some affinity for the proteolyzed form of PodJ[163]. Interestingly, each of these PleC domain deletions resulted in elongated cells, especially the deletion of PAS B only

(Figure 4.15A-B). Future studies using these strains should include a Western blot or fluorescence intensity analysis to determine if there are differences in expression levels of the PleC-mCherry variants in the *C. crescentus* Δ*podJ* Δ*pleC* strain and Δ*pleC* strain.
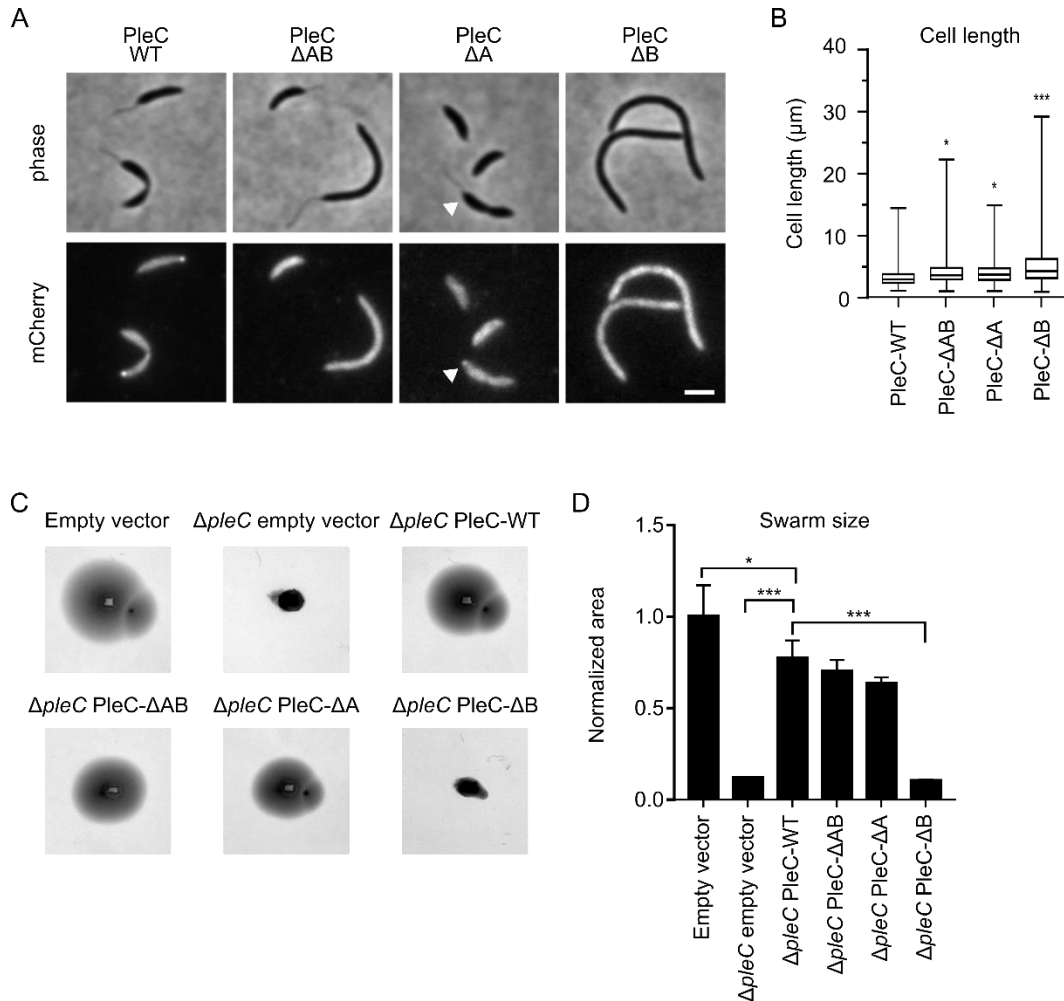
Figure 4.15: The interaction between PodJ and PleC has downstream affects in *C. crescentus* PleC-mCherry domain deletions were expressed in *C. crescentus* wild-type or Δ*pleC* strains. (A) Localization of PleC-mCherry domain deletions. PleC-mCherry variants were expressed from a high-copy plasmid with 0.5 mM vanillate for 3 hours in PYE medium. White arrow points to a focus at the old cell pole. Scale bar denotes 2 μm. (B) Cell lengths of the populations in A. The center line is the median and the box extends to the 25th and 75th percentiles. The whiskers lie

at the minimum and maximum values. n>126 cells. (C) Motility assay of *C. crescentus* were stabbed into 0.3% PYE agar and incubated at 28 ºC for 3 days. (D) Quantification of the motility assay of *C. crescentus* strains expressing PleC domain deletions. Significance was determined with a Dunnett's multiple comparisons test. Comparisons not shown are not significant. (ns: P>0.05, *: P ≤ 0.05, **: P ≤ 0.01, ***: P ≤ 0.001).

We performed a swarm motility assay to interrogate the role of proper PleC localization on not only division defects, but motility as well (Figure 4.15C-D). When *pleC* was deleted, the swarm size was drastically reduced compared to *C. crescentus* expressing an empty vector. Background levels of induction of PleC-WT from the over-expression plasmid nearly recovered the cells' swarming ability. The PleC-ΔPAS A and PleC-ΔPAS AB variants were similarly able to rescue the swarm phenotype of full-length PleC, but PleC-Δ PAS B was not able to recover the swarm phenotype. This correlates with the cell length analysis of the same strains (Figure 4.15A-B) such that the longer cells formed a smaller swarm.

It was unexpected that the deletion of both PAS A and B resulted in a milder phenotype than the deletion of PAS B alone in both assays. In deleting a PAS domain, a new sensor-kinase junction site is created. Engineering chimeric HKs has shown that the linker composition between the sensor and kinase domains can result in constitutive activity, deactivation, or even switching input response[7, 30]. It is possible, then, that PleC-ΔPAS B is locked in a conformation that mis-regulates DivK~P phoshorylation and downstream CtrA-mediated phenotypes. Alternatively, PAS A and PAS B may have antagonistic roles.

Given the differences in cell lengths due to native or induced PodJ expression levels Figure 4.14B, 4.15A-B), we hypothesized that swarm size would also be affected by varying the expression of PodJ. We performed a swarm assay using a strain with xylose-inducible sfGFP-PodJ and vanillate-inducible PleC-mCherry in a Δ*podJ* Δ*pleC* background (Figure 4.16A). This is the

same strain that was imaged using 0.03% xylose to induce sfGFP-PodJ expression in Figure 4.14B. In this experiment, PodJ expression was repressed using 0.2% glucose and induced using 0.003% xylose. We observed a mild but significant increase in swarm size for the non-induced condition, which may allow for "leaky" background expression levels. This increase was only observed in the strains expressing PleC-WT and PleC-ΔPAS A. The PleC variants that did not contain PAS B, PleC-ΔPAS B or PleC-ΔPAS AB, were not responsive to changes in PodJ expression. This suggests that PAS B maintains an interaction with PodJ that is important for swarm motility. We recall that we did not observe differences in cell length in any of the same strains (Figure 4.14B), indicating that the defects caused by the PAS B deletion are related to motility and not cell length or division. A trend in swarm size emerged for all of the PleC variants, such that as more PodJ was expressed, swarm size increased, and then decreased (Figure 4.16A). A precise PodJ and PleC stoichiometry may be required for proper regulation of the downstream pathway, or abnormal PodJ concentrations may mis-regulate other components of cell-cycle progression.

PodJ(1-635) represses the kinase activity of PleC in an *in vitro* coupled enzyme assay

The *C. crescentus* experiments demonstrated that loss of the spatial interaction between PodJ and PleC leads to downstream cell cycle defects. To further evaluate the impact of PodJ(1-635) upon PleC activity, we employed a coupled enzyme ATPase assay (Figure 4.16B)[145, 160]. Purified PleC AB-HK was combined with varying amounts of the purified cytoplasmic portion of PodJ(1-635). 2.5 μM PleC alone resulted in a 3 x 10^{-9} M/s ATP hydrolysis rateThe ATP hydrolysis rate decreased in response to the addition of PodJ(1-635). Addition of 2.5 μM PodJ(1-635) decreased the rate of by about 60%. Upon addition of 7.5 μM PodJ(1-635) to PleC AB-HK, we observed a 90% decrease in the ATP hydrolysis rate compared to PleC alone. In contrast, the addition of 2.5 μM of the BSA negative control resulted in a 25% decrease in PleC ATP hydrolysis activity. This

decrease in the PleC ATP hydrolysis rate indicates that the cytoplasmic region of PodJ represses PleC kinase activity. Further studies are required to determine whether this PodJ merely represses PleC kinase activity or serves to activate phosphatase activity. However, we have evidence that PodJ can allosterically regulate PleC activity.
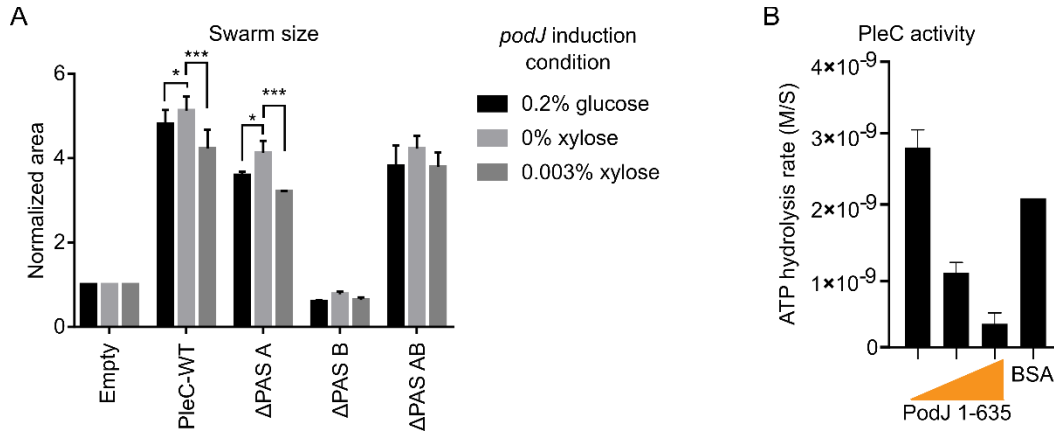
Figure 4.16: PodJ regulates the cell cycle and purified PleC activity in a dose-dependent manner (A) Quantification of the motility assay of *C. crescentus* strains expressing PleC-mCherry domain deletions with varying induction of sfGFP-PodJ. *C. crescentus* were stabbed into PYE agar with the appropriate glucose or xylose concentration and incubated at 28 ℃ for 3 days. Significance was determined with a Tukey's multiple comparisons test. Comparisons not shown are not significant. (ns: $P > 0.05$, *: $P \leq 0.05$, **: $P \leq 0.01$, ***: $P \leq 0.001$). (B) Coupled enzyme assay with PleC and PodJ concentrations. 2.5 µM of PleC AB-HK was incubated with 125 µM ATP and 0, 2.5 or 7.5 µM of PodJ(1-635) or 2.5 µM of BSA. The ATP hydrolysis rate was calculated from the linear region in the A_{340} versus time. ATP hydrolysis rate in the coupled enzyme buffer has been subtracted to account for the background hydrolysis of ATP. Error bars represent the standard deviation from two independent replicates. ATP hydrolysis assay was performed in collaboration with Chao Zhang.

A chimeric PleC activity reporter responds to PodJ expression in *E. coli* We have shown that the PodJ-PleC interaction can modulate PleC activity. We next wanted to answer whether proteolysis or a signal binding event within the periplasm can act to switch PleC's kinase

and phosphatase states. A limitation of the PodJ coupled enzyme ATPase assay is that purification of full-length PodJ is difficult, and optimal conditions are still being sought. Chao Zhang in our lab developed a chimeric sensor-HK activity reporter to assess the effect of various PodJ constructs on the PleC sensor in *E. coli*. A library of chimeric constructs was built and screened for response to PodJ expression. The design of the most responsive chimeric histidine kinase reporter included PleC's PAS A and PAS B directly fused to the HK of the light-sensing TCS CcaS/R[218] (Figure 4.17A). This reporter couples PleC's sensory domain with a HK from a two-component system with a programmable and measurable output; in this case, mCherry expression (Figure 4.17B). The system utilizes the response regulator CcaR, which upon phosphorylation activates transcription of *mCherry* through the P_{cpc}G2-172 promoter[219]. We confirmed the co-localization between the PleC-CcaS reporter and CFP-PodJ in *E. coli* (Figure 4.17C). This result indicates that the fusion of PAS AB to a different HK domain does not impact PAS AB's binding to PodJ.
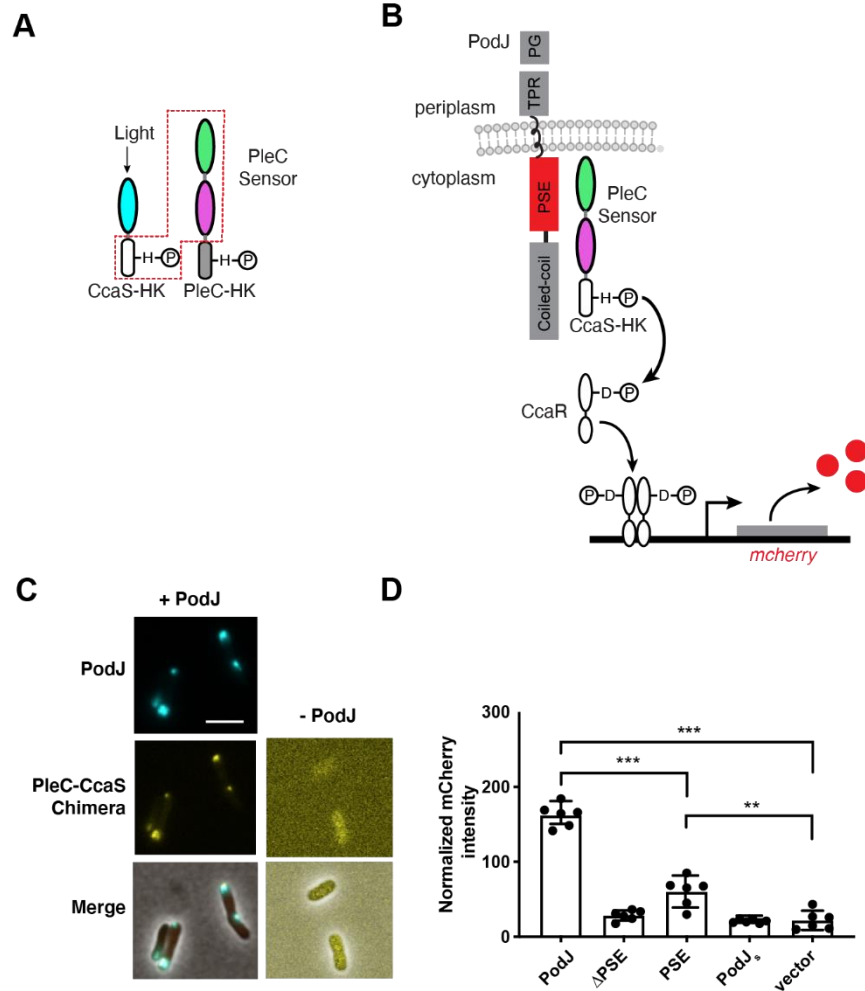
Figure 4.17: PodJ stimulates the kinase activity of PodJ-CcaS chimera in *E. coli* (A) Design of a PleC-CcaS chimera reporter system. PleC's cytoplasmic sensory domains were fused to the histidine kinase domain of CcaS. (B) The chimeric sensor is designed to test the impact of the PodJ-PleC interaction upon PleC signaling. (C) Heterologous co-expression of CFP-PodJ with YFP-PleC-CcaS in *E. coli*. CFP-PodJ was induced with 0.5 mM IPTG for 3 hours and PleC-CcaS-YFP was constitutively expressed. Scale bar denotes 2 μm. (D) Co-expression of the PleC-CcaS chimera gene reporter system with PodJ domain deletion variants. Significance was calculated using a two-tailed t-test. (ns: P>0.05, *: P ≤ 0.05, **: P ≤ 0.01, ***: P ≤ 0.001). Error bars represent the standard deviation from three independent biological replicates performed on different days. Experiments were completed in collaboration with Chao Zhang.

The stimulation of the PleC-CcaS reporter requires PodJ's intrinsically disordered (PSE-rich) and periplasmic domains To determine whether the PleC activity reporter would respond to interaction with PodJ, we compared the effects of expressing PodJ domain deletion variants in the system (Figure 4.17D). We measured mCherry fluorescence as an output of the PleC-CcaS reporter. Relative to the addition of the empty vector, expression of full-length PodJ resulted in a 10-fold increase in mCherry expression, which indicates that PodJ stimulated kinase activity of the PleC-CcaS chimera (Figure 4.17D). A variant that lacks the intrinsically disordered PSE domain, PodJ-ΔPSE, was unable to stimulate PleC-CcaS mediated mCherry expression. In contrast, expression of the PSE-rich domain alone led to a moderate 3-fold activation of mCherry expression. This suggests that stimulation of the PleC-CcaS chimera is dependent upon the interaction between PodJ's PSE-rich domain and PleC's sensory domain.

Next, we asked if PleC-CcaS responds differently to the long-form of PodJ (PodJ$_L$) and the short form of PodJ (PodJ$_S$). Past experiments indicated that loss of the periplasmic domain of PodJ leads to a reduction in expression of CtrA mediated genes in *C. crescentus*[121]. We observed that both PodJ$_L$ and PodJ$_S$ could recruit PleC to the cell poles when heterologously expressed in *E. coli* (Figure 12), consistent with the past observation in *C. crescentus*[209]. Therefore, our studies combined with previous work suggest that down-regulation of the CtrA pathway that occurs upon PodJ proteolysis but not due to a loss of PleC-PodJ binding. One possibility is that PodJ$_L$ and PodJ$_S$ may exert different allosteric effects upon PleC signaling activity. We observed that expression of full-length PodJ stimulated mCherry expression via the PleC-CcaS chimera. However, the expression of PodJ$_S$ was unable to stimulate mCherry expression (Figure 4.17D). Therefore, while both PodJ$_L$ and PodJ$_S$ can interact with PleC (Figure 10), only the long form of PodJ allosterically stimulates PleC-CcaS function (Figure 14D). For each of these assays, PodJ variant expression

levels were confirmed through the measurement of PodJ's fluorescent label. Analysis of PodJ variant induction levels indicates total cell intensities are within 2-fold of one another, and the activities did not correlate to PodJ expression level. While future experimental design will include more strict regulation of PodJ expression, we believe that the effects on the PleC activity reporter were not only due to PodJ concentration. Overall, we have demonstrated that the two forms of PodJ can both interact with PleC (Figure 4.12) but have different regulatory effects upon PleC activity (Figure 4.17).

Notably, PleC and PleC-CcaS behave differently in the *in vivo* mCherry expression assays and *in vitro* coupled enzyme assays. In our *in vitro* assays, PleC exhibits kinase activity in solution, but the addition of PodJ(1-635) represses kinase activity (Figure 4.16B). In contrast, the PleC activity reporter is inactive alone and when co-expressed with PodJ(1-702), but kinase activity is turned on with the addition of PodJ$_L$ (Figure 4.17D). The differences in regulation are likely rooted in one of two aspects of the PleC-CcaS chimeric reporter design: removal of PleC's periplasmic sensor that may directly regulate the cytoplasmic sensor or fusion of the PleC cytoplasmic sensor to a divergent histidine kinase CcaS. Past studies of the YF1 kinase have shown that alterations of the N-terminus or C-terminus of PAS sensory domains can impact sensor functions as an activator or repressor upon sensor stimulation[7]. Similarly, we suspect that N-terminal or C-terminal modifications to PleC's sensor have switched its mode of regulation compared to the wild-type PleC (on-switch versus off-switch). Nevertheless, both experimental sets provide evidence that PodJ can allosterically regulate PleC signaling.

PodJ's intrinsically disordered domain binds to PleC's tandem sensory domain and allosterically modulates PleC activity We have demonstrated that the domain of PodJ that recruits PleC to the new cell pole is its intrinsically disordered domain (Figures 4.12, 4.14A, and

4.18). This type of flexible, charged protein motif has been shown to act as a recruitment hub for other scaffolds, such as PopZ[122, 193, 197]. We have also discovered that PleC uses its PAS A and PAS B sensory domains to bind to PodJ at the new cell pole (Figures 4.13 and 14B-C), and that this interaction is critical for maintaining control over CtrA throughout the cell cycle (Figures 4.15A-D, 4.16A). Finally, we found that PodJ has an allosteric effect on PleC activity (Figure 4.16B), and that this requires both the direct interaction between PodJ and PleC (PSE-rich domain) and the periplasmic domain (PodJL) (Figure 4.17D).
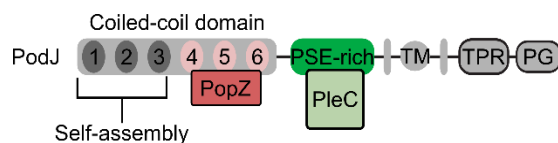
Figure 4.18: Model of the interaction sites for PodJ-self assembly and PopZ and PleC binding within the PodJ domain architecture

4.3 Discussion

PodJ self-assembles and recruits PopZ to the new cell pole to create a distinct signaling hub Recently, biomolecular condensation has emerged as an organizing principle of the bacterial cytoplasm[196, 220-223]. Here we have provided evidence that PodJ self-assembles and forms a liquid-like droplet in solution (Figures 4.7 and 4.8) and accumulates at the cell pole. We predict that accumulation occurs through negative curvature sensing. We discovered a direct interaction between the PopZ and PodJ scaffolds (Figure 4.9) that triggers the robust accumulation of PopZ at the new cell pole as a biomolecular condensate (Figure 4.10)[196]. In the absence of PodJ, we observed a 3-4-fold reduction in the amount of PopZ that localized to the new cell pole (Figure

4.10). Overall, the observed segregation and division phenotypes in cells decreased PopZ at the new cell pole were mild. In the PodJ over-expression strains exhibiting ectopic poles, PopZ almost always accumulated at the stalked or swarmer poles, and not a newly forming pole. These observations indicate that redundant proteins play a role in PopZ recruitment at the new cell pole[206, 224].

Super-resolution imaging of the new cell pole suggests that the molecular organization is well mixed at the spatial resolution of approximately 20 nm[225]. In the absence of protein-protein interaction information, the PopZ-CckA-DivL complex and PodJ-PleC complexes could either be interacting or non-interacting and phase-separated into discrete clusters at the cell pole. Our observation of a direct-scaffold interaction between PodJ and PopZ (Figures 4.9 and 4.10) likely mediates placement of PleC, CckA, DivL as a well-defined signaling complex. This proximity would support previously proposed models in which PleC's dephosphorylation of DivK~P may generate localized zones of unphosphorylated DivK~P[108, 208]. In contrast, simple co-localization of signaling proteins at the cell poles as heterogeneous clusters and without direct interactions may not overcome the rapid DivK diffusion rates that generate shallow DivK~P gradients across the cell[226]. Within bacteria, many histidine kinases form foci[227, 228] or display patchy localization patterns[229, 230], raising the question of how this organization impacts signaling protein function. This raises questions of how localization factors such as the PodJ scaffold regulate signaling protein biochemistry.

PleC is regulated by protein-protein interactions throughout the cell cycle We demonstrated distinct PodJ-PleC interacting domains that are required for co-localization at the new cell pole (Figure 4.17) and allosteric regulation of PleC activity. In light of recent discovery of another allosteric regulator of PleC[231], we propose a model in which the timing and processing

154

of two protein-protein interactions regulate PleC signaling (Figure 4.19). The first of these protein-protein interactions are between PilA and PleC[231]. A recent study has demonstrated that PleC signaling activity is regulated by pilus retraction upon surface contact[231]. Swarmer *C. crescentus* cells extend pili until a surface is encountered, at which point the pili are retracted and holdfast production is initiated[232]. In this model, pilus retraction leads to an accumulation of PilA monomers in the periplasm[232, 233], that directly contacts the transmembrane helices of the PleC kinase[231]. This leads to an increase in cellular cyclic-di-GMP levels that occurs through a PleC response regulator, the diguanylate cyclase PleD[231]. This biochemical event drives the morphological transition from swarmer cells to stalked cells. Also, during this swarmer to stalk-to-stalk transition, PilA is lost from cells either through the ejection of the pili or proteolysis[234].
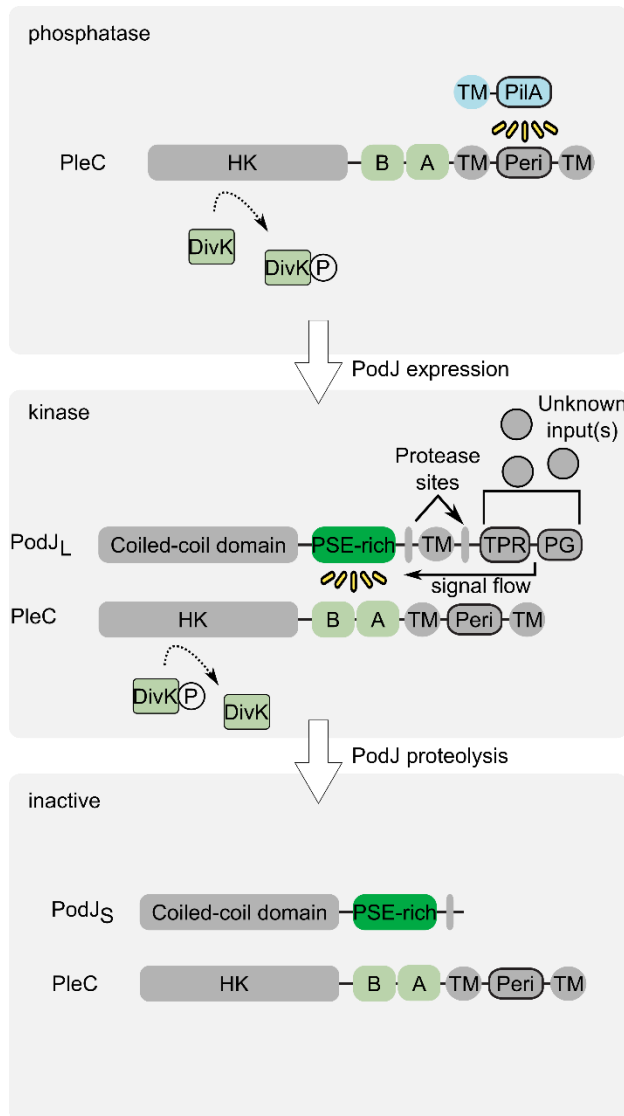
Figure 4.19: Model of PodJ recruitment and activation of the PleC phosphatase at the new cell pole throughout the cell cycle

Later, in the pre-divisional stage of the cell-cycle, PleC functions as a DivK phosphatase to promote robust activation of CckA signaling. The scaffolding protein PodJ is expressed in the early pre-divisional stage of the cell cycle to stimulate PleC phosphatase activity. The PodJ interaction site in the cytoplasmic PAS sensor is downstream of the PilA interaction site, and we speculate that PodJ$_L$ overrides premature PilA stimulation of kinase function (Figure 4.19). This

156

may also indicate that one or more unknown signals are recognized by PodJ's periplasmic domain, which can only occur before proteolysis.

However, during late swarmer cell phase, it's critical to reset PleC's ability for surface sensing. This is achieved by stepwise proteolysis of the PodJ scaffold, which clears the PodJ signal[130, 235]. At the same time that PodJ protease expression is up-regulated[130], the expression of PilA is also upregulated[234]. These two biochemical events lead to conditions where PleC functions primarily as an extracellular sensor for interaction with surfaces. Further biochemical assays will be needed to understand how PodJ and PleC's structure encodes a complex interplay of extracellular and intracellular signal processing.

4.4 Future Directions

Biomolecular condensate formation and effects on kinase activity Our preliminary studies of sfGFP-PodJ in solution indicated that PodJ can form liquid-like biomolecular condensates. While PEG and other crowding agents have been used to induce the formation of such condensates, its use is cautioned. The crowding agent may have a distinct interaction with the components of the condensate, and other crowding agents should be used as controls to rule out specific effects from a certain chemical structure[214]. Given the potential complications with use of crowding agents, I propose that a more appropriate way to mimic the cellular environment is to place the PodJ protein solution onto a lipid-coated slide[236]. Given PodJ's membrane anchoring, I hypothesize that PodJ-membrane interactions may influence condensate formation.

Another possibility is that the appearance of liquid-like droplets is a result of the weak interaction between the sfGFP fluorescent labels[237]. Therefore, I propose to purify and image

157

sfGFP under the same conditions that mediate sfGFP-PodJ condensation formation. Additionally, replacement of the fluorescent protein with small molecule dye labeling strategies[238] or with the antibody-based fluorogenic DL5 tag[239] could circumvent the potential issues with using fluorescent proteins.

The combination of condensate formation and allosteric activation of a kinase leads to the exciting possibility of visualizing kinase activity inside and outside of the condensate. We propose combining fluorescently labeled PodJ and PleC in solution and screen for conditions that promote their co-assembly as well as exclusion of PleC from the PodJ droplet. Genetically encoded fluorescent ATP sensors such as iATPSnFR have been developed[240] and can be used in solution or fused to PleC in order to visualize ATP consumption to measure kinase activity. We envision being able to see where PleC is localized (within or outside a droplet) and where PleC is acting as a kinase. Controls to test whether the ATP sensor is affecting droplet formation or composition will be performed. We will also need to correct our measurements for the loss of fluorescence due to photobleaching, and not a decrease in ATP concentration. Based on the coupled enzyme ATPase assay results (Figure 4.16B), we predict that if PleC is localized inside of the PodJ variant droplet, it will not act as a kinase. However, if it localizes outside of the droplet, it will act as a kinase, and the fluorescence of the ATP sensor will change outside of the droplet over time. We predict that PodJ PSE-only will not form liquid-like condensates, but can interact with PleC in solution, and we would not observe kinase activity. However, while PodJ CC4-6 may co-localize with PleC in solution, we would not expect this PodJ variant to inhibit kinase activity.

Detection of CtrA activity in *C. crescentus* A limitation of any PodJ biochemistry experiment at this time is the inability to purify sufficient quantities of full-length PodJ. We want to be able to test for CtrA activity directly in *C. crescentus*. This technology will be useful for

studying the effects of PleC and PodJ variants, as well as other ongoing *C. crescentus* signaling projects in our lab. A common assay for detecting transcriptional activity is the fluorescent reporter, in which the gene for a fluorescent protein is placed under transcriptional control of the regulator of interest. This type of reporter has been improved for transient processes with the creation of degradable fluorescent proteins[241]. With these proteins, the signal can quickly dissipate if the transcription of the gene decreases. Degradation strategies have been developed in *C. crescentus* as well, but they require the gene of interest to be fused to a degradation tag and the additional expression of an inducible protease[242].

CtrA itself is regulated by phosphorylation and degradation throughout the cell cycle[243]. A CtrA degradation reporter was developed by fusing its receiver domain to the C-terminal 15 amino acids that are required for degradation. This construct is lacking the DNA binding domain and thus has no transcriptional activity but does allow for the visualization of CtrA presence and asymmetric degradation throughout the cell cycle (Figure 4.20A). We took inspiration from this reporter and created a similar system, but with the reporter gene under transcriptional control over CtrA-regulated genes (Figure 4.20B-D). This resulted in a fluorescent reporter that can be used to measure CtrA gene activation and that degrades every cell cycle. We will analyze CtrA-mediated expression by measuring total cell fluorescence by either imaging cells or flow cytometry. Three promoters were chosen for our initial panel of CtrA-regulated gene reporters. PilA is present at high levels and SciP is present at a lower, but more steady level throughout the cell cycle[244]. We also put the reporter under a xylose inducible promoter to test for fluorescence and localization pattern.
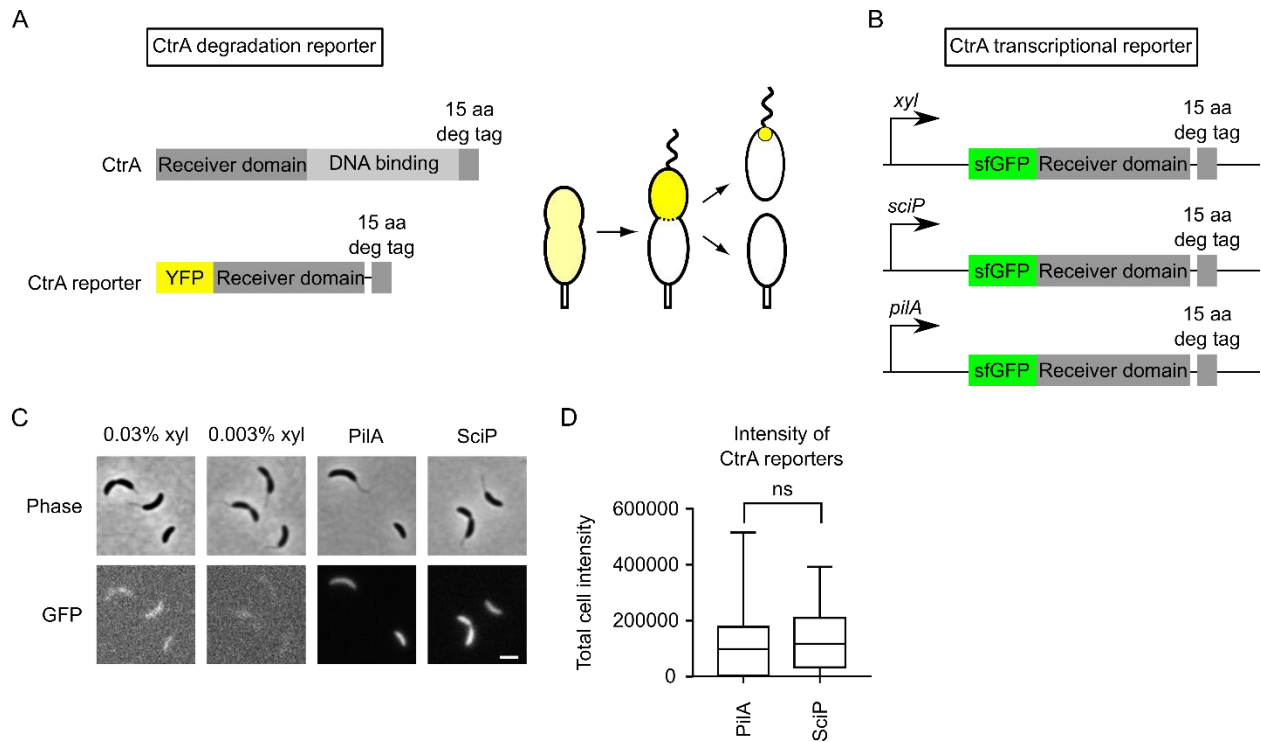
Figure 4.20: Design and initial visualization of the CtrA-based fluorescent reporters (A) A CtrA degradation reporter was previously designed[243]. (B) Design of the new gene transcription reporter based on the CtrA degradation reporter. (C) Initial visualization of the strains. Inducible strains were grown with the reported xylose concentration overnight. (D) Quantification of the total cell intensities for the PilA and SciP reporters. The center line is the median and the box extends to the 25th and 75th percentiles. The whiskers lie at the minimum and maximum values. Significance was determined using Dunnett's multiple comparisons test.

An initial localization screen showed that the reporter did not have the characteristic asymmetric localization of the original CtrA degradation reporter[243] (Figure 20C). Expression levels from the two CtrA-regulated promoters measured by total cell intensities were not different from one another, as predicted (Figure 20D). It appears that the machinery required for degradation could not effectively clear the amount of reporter that was being expressed. Alternatively, photoswitchable fluorescent proteins offer the ability to visualize old and newly translated proteins separately[245], proving to be another effective strategy for reporter design in *C. crescentus*[246]. The

reporter strain will be validated by using it to measure the effect of *podJ* deletion upon *pilA* expression levels compared to previous studies. It can then be used to screen PodJ variants for their effects on the CtrA pathway in combination with or in lieu of other assays such as the more expensive qRT-PCR or Western blots with unique antibodies.

4.5 Methods

Bacterial strains All experiments were performed using *Caulobacter crescentus* NA1000 (also known as CB15N) and *Escherichia coli* BL21. *E. coli* BL21 was purchased from Promega. *C. crescentus* NA1000 was a kind gift from Dr. Lucy Shapiro (Stanford University School of Medicine). C. crescentus and E. coli strains used in this study are listed in Table 4.1. Transformations and phage transductions were carried out as described[247].

Growth conditions and inducer concentrations *C. crescentus* strains were grown at 28°C in PYE (peptone yeast extract) or M2G (minimal medium supplemented with glucose)[247]. When needed, *C. crescentus* cells were synchronized as described[248], and swarmer cells were harvested by Percoll density-gradient centrifugation. *E. coli* strains used for protein purifications and microscopy experiments were grown at 37 °C in LB medium unless otherwise stated. When required, protein expression was induced by adding 0.002-0.5 mM Isopropyl β-D-1-thiogalactopyranoside (IPTG) or 0.5-10 mM arabinose in *E. coli*, and 0.003%–0.3% xylose or 0.05-0.5 mM vanillic acid in *C. crescentus* unless otherwise stated. The induction time for microscopy experiments is 2 hours in *E. coli* and 3 hours in *C. crescentus*. Generalized CR30 phage transduction was performed as described[247].

Plasmid cloning strategies Fragments of target genes plasmid backbone were amplified via PCR using Phusion polymerase (Thermo Scientific). PCR reactions were performed in 50 μL reaction mixtures containing 3% (v/v) DMSO, 1.3 M betaine, 0.3 μM each primer, and 0.2 mM each dNTP, and 1U Phusion High-Fidelity DNA Polymerase (Thermo Scientific). Both fragments were purified via gel extraction. Gibson assembly[249] reactions were performed in 20 μL with 100 ng backbone and typically a 1:10 backbone: insert ratio. A Gibson reaction master mix was prepared from 5x reaction buffer, T5 exonuclease (NEB), Phusion polymerase (NEB), Taq ligase (NEB), and stored as aliquots of 15 μl at -20°C. An annealing temperature of 55°C was used for most reactions unless specified followed by 10 min at 4°C and 10 μl were then transformed into chemically competent *E. coli* DH5a cells using KCM transformation method. Oligonucleotide primers applied for amplification of the gene insert are designed using j5 online program[250]. Oligonucleotides were synthesized by IDT (Coralville, IA), and all DNA sequencing reactions were performed by Genewiz (South Plainfield, NJ).

Phase contrast, DIC, and epifluorescence microscopy Cells were imaged after being immobilized on a 1.5% agarose pad containing corresponding inducers when required. Phase microscopy was performed by using a Nikon Eclipse T*i*-E inverted microscope equipped with an Andor Ixon Ultra DU897 EMCCD camera and a Nikon CFI Plan-Apochromat 100X/1.45 Oil objective. DIC (differential interference contrast) microscopy was performed using the same microscope and camera but with a Nikon CFI Plan-Apochromat 100X/1.45 Oil DIC objective with a Nikon DIC polarizer and slider in place. The excitation source was a Lumencor SpectraX light engine. Chroma filter cube CFP/YFP/MCHRY MTD TI was used to image ECFP (465/25M), EYFP (545/30M), and mCherry (630/60M). Chroma filter cube DAPI/GFP/TRITC was used to

162

image EGFP, sfGFP, and mNeonGreen (515/30M). Images were collected and processed with Nikon NIS-Elements AR software.

Fluorescence intensity profile analysis sfGFP-PodJ variants expressing mCherry-PopZ from the native PopZ promoter were imaged using the above methods. After imaging, predivisional cells expressing sfGFP-PodJ variants were oriented by visualization of the stalk. The average fluorescence intensity profile using normalized cell length was generated using MicrobeJ[136] with the new pole at 0.0 and old pole at 1.0. mCherry-PopZ was made in the same way in the same strains.

Purification of PodJ and PleC Protein expression of all variants followed the same protocol and is described in detail below for PodJ (1-635). To purify the cytoplasmic portion of PodJ(1-635), Rosetta (DE3) containing plasmid pwz091 was grown in 6 liters LB medium (20 µg/ml chloramphenicol and 100 µg/ml ampicillin) at 37°C. The culture was then induced at an OD_{600} of 0.4–0.6 with 0.5 mM IPTG overnight at 18°C. The cells were harvested, resuspended in the lysis buffer (50 mM Tris-HCl, 700 mM KCl, 20 mM Imidazole, 0.05% dextran sulfate, pH 8.0), in the presence of protease inhibitor cocktail tablets without EDTA (Roche).

The cell suspension was lysed with three passes through an EmulsiFlex-C5 cell disruptor (AVESTIN, Inc., Ottawa, Canada), and the supernatant was collected by centrifuging at 13000 g for 30 min at 4°C. Also, the insoluble cell debris was resuspended by the recovery buffer (50 mM Tris-HCl, 1000 mM KCl, 20 mM Imidazole, 0.05% dextran sulfate, pH 8.0) and its supernatant was collected as well as the previous centrifugation. The combined supernatants were loaded onto a 5 ml HisTrap™ HP column (GE Healthcare) and purified with the ÄKTA™ FPLC System. After washing with 10 volumes of wash buffer (50 mM Tris-HCl, 300 mM KCl, and 25 mM imidazole, pH 8.0), the protein was collected by elution from the system with elution buffer (50 mM Tris-

HCl, 300 mM KCl, and 500 mM imidazole, pH 8.0), and concentrated to a 3 ml volume using Amicon Centrifugal Filter Units, resulting in > 95% purity. All PodJ variants were dialyzed with a buffer containing 50 mM Tris-HCl (pH 8.0), 300 mM KCl, and then aliquoted to a small volume (100 µl) and kept frozen at -80°C until use.

PleC-CcaS chimera reporter assay PleC-CcaS chimera reporter assays were performed based on following steps. Starting from a −80 °C DMSO freezer stock, strains were inoculated into 5 mL LB Miller Broth in culture tubes containing appropriate antibiotics and grown at 37 °C 220 rpm for overnight. Cultures were then diluted with fresh and sterile LB media to OD_{600} =1.0 using a UV/Vis spectrophotometer (VWR, USA). The cells are then inoculated into fresh LB media with inoculation density of 25 µl per 1mL LB media with appropriate antibiotics. The tubes were placed in shaker and shaked at 37 °C 220 rpm until OD_{600} reaches 0.4. Then PodJ was induced with 5 mM arabinose for another 4h. After that, cells were harvested and transferred into 96-well plates. Fluorescent protein signals were measured using Tecan M1000 plate reader. Fluorescence was measured using a 5 nm bandpass with excitation/emission for mCherry (585/nm/610nm)/CFP (456nm/480nm)/ YFP (513nm/527nm) with a manually set gain of 50. Each construct was repeated with three independent biological replicates as indicated in the standard error in the bar graph.

Swarmer motility assay Cells were grown to mid-log phase overnight in PYE medium and the appropriate antibiotic. Cells were normalized by dilution in PYE medium to the culture with the lowest OD_{600}. Cells were stabbed into 0.3% PYE agar with the appropriate antibiotic in 15 cm diameter culture plates using a Boekel replicator. Plates were incubated at 28 °C for 3 days. Plates were visualized using a ChemiDoc XRS+ system (Bio-Rad). Three replicate plates were analyzed. Swarm area was measured using ImageJ. Swarm areas were normalized to the empty

vector control on each plate. The error for the empty vector control was calculated by dividing the standard deviation of the areas by the average area. The error for the experimental areas was calculated as the standard deviation of the areas after normalization to the empty vector control. Significance was determined using Prism (GraphPad) with a Dunnett's multiple comparisons test by comparing the mean area of each strain to the mean area of WT (ns: P>0.05, *: P ≤ 0.05, **: P ≤ 0.01, ***: P ≤ 0.001).

Coupled enzyme ATPase assay Kinase and phosphatase activity were measured using a coupled-enzyme assay[145, 160]. Purified PleC CD-HK protein (2.5 µM) was mixed in kinase buffer supplemented with 75 µM ATP, 10 mM $MgCl_2$, 3 mM phosphoenolpyruvate, 0.2 mM NADH, 2 units of pyruvate kinase, and 6.6 units of lactate dehydrogenase (P0294, Sigma). Reactions were performed in two replicates in a 100 µL volume and loaded into a clear polystyrene 384 well-plate. Each reaction was initiated by the addition of ATP, and 340 nm absorbance was recorded every 10 s for 180 min on a Tecan M1000 microplate reader (Tecan, Switzerland). The slope of a stable, linear absorbance decay was measured to calculate ATP hydrolysis rates[251]. Background rates of ATP hydrolysis and NADH oxidation were measured and subtracted from observed ATP hydrolysis rates without addition of any protein. The mean observed rate and SD were determined and analyzed using Prism (GraphPad).

Native gel assay His-PodJ(1-635) was also analyzed by running a native gel. Protein was separated by gel electrophoresis (8% resolving gel) at 80 V for at least 4 hours at 4°C, using a native protein ladder (range from 66 to 669 kDa, Thermo Fisher).

Quantification and statistical analyses FIJI/ImageJ[252, 253], and MicrobeJ [136] were used for image analysis. The number of replicates and the number of cells analyzed per replicate is specified in corresponding legends. All experiments were replicated at least 2 times, and statistical

comparisons were carried out using GraphPad Prism. Differences were considered to be significant when p values were below 0.05. In all figures, measurements are shown as mean ± standard deviations (s.d.).

Intrinsically disordered region analysis The probability of intrinsically disordered regions over the primary sequence of PodJ was predicted (Figure 2C) by three independent programs, *i.e.*, Metadisorder MD2 [254] SPOT [255], and Cspritz [256]. The average scores of these programs were plotted against the PodJ sequence. Regions with probability > 75% were considered disordered in this study.

Table 4.1: *C. crescentus* and *E. coli* strains

Name	Genotype/description	Reference
WSC1123	BL21 Rosetta, F⁻ *ompT hsdSB*(Rb⁻ Mb⁻) *gal dcm* (DE3) Prare (CamR)	Novagen
WSC1119	DH5α	Novagen
WSC0439	*C. crescentus* NA1000	Lucy Shapiro
WSC1141	*C. crescentus* NA1000 *parB::CFP-parB, popZ::popZ-mCherry*	210, 257
LS3778	*C. crescentus* NA1000 Δ*podJ42-959*	210
LS3797	*C. crescentus NA1000 ΔpodJ, ΔpleC*	210
LS4367	*C. crescentus* NA1000 Δ*tipN*	258
WSC1018	*C. crescentus* NA1000 Δ*popZ, vanA::mCherry-popZ*	216
WSC1140	*C. crescentus NA1000 ΔpleC*	161
CZ388	BW29655, pACYCDuet-CcaS(1-57)-pleC(302-548)-CcaS(502-753), pBAD-YFP-PodJ,pProTet.E333-CcaR	this study
CZ442	BW29655, pACYCDuet-J23102-YFP-pleC(302-548)-CcaS(502-753), pBAD-CFP-PodJ,pProTet.E333-CcaR	this study
CZ446	BW29655, pACYCDuet-J23102-YFP-pleC(302-548)-CcaS(502-753)	this study
CZ611	BW29655, pACYCDuet-CcaS(1-57)-pleC(302-548)-CcaS(502-753), pBAD-YFP-PodJ(1-470, 636-974),pProTet.E333-CcaR	this study
CZ612	BW29655, pACYCDuet-CcaS(1-57)-pleC(302-548)-CcaS(502-753), pBAD vector,pProTet.E333-CcaR	this study
CZ639	BW29655, pACYCDuet-CcaS(1-57)-pleC(302-548)-CcaS(502-753), pBAD-YFP-PodJ(1-702),pProTet.E333-CcaR	this study
CZ668	BL21(DE3) pBAD-YFP-PodJ	this study
CZ84	BW29655, pACYCDuet-CcaS(1-57)-pleC(302-548)-CcaS(502-753), pBAD-YFP-PodJ(470-635),pProTet.E333-CcaR	this study
KAK314	*C. crescentus* NA1000 Δ*podJ* Δ*pleC* pbVMCS-6-pleC-ΔA-mCherry	this study
KAK315	*C. crescentus* NA1000 Δ*podJ* Δ*pleC* pbVMCS-6-pleC-ΔAB-mCherry	this study
KAK329	*C. crescentus* NA1000 *ΔpodJ* Δ*pleC* pbVMCS-6-pleC -mCherry	this study
KAK338	*C. crescentus* NA1000 *ΔpodJ* Δ*pleC* pbVMCS-6-pleC-ΔB-mCherry	this study
KAK343	*C. crescentus* NA1000 *Δ pleC*, pBVMCS-6-pleC-mCherry	this study
KAK344	*C. crescentus* NA1000 *ΔpleC*, pBVMCS-6-pleC Δ AB-mCherry	this study
KAK345	*C. crescentus* NA1000 *ΔpleC*, pBVMCS-6-pleC Δ A-mCherry	this study

KAK346	*C. crescentus* NA1000 Δ*pleC*, pBVMCS-6-pleC Δ B-mCherry	this study
KAK465	*C. crescentus* NA1000, pBVMCS-2	this study
KAK466	*C. crescentus* NA1000 Δ *pleC, pBVMCS-2*	this study
MJC120	*C. crescentus* NA1000 Δ *pleC* pBVMCS-6	this study
MJC122	*C. crescentus* NA1000 pBVMCS-6	this study
WSC1208	*C. crescentus* NA1000 pBVMCS-6-Pvan-pleC-mCherry	this study
WSC1209	*C. crescentus* NA1000 Δ *podJ*, pBVMCS-6-Pvan-pleC-mCherry	this study
WSC1210	*C. crescentus* NA1000 Δ *podJ*, pBVMCS-6-Pvan-pleC-mCherry, pXYFPN-2-Pxyl-sfGFP-PodJ	this study
WSC1210	*C. crescentus* NA1000 Δ*podJ,* pBVMCS-6-Pvan-pleC-mCh, pXYFPN-2-Pxyl-sfGFP-PodJ	this study
WSC1221	*C. crescentus* NA1000 Δ *podJ*, pXYFPN-2-Pxyl-sfGFP-PodJΔ471-635, pBVMCS-6-Pvan-pleC-mCherry	this study
WSC1231	pCDFDuet1-PodJ-YPF	this study
WSC1232	DH5α pCDF-YFP-PodJ	this study
WSC1232	pCDFDuet1-YFP-PodJ	this study
WSC1233	pCDFDuet1-mCherry-PodJ	this study
WSC1234	DH5α pBAD-YFP-PodJ	this study
WSC1234	pBAD-YFP-PodJ	this study
WSC1235	pBAD-CFP-PodJ	this study
WSC1236	pCDFDuet1-YFP-PodJ(1-894)	this study
WSC1237	DH5α pCDF-YFP-PodJ(1-702)	this study
WSC1237	pCDFDuet1-YFP-PodJ(1-702)	this study
WSC1238	pCDFDuet1-YFP-PodJ(703-974)	this study
WSC1239	pCDFDuet1-YFP-PodJ(703-894)	this study
WSC1240	pCDFDuet1-YFP-PodJ(1-642)	this study
WSC1241	pCDFDuet1-YFP-PodJ(643-974)	this study
WSC1242	pCDFDuet1-mCherry-PodJ(1-470)	this study
WSC1243	pCDFDuet1-mCherry-PodJ(471-642)	this study
WSC1244	pCDFDuet1-mCherry-PodJ(703-974)	this study
WSC1245	pCDFDuet1-mCherry-PodJ(703-894)	this study
WSC1246	pCDFDuet1-mCherry-PodJ(643-974)	this study
WSC1247	pCDFDuet1-mCherry-PodJ(660-756)	this study
WSC1248	pCDFDuet1-PodJ-mCherry(703-974)	this study
WSC1249	pCDFDuet1-mCherry-PodJ(643-756)	this study
WSC1250	pCDFDuet1-mCherry-PodJ(643-894)	this study
WSC1251	pCDFDuet1-mCherry-PodJ(471-702)	this study
WSC1252	DH5α pCDF--YFP-PodJ(1-470, 643-702)	this study
WSC1252	pCDFDuet1-YFP-PodJ(1-470, 643-702)	this study
WSC1253	pCDFDuet1-mCherry-PodJ(643-702)	this study
WSC1254	pCDFDuet1-YFP-PodJ(128-702)	this study
WSC1255	pCDFDuet1-YFP-PodJ(170-702)	this study

WSC1256	pCDFDuet1-YFP-PodJ(250-702)	this study
WSC1257	pCDFDuet1-YFP-PodJ(430-702)	this study
WSC1258	pCDFDuet1-YFP-PodJ(1-635)	this study
WSC1259	pCDFDuet1-mCherry-PodJ(250-430)	this study
WSC1260	pCDFDuet1-mCherry-PodJ(36-635)	this study
WSC1261	pCDFDuet1-mCherry-PodJ(36-702)	this study
WSC1262	pCDFDuet1-YFP-PodJ(42-702)	this study
WSC1263	pCDFDuet1-YFP-PodJ(1-601)	this study
WSC1264	pCDFDuet1-mCherry-PodJ(643-656)	this study
WSC1265	pCDFDuet1-mCherry-PodJ(657-702)	this study
WSC1266	DH5α pCDF-YFP-PodJ(1-588, 643-702)	this study
WSC1266	pCDFDuet1-YFP-PodJ(1-588, 643-702)	this study
WSC1267	DH5α pCDF-YFP-PodJ(1-470, PopZ 24-102, 643-702)	this study
WSC1267	pCDFDuet1-YFP-PodJ(1-470, popz24-102, 643-702)	this study
WSC1268	DH5α pCDF-YFP-PodJ(1-470, 589-702)	this study
WSC1268	pCDFDuet1-YFP-PodJ(1-470, 589-702)	this study
WSC1269	pCDFDuet1-YFP-PodJΔ250-430	this study
WSC1273	pCDFDuet1-mCherry-PopZ	this study
WSC1274	pBAD-CFP-PopZ	this study
WSC1292	DH5α pACYC-pleC-mCherry	this study
WSC1297	DH5α pBAD-pleC(1-53, 302-842)-mcherry	this study
WSC1298	DH5α pBAD-pleC(1-301, 551-842)-mcherry	this study
WSC1299	DH5α pBAD-pleC(1-550)-mcherry	this study
WSC1300	DH5α pBAD-pleC-PAS C-mcherry	this study
WSC1301	DH5α pBAD-pleC-PAS D-mcherry	this study
WSC1302	DH5α pBAD-pleC-PAS CD-mcherry	this study
WSC1303	DH5α pBAD-pleC-Δ PAS C-mcherry	this study
WSC1304	BL21(DE3) pBAD-pleC-Δ PAS D-mcherry	this study
WSC1341	BL21(DE3) pCDF-YFP-PodJ(1-588, 643-702)	this study
WSC1342	BL21(DE3) pCDF-YFP-PodJ(1-470, 589-702)	this study
WSC1343	BL21(DE3) pCDF-YFP-PodJ	this study
WSC1344	BL21(DE3) pCDF--YFP-PodJ(1-470, 643-702)	this study
WSC1347	BL21(DE3) pACYC-pleC-mCherry	this study
WSC1348	BL21(DE3) pCDF-YFP-PodJ(1-588, 643-702), pACYC-pleC-mCherry	this study
WSC1351	BL21(DE3) pCDF-YFP-PodJ(1-470, 589-702), pACYC-pleC-mcherry	this study
WSC1354	BL21(DE3) pCDF-YFP-PodJ, pACYC-pleC-mCherry	this study
WSC1367	BL21(DE3) pCDF-YFP-PodJ(1-702)	this study
WSC1396	*C. crescentus* NA1000 *ppopZ::mCherry-popZ*	[216]
WSC1397	*C. crescentus* NA1000 *podJ::chlor, ppopZ::mCherry-popZ*	this study (Bowman et al., 2013)
WSC1398	*C. crescentus* NA1000 *podJ::chlor, ppopZ::mCherry-popZ, pCZ393*	this study (Bowman et al., 2013)

WSC1401	*C. crescentus* NA1000 *podJ::chlor, ppopZ::mCherry-popZ, xylX:: sfGFP-podJ1-635*	this study
WSC1402	*C. crescentus* NA1000 *podJ::chlor, ppopZ::mCherry-popZ, xylX::sfGFP-podJΔ471-635*	this study
WSC1403	*C. crescentus* NA1000 *podJ::chlor, ppopZ::mCherry-popZ, xylX::sfGFP-podJΔ250-430*	this study
WSC1404	*C. crescentus* NA1000 *podJ::chlor, ppopZ::mCherry-popZ, xylX::sfGFP-podJΔ1-249*	this study
WSC1407	*C. crescentus* NA1000 *podJ::chlor*	this study

Bibliography

[1] Gao, R., and Stock, A. M. (2009) Biological insights from structures of two-component proteins, *Annu. Rev. Microbiol. 63*, 133-154.

[2] Zschiedrich, C. P., Keidel, V., and Szurmant, H. (2016) Molecular Mechanisms of Two-Component Signal Transduction, *J. Mol. Biol. 428*, 3752-3775.

[3] Galperin, M. Y. (2006) Structural classification of bacterial response regulators: diversity of output domains and domain combinations, *J. Bacteriol. 188*, 4169-4182.

[4] Lin, Y. H., Pierce, B. D., Fang, F., Wise, A., Binns, A. N., and Lynn, D. G. (2014) Role of the VirA histidine autokinase of Agrobacterium tumefaciens in the initial steps of pathogenesis, *Front Plant Sci 5*, 195.

[5] Matamouros, S., Hager, K. R., and Miller, S. I. (2015) HAMP Domain Rotation and Tilting Movements Associated with Signal Transduction in the PhoQ Sensor Kinase, *MBio 6*, e00616-00615.

[6] Schultz, J. E., Kanchan, K., and Ziegler, M. (2015) Intraprotein signal transduction by HAMP domains: a balancing act, *Int. J. Med. Microbiol. 305*, 243-251.

[7] Diensthuber, R. P., Bommer, M., Gleichmann, T., and Moglich, A. (2013) Full-length structure of a sensor histidine kinase pinpoints coaxial coiled coils as signal transducers and modulators, *Structure 21*, 1127-1136.

[8] Lesne, E., Dupre, E., Lensink, M. F., Locht, C., Antoine, R., and Jacob-Dubuisson, F. (2018) Coiled-Coil Antagonism Regulates Activity of Venus Flytrap-Domain-Containing Sensor Kinases of the BvgS Family, *MBio 9*.

[9] Eguchi, Y., Okajima, T., Tochio, N., Inukai, Y., Shimizu, R., Ueda, S., Shinya, S., Kigawa, T., Fukamizo, T., Igarashi, M., and Utsumi, R. (2017) Angucycline antibiotic waldiomycin recognizes common structural motif conserved in bacterial histidine kinases, *The Journal of antibiotics 70*, 251-258.

[10] Casino, P., Rubio, V., and Marina, A. (2009) Structural insight into partner specificity and phosphoryl transfer in two-component signal transduction, *Cell 139*, 325-336.

[11] Wang, B., Zhao, A., Novick, R. P., and Muir, T. W. (2014) Activation and inhibition of the receptor histidine kinase AgrC occurs through opposite helical transduction motions, *Mol. Cell 53*, 929-940.

[12] Marina, A., Waldburger, C. D., and Hendrickson, W. A. (2005) Structure of the entire cytoplasmic portion of a sensor histidine-kinase protein, *EMBO J. 24*, 4247-4259.

[13] Albanesi, D., Martin, M., Trajtenberg, F., Mansilla, M. C., Haouz, A., Alzari, P. M., de Mendoza, D., and Buschiazzo, A. (2009) Structural plasticity and catalysis regulation of a thermosensor histidine kinase, *Proc. Natl. Acad. Sci. U. S. A. 106*, 16185-16190.

[14] Ferris, H. U., Zeth, K., Hulko, M., Dunin-Horkawicz, S., and Lupas, A. N. (2014) Axial helix rotation as a mechanism for signal regulation inferred from the crystallographic analysis of the E. coli serine chemoreceptor, *J. Struct. Biol. 186*, 349-356.

[15] Wang, C., Sang, J., Wang, J., Su, M., Downey, J. S., Wu, Q., Wang, S., Cai, Y., Xu, X., Wu, J., Senadheera, D. B., Cvitkovitch, D. G., Chen, L., Goodman, S. D., and Han, A. (2013) Mechanistic insights revealed by the crystal structure of a histidine kinase with signal transducer and sensor domains, *PLoS Biol. 11*, e1001493.

[16] Mechaly, A. E., Sassoon, N., Betton, J. M., and Alzari, P. M. (2014) Segmental helical motions and dynamical asymmetry modulate histidine kinase autophosphorylation, *PLoS Biol. 12*, e1001776.

[17] Szurmant, H., Bu, L., Brooks, C. L., 3rd, and Hoch, J. A. (2008) An essential sensor histidine kinase controlled by transmembrane helix interactions with its auxiliary proteins, *Proc. Natl. Acad. Sci. U. S. A. 105*, 5891-5896.

[18] Goldberg, S. D., Clinthorne, G. D., Goulian, M., and DeGrado, W. F. (2010) Transmembrane polar interactions are required for signaling in the Escherichia coli sensor kinase PhoQ, *Proc. Natl. Acad. Sci. U. S. A. 107*, 8141-8146.

[19] Utsumi, R., Brissette, R. E., Rampersaud, A., Forst, S. A., Oosawa, K., and Inouye, M. (1989) Activation of Bacterial Porin Gene-Expression by a Chimeric Signal Transducer in Response to Aspartate, *Science 245*, 1246-1249.

[20] Moglich, A., Ayers, R. A., and Moffat, K. (2009) Design and signaling mechanism of light-regulated histidine kinases, *J. Mol. Biol. 385*, 1433-1444.

[21] Iniesta, A. A., Hillson, N. J., and Shapiro, L. (2010) Cell pole-specific activation of a critical bacterial cell cycle kinase, *Proc. Natl. Acad. Sci. U. S. A. 107*, 7012-7017.

[22] Lopez, D., Fischbach, M. A., Chu, F., Losick, R., and Kolter, R. (2009) Structurally diverse natural products that cause potassium leakage trigger multicellularity in Bacillus subtilis, *Proc. Natl. Acad. Sci. U. S. A. 106*, 280-285.

[23] Ganesh, I., Ravikumar, S., Lee, S. H., Park, S. J., and Hong, S. H. (2013) Engineered fumarate sensing Escherichia coli based on novel chimeric two-component system, *Journal of biotechnology 168*, 560-566.

[24] Ganesh, I., Ravikumar, S., Yoo, I. K., and Hong, S. H. (2015) Construction of malate-sensing Escherichia coli by introduction of a novel chimeric two-component system, *Bioprocess and biosystems engineering 38*, 797-804.

[25] Ashenberg, O., Rozen-Gagnon, K., Laub, M. T., and Keating, A. E. (2011) Determinants of homodimerization specificity in histidine kinases, *J. Mol. Biol. 413*, 222-235.

[26] Skerker, J. M., Perchuk, B. S., Siryaporn, A., Lubin, E. A., Ashenberg, O., Goulian, M., and Laub, M. T. (2008) Rewiring the specificity of two-component signal transduction systems, *Cell 133*, 1043-1054.

[27] Whitaker, W. R., Davis, S. A., Arkin, A. P., and Dueber, J. E. (2012) Engineering robust control of two-component system phosphotransfer using modular scaffolds, *Proc. Natl. Acad. Sci. U. S. A. 109*, 18090-18095.

[28] Krikos, A., Conley, M. P., Boyd, A., Berg, H. C., and Simon, M. I. (1985) Chimeric chemosensory transducers of Escherichia coli, *Proc. Natl. Acad. Sci. U. S. A. 82*, 1326-1330.

[29] Jin, T., and Inouye, M. (1994) Mutational Analysis of the Cytoplasmic Linker Region of Taz1-1, a Tar-Envz Chimeric Receptor in Escherichia-Coli, *Journal of molecular biology 244*, 477-481.

[30] Zhu, Y., and Inouye, M. (2003) Analysis of the role of the EnvZ linker region in signal transduction using a chimeric Tar/EnvZ receptor protein, Tez1, *J. Biol. Chem. 278*, 22812-22819.

[31] Moglich, A., Ayers, R. A., and Moffat, K. (2009) Structure and signaling mechanism of Per-ARNT-Sim domains, *Structure 17*, 1282-1294.

[32] Harper, S. M., Christie, J. M., and Gardner, K. H. (2004) Disruption of the LOV-Jalpha helix interaction activates phototropin kinase activity, *Biochemistry 43*, 16184-16192.

[33] Crosson, S., Rajagopal, S., and Moffat, K. (2003) The LOV domain family: photoresponsive signaling modules coupled to diverse output domains, *Biochemistry 42*, 2-10.

[34] Bury, A., and Hellingwerf, K. J. (2018) Design, characterization and in vivo functioning of a light-dependent histidine protein kinase in the yeast Saccharomyces cerevisiae, *AMB Express 8*, 53.

[35] Shivaji, S., and Prakash, J. S. (2010) How do bacteria sense and respond to low temperature?, *Arch. Microbiol. 192*, 85-95.

[36] Draheim, R. R., Bormans, A. F., Lai, R. Z., and Manson, M. D. (2006) Tuning a bacterial chemoreceptor with protein-membrane interactions, *Biochemistry 45*, 14655-14664.

[37] Norholm, M. H., von Heijne, G., and Draheim, R. R. (2015) Forcing the issue: aromatic tuning facilitates stimulus-independent modulation of a two-component signaling circuit, *ACS Synth Biol 4*, 474-481.

[38] Lehning, C. E., Heidelberger, J. B., Reinhard, J., Norholm, M. H. H., and Draheim, R. R. (2017) A Modular High-Throughput In Vivo Screening Platform Based on Chimeric Bacterial Receptors, *ACS Synth Biol 6*, 1315-1326.

[39] de Planque, M. R., Boots, J. W., Rijkers, D. T., Liskamp, R. M., Greathouse, D. V., and Killian, J. A. (2002) The effects of hydrophobic mismatch between phosphatidylcholine bilayers and transmembrane alpha-helical peptides depend on the nature of interfacially exposed aromatic and charged residues, *Biochemistry 41*, 8396-8404.

[40] de Planque, M. R., Goormaghtigh, E., Greathouse, D. V., Koeppe, R. E., 2nd, Kruijtzer, J. A., Liskamp, R. M., de Kruijff, B., and Killian, J. A. (2001) Sensitivity of single membrane-spanning alpha-helical peptides to hydrophobic mismatch with a lipid bilayer: effects on

backbone structure, orientation, and extent of membrane incorporation, *Biochemistry 40*, 5000-5010.

[41] Crosson, S., McGrath, P. T., Stephens, C., McAdams, H. H., and Shapiro, L. (2005) Conserved modular design of an oxygen sensory/signaling network with species-specific output, *Proc. Natl. Acad. Sci. U. S. A. 102*, 8018-8023.

[42] Ravikumar, S., David, Y., Park, S. J., and Choi, J. I. (2018) A Chimeric Two-Component Regulatory System-Based Escherichia coli Biosensor Engineered to Detect Glutamate, *Applied biochemistry and biotechnology*.

[43] Selvamani, V., Ganesh, I., Maruthamuthu, M. K., Eom, G. T., and Hong, S. H. (2017) Engineering chimeric two-component system into Escherichia coli from Paracoccus denitrificans to sense methanol, *Biotechnol Bioproc E 22*, 225-230.

[44] Tabor, J. J., Levskaya, A., and Voigt, C. A. (2011) Multichromatic control of gene expression in Escherichia coli, *J. Mol. Biol. 405*, 315-324.

[45] Daeffler, K. N., Galley, J. D., Sheth, R. U., Ortiz-Velez, L. C., Bibb, C. O., Shroyer, N. F., Britton, R. A., and Tabor, J. J. (2017) Engineering bacterial thiosulfate and tetrathionate sensors for detecting gut inflammation, *Mol. Syst. Biol. 13*, 923.

[46] Schrader, J., Schilling, M., Holtmann, D., Sell, D., Filho, M. V., Marx, A., and Vorholt, J. A. (2009) Methanol-based industrial biotechnology: current status and future perspectives of methylotrophic bacteria, *Trends in biotechnology 27*, 107-115.

[47] Ziolkowska, J. R. (2014) Prospective technologies, feedstocks and market innovations for ethanol and biodiesel production in the US, *Biotechnology reports 4*, 94-98.

[48] Ang, J., Harris, E., Hussey, B. J., Kil, R., and McMillen, D. R. (2013) Tuning response curves for synthetic biology, *ACS Synth Biol 2*, 547-567.

[49] Batchelor, E., and Goulian, M. (2003) Robustness and the cycle of phosphorylation and dephosphorylation in a two-component regulatory system, *Proc. Natl. Acad. Sci. U. S. A. 100*, 691-696.

[50] Landry, B. P., Palanki, R., Dyulgyarov, N., Hartsough, L. A., and Tabor, J. J. (2018) Phosphatase activity tunes two-component system sensor detection threshold, *Nat Commun 9*, 1433.

[51] Huynh, T. N., Noriega, C. E., and Stewart, V. (2010) Conserved mechanism for sensor phosphatase control of two-component signaling revealed in the nitrate sensor NarX, *Proc. Natl. Acad. Sci. U. S. A. 107*, 21140-21145.

[52] Huynh, T. N., Noriega, C. E., and Stewart, V. (2013) Missense substitutions reflecting regulatory control of transmitter phosphatase activity in two-component signalling, *Mol. Microbiol. 88*, 459-472.

[53] Zhu, Y., and Inouye, M. (2002) The role of the G2 box, a conserved motif in the histidine kinase superfamily, in modulating the function of EnvZ, *Mol. Microbiol. 45*, 653-663.

[54] Sutton, M. A., Howard, C. M., Erisman, J. W., Billen, G., Bleeker, A., Grennfelt, P., Van Grinsven, H., and Grizzetti, B. (2011) *The European Nitrogen Assessment : Sources, Effects and Policy Perspectives*, Cambridge University Press, Leiden.

[55] Smanski, M. J., Bhatia, S., Zhao, D., Park, Y., L, B. A. W., Giannoukos, G., Ciulla, D., Busby, M., Calderon, J., Nicol, R., Gordon, D. B., Densmore, D., and Voigt, C. A. (2014) Functional optimization of gene clusters by combinatorial design and assembly, *Nature biotechnology 32*, 1241-1249.

[56] Casino, P., Rubio, V., and Marina, A. (2010) The mechanism of signal transduction by two-component systems, *Curr. Opin. Struct. Biol. 20*, 763-771.

[57] Ferris, H. U., Dunin-Horkawicz, S., Hornig, N., Hulko, M., Martin, J., Schultz, J. E., Zeth, K., Lupas, A. N., and Coles, M. (2012) Mechanism of regulation of receptor histidine kinases, *Structure 20*, 56-66.

[58] Zitzewitz, J. A., Ibarra-Molero, B., Fishel, D. R., Terry, K. L., and Matthews, C. R. (2000) Preformed secondary structure drives the association reaction of GCN4-p1, a model coiled-coil system, *J. Mol. Biol. 296*, 1105-1116.

[59] Hidaka, Y., Park, H., and Inouye, M. (1997) Demonstration of dimer formation of the cytoplasmic domain of a transmembrane osmosensor protein, EnvZ, of Escherichia coli using Ni-histidine tag affinity chromatography, *FEBS Lett. 400*, 238-242.

[60] Cochran, A. G., and Kim, P. S. (1996) Imitation of Escherichia coli aspartate receptor signaling in engineered dimers of the cytoplasmic domain, *Science 271*, 1113-1116.

[61] Wang, Y., Gao, R., and Lynn, D. G. (2002) Ratcheting up vir gene expression in Agrobacterium tumefaciens: coiled coils in histidine kinase signal transduction, *ChemBioChem 3*, 311-317.

[62] Gao, R., and Lynn, D. G. (2007) Integration of rotation and piston motions in coiled-coil signal transduction, *J. Bacteriol. 189*, 6048-6056.

[63] Wang, B., Zhao, A., Xie, Q., Olinares, P. D., Chait, B. T., Novick, R. P., and Muir, T. W. (2017) Functional Plasticity of the AgrC Receptor Histidine Kinase Required for Staphylococcal Virulence, *Cell Chem Biol 24*, 76-86.

[64] Winans, S. C. (1992) Two-way chemical signaling in Agrobacterium-plant interactions, *Microbiol Rev 56*, 12-31.

[65] Doty, S. L., Yu, M. C., Lundin, J. I., Heath, J. D., and Nester, E. W. (1996) Mutational analysis of the input domain of the VirA protein of Agrobacterium tumefaciens, *J. Bacteriol. 178*, 961-970.

[66] Zimmermann, L., Stephens, A., Nam, S. Z., Rau, D., Kubler, J., Lozajic, M., Gabler, F., Soding, J., Lupas, A. N., and Alva, V. (2017) A Completely Reimplemented MPI Bioinformatics Toolkit with a New HHpred Server at its Core, *J. Mol. Biol.*

[67] McLean, B. G., Greene, E. A., and Zambryski, P. C. (1994) Mutants of Agrobacterium VirA that activate vir gene expression in the absence of the inducer acetosyringone, *J. Biol. Chem. 269*, 2645-2651.

[68] Reyes, D., Andrey, D. O., Monod, A., Kelley, W. L., Zhang, G., and Cheung, A. L. (2011) Coordinated regulation by AgrA, SarA, and SarR to control agr expression in Staphylococcus aureus, *J. Bacteriol. 193*, 6020-6031.

[69] Childers, W. S., Xu, Q., Mann, T. H., Mathews, II, Blair, J. A., Deacon, A. M., and Shapiro, L. (2014) Cell fate regulation governed by a repurposed bacterial histidine kinase, *PLoS Biol. 12*, e1001979.

[70] Ozaki, S., Schalch-Moser, A., Zumthor, L., Manfredi, P., Ebbensgaard, A., Schirmer, T., and Jenal, U. (2014) Activation and polar sequestration of PopA, a c-di-GMP effector protein involved in Caulobacter crescentus cell cycle control, *Mol. Microbiol. 94*, 580-594.

[71] Gao, R., and Lynn, D. G. (2005) Environmental pH sensing: resolving the VirA/VirG two-component system inputs for Agrobacterium pathogenesis, *Journal of bacteriology 187*, 2182-2189.

[72] Moglich, A., Ayers, R. A., and Moffat, K. (2010) Addition at the Molecular Level: Signal Integration in Designed Per-ARNT-Sim Receptor Proteins, *Journal of molecular biology 400*, 477-486.

[73] Eswaramoorthy, P., Dravis, A., Devi, S. N., Vishnoi, M., Dao, H. A., and Fujita, M. (2011) Expression level of a chimeric kinase governs entry into sporulation in Bacillus subtilis, *Journal of bacteriology 193*, 6113-6122.

[74] Mann, T. H., and Shapiro, L. (2018) Integration of cell cycle signals by multi-PAS domain kinases, *bioRxiv*.

[75] Eswaramoorthy, P., Guo, T., and Fujita, M. (2009) In vivo domain-based functional analysis of the major sporulation sensor kinase, KinA, in Bacillus subtilis, *J. Bacteriol. 191*, 5358-5368.

[76] Eswaramoorthy, P., Dravis, A., Devi, S. N., Vishnoi, M., Dao, H. A., and Fujita, M. (2011) Expression Level of a Chimeric Kinase Governs Entry into Sporulation in Bacillus subtilis, *J. Bacteriol. 193*, 6113-6122.

[77] Rowland, M. A., and Deeds, E. J. (2014) Crosstalk and the evolution of specificity in two-component signaling, *Proc. Natl. Acad. Sci. U. S. A. 111*, 5550-5555.

[78] Chambonnier, G., Roux, L., Redelberger, D., Fadel, F., Filloux, A., Sivaneson, M., de Bentzmann, S., and Bordi, C. (2016) The Hybrid Histidine Kinase LadS Forms a Multicomponent Signal Transduction System with the GacS/GacA Two-Component System in Pseudomonas aeruginosa, *PLoS Genet. 12*, e1006032.

[79] Goodman, A. L., Merighi, M., Hyodo, M., Ventre, I., Filloux, A., and Lory, S. (2009) Direct interaction between sensor kinase proteins mediates acute and chronic disease phenotypes in a bacterial pathogen, *Genes Dev. 23*, 249-259.

[80] Capra, E. J., and Laub, M. T. (2012) Evolution of two-component signal transduction systems, *Annu. Rev. Microbiol. 66*, 325-347.

[81] Atchley, W. R., Wollenberg, K. R., Fitch, W. M., Terhalle, W., and Dress, A. W. (2000) Correlations among amino acid sites in bHLH protein domains: an information theoretic analysis, *Mol. Biol. Evol. 17*, 164-178.

[82] Fodor, A. A., and Aldrich, R. W. (2004) Influence of conservation on calculations of amino acid covariance in multiple sequence alignments, *Proteins 56*, 211-221.

[83] Varughese, K. I., Tsigelny, I., and Zhao, H. (2006) The crystal structure of beryllofluoride Spo0F in complex with the phosphotransferase Spo0B represents a phosphotransfer pretransition state, *Journal of bacteriology 188*, 4970-4977.

[84] Podgornaia, A. I., Casino, P., Marina, A., and Laub, M. T. (2013) Structural basis of a rationally rewired protein-protein interface critical to bacterial signaling, *Structure 21*, 1636-1647.

[85] Bhattacharyya, R. P., Reményi, A., Yeh, B. J., and Lim, W. A. (2006) Domains, Motifs, and Scaffolds: The Role of Modular Interactions in the Evolution and Wiring of Cell Signaling Circuits, *Annu. Rev. Biochem. 75*, 655-680.

[86] Jin, T., and Inouye, M. (1993) Ligand binding to the receptor domain regulates the ratio of kinase to phosphatase activities of the signaling domain of the hybrid Escherichia coli transmembrane receptor, Taz1, *J. Mol. Biol. 232*, 484-492.

[87] Skerker, J. M., Prasol, M. S., Perchuk, B. S., Biondi, E. G., and Laub, M. T. (2005) Two-component signal transduction pathways regulating growth and cell cycle progression in a bacterium: a system-level analysis, *PLoS Biol. 3*, e334.

[88] Townsend, G. E., Raghavan, V., Zwir, I., and Groisman, E. A. (2013) Intramolecular arrangement of sensor and regulator overcomes relaxed specificity in hybrid two-component systems, *Proceedings of the National Academy of Sciences 110*, E161-E169.

[89] Capra, E. J., Perchuk, B. S., Ashenberg, O., Seid, C. A., Snow, H. R., Skerker, J. M., and Laub, M. T. (2012) Spatial tethering of kinases to their substrates relaxes evolutionary constraints on specificity, *Mol. Microbiol. 86*, 1393-1403.

[90] Tsokos, C. G., Perchuk, B. S., and Laub, M. T. (2011) A dynamic complex of signaling proteins uses polar localization to regulate cell-fate asymmetry in Caulobacter crescentus, *Dev. Cell 20*, 329-341.

[91] Podgornaia, A. I., and Laub, M. T. (2013) Determinants of specificity in two-component signal transduction, *Current opinion in microbiology 16*, 156-162.

[92] Jiang, M., Shao, W., Perego, M., and Hoch, J. A. (2000) Multiple histidine kinases regulate entry into stationary phase and sporulation in Bacillus subtilis, *Mol Microbiol 38*, 535-542.

[93] Francis, V. I., Waters, E. M., Finton-James, S. E., Gori, A., Kadioglu, A., Brown, A. R., and Porter, S. L. (2018) Multiple communication mechanisms between sensor kinases are crucial for virulence in Pseudomonas aeruginosa, *Nat Commun 9*, 2219.

[94] Hurley, A., and Bassler, B. L. (2017) Asymmetric regulation of quorum-sensing receptors drives autoinducer-specific gene expression programs in Vibrio cholerae, *PLoS genetics 13*, e1006826.

[95] Jagadeesan, S., Mann, P., Schink, C. W., and Higgs, P. I. (2009) A novel "four-component" two-component signal transduction mechanism regulates developmental progression in Myxococcus xanthus, *The Journal of biological chemistry 284*, 21435-21445.

[96] Lynskey, N. N., Velarde, J. J., Finn, M. B., Dove, S. L., and Wessels, M. R. (2019) RocA Binds CsrS To Modulate CsrRS-Mediated Gene Regulation in Group A Streptococcus, *MBio 10*.

[97] Mancl, J. M., Ray, W. K., Helm, R. F., and Schubot, F. D. (2019) Helix Cracking Regulates the Critical Interaction between RetS and GacS in Pseudomonas aeruginosa, *Structure 27*, 785-793 e785.

[98] Miller, E. W., Danger, J. L., Ramalinga, A. B., Horstmann, N., Shelburne, S. A., and Sumby, P. (2015) Regulatory rewiring confers serotype-specific hyper-virulence in the human pathogen group A Streptococcus, *Mol. Microbiol. 98*, 473-489.

[99] Schramm, A., Lee, B., and Higgs, P. I. (2012) Intra- and interprotein phosphorylation between two-hybrid histidine kinases controls Myxococcus xanthus developmental progression, *J. Biol. Chem. 287*, 25060-25072.

[100] Childers, W. S., and Shapiro, L. (2014) A pseudokinase couples signaling pathways to enable asymmetric cell division in a bacterium, *Microbial cell (Graz, Austria) 2*, 29-32.

[101] Rollen, K., Granzin, J., Panwalkar, V., Arinkin, V., Rani, R., Hartmann, R., Krauss, U., Jaeger, K. E., Willbold, D., and Batra-Safferling, R. (2016) Signaling States of a Short

Blue-Light Photoreceptor Protein PpSB1-LOV Revealed from Crystal Structures and Solution NMR Spectroscopy, *J. Mol. Biol. 428*, 3721-3736.

[102] Curtis, P. D., and Brun, Y. V. (2010) Getting in the loop: regulation of development in Caulobacter crescentus, *Microbiology and molecular biology reviews : MMBR 74*, 13-41.

[103] Lasker, K., Mann, T. H., and Shapiro, L. (2016) An intracellular compass spatially coordinates cell cycle modules in Caulobacter crescentus, *Current opinion in microbiology 33*, 131-139.

[104] Tsokos, C. G., and Laub, M. T. (2012) Polarity and cell fate asymmetry in Caulobacter crescentus, *Current opinion in microbiology 15*, 744-750.

[105] Laub, M. T., Chen, S. L., Shapiro, L., and McAdams, H. H. (2002) Genes directly controlled by CtrA, a master regulator of the Caulobacter cell cycle, *Proc. Natl. Acad. Sci. U. S. A. 99*, 4632-4637.

[106] Iniesta, A. A., Hillson, N. J., and Shapiro, L. (2010) Cell pole-specific activation of a critical bacterial cell cycle kinase, *Proceedings of the National Academy of Sciences of the United States of America 107*, 7012-7017.

[107] Mann, T. H., and Shapiro, L. (2018) Integration of cell cycle signals by multi-PAS domain kinases, *Proc. Natl. Acad. Sci. U. S. A. 115*, E7166-E7173.

[108] Tsokos, C. G., Perchuk, B. S., and Laub, M. T. (2011) A Dynamic Complex of Signaling Proteins Uses Polar Localization to Regulate Cell-Fate Asymmetry in Caulobacter crescentus, *Developmental Cell 20*, 329-341.

[109] Reisinger, S. J., Huntwork, S., Viollier, P. H., and Ryan, K. R. (2007) DivL performs critical cell cycle functions in Caulobacter crescentus independent of kinase activity, *Journal of bacteriology 189*, 8308-8320.

[110] Bhate, M. P., Molnar, K. S., Goulian, M., and DeGrado, W. F. (2015) Signal transduction in histidine kinases: insights from new structures, *Structure 23*, 981-994.

[111] Gushchin, I., Melnikov, I., Polovinkin, V., Ishchenko, A., Yuzhakova, A., Buslaev, P., Bourenkov, G., Grudinin, S., Round, E., Balandin, T., Borshchevskiy, V., Willbold, D., Leonard, G., Buldt, G., Popov, A., and Gordeliy, V. (2017) Mechanism of transmembrane signaling by sensor histidine kinases, *Science 356*.

181

[112] Gushchin, I., and Gordeliy, V. (2018) Transmembrane Signal Transduction in Two-Component Systems: Piston, Scissoring, or Helical Rotation?, *BioEssays 40*.

[113] Möglich, A. (2019) Signal transduction in photoreceptor histidine kinases, *Protein Sci. 28*, 1923-1946.

[114] Buschiazzo, A., and Trajtenberg, F. (2019) Two-Component Sensing and Regulation: How Do Histidine Kinases Talk with Response Regulators at the Molecular Level?, *Annu. Rev. Microbiol. 73*, 507-528.

[115] Dubey, B. N., Lori, C., Ozaki, S., Fucile, G., Plaza-Menacho, I., Jenal, U., and Schirmer, T. (2016) Cyclic di-GMP mediates a histidine kinase/phosphatase switch by noncovalent domain cross-linking, *Sci Adv 2*, e1600823.

[116] Moglich, A., and Moffat, K. (2007) Structural basis for light-dependent signaling in the dimeric LOV domain of the photosensor YtvA, *J. Mol. Biol. 373*, 112-126.

[117] Engelhard, C., Diensthuber, R. P., Moglich, A., and Bittl, R. (2017) Blue-light reception through quaternary transitions, *Sci Rep 7*, 1385.

[118] Childers, W. S., and Shapiro, L. (2014) A pseudokinase couples signaling pathways to enable asymmetric cell division in a bacterium, *Microbial Cell 2*, 29-32.

[119] Domian, I. J., Quon, K. C., and Shapiro, L. (1997) Cell type-specific phosphorylation and proteolysis of a transcriptional regulator controls the G1-to-S transition in a bacterial cell cycle, *Cell 90*, 415-424.

[120] Iniesta, A. A., Hillson, N. J., and Shapiro, L. (2010) Polar Remodeling and Histidine Kinase Activation, Which Is Essential for Caulobacter Cell Cycle Progression, Are Dependent on DNA Replication Initiation, *Journal of bacteriology 192*, 3893-3902.

[121] Curtis, P. D., Quardokus, E. M., Lawler, M. L., Guo, X., Klein, D., Chen, J. C., Arnold, R. J., and Brun, Y. V. (2012) The scaffolding and signalling functions of a localization factor impact polar development, *Mol. Microbiol. 84*, 712-735.

[122] Holmes, J. A., Follett, S. E., Wang, H., Meadows, C. P., Varga, K., and Bowman, G. R. (2016) Caulobacter PopZ forms an intrinsically disordered hub in organizing bacterial cell poles, *Proc. Natl. Acad. Sci. U. S. A. 113*, 12490-12495.

[123] Sommer, J. M., and Newton, A. (1991) Pseudoreversion analysis indicates a direct role of cell division genes in polar morphogenesis and differentiation in Caulobacter crescentus, *Genetics 129*, 623-630.

[124] Christen, B., Abeliuk, E., Collier, J. M., Kalogeraki, V. S., Passarelli, B., Coller, J. A., Fero, M. J., McAdams, H. H., and Shapiro, L. (2011) The essential genome of a bacterium, *Molecular systems biology 7*.

[125] Jacobs, C., Domian, I. J., Maddock, J. R., and Shapiro, L. (1999) Cell cycle-dependent polar localization of an essential bacterial histidine kinase that controls DNA replication and cell division, *Cell 97*, 111-120.

[126] Sciochetti, S. A., Ohta, N., and Newton, A. (2005) The role of polar localization in the function of an essential Caulobacter crescentus tyrosine kinase, *Molecular Microbiology 56*, 1467-1480.

[127] Grigoryan, G., and Keating, A. E. (2008) Structural specificity in coiled-coil interactions, *Curr. Opin. Struct. Biol. 18*, 477-483.

[128] Hecht, G. B., Lane, T., Ohta, N., Sommer, J. M., and Newton, A. (1995) An essential single domain response regulator required for normal cell division and differentiation in Caulobacter crescentus, *EMBO J. 14*, 3915-3924.

[129] Hung, D. Y., and Shapiro, L. (2002) A signal transduction protein cues proteolytic events critical to Caulobacter cell cycle progression, *Proc. Natl. Acad. Sci. U. S. A. 99*, 13160-13165.

[130] Chen, J. C., Hottes, A. K., McAdams, H. H., McGrath, P. T., Viollier, P. H., and Shapiro, L. (2006) Cytokinesis signals truncation of the PodJ polarity factor by a cell cycle-regulated protease, *The EMBO journal 25*, 377-386.

[131] Manning, G., Whyte, D. B., Martinez, R., Hunter, T., and Sudarsanam, S. (2002) The protein kinase complement of the human genome, *Science 298*, 1912-1934.

[132] Reiterer, V., Eyers, P. A., and Farhan, H. (2014) Day of the dead: pseudokinases and pseudophosphatases in physiology and disease, *Trends Cell Biol. 24*, 489-505.

[133] Ribeiro, A. J. M., Das, S., Dawson, N., Zaru, R., Orchard, S., Thornton, J. M., Orengo, C., Zeqiraj, E., Murphy, J. M., and Eyers, P. A. (2019) Emerging concepts in pseudoenzyme classification, evolution, and signaling, *Sci Signal 12*.

[134] Henry, J. T., and Crosson, S. (2011) Ligand-binding PAS domains in a genomic, cellular, and structural context, *Annu. Rev. Microbiol. 65*, 261-286.

[135] Schneider, C. A., Rasband, W. S., and Eliceiri, K. W. (2012) NIH Image to ImageJ: 25 years of image analysis, *Nat. Methods 9*, 671-675.

[136] Ducret, A., Quardokus, E. M., and Brun, Y. V. (2016) MicrobeJ, a tool for high throughput bacterial cell detection and quantitative analysis, *Nat Microbiol 1*, 16077.

[137] Brilli, M., Fondi, M., Fani, R., Mengoni, A., Ferri, L., Bazzicalupo, M., and Biondi, E. G. (2010) The diversity and evolution of cell cycle regulation in alpha-proteobacteria: a comparative genomic analysis, *BMC Syst Biol 4*, 52.

[138] Zimmermann, L., Stephens, A., Nam, S. Z., Rau, D., Kubler, J., Lozajic, M., Gabler, F., Soding, J., Lupas, A. N., and Alva, V. (2018) A Completely Reimplemented MPI Bioinformatics Toolkit with a New HHpred Server at its Core, *J. Mol. Biol. 430*, 2237-2243.

[139] Waterhouse, A. M., Procter, J. B., Martin, D. M., Clamp, M., and Barton, G. J. (2009) Jalview Version 2--a multiple sequence alignment editor and analysis workbench, *Bioinformatics 25*, 1189-1191.

[140] Pettersen, E. F., Goddard, T. D., Huang, C. C., Couch, G. S., Greenblatt, D. M., Meng, E. C., and Ferrin, T. E. (2004) UCSF Chimera--a visualization system for exploratory research and analysis, *J. Comput. Chem. 25*, 1605-1612.

[141] Rocco, C. J., Dennison, K. L., Klenchin, V. A., Rayment, I., and Escalante-Semerena, J. C. (2008) Construction and use of new cloning vectors for the rapid isolation of recombinant proteins from Escherichia coli, *Plasmid 59*, 231-237.

[142] Thanbichler, M., Iniesta, A. A., and Shapiro, L. (2007) A comprehensive set of plasmids for vanillate- and xylose-inducible gene expression in Caulobacter crescentus, *Nucleic Acids Res. 35*, e137.

[143] Reisinger, S. J., Huntwork, S., Viollier, P. H., and Ryan, K. R. (2007) DivL performs critical cell cycle functions in Caulobacter crescentus independent of kinase activity, *J. Bacteriol. 189*, 8308-8320.

[144] Kwon, A., Scott, S., Taujale, R., Yeung, W., Kochut, K. J., Eyers, P. A., and Kannan, N. (2019) Tracing the origin and evolution of pseudokinases across the tree of life, *Science Signaling 12*, eaav3810.

[145] Blair, J. A., Xu, Q., Childers, W. S., Mathews, II, Kern, J. W., Eckart, M., Deacon, A. M., and Shapiro, L. (2013) Branched signal wiring of an essential bacterial cell-cycle phosphotransfer protein, *Structure 21*, 1590-1601.

[146] Jain, I., Miller, E. W., Danger, J. L., Pflughoeft, K. J., and Sumby, P. (2017) RocA Is an Accessory Protein to the Virulence-Regulating CovRS Two-Component System in Group A Streptococcus, *Infect. Immun. 85*.

[147] Black, M. H., Osinski, A., Gradowski, M., Servage, K. A., Pawłowski, K., Tomchick, D. R., and Tagliabracci, V. S. (2019) Bacterial pseudokinase catalyzes protein polyglutamylation to inhibit the SidE-family ubiquitin ligases, *Science 364*, 787-792.

[148] Sulpizio, A., Minelli, M. E., Wan, M., Burrowes, P. D., Wu, X., Sanford, E. J., Shin, J.-H., Williams, B. C., Goldberg, M. L., Smolka, M. B., and Mao, Y. (2019) Protein polyglutamylation catalyzed by the bacterial calmodulin-dependent pseudokinase SidJ, *eLife 8*, e51162.

[149] Furuya, K., and Hutchinson, C. R. (1996) The DnrN protein of Streptomyces peucetius, a pseudo-response regulator, is a DNA-binding protein involved in the regulation of daunorubicin biosynthesis, *J. Bacteriol. 178*, 6310-6318.

[150] Mizuno, T., and Nakamichi, N. (2005) Pseudo-Response Regulators (PRRs) or True Oscillator Components (TOCs), *Plant Cell Physiol. 46*, 677-685.

[151] Biondi, E. G., Reisinger, S. J., Skerker, J. M., Arif, M., Perchuk, B. S., Ryan, K. R., and Laub, M. T. (2006) Regulation of the bacterial cell cycle by an integrated genetic circuit, *Nature 444*, 899-904.

[152] Angelastro, P. S., Sliusarenko, O., and Jacobs-Wagner, C. (2010) Polar localization of the CckA histidine kinase and cell cycle periodicity of the essential master regulator CtrA in Caulobacter crescentus, *J. Bacteriol. 192*, 539-552.

[153] Varughese, K. I., Madhusudan, Zhou, X. Z., Whiteley, J. M., and Hoch, J. A. (1998) Formation of a Novel Four-Helix Bundle and Molecular Recognition Sites by Dimerization of a Response Regulator Phosphotransferase, *Mol. Cell 2*, 485-493.

[154] Eswaran, J., Patnaik, D., Filippakopoulos, P., Wang, F., Stein, R. L., Murray, J. W., Higgins, J. M. G., and Knapp, S. (2009) Structure and functional characterization of the atypical human kinase haspin, *Proceedings of the National Academy of Sciences 106*, 20198-20203.

[155] Christen, B., Abeliuk, E., Collier, J. M., Kalogeraki, V. S., Passarelli, B., Coller, J. A., Fero, M. J., McAdams, H. H., and Shapiro, L. (2011) The essential genome of a bacterium, *Mol. Syst. Biol. 7*, 528.

[156] Chen, Y. E., Tropini, C., Jonas, K., Tsokos, C. G., Huang, K. C., and Laub, M. T. (2011) Spatial gradient of protein phosphorylation underlies replicative asymmetry in a bacterium, *Proc Natl Acad Sci U S A 108*, 1052-1057.

[157] Cunningham, M. W. (2000) Pathogenesis of group A streptococcal infections, *Clin. Microbiol. Rev. 13*, 470-511.

[158] Kowallis, K. A., Silfani, E. M., Kasumu, A., Rong, G., So, V., and Childers, W. S. (2020) Synthetic Control of Signal Flow Within a Bacterial Multi-Kinase Network, *ACS Synthetic Biology*.

[159] Kowallis, K. A., Duvall, S. W., Zhao, W., and Childers, W. S. (2020) Manipulation of Bacterial Signaling Using Engineered Histidine Kinases, *Methods Mol Biol 2077*, 141-163.

[160] Chen, Y. E., Tsokos, C. G., Biondi, E. G., Perchuk, B. S., and Laub, M. T. (2009) Dynamics of two Phosphorelays controlling cell cycle progression in Caulobacter crescentus, *J. Bacteriol. 191*, 7417-7429.

[161] Wheeler, R. T., and Shapiro, L. (1999) Differential localization of two histidine kinases controlling bacterial cell differentiation, *Mol. Cell 4*, 683-694.

[162] Holmes, J. A., Follett, S. E., Wang, H., Meadows, C. P., Varga, K., and Bowman, G. R. (2016) Caulobacter PopZ forms an intrinsically disordered hub in organizing bacterial cell poles, *Proceedings of the National Academy of Sciences*.

[163] Chen, J. C., Hottes, A. K., McAdams, H. H., McGrath, P. T., Viollier, P. H., and Shapiro, L. (2006) Cytokinesis signals truncation of the PodJ polarity factor by a cell cycle-regulated protease, *The EMBO journal 25*, 377-386.

[164] Hofmann, K. S., W. (1993) TMbase-A databade of membrane spanning proteins segments, *Biol. Chem. Hoppe-Seyler 374*.

[165] Jones, D. T. (1999) Protein secondary structure prediction based on position-specific scoring matrices, *J. Mol. Biol. 292*, 195-202.

[166] Duvall, S. W., and Childers, W. S. (2020) Design of a histidine kinase FRET sensor to detect complex signal integration within living bacteria, *ACS Sensors*.

[167] Jacobs, C., Ausmees, N., Cordwell, S. J., Shapiro, L., and Laub, M. T. (2003) Functions of the CckA histidine kinase in Caulobacter cell cycle control, *Mol. Microbiol. 47*, 1279-1290.

[168] Mann, T. H., Childers, W. S., Blair, J. A., Eckart, M. R., and Shapiro, L. (2016) A multi-sensor kinase integrates sub-cellular density and second messenger cues to toggle between functional states.

[169] Vo, C. D., Shebert, H. L., Zikovich, S., Dryer, R. A., Huang, T. P., Moran, L. J., Cho, J., Wassarman, D. R., Falahee, B. E., Young, P. D., Gu, G. H., Heinl, J. F., Hammond, J. W., Jackvony, T. N., Frederick, T. E., and Blair, J. A. (2017) Repurposing Hsp90 inhibitors as antibiotics targeting histidine kinases, *Bioorg. Med. Chem. Lett. 27*, 5235-5244.

[170] Bowman, G. R., Comolli, L. R., Gaietta, G. M., Fero, M., Hong, S. H., Jones, Y., Lee, J. H., Downing, K. H., Ellisman, M. H., McAdams, H. H., and Shapiro, L. (2010) Caulobacter PopZ forms a polar subdomain dictating sequential changes in pole composition and function, *Mol. Microbiol. 76*, 173-189.

[171] Jacobs, C., Hung, D., and Shapiro, L. (2001) Dynamic localization of a cytoplasmic signal transduction response regulator controls morphogenesis during the Caulobacter cell cycle, *Proc. Natl. Acad. Sci. U. S. A. 98*, 4095-4100.

[172] Bergé, M., Campagne, S., Mignolet, J., Holden, S., Théraulaz, L., Manley, S., Allain, F., and Viollier, P. (2016) Modularity and determinants of a (bi-)polarization control system from free-living and obligate intracellular bacteria, *eLife 5*.

[173] Ghai, R., Falconer, R. J., and Collins, B. M. (2012) Applications of isothermal titration calorimetry in pure and applied research--survey of the literature from 2010, *J. Mol. Recognit. 25*, 32-52.

[174] Zhao, W., Duvall, S. W., Kowallis, K. A., Tomares, D. T., Petitjean, H. N., and Childers, W. S. (2018) A circuit of protein-protein regulatory interactions enables polarity establishment in a bacterium, *bioRxiv*, 503250.

[175] Lawler, M. L., Larson, D. E., Hinz, A. J., Klein, D., and Brun, Y. V. (2006) Dissection of functional domains of the polar localization factor PodJ in Caulobacter crescentus, *Mol. Microbiol. 59*, 301-316.

[176] Lynskey, N. N., Goulding, D., Gierula, M., Turner, C. E., Dougan, G., Edwards, R. J., and Sriskandan, S. (2013) RocA truncation underpins hyper-encapsulation, carriage longevity and transmissibility of serotype M18 group A streptococci, *PLoS Pathog. 9*, e1003842.

[177] Matroule, J. Y., Lam, H., Burnette, D. T., and Jacobs-Wagner, C. (2004) Cytokinesis monitoring during development; rapid pole-to-pole shuttling of a signaling protein by localized kinase and phosphatase in Caulobacter, *Cell 118*, 579-590.

[178] Chiang-Ni, C., Chiou, H.-J., Tseng, H.-C., Hsu, C.-Y., and Chiu, C.-H. (2020) RocA Regulates Phosphatase Activity of Virulence Sensor CovS of Group A Streptococcus in Growth Phase- and pH-Dependent Manners, *mSphere 5*, e00361-00320.

[179] Kreikemeyer, B., Boyle, M. D. P., Buttaro, B. A., Heinemann, M., and Podbielski, A. (2001) Group A streptococcal growth phase-associated virulence factor regulation by a novel operon (Fas) with homologies to two-component-type regulators requires a small RNA molecule, *Mol. Microbiol. 39*, 392-406.

[180] Ichikawa, M., Minami, M., Isaka, M., Tatsuno, I., and Hasegawa, T. (2011) Analysis of two-component sensor proteins involved in the response to acid stimuli in Streptococcus pyogenes, *Microbiology 157*, 3187-3194.

[181] Denisov, I. G., Grinkova, Y. V., Lazarides, A. A., and Sligar, S. G. (2004) Directed Self-Assembly of Monodisperse Phospholipid Bilayer Nanodiscs with Controlled Size, *J. Am. Chem. Soc. 126*, 3477-3487.

[182] Good, M. C., Zalatan, J. G., and Lim, W. A. (2011) Scaffold proteins: hubs for controlling the flow of cellular information, *Science 332*, 680-686.

[183] Perez, A. M., Mann, T. H., Lasker, K., Ahrens, D. G., Eckart, M. R., and Shapiro, L. (2017) A Localized Complex of Two Protein Oligomers Controls the Orientation of Cell Polarity, *MBio 8*.

[184] Thompson, B. J. (2013) Cell polarity: models and mechanisms from yeast, worms and flies, *Development 140*, 13-21.

[185] Van der Henst, C., de Barsy, M., Zorreguieta, A., Letesson, J. J., and De Bolle, X. (2013) The Brucella pathogens are polarized bacteria, *Microbes and infection 15*, 998-1004.

[186] Laventie, B. J., Sangermani, M., Estermann, F., Manfredi, P., Planes, R., Hug, I., Jaeger, T., Meunier, E., Broz, P., and Jenal, U. (2019) A Surface-Induced Asymmetric Program Promotes Tissue Colonization by Pseudomonas aeruginosa, *Cell Host Microbe 25*, 140-152.e146.

[187] Aakre, C. D., and Laub, M. T. (2012) Asymmetric cell division: a persistent issue?, *Developmental cell 22*, 235-236.

[188] Laloux, G., and Jacobs-Wagner, C. (2014) How do bacteria localize proteins to the cell pole?, *J. Cell Sci. 127*, 11-19.

[189] Renner, L. D., and Weibel, D. B. (2012) MinD and MinE interact with anionic phospholipids and regulate division plane formation in Escherichia coli, *J. Biol. Chem. 287*, 38835-38844.

[190] Huang, K. C., and Ramamurthi, K. S. (2010) Macromolecules that prefer their membranes curvy, *Mol. Microbiol. 76*, 822-832.

[191] Bowman, G. R., Comolli, L. R., Zhu, J., Eckart, M., Koenig, M., Downing, K. H., Moerner, W. E., Earnest, T., and Shapiro, L. (2008) A polymeric protein anchors the chromosomal origin/ParB complex at a bacterial cell pole, *Cell 134*, 945-955.

[192] Ebersbach, G., Briegel, A., Jensen, G. J., and Jacobs-Wagner, C. (2008) A self-associating protein critical for chromosome attachment, division, and polar organization in caulobacter, *Cell 134*, 956-968.

[193] Banani, S. F., Lee, H. O., Hyman, A. A., and Rosen, M. K. (2017) Biomolecular condensates: organizers of cellular biochemistry, *Nat. Rev. Mol. Cell Biol. 18*, 285-298.

[194] Al-Husini, N., Tomares, D. T., Bitar, O., Childers, W. S., and Schrader, J. M. (2018) alpha-Proteobacterial RNA Degradosomes Assemble Liquid-Liquid Phase-Separated RNP Bodies, *Mol. Cell 71*, 1027-1039 e1014.

[195] Al-Husini, N., Tomares, D. T., Pfaffenberger, Z. J., Muthunayake, N. S., Samad, M. A., Zuo, T., Bitar, O., Aretakis, J. R., Bharmal, M.-H. M., Gega, A., Biteen, J. S., Childers, W. S., and Schrader, J. M. (2020) BR-Bodies Provide Selectively Permeable Condensates that Stimulate mRNA Decay and Prevent Release of Decay Intermediates, *Mol. Cell 78*, 670-682.e678.

[196] Lasker, K., von Diezmann, L., Zhou, X., Ahrens, D. G., Mann, T. H., Moerner, W. E., and Shapiro, L. (2020) Selective sequestration of signalling proteins in a membraneless organelle reinforces the spatial regulation of asymmetry in Caulobacter crescentus, *Nat Microbiol 5*, 418-429.

[197] Boeynaems, S., Alberti, S., Fawzi, N. L., Mittag, T., Polymenidou, M., Rousseau, F., Schymkowitz, J., Shorter, J., Wolozin, B., Van Den Bosch, L., Tompa, P., and Fuxreiter, M. (2018) Protein Phase Separation: A New Phase in Cell Biology, *Trends Cell Biol. 28*, 420-435.

[198] Shaw, A. S., and Filbert, E. L. (2009) Scaffold proteins and immune-cell signalling, *Nat. Rev. Immunol. 9*, 47-56.

[199] Saha, A., and Deshaies, R. J. (2008) Multimodal Activation of the Ubiquitin Ligase SCF by Nedd8 Conjugation, *Mol. Cell 32*, 21-31.

[200] Strickfaden, S. C., Winters, M. J., Ben-Ari, G., Lamson, R. E., Tyers, M., and Pryciak, P. M. (2007) A mechanism for cell-cycle regulation of MAP kinase signaling in a yeast differentiation pathway, *Cell 128*, 519-531.

[201] Good, M., Tang, G., Singleton, J., Reményi, A., and Lim, W. A. (2009) The Ste5 Scaffold Directs Mating Signaling by Catalytically Unlocking the Fus3 MAP Kinase for Activation, *Cell 136*, 1085-1097.

[202] Bergé, M., and Viollier, P. H. (2018) End-in-Sight: Cell Polarization by the Polygamic Organizer PopZ, *Trends in Microbiology 26*, 363-375.

[203] Jensen, R. B., Wang, S. C., and Shapiro, L. (2002) Dynamic localization of proteins and DNA during a bacterial cell cycle, *Nat. Rev. Mol. Cell Biol. 3*, 167-176.

[204] Jacobs, C., Hung, D., and Shapiro, L. (2001) Dynamic localization of a cytoplasmic signal transduction response regulator controls morphogenesis during the Caulobacter cell cycle, *Proceedings of the National Academy of Sciences of the United States of America 98*, 4095-4100.

[205] Quon, K. C., Yang, B., Domian, I. J., Shapiro, L., and Marczynski, G. T. (1998) Negative control of bacterial DNA replication by a cell cycle regulatory protein that binds at the chromosome origin, *Proceedings of the National Academy of Sciences 95*, 120-125.

[206] Laloux, G., and Jacobs-Wagner, C. (2013) Spatiotemporal control of PopZ localization through cell cycle-coupled multimerization, *J. Cell Biol. 201*, 827-841.

[207] Young, K. D. (2003) Bacterial shape, *Mol. Microbiol. 49*, 571-580.

[208] Viollier, P. H., Sternheim, N., and Shapiro, L. (2002) Identification of a localization factor for the polar positioning of bacterial structural and regulatory proteins, *Proc. Natl. Acad. Sci. U. S. A. 99*, 13831-13836.

[209] Hinz, A. J., Larson, D. E., Smith, C. S., and Brun, Y. V. (2003) The Caulobacter crescentus polar organelle development protein PodJ is differentially localized and is required for polar targeting of the PleC development regulator, *Mol. Microbiol. 47*, 929-941.

[210] Viollier, P. H., Sternheim, N., and Shapiro, L. (2002) A dynamically localized histidine kinase controls the asymmetric distribution of polar pili proteins, *The EMBO Journal 21*, 4420-4428.

[211] Wang, S. P., Sharma, P. L., Schoenlein, P. V., and Ely, B. (1993) A histidine protein kinase is involved in polar organelle development in Caulobacter crescentus, *Proceedings of the National Academy of Sciences 90*, 630-634.

[212] Paul, R., Jaeger, T., Abel, S., Wiederkehr, I., Folcher, M., Biondi, E. G., Laub, M. T., and Jenal, U. (2008) Allosteric regulation of histidine kinases by their cognate response regulator determines cell fate, *Cell 133*, 452-461.

[213] Chen, J. C., Viollier, P. H., and Shapiro, L. (2005) A membrane metalloprotease participates in the sequential degradation of a Caulobacter polarity determinant, *Mol. Microbiol. 55*, 1085-1103.

[214] Alberti, S., Gladfelter, A., and Mittag, T. (2019) Considerations and Challenges in Studying Liquid-Liquid Phase Separation and Biomolecular Condensates, *Cell 176*, 419-434.

[215] Lawler, M. L., and Brun, Y. V. (2006) A Molecular Beacon Defines Bacterial Cell Asymmetry, *Cell 124*, 891-893.

[216] Bowman, G. R., Perez, A. M., Ptacin, J. L., Ighodaro, E., Folta-Stogniew, E., Comolli, L. R., and Shapiro, L. (2013) Oligomerization and higher-order assembly contribute to sub-cellular localization of a bacterial scaffold, *Mol. Microbiol. 90*, 776-795.

[217] Wheeler, R. T., and Shapiro, L. (1999) Differential localization of two histidine kinases controlling bacterial cell differentiation, *Molecular cell 4*, 683-694.

[218] Schmidl, S. R., Sheth, R. U., Wu, A., and Tabor, J. J. (2014) Refactoring and optimization of light-switchable Escherichia coli two-component systems, *ACS Synth Biol 3*, 820-831.

[219] Schmidl, S. R., Sheth, R. U., Wu, A., and Tabor, J. J. (2014) Refactoring and Optimization of Light-Switchable Escherichia coli Two-Component Systems, *ACS Synthetic Biology 3*, 820-831.

[220] Al-Husini, N., Tomares, D. T., Childers, W. S., and Schrader, J. (2018) α-proteobacterial RNA degradosomes assemble liquid-liquid phase separated RNP bodies, *Molecular cell*.

[221] Al-Husini, N., Tomares, D. T., Pfaffenberger, Z. J., Muthunayake, N. S., Samad, M. A., Zuo, T., Bitar, O., Aretakis, J. R., Bharmal, M. M., Gega, A., Biteen, J. S., Childers, W. S., and Schrader, J. M. (2020) BR-Bodies Provide Selectively Permeable Condensates that Stimulate mRNA Decay and Prevent Release of Decay Intermediates, *Molecular cell*.

[222] Monterroso, B., Zorrilla, S., Sobrinos-Sanguino, M., Robles-Ramos, M. A., Lopez-Alvarez, M., Margolin, W., Keating, C. D., and Rivas, G. (2019) Bacterial FtsZ protein forms phase-separated condensates with its nucleoid-associated inhibitor SlmA, *EMBO reports 20*.

[223] Heinkel, F., Abraham, L., Ko, M., Chao, J., Bach, H., Hui, L. T., Li, H., Zhu, M., Ling, Y. M., Rogalski, J. C., Scurll, J., Bui, J. M., Mayor, T., Gold, M. R., Chou, K. C., Av-Gay, Y., McIntosh, L. P., and Gsponer, J. (2019) Phase separation and clustering of an ABC transporter in Mycobacterium tuberculosis, *Proceedings of the National Academy of Sciences of the United States of America 116*, 16326-16331.

[224] Berge, M., Campagne, S., Mignolet, J., Holden, S., Theraulaz, L., Manley, S., Allain, F. H., and Viollier, P. H. (2016) Modularity and determinants of a (bi-)polarization control system from free-living and obligate intracellular bacteria, *Elife 5*.

[225] Lasker, K., von Diezmann, L., Zhou, X., Ahrens, D. G., Mann, T. H., Moerner, W. E., and Shapiro, L. (2020) Selective sequestration of signalling proteins in a membraneless organelle reinforces the spatial regulation of asymmetry in Caulobacter crescentus, *Nature microbiology*.

[226] Tropini, C., and Huang, K. C. (2012) Interplay between the localization and kinetics of phosphorylation in flagellar pole development of the bacterium Caulobacter crescentus, *PLoS Comput. Biol. 8*, e1002602.

[227] Mignolet, J., Van der Henst, C., Nicolas, C., Deghelt, M., Dotreppe, D., Letesson, J.-J., and De Bolle, X. (2010) PdhS, an Old-Pole-Localized Histidine Kinase, Recruits the Fumarase FumC in Brucella abortus, *Journal of bacteriology 192*, 3235.

[228] Angelastro, P. S., Sliusarenko, O., and Jacobs-Wagner, C. (2010) Polar Localization of the CckA Histidine Kinase and Cell Cycle Periodicity of the Essential Master Regulator CtrA in Caulobacter crescentus, *Journal of bacteriology 192*, 539-552.

[229] Devi, S. N., Vishnoi, M., Kiehler, B., Haggett, L., and Fujita, M. (2015) In vivo functional characterization of the transmembrane histidine kinase KinC in Bacillus subtilis, *Microbiology 161*, 1092-1104.

[230] Monteagudo-Cascales, E., García-Mauriño, S. M., Santero, E., and Canosa, I. (2019) Unraveling the role of the CbrA histidine kinase in the signal transduction of the CbrAB two-component system in Pseudomonas putida, *Scientific reports 9*, 9110.

[231] Del Medico, L., Cerletti, D., Schachle, P., Christen, M., and Christen, B. (2020) The type IV pilin PilA couples surface attachment and cell-cycle initiation in Caulobacter crescentus, *Proc Natl Acad Sci U S A*.

[232] Ellison, C. K., Kan, J., Dillard, R. S., Kysela, D. T., Ducret, A., Berne, C., Hampton, C. M., Ke, Z., Wright, E. R., Biais, N., Dalia, A. B., and Brun, Y. V. (2017) Obstruction of pilus retraction stimulates bacterial surface sensing, *Science 358*, 535-538.

[233] Craig, L., Forest, K. T., and Maier, B. (2019) Type IV pili: dynamics, biophysics and functional consequences, *Nat Rev Microbiol 17*, 429-440.

[234] Viollier, P. H., Sternheim, N., and Shapiro, L. (2002) A dynamically localized histidine kinase controls the asymmetric distribution of polar pili proteins, *EMBO J 21*, 4420-4428.

[235] Chen, J. C., Viollier, P. H., and Shapiro, L. (2005) A membrane metalloprotease participates in the sequential degradation of a Caulobacter polarity determinant, *Molecular microbiology 55*, 1085-1103.

[236] Alberti, S., Saha, S., Woodruff, J. B., Franzmann, T. M., Wang, J., and Hyman, A. A. (2018) A User's Guide for Phase Separation Assays with Purified Proteins, *J. Mol. Biol. 430*, 4806-4820.

[237] Scott, D. J., Gunn, N. J., Yong, K. J., Wimmer, V. C., Veldhuis, N. A., Challis, L. M., Haidar, M., Petrou, S., Bathgate, R. A. D., and Griffin, M. D. W. (2018) A Novel Ultra-Stable, Monomeric Green Fluorescent Protein For Direct Volumetric Imaging of Whole Organs Using CLARITY, *Scientific Reports 8*, 667.

[238] Toseland, C. P. (2013) Fluorescent labeling and modification of proteins, *J Chem Biol 6*, 85-95.

[239] Saurabh, S., Perez, A. M., Comerci, C. J., Shapiro, L., and Moerner, W. E. (2016) Super-resolution Imaging of Live Bacteria Cells Using a Genetically Directed, Highly Photostable Fluoromodule, *J. Am. Chem. Soc. 138*, 10398-10401.

[240] Tantama, M., Martínez-François, J. R., Mongeon, R., and Yellen, G. (2013) Imaging energy status in live cells with a fluorescent biosensor of the intracellular ATP-to-ADP ratio, *Nature Communications 4*, 2550.

[241] Li, X., Zhao, X., Fang, Y., Jiang, X., Duong, T., Fan, C., Huang, C. C., and Kain, S. R. (1998) Generation of destabilized green fluorescent protein as a transcription reporter, *J. Biol. Chem. 273*, 34970-34975.

[242] Ricci, D. P., Melfi, M. D., Lasker, K., Dill, D. L., McAdams, H. H., and Shapiro, L. (2016) Cell cycle progression in Caulobacter requires a nucleoid-associated protein with high AT sequence recognition, *Proceedings of the National Academy of Sciences 113*, E5952-E5961.

[243] Ryan, K. R., Judd, E. M., and Shapiro, L. (2002) The CtrA response regulator essential for Caulobacter crescentus cell-cycle progression requires a bipartite degradation signal for temporally controlled proteolysis, *J. Mol. Biol. 324*, 443-455.

[244] Schrader, J. M., Li, G. W., Childers, W. S., Perez, A. M., Weissman, J. S., Shapiro, L., and McAdams, H. H. (2016) Dynamic translation regulation in Caulobacter cell cycle control, *Proc. Natl. Acad. Sci. U. S. A. 113*, E6859-E6867.

[245] Gurskaya, N. G., Verkhusha, V. V., Shcheglov, A. S., Staroverov, D. B., Chepurnykh, T. V., Fradkov, A. F., Lukyanov, S., and Lukyanov, K. A. (2006) Engineering of a monomeric green-to-red photoactivatable fluorescent protein induced by blue light, *Nat. Biotechnol. 24*, 461-465.

[246] Kaczmarczyk, A., Hempel, A. M., von Arx, C., Bohm, R., Dubey, B. N., Nesper, J., Schirmer, T., Hiller, S., and Jenal, U. (2020) Precise timing of transcription by c-di-GMP coordinates cell cycle and morphogenesis in Caulobacter, *Nat Commun 11*, 816.

[247] Ely, B. (1991) Genetics of Caulobacter crescentus, *Methods in enzymology 204*, 372-384.

[248] Evinger, M., and Agabian, N. (1977) Envelope-associated nucleoid from Caulobacter crescentus stalked and swarmer cells, *Journal of bacteriology 132*, 294-301.

[249] Gibson, D. G., Young, L., Chuang, R. Y., Venter, J. C., Hutchison, C. A., 3rd, and Smith, H. O. (2009) Enzymatic assembly of DNA molecules up to several hundred kilobases, *Nat. Methods 6*, 343-345.

[250] Hillson, N. J., Rosengarten, R. D., and Keasling, J. D. (2012) j5 DNA assembly design automation software, *ACS Synth Biol 1*, 14-21.

[251] Kiianitsa, K., Solinger, J. A., and Heyer, W. D. (2003) NADH-coupled microplate photometric assay for kinetic studies of ATP-hydrolyzing enzymes with low and high specific activities, *Anal Biochem 321*, 266-271.

[252] Schindelin, J., Arganda-Carreras, I., Frise, E., Kaynig, V., Longair, M., Pietzsch, T., Preibisch, S., Rueden, C., Saalfeld, S., Schmid, B., Tinevez, J. Y., White, D. J., Hartenstein, V., Eliceiri, K., Tomancak, P., and Cardona, A. (2012) Fiji: an open-source platform for biological-image analysis, *Nature methods 9*, 676-682.

[253] Preibisch, S., Saalfeld, S., and Tomancak, P. (2009) Globally optimal stitching of tiled 3D microscopic image acquisitions, *Bioinformatics 25*, 1463-1465.

[254] Kozlowski, L. P., and Bujnicki, J. M. (2012) MetaDisorder: a meta-server for the prediction of intrinsic disorder in proteins, *BMC bioinformatics 13*, 111.

[255] Hanson, J., Yang, Y., Paliwal, K., and Zhou, Y. (2017) Improving protein disorder prediction by deep bidirectional long short-term memory recurrent neural networks, *Bioinformatics 33*, 685-692.

[256] Walsh, I., Martin, A. J., Di Domenico, T., Vullo, A., Pollastri, G., and Tosatto, S. C. (2011) CSpritz: accurate prediction of protein disorder segments with annotation for homology, secondary structure and linear motifs, *Nucleic Acids Res 39*, W190-196.

[257] Ptacin, J. L., Gahlmann, A., Bowman, G. R., Perez, A. M., von Diezmann, A. R. S., Eckart, M. R., Moerner, W. E., and Shapiro, L. (2014) Bacterial scaffold directs pole-specific centromere segregation, *Proceedings of the National Academy of Sciences 111*, E2046-E2055.

[258] Huitema, E., Pritchard, S., Matteson, D., Radhakrishnan, S. K., and Viollier, P. H. (2006) Bacterial birth scar proteins mark future flagellum assembly site, *Cell 124*, 1025-1037.